THE BELL SYSTEM
TECHNICAL JOURNAL
DEVOTED TO THE SCIENTIFIC AND ENGINEERING
ASPECTS OF ELECTRICAL COMMUNICATION

Volume 50 April 1971 Number 4

Statistical Circuit Design:

History and Introduction

By A. C. DICKIESON and J. CHERNAK

(Manuscript received January 8, 1971)

The papers in this series describe the status of a continuing program at Bell Telephone Laboratories to apply computers to all phases of transmission circuit design. The process involves the same steps now that it has historically. Given a set of circuit objectives, the designer:

(*i*) Synthesizes a circuit, using known or assumed characterizations of the devices and components involved.
(*ii*) Analyzes circuit performance, either by measurements of laboratory samples or by calculations based on simulation or modeling.
(*iii*) Optimizes design performance and cost by changing topology or element values.
(*iv*) Examines the design for compliance with objectives under all expected conditions of manufacturing tolerances and the environment of application.
(*v*) Iterates some or all of these steps until a satisfactory, if not optimum, design is achieved.

The first large-scale application of a digital computer to the anal-

ysis of linear filter and equalizer designs came in 1950. The computer was the BTL Mod VI, an early version using telephone relays. As computers gained in speed and versatility and programmers developed new algorithms, strides were taken in synthesis and optimization.

Paralleling this work was a continuous effort to improve the frequency range, speed, precision, and accuracy of transmission measurements. A major milestone was reached in 1953 with the announcement by Thaddeus Slonczewski of the "micro-bel" technique. This achieved measurement accuracies of ± 0.001 decibel by a method that can be applied over very wide frequency ranges.

In 1966, the important step was achieved of using a dedicated general-purpose computer to control the transmission measuring set, and also to process, collate, and output the data in various forms. The next step, of using this computer also to play a role in the iterative process used in design and production, is described in this series.

The advantages of modeling and simulation were recognized early. Both digital and analog computers were put to this task. In 1962, a hybrid interconnection of the two produced great flexibility in dealing with both linear and nonlinear systems.

An obvious requisite to useful modeling is an adequate characterization of the elements to be modeled. The computer-operated test sets have been used extensively in measurements characterizing transistors and other devices, coupled with efforts to relate the measurements to the physics and geometry of the device.

Most recently, algorithms and programs have been developed to use the computer in the process of analyzing the performance of networks under realistic conditions of manufacturing tolerances, variations of the environment, and manufacturing adjustments. The next step is to have the machine apply the results of this analysis in the iterative process to achieve something near an optimum design.

This brief history of two decades in computer-aided design in transmission development provides a useful perspective in viewing this series of papers dealing with statistical analysis. The notion of using statistical procedures was proposed[1] many years ago and successful applications have been reported[2] in the past in the analysis of logic circuits. The catalyst which has led to the present effectiveness on a wide class of circuits and systems, however, has its roots in this twenty-year-old effort in device characterization, development of algorithms for general-purpose programs, and the effort to improve the factory transmission measurement and adjustment capabilities. Consider what has occurred in the past several years of statistical analysis as described in this series.

During 1968 several versions of a general-purpose, statistical analysis program (TAP)[3, 4] were written and used effectively for a range of circuits from passive filter designs to highly nonlinear systems. In their original conception, the tolerance analysis procedures were visualized as a final step in the design process. They belonged to the class of computer aids that allows the computer to manipulate an analysis or simulation in a fashion similar to the general-purpose optimization programs. The computer-aided design process was viewed as consisting of the following three steps:

(*i*) *Analysis*—Components are modeled and the circuit is analyzed. Components and the network topology are changed until the circuit performance approaches the designer's expectations.

(*ii*) *Optimization*—The designer identifies a desired measure of performance and the analysis is embedded in a general-purpose optimization program. These optimization programs use various strategies to alter the circuit parameters to bring the performance within the desired bounds.

(*iii*) *Tolerance Analysis*—Using a similar measure of performance, the optimized model parameters are varied within their anticipated distributions with the appropriate correlation between parameters. The circuit performance is repetitively analyzed with these different parameters until a histogram of the performance measure can be interpreted with confidence.

Our experience in the past several years has shown that the use of statistical analysis is not the simple final step in the design process. Our present view is that this technique forms new bridges among design, manufacture, and field failure problems. These bridges carry information in both directions with a substantial impact on both design and manufacturing technologies.

Consider what occurs when the designer takes the first step into the use of tolerance analysis. If he is using the same performance measure as was used in the optimization procedure, he can build histograms as he accumulates the statistics of many designs. For this to be related to the manufacturing yield, however, he must include anticipated bench adjustments on selected components. These adjustments may be as simple as tuning inductors to resonance or as involved as anodizing resistors (a one-directional adjustment) while monitoring a complicated performance measure of some subsystem.

When he considers the manufacturability of the circuit in the factory environment, he faces the issue of relating factory testing procedures to his performance measures used for design. These are often only

casually related to each other in spite of the increasing reliance on computer-operated measurement equipment. This factory test equipment can often be adapted to do "go/no-go" testing using the *same* performance criteria used in the tolerance analysis program.

To simplify the problem, let us presume that the same performance criteria are used for both design and manufacture. The bridge for information flow in both directions becomes critical. In his tolerance analysis, was the designer detecting failures discernible in manufacturing or in the field environment? Can he devise a set of conditions for factory testing (a particular temperature, bias supply voltage, etc.) that will detect most failures predicted for the field? Is there an alternate technique for component adjustment which will increase yield and decrease field failures? If so, should not this adjustment procedure be brought back into his optimization and tolerance analysis programs to see if he still has the optimum nominal values for his components?

Obviously, the answers to these questions depend on the specific circuit or system being designed. These questions, however, are not peripheral to the design process but often introduce overriding considerations which should be considered at every stage of the design process.

The first three papers in this series deal with the current capabilities in tolerance analysis. The first paper by J. Logan[5] introduces the characterization and modeling of components. This characterization capability enables the designer to analyze manufacturing yield (correlation between devices, adjustments, etc.) as separate from field failures (temperature effects, aging, etc.). The second paper by C. L. Semmelman, E. D. Walsh, and G. T. Daryanani[6] traces the development of a linear circuit analysis capability that allows the designer to specify the factory and field environments for a class of active circuits. The third paper by I. A. Cermak and Mrs. D. B. Kirby[7] describes the extension of these techniques to nonlinear circuits.

The fourth paper by G. D. Haynie and S. Yang[8] develops the relationships between the design process and the measurement and testing process. The next two papers by E. M. Butler[9] and B. J. Karafin[10] examine the question of using tolerance analysis for optimum design. The first deals with techniques to optimize the component sensitivity and the second to optimize cost.

The last three papers by L. A. O'Neill;[11] P. Balaban, et al.;[12] and R. G. Olsen[13] provide a view of these techniques as applied to the design of a complex linear circuit, a nonlinear hybrid integrated circuit, and finally a waveguide system analysis. In each of these cases the

ability to extend the designer's capability past the traditional worst-case design estimate was an important factor in the successful design.

This series of papers documents the establishment of analytic bridges between design, manufacturing, and field environment problems. The effective use of these techniques places substantial demands on the design experience of the engineer. The designer must have insight into the factory capabilities and procedures and consider these effects at an early stage of design. This ability, however, to bring these manufacturing and field environments into the design process results in substantially more reliable and economical designs. Major advances still lie ahead, so that one cannot say the program has reached maturity: it is possible to see it as in sturdy adolescence.

REFERENCES

1. Bode, H. W., unpublished work, 1933.
2. Nussbaum, E., Irland, E. A., and Young, C. E., "Statistical Analysis of Logic Circuit Performance in Digital Systems," Proc. of IRE, *49*, (January 1961), pp. 236–244.
3. O'Neill, L. A., "Interactive Tolerance Analysis with Graphic Display," Proc. of Spring Joint Computer Conf., 1969, pp. 207–213.
4. Bohling, D. M., and O'Neill, L. A., "An Interactive Computer Approach to Tolerance Analysis," IEEE Trans. on Computers, *C-19*, (January 1970), pp. 10–16.
5. Logan, J., "Characterization and Modeling for Statistical Design," B.S.T.J., this issue, pp. 1105–1147.
6. Semmelman, C. L., Walsh, E. D., and Daryanani, G. T., "Linear Circuits and Statistical Design," B.S.T.J., this issue, pp. 1149–1171.
7. Cermak, I. A., and Kirby, Mrs. D. B., "Nonlinear Circuits and Statistical Design," B.S.T.J., this issue, pp. 1173–1195.
8. Haynie, G. D., and Yang, S., "Confirmation of Design Using Computer-Controlled Test Sets," B.S.T.J., this issue, p. 1197–1208.
9. Butler, E. M., "Large Change Sensitivities for Statistical Design," B.S.T.J., this issue, pp. 1209–1224.
10. Karafin, B. J., "The Optimum Assignment of Component Tolerances for Electrical Networks," B.S.T.J., this issue, pp. 1225–1242.
11. O'Neill, L. A., "A Case Study of the Use of Computer Aids in Circuit Design—Pulse Equalizers for the T2 Digital Transmission Line," B.S.T.J., this issue, pp. 1243–1262.
12. Balaban, P., Karafin, B. J., and Snyder, Mrs. D. B., "A Monte Carlo Tolerance Analysis of the Integrated, Single-Substrate, RC, *Touch-Tone*® Oscillator," B.S.T.J., this issue, pp. 1263–1291.
13. Olsen, R. G., "The Application of Monte Carlo Techniques to the Study of Impairments in the Waveguide Transmission System," B.S.T.J., this issue, pp. 1293–1310.

THE BELL SYSTEM TECHNICAL JOURNAL
Vol. 50, No. 4, April, 1971
Printed in U.S.A.

Statistical Circuit Design:

Characterization and Modeling for Statistical Design

By JOHN LOGAN

(Manuscript received November 30, 1970)

Analysis of the variation in the electrical performance of integrated circuit structures requires a knowledge of the distributions and interrelationships of device parameter values. This article presents new techniques for more accurate transistor modeling and describes the statistical characterization procedure developed to describe the integrated circuit manufacturing process as far as the measurable electrical parameters are concerned.

I. INTRODUCTION

In statistical design work involving discrete passive elements, nominal parameter values and production distributions give an adequate description. The situation is more complicated for active devices in which the equivalent circuit used to describe these devices requires parameters which are interrelated.

With integrated circuits, conditions are further compounded by the fact that the parameters of different devices on an IC chip are interdependent. Experimentally, however, it has been found that the integrated circuit case can be conveniently decoupled to a manageable degree of complexity even when temperature effects are considered.

In the following sections, the philosophy underlying both our modeling approach and the measurement techniques is outlined. This is followed by a description of the transistor model favored for statistical analysis work, highlighting some popular misconceptions arising from inadequate past measurements. The implications for device modeling in an integrated circuit environment are then considered, followed by a description of the practical methods which have been successfully used to predict the variability in circuit performance arising from variations in the manufacturing process.

II. PRACTICAL MODELING

2.1 *Modeling Philosophy*

The modeling approach found to be most effective is to carry device physics as far as possible, then verify or modify the results by practical experience. To be truly useful, modeling has to be considered simultaneously from three fronts, in that the model must:

(*i*) Give an adequate qualitative description of the electrical behavior of the device.
(*ii*) Have efficient* parameters which are readily measurable (or calculable) and amenable to statistical description.
(*iii*) Be compatible with numerical circuit analysis techniques.

In the literature most attention has been given to items (*i*)[1,2] and (*iii*)[3,4]; in fact, the greatest impediment to meaningful statistical design work is the lack of attention to item (*ii*). In consequence, this discussion will dwell on the hard facts of what has to be done in practice when real data is required to get meaningful results.

There are at least two schools of thought on the subject of device modeling: modeling to get an understanding of the device physics and modeling for the purpose of circuit analysis. Although it is desirable to have one model for both situations, it is frequently expedient to make simplifications in the case of circuit analysis. In a statistical design, particularly one involving integrated circuits, the general properties of the system have to be represented. With transistors, the important points are:

(*i*) The matching of characteristics such as gain or junction voltages.
(*ii*) The tracking of parameters within a device and from device to device on an integrated circuit chip.
(*iii*) The temperature characteristics, vitally important in Bell System work, both from the standpoint of the variation of system performance with temperature and also for any aging effects which may be temperature dependent.

A general description of the above properties is therefore required in statistical design rather than an elaborate precision model which may greatly exceed the accuracy of available data.

Comparisons[1,2] of generic model types, which appear to indicate a mathematical equivalence, neglect some very important facts applicable to transistor models in common use. These facts relate to

* Efficient parameters are ones whose values are simply related to changes in device environmental conditions—preferably constants.

the choice of the independent variables in the model and the significance of this is discussed in Section III.

2.2 *Measurement Philosophy*

From the measurement standpoint the most important consideration is that of effectively decoupling the model parameters. This is done such that each measurement, or set of measurements, uniquely defines specific parameters. The ability to do this depends very much on the complexity of the model structure and may be difficult to achieve in more detailed physical models.[5]

Statistical data is expensive; it is necessary, then, to depend on the minimum set of data points and to maximize their use. In addition, it is expedient to identify parameters which are consistently the same in a given family of devices. This is considered further in Section III which to some extent dictates the form of model desired. Further, to minimize measurement effort, it is essential to use the same statistical data for both nonlinear and small signal models. The development of a suitable small signal model for this purpose is considered in Section IV.

Two approaches exist for determining the model parameters.

(*i*) Obtain the physical properties of the device, such as geometry and doping profile, and calculate the theoretical parameter values for the model.

(*ii*) Derive the parameters from electrical measurements at the device terminals.

In statistical work, item (*ii*) is more attractive as the process variability may not be well known. In addition, complex interactions may be compensated for in the direct measurement technique. For device design prior to fabrication, obviously a combination of (*i*) and (*ii*) has to be used, drawing on measured data from previous similar devices.

III. NONLINEAR TRANSISTOR MODELS

3.1 *Models in Common Use*

At the present time, two forms[6,7] of nonlinear transistor models appear to be in vogue in general purpose network analysis programs. The major difference between the two approaches lies in the reference currents used in the representation of the dependent parameters. The two manifestations have been identified as:

(*i*)[6] The injection model, based on the diode currents injected at the junctions.

(*ii*)[7] The transport model, based on the currents traversing the base region.

In the past it has been said[7] that since the two models appear to be mathematically equivalent, there is a simple transformation between the parameters and it makes little difference which one is used. In fact, this ignores the approximations inherent in the model derivation. It turns out that the functional dependencies of the model parameters in case (*ii*) are more realistic from a physical viewpoint and at the same time simplify the measurement procedures required for parameter determination.

3.2 *Evaluation of the Popular Models*

To stress the significance of the claim for the transport model, the following argument is presented to show the simpler measurement requirements and the more accurate dynamic characterization of this model.

3.2.1 *DC Model*

Figure 1 shows the equivalent circuits of the intrinsic transistor for the two models under consideration; the elements making up the two equivalent circuits are identical, consisting of two semiconductor diodes to provide for minority carrier injection and two current sources to account for minority carrier transport across the base region. The coefficients α_F , α_R , B_N , B_I are current dependent and are represented by either functional or tabular dependence on the currents I_F , I_R , I_N , and I_I respectively. The important differences between the two models are the reference currents used as mentioned in Section 3.1.

The defining equations* are

(a) *Injection Model*	(b) *Transport Model*	
Emitter junction injection:	Transport from emitter to collector:	
$I_F = I_{EF}[\exp(qV_{be}/n_e kT) - 1].$	$I_N = I_{ES}[\exp(\theta_N V_{be}) - 1].$	(1)
Collector junction injection:	Transport from collector to emitter:	
$I_R = I_{CR}[\exp(qV_{bc}/n_c kT) - 1].$	$I_I = I_{CS}[\exp(\theta_I V_{bc}) - 1].$	(2)

The equations for the terminal currents representing the transistor

* The choice of parameter names for the transport model are identical with the CIRCUS[7] convention; the injection model parameter names are selected to prevent ambiguity. The parameters used are defined in Table I.

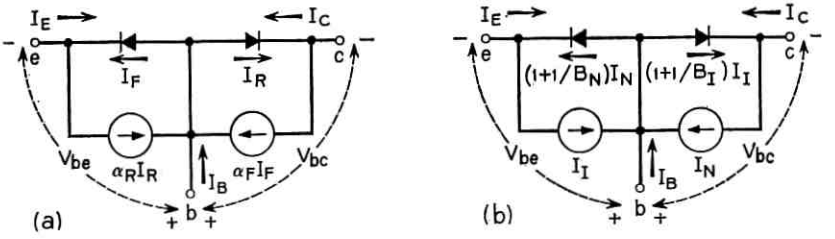

Fig. 1—Equivalent circuits for transistor models. (a) Injection model, (b) Transport model.

nonlinearities are

$$I_E = -I_F + \alpha_R I_R , \qquad I_E = -\left(1 + \frac{1}{B_N}\right) I_N + I_I , \tag{3}$$

$$I_C = \alpha_F I_F - I_R , \qquad I_C = I_N - \left(1 + \frac{1}{B_I}\right) I_I , \tag{4}$$

$$I_B = (1 - \alpha_F) I_F + (1 - \alpha_R) I_R , \qquad I_B = \frac{I_N}{B_N} + \frac{I_I}{B_I} . \tag{5}$$

If the emitter junction is forward biased with $V_{bc} = 0$ such that $I_R = 0$, and $I_I = 0$, then,

$$I_F = -I_E = I_C + I_B , \qquad I_N = I_C . \tag{6}$$

(ideal component) (nonideal component) (ideal component)

Equation (6) shows the fundamental difference between the two models by virtue of the make-up of the reference currents I_F and I_N. I_N represents an ideal component of current in the sense that the collector current and emitter-base voltage are related[5] by the "ideal" diode law. I_F, on the other hand, is made up of two components of currents of which I_B, the base current, is nonideal.[8]

This gives the first reason for preferring the transport model, in that it is intuitively more satisfying to work with the components approximating theoretical behavior. Other experimental reasons now follow:

By measuring I_E and I_C as functions of V_{be}, it is possible to plot the voltage dependence of I_F and I_N as shown on the semilogarithmic plots in Fig. 2.

TABLE I—COEFFICIENTS USED IN COMPARING NONLINEAR MODELS

α_F	Common base current gain in normal mode.
α_R	Common base current gain in inverse mode.
B_N	Common emitter current gain in normal mode.
B_I	Common "emitter" current gain in inverse mode.
I_{CR}	Collector intercept current for the injection model.
I_{CS}	Collector intercept current for the transport model.
I_{EF}	Emitter intercept current for the injection model.
I_{ES}	Emitter intercept current for the transport model.
k	Boltzman's constant.
n_c	Collector injection factor.
n_e	Emitter injection factor.
q	Charge on electron.
T	Absolute temperature.
θ_N	Slope factor for normal mode.
θ_I	Slope factor for inverse mode.

In the inverted mode of transistor operation, if the collector junction is forward biased with $V_{bc} = 0$, then $I_F = 0$ and $I_N = 0$ giving

$$I_R = -I_C = I_E + I_B, \qquad I_I = I_E. \tag{7}$$

(ideal component) (nonideal component) (ideal component)

In this situation I_I represents an ideal component of current and I_R is made up of ideal and nonideal terms. Measurement of I_E and I_C for the inverted transistor gives the voltage dependence of I_I and I_R as shown in Fig. 2.

The redundancy in the injection model is shown by the fact that the slopes and intercepts are different for I_F and I_R in the linear portion of the curves where leakage and high-level effects are not significant. The transport model gives identical slopes and intercepts as a result of the common dependency on the base charge.[9] Thus

$$I_{ES} = I_{CS} \tag{8}$$

and

$$\theta_N = \theta_I = \frac{q}{kT}. \tag{9}$$

This has been found to be the case experimentally within the accuracy of the measurements, and follows from the one-dimensional model derivation in elementary transistor theory. In the interests of generality, however, four parameters rather than two are retained in the model used in nonlinear analysis[10] to allow for possible deviations[11] in very high-frequency transistors. It is important to note that the redundancy in the injection model is absorbed in the current dependent

parameters $B_N(I_N)$ and $B_I(I_I)$ used in the transport model to define the base current in equation (5).

3.2.2 *Dynamic Behavior*

In a transistor, charge storage can be divided into two types:

(*i*) Fixed charge in the depletion regions (voltage dependent).
(*ii*) Mobile charge in transit (current dependent).

To account for the charging currents which flow under dynamic conditions, two capacitances are included across each junction as shown in Fig. 3. C_{ej} and C_{cj} are the voltage dependent capacitances representing the emitter and collector depletion regions.

Capacitances C_{de} and C_{dc} are current dependent and represent the minority carrier charge stored on account of the current flow.

According to charge control theory[12] the charges are directly proportional to the reference currents such that the capacitances, which are the incremental changes of charge with junction voltage, then become

(a) *Injection Model* (b) *Transport Model*

$$C_{de} = \frac{qT_{EF}}{n_e kT}[I_F + I_{EF}], \qquad C_{de} = \theta_N T_{CN}[I_N + I_{ES}], \tag{10}$$

$$C_{dc} = \frac{qT_{CR}}{n_c kT}[I_R + I_{CR}]. \qquad C_{dc} = \theta_I T_{CI}[I_I + I_{CS}]. \tag{11}$$

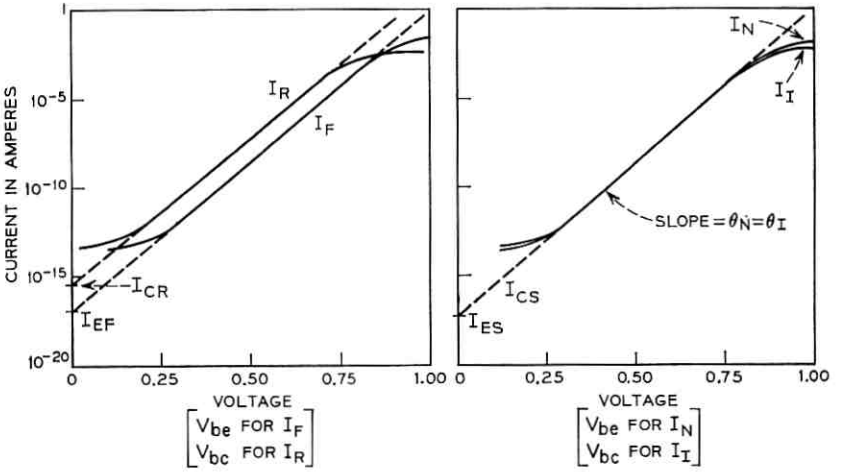

Fig. 2—Transistor nonlinear behavior. (a) Injection model, (b) Transport model.

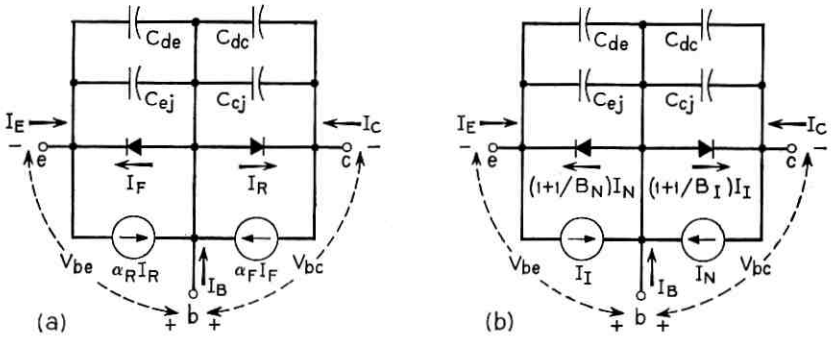

Fig. 3—Dynamic transistor model. (a) Injection model, (b) Transport model.

In practice the parameters* $T_{EF}(I_F)$, $T_{CR}(I_R)$, $T_{CN}(I_N)$, $T_{CI}(I_I)$ have to account for a multitude of effects, for example high-level injection effects, and storage in the collector remote from the base. To represent these effects the parameters are made functions of current as shown.

The parameters $T_{EF}(I_F)$ and $T_{CR}(I_R)$ depend on current terms which consist of ideal and nonideal components. More importantly these characteristic times describe both transit time and recombination time effects. This is both bad and unnecessary.

It is bad since the recombination phenomena are not nearly as well understood (mainly because of surface effects) as transit times; hence, large variations from unit to unit can be expected and in fact are found in practice.

It is unnecessary since the information relating the transit time and recombination time is already contained[13] in the nonlinear current gain terms B_N and B_I (or α_F and α_R). Thus, the effect of basing the characteristic times on the injection currents is to force the introduction of redundant nonidealities in the dynamic parameters. This is much more significant for $T_{CR}(I_R)$ than for $T_{EF}(I_F)$.

3.2.3 *Experimental Evidence*

Indication that the injection model was in trouble came about from actual storage time measurements on high-frequency devices. These showed that $T_{CR}(I_R)$ was a strong function of I_F which could not be

* D. Koehler[2] has defined a consistent set of characteristic time parameters which gave the rationale for the parameter terminology for the injection model. The parameters T_{CN} and T_{CI} for the transport model follow the familiar CIRCUS[7] format, but strictly speaking for consistency[2] these should be T_{CN} and T_{EI}, where C and E refer to collector and emitter, respectively. If T_C signifies "time constant," then perhaps a better unambiguous pair of time parameters would be T_N and T_I.

accounted for in the model and, in fact, it was impossible to assign meaningful values to T_{CR}.

The parameter $T_{CI}(I_I)$, in the transport model on the other hand, was found to be essentially independent of I_N. More importantly, for the devices in question, T_{CI} was constant over a wide range of I_I and in fact showed little variation from device to device. In addition, it was found that devices of the same family which had different gold spiking treatment gave approximately the same value of T_{CI}. Differing amounts of gold doping control the recombination lifetime which is already accounted for by the dc parameter $B_I(I_I)$.

3.2.4 *Important Properties for Tolerance Analysis*

Consistency of T_{CI} for families of device types is vitally important in tolerance analysis work since it requires fewer measurements, and can be given a simple statistical description, yet still yields good answers. The explanation for this superior performance of the transport model parameters is that T_{CN} and T_{CI} are effective transit times which, as mentioned earlier, are much better behaved than recombination times. Thus for the dynamic response as well as the dc situation, the transport model description eliminates the redundancy of the injection model.

3.2.5 *Transistor Model Most Suited to Statistical Design*

The conclusion drawn from these experimental results is that the transport model as outlined above is to be preferred for the following reasons:

(*i*) Nonideal components of current do not occur in the equations relating input voltage and output current.

(*ii*) Intercept currents and slope factors are obtained from one set of measurements instead of two.

(*iii*) Parameters are decoupled in that the dc nonlinearities are contained only in the parameters $B_N(I_N)$ and $B_I(I_I)$.

(*iv*) Characteristic time parameters describing dynamic behavior are constant over a wider range of currents and vary less from device to device, thereby simplifying the measurement procedure.

(*v*) Dynamic behavior is more accurately modeled and the effect of process variation is decoupled from T_{CI} and contained predominantly in $B_I(I_I)$.

Thus from considerations of both accuracy and measurement convenience, the transport model is preferable and has, in fact, been used with considerable success in network analysis programs.[10]

3.3 *Transistor Output Characteristics*

3.3.1 *Defects of the Model*

To account for the effects of bulk material in the base, collector and emitter, resistances R_B , R_C and R_E are added to the intrinsic model of Fig. 3(b) as shown in Fig. 4.

Two effects not accounted for in this model as it stands are:

(*i*) Collector output resistance.
(*ii*) Avalanche multiplication.

Collector avalanche multiplication is usually accounted for by multiplying the parameter I_{CS} by a factor of the form $1/[1 - (V_{cb}/V_B)^n]$ where n and V_B are constants. Since the avalanche mode is not of concern in most circuit analysis encountered in this discussion, it will not be considered further.

Item (*i*) is very significant, particularly for devices in high-resistance circuits, and some simple means had to be found to represent the output resistance. The approach used is described in Section 3.3.2 and the equivalent output resistance is calculated in Appendix C.

3.3.2 *Thermal Considerations*

Measurements of B_N as a function of V_{CB} for constant base current are shown in Fig. 5 where two important effects should be noted.

(*i*) Heating effects due to increased power dissipation greatly increase the change in B_N .

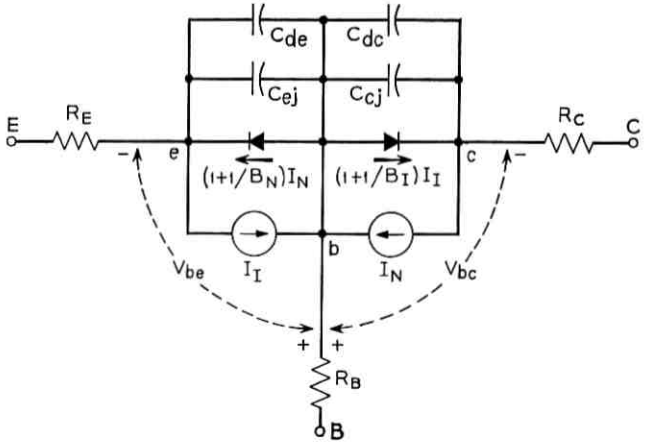

Fig. 4—Nonlinear transistor model.

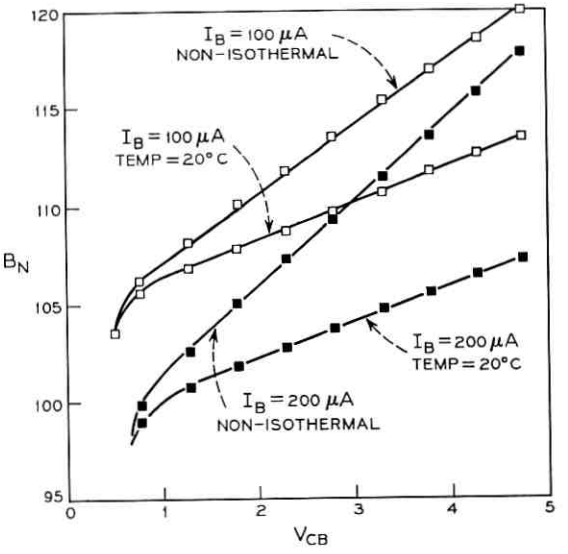

Fig. 5—Variation of B_N with V_{CB}.

(*ii*) When junction temperature is held constant the change in B_N is considerably reduced but more importantly the curves are essentially parallel.

This suggested representing the current gain term in the form

$$B_N = \beta_N(I_N , T) + V_{cb}/V_N \tag{12}$$

where $\beta_N(I_N , T)$ is a function of current and temperature and V_N is a constant.

Further investigation of a range of devices of different structural and manufacturing processes yielded three useful results.

(*i*) At constant junction temperature* the curves for B_N as a function of V_{CB} with I_B as a parameter were parallel [Fig. 6(a)].

(*ii*) At different constant temperatures the curves remained parallel [Fig. 6(b)].

(*iii*) Devices with the same geometry but different gold spiking gave parallel curves (Fig. 7).

* Note that it is not adequate to hold a transistor can or substrate at constant temperature and assume that the junction remains at constant temperature even under pulsed conditions. V_{be} at a low reference current was used as a temperature monitor and a "Themospot" probe (manufactured by EG&G Boston, Mass.) was used to adjust the environment temperature such that V_{be} remained constant.

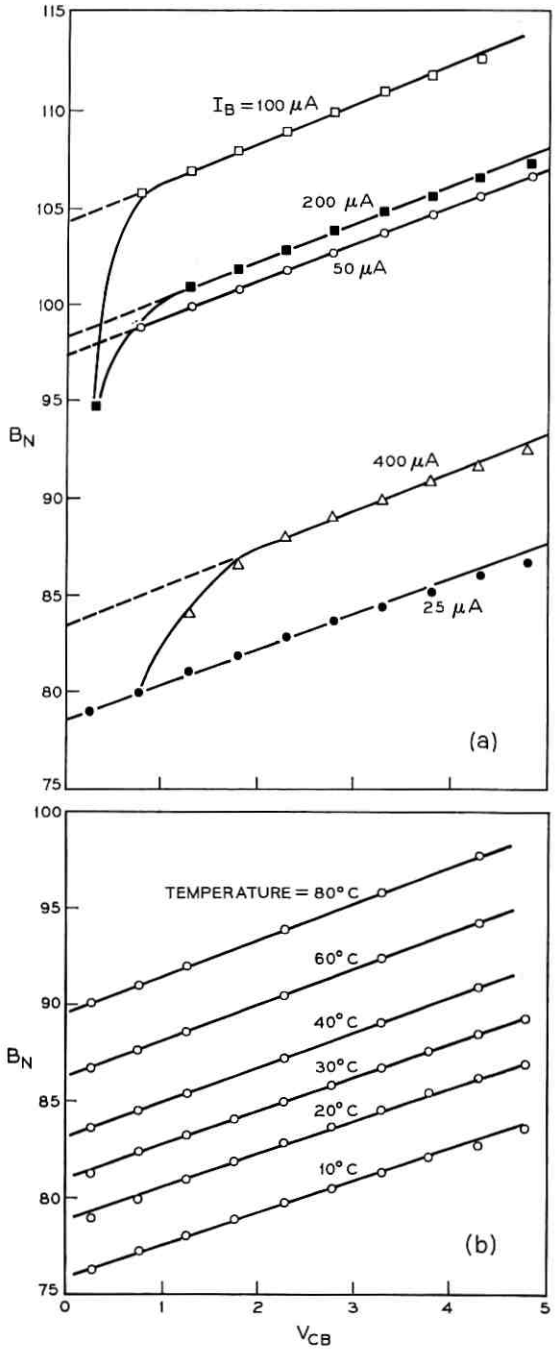

Fig. 6a—B_N as a function of V_{CB} at temperature of 20° C.
Fig. 6b—Variation of B_N with V_{CB} and temperature for base current $I_B = 25\ \mu A$.

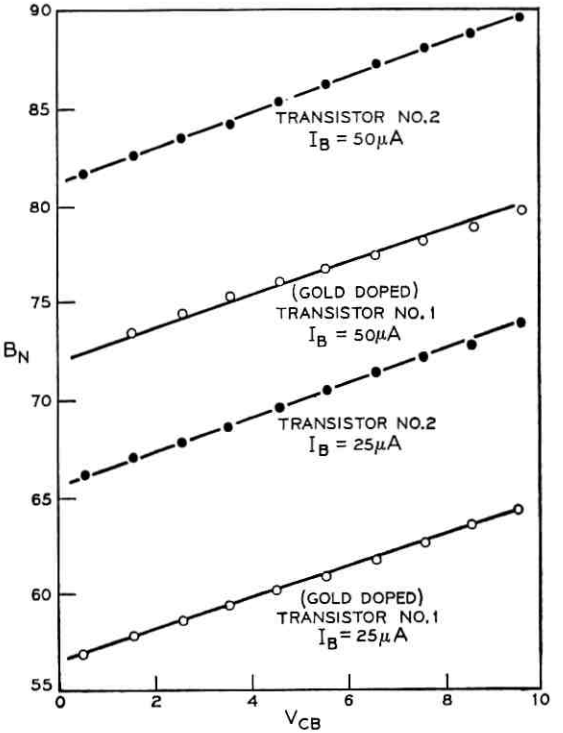

Fig. 7—Variation of B_N with V_{CB} for two devices with the same geometry.

Thus equation (12) has vital properties for statistical design in that the current and temperature dependence is contained in $\beta_N(I_N, T)$ and parameter V_N can be regarded as a constant for a given device geometry. Since the lines in Fig. 6 are all parallel, it is only necessary to take measurements for one value of I_B at room temperature to determine V_N. This value of I_B can be small enough that no significant heating occurs on pulsed measurements obviating the need for a heat sink.

Equation (12) was very easily added to the model in the computer program[10] and Fig. 8 shows a comparison of measured curves and computer predictions.

IV. SMALL SIGNAL TRANSISTOR MODELING

4.1 *Types of Models*

Small signal models used in linear steady-state analysis programs may be divided into two categories:

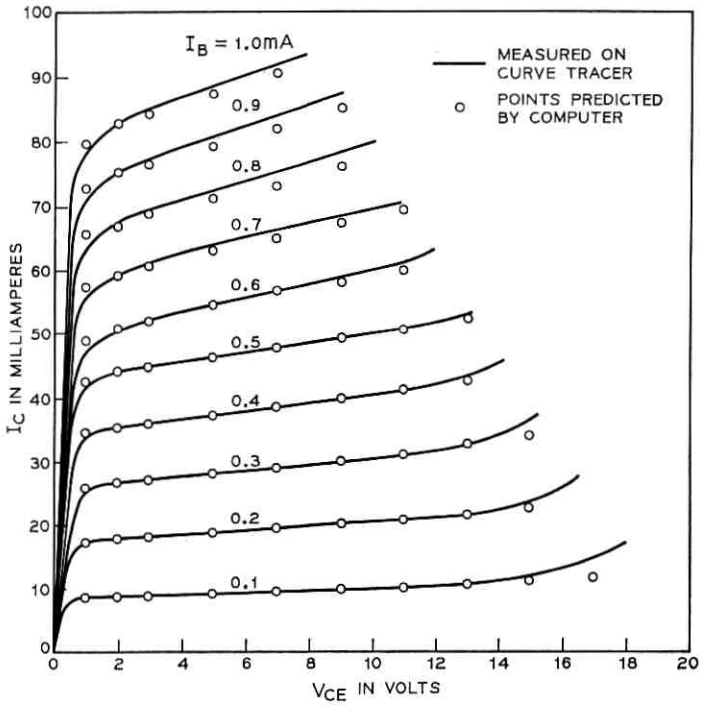

Fig. 8—Transistor output characteristics.

(*i*) Terminal models—measured two-port parameter data at the required operating point over the desired frequency range.
(*ii*) Physical models—equivalent circuit representation of the device at the operating point in question.

Both approaches have advantages and disadvantages for variability analysis.

4.1.1 *Terminal Models*

The measured data can be obtained extremely precisely and used directly in linear analysis programs to investigate circuit performance. This gives no loss of accuracy in the representation of the specific transistors in question.

The main problems with this technique are:

(*i*) Data at different temperatures at several bias points over a range of frequencies imposes a prohibitive storage problem.

(*ii*) Devices have to be available on which measurements can be made and hence new devices cannot be handled this way.

(*iii*) Statistical descriptions of devices cannot be generated, but have to depend on past measured data.

4.1.2 *Equivalent Circuit Model*

The equivalent circuit model eliminates a number of these difficulties and has the following advantages:

(*i*) The number of parameters at a given bias point is dependent only on the complexity of the model for all frequencies in the range of applicability. In addition, the model can easily be made a function of bias, as shown below.

(*ii*) Reasonable first-order estimates for the equivalent circuit model of new devices can be made from a knowledge of similar previously characterized devices.

(*iii*) Variability and interdependence of the equivalent circuit elements of the model can be characterized to give a statistical description for Monte Carlo analysis.

The main problem with the equivalent circuit is its range of applicability, usually requiring more complexity for adequate representation as the frequency is increased.

4.2 *The Hybrid-Pi Model*

Many forms of equivalent circuit representation for the transistor are possible.[14] The hybrid-Pi model is particularly attractive and can be readily derived from the nonlinear model of Fig. 4 showing that the hybrid-Pi model is simply the incremental version of the nonlinear model. Thus, once we have a statistical characterization of the nonlinear model, by appropriate choice of the parameters for the hybrid-Pi model, we have complete statistical information for small signal analysis work.[15]

In the active region of operation, the collector junction is reverse-biased, and from equations (2) and (11)

$$I_I \approx 0,$$

$$C_{dc} \approx 0.$$

Figure 4 can then be simplified and redrawn as Fig. 9. At low frequencies, the currents are:

$$I_E = -(1 + 1/B_N)I_N ,$$
$$I_C = I_N ,$$
$$I_B = I_N/B_N .$$

Thus, the current generators in Fig. 9 can be rearranged to give the configuration of Fig. 10 and satisfy the above equations.

The incremental behavior of the two current sources in Fig. 10 has to be evaluated to give the small signal model. The linear equivalents of the current sources are derived from the following equations:

$$\delta I_B = \delta V_{be} \frac{\partial I_B}{\partial V_{be}} , \qquad (13)$$
$$= \delta V_{be}/R_{be} ,$$

$$\delta I_C = \delta I_B \frac{\partial I_C}{\partial I_B} + \delta V_{ce} \frac{\partial I_C}{\partial V_{ce}} , \qquad (14)$$
$$= i\beta + \delta V_{ce}/R_0 ,$$

where δ signifies an incremental change and i is the incremental change in the low frequency base current I_B.

The hybrid-Pi model incorporating the linear elements defined in equations (13) and (14) is shown in Fig. 11. Also included in the model are capacitances C_1, C_2 and C_3 to account for header capacitances in discrete devices and parasitic capacitances in integrated circuits.

The relationship between the linear elements in Fig. 11 and the parameters previously used for the nonlinear model of Fig. 4 are:

$$C_{be} = C_{ej} + C_{de} , \qquad (15)$$

$$\left.\begin{aligned} \beta &= B_N/[1 - S/B_N] \\ R_{be} &= \beta/[I_N\theta_N] \\ R_0 &= B_N V_N/I_N \end{aligned}\right\} . \qquad (16)$$

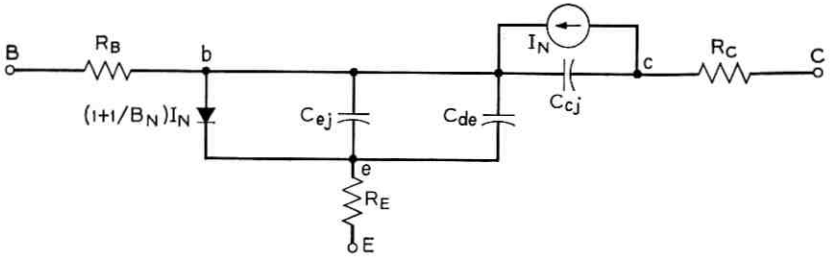

Fig. 9—Simplified model for active region.

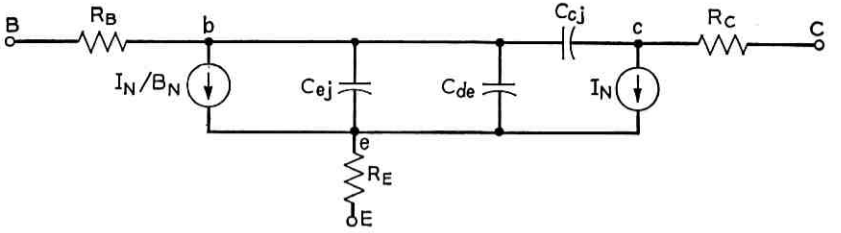

Fig. 10—Equivalent π model.

The derivation of the relationships constituting equation (16) are given in Appendices A, B and C. Thus at any bias condition, the value of C_{cj} is determined by the voltage V_{bc} ; the value of C_{ej} is determined by the voltage V_{be} ; and the collector current I_N determines the values of C_{de} , β, R_{be} and R_0 .

The model in Fig. 11 represents the transistor at any bias condition over the desired frequency range of applicability. No parameters other than those required for the nonlinear model are used in this representation. In consequence, all the relationships for temperature dependence, parameter variation and correlation which are developed in Section 6.3 for the nonlinear model, can be applied directly for small signal tolerance analysis work.

4.2.1 *Excess Phase*

The frequency dependences of the junctions are represented by the single pole type of response in each case. Excess phase resulting from

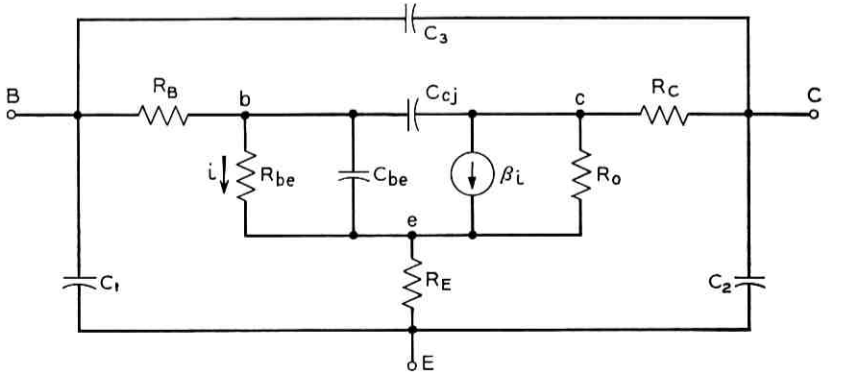

Fig. 11—Hybrid-Pi small signal model.

other nondominant poles is not accounted for explicitly in the model of Fig. 11. However, the additional capacitors C_1, C_2 and C_3 have been found to give the additional degrees of freedom to account not only for the stray capacitances but also to satisfy the excess phase requirement. The model in Fig. 11 has in fact been very accurate up to 1 GHz, the highest frequency at which reliable measurement data is currently available.

V. INTEGRATED CIRCUIT DEVICE MODELING

5.1 *Monolithic Integrated Circuit Environment*

Passive components, such as resistors and capacitors, are used in three forms: discrete, thin-film and planar diffused, along with discrete and planar diffused transistors. Of these, the monolithic integrated circuit situation imposes the greatest requirement on both device modeling[16] and statistical characterization. Modeling problems arise from the junction isolation which result in various parasitic elements in addition to the desired components. Characterization difficulties occur because of the parameter interdependence resulting from the simultaneous fabrication of complete circuits in which the components have a common dependency on the various processing steps. The effect of the integrated circuit environment is considered in the next sections.

5.2 *Resistor Models*

The integrated circuit resistor consisting of a base diffusion, as shown in Fig. 12(a), is really a distributed diode which is reverse-biased. However, the pnp structure also gives rise to a possible parasitic transistor and distributed capacitance as shown in Fig. 12(b). Under normal circumstances, C is taken to the most positive circuit voltage and S to the most negative which effectively eliminates the transistor and leaves only the distributed capacitance. This can be lumped at each

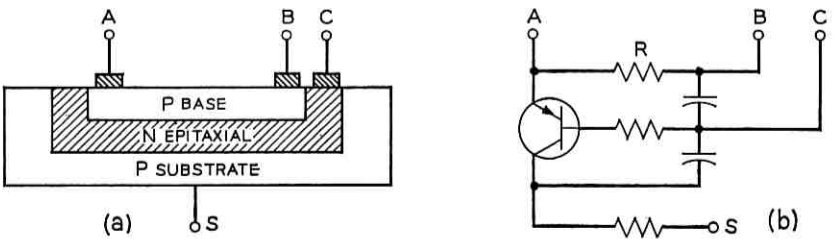

Fig. 12—(a) Diffused resistor, (b) Resistor equivalent circuit.

end of the resistor. Long narrow resistors, however, would be poorly modeled by such an approximation and a distributed representation would be more appropriate.

In manufacture, the variation in resistor values depends on a number of factors, of which the most important are

(*i*) Error in the resistor shape calculation.
(*ii*) Error in the photomask.
(*iii*) Variation in the processing.

Items (*i*) and (*ii*) relate to the resistor geometry and will result in different variations depending on the shape, dictated by the resistor magnitude. Item (*iii*) accounts for the tracking of resistors on an IC chip and is discussed further in Sections 6.3.1 and 6.3.5.

Thin-film resistors can be modeled by ideal resistors except at higher frequencies where stray capacitances become significant. These are obviously layout dependent and have to be estimated in each particular situation. One advantage of the thin-film situation is that resistors can be trimmed to value when required. Such an adjustment has frequently to be performed in simulations[17] and greatly influences the analysis procedure.

An important source of common variation in integrated circuits results from temperature changes on the chip which causes the resistance to change according to the formula

$$R_T = R_{T_0}[1 + \alpha(T - T_0)] \tag{17}$$

where α is the temperature coefficient.

It should be noted in passing that thermal modeling should be performed in integrated circuit structures to account for possible thermal feedback. The electrical parameters of the various devices are temperature dependent and if the devices dissipate significant power, there is coupling between the thermal and electrical behavior of the system. In practice, this can be a prohibitively expensive study and it is either assumed that thermal feedback poses no problem or a very crude static thermal analysis is performed.

6.3 *Capacitor Models*

Two forms of capacitors are in common use in integrated circuit work.

(*i*) Reverse-biased junctions.
(*ii*) Oxide film dielectric.

For item (*i*), any of the three junctions, emitter-base, base-collector or collector-substrate, can be used. The collector-base situation and its equivalent circuit are shown in Fig. 13.

The main problems with the junction capacitance are the variation with voltage, the need to stay reverse-biased and the high series resistance.

The oxide film capacitor overcomes these disadvantages since it is constant and nonpolar. As shown in Fig. 14, it also has a simpler equivalent circuit.

5.4 *Transistors*

As with passive elements, the main difference between the integrated circuit transistor model and its discrete counterpart described in Sections III and IV relates to the parasitic elements encountered in the junction isolation environment. As Fig. 15 shows, the IC transistor should really be considered as a four-layer device to fully account for the device behavior. This is particularly true for transistors which saturate and forward-bias the collector junction such that the substrate behaves like the collector of a poor transistor. Figure 15(b) shows the equivalent circuit for this situation. Steps are usually taken in the processing to minimize the effect of the parasitic pnp transistors. Characterizing this equivalent circuit is difficult since there is no way of identifying the currents in the two transistors to obtain the parameters for each device. Several authors have considered this problem[18] and some computer programs[7] provide four-layer device capability for the IC structure. In many applications, as with the passive elements, only the capacitance effects of the collector-substrate isolation need be taken into consideration in computer analysis. Another characteristic of the integrated circuit environment is the top collector contact which results in parasitic resistance between the collector terminal and

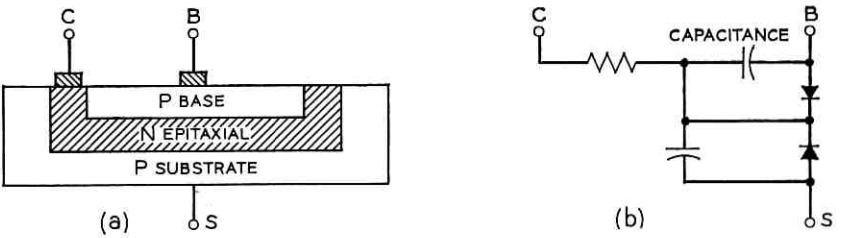

Fig. 13—Diffused junction capacitance. (a) Collector-base capacitor, (b) Equivalent circuit.

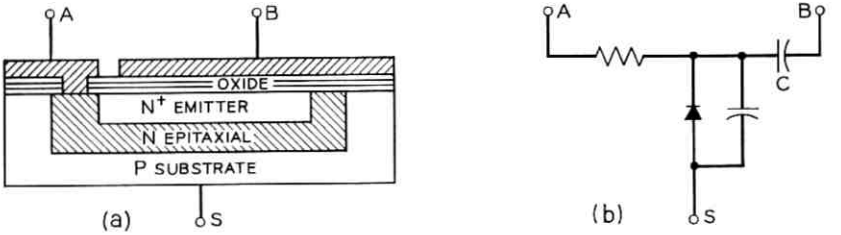

Fig. 14—Oxide capacitor. (a) Oxide film capacitor, (b) Equivalent circuit.

the active region of the collector junction. This can be accounted for by R_c in Fig. 4.

VI. STATISTICAL CHARACTERIZATION

6.1 *Monte Carlo Analysis*

In Monte Carlo analysis, the objective is to predict the electrical behavior of circuits in the light of device variability resulting from a manufacturing process. When the process is well understood, a statistical description of the device behavior in terms of the process variables is desired. Some attempts along these lines have been made[19,20] in semiconductor device work but the transformation from process variables to electrical parameters is complex. The result of these studies has generally been to guide device designers in the optimization of their fabrication process rather than to provide circuit designers with statiscal information on device parameters.

Assuming that the process is under good control, a practical solution to the problem of describing the electrical parameters of the devices in terms of the process variability is to measure the actual electrical parameters of a statistically significant quantity of the product. This

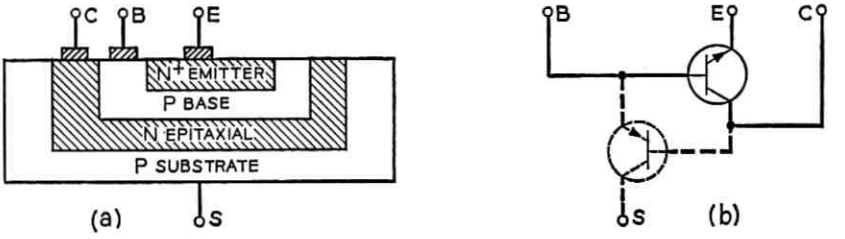

Fig. 15—Integrated circuit transistor. (a) Transistor structure, (b) Equivalent circuit.

eliminates the uncertainty in transformation and, more importantly, puts the statistical description as close as possible to the desired objective. The only requirement of this statistical description is that it must permit the generation of groups of devices with parameters which have the same statistical characteristics as the output from the process.

The problem, then, is divided into two parts:

(*i*) Measurement procedures to estimate the device parameters.

(*ii*) Statistical analysis of the measured parameter values to find their distributions and interrelationships and synthesis procedures for computer generation of parameter values with the same distributions and interrelationships.

Item (*i*) is reasonably well understood and will be described briefly. Item (*ii*) is more of an evolving art with much left to expediency at the present time. It will be described in some detail to show the current state of this art as applied to very significant Bell System Projects.[10,17]

6.2 *Transistor Parameter Measurement*

6.2.1 *Model Parameters*

The most difficult integrated circuit device to characterize is undoubtedly the transistor. Earlier sections have described an adequate model for this device and the modifications required to account for the integrated circuit environment.

For convenience, the essential parameters of the model* of Fig. 4 are listed in Table II along with the measurement techniques used to evaluate the parameters. The model parameters are related as closely as possible to the measurements, both to minimize the amount of data reduction and also to provide parameters, the significance of which is well understood by circuit designers. In addition, the measurements are highly decoupled such that parameters are uniquely defined by each set of measurements. This eliminates the need for optimization to sort out parameters on a best-fit basis which is not practical for a system geared to measuring statistically significant quantities of data.

6.2.2 *DC Measurements*

Figure 4 shows that terminal measurements will always result in at least two of the bulk resistances appearing in series. In principle, by

* Note that the additional capacitance C_{cs} between collector and substrate is included to account for the integrated circuit environment.

TABLE II—PARAMETERS FOR THE NONLINEAR TRANSISTOR MODEL

R_B	Base bulk resistance,	DC Measurements.
R_C	Collector bulk resistance,	
R_E	Emitter bulk resistance,	
I_{ES}	Intercept current,	
θ_N	Slope factor,	
V_N	Gain voltage factor in nominal mode,	
β_N	Current gain factor in normal mode,	
β_I	Current gain factor in inverse mode,	
C_{ej}	Emitter depletion capacitance,	Capacitance Bridge.
C_{cj}	Collector depletion capacitance,	
C_{cs}	Collector-substrate junction capacitance,	
T_{CN}	Characteristic time for normal mode,	frequency domain.
T_{CI}	Characteristic time for inverse mode,	time domain.

making two or more measurements, it should be possible to solve the simultaneous equations for the bulk resistances. In practice, R_E is very much less than R_B or R_C such that conductivity modulation, emitter crowding and other second-order effects cause small changes in R_B and R_C which may exceed R_E. A consistent set of measurements does not exist and severe errors would result from estimating the parameters under such circumstances. For discrete devices, R_E is frequently neglected as a first approximation, but for statistical design involving integrated circuit transistors, the technique described in Section 6.3.4 gives an effective way of estimating R_E.

The equation for the collector-emitter saturation voltage in terms of the variables in Fig. 4 is

$$V_{CE(sat)} = I_C R_C + \frac{1}{\theta_N} \ln \left\{ \frac{1 + 1/B_I + I_C/I_B B_I}{1 + I_C/I_B B_N} \right\}. \tag{18}$$

If B_N and B_I have small variation in the current range of interest, then measurements of $V_{CE(sat)}$ as a function of I_C with constant I_C/I_B will give a straight line with slope R_C. Figure 16 shows typical results.

There are many ways[21] of estimating R_B. For statistical design, it is essential to evaluate this parameter from readily available measured data. R_B is estimated from the plot of log I_C versus V_{BE} similar to Fig. 2(b). The initial deviation from the ideal exponential function at high currents is assumed to result from ohmic voltage drop such that at any current level

$$\Delta V_{BE} = I_B R_B + I_E R_E , \tag{19}$$

$$\approx I_B R_B . \tag{20}$$

Since I_B and ΔV_{BE} are known, R_B can be calculated.

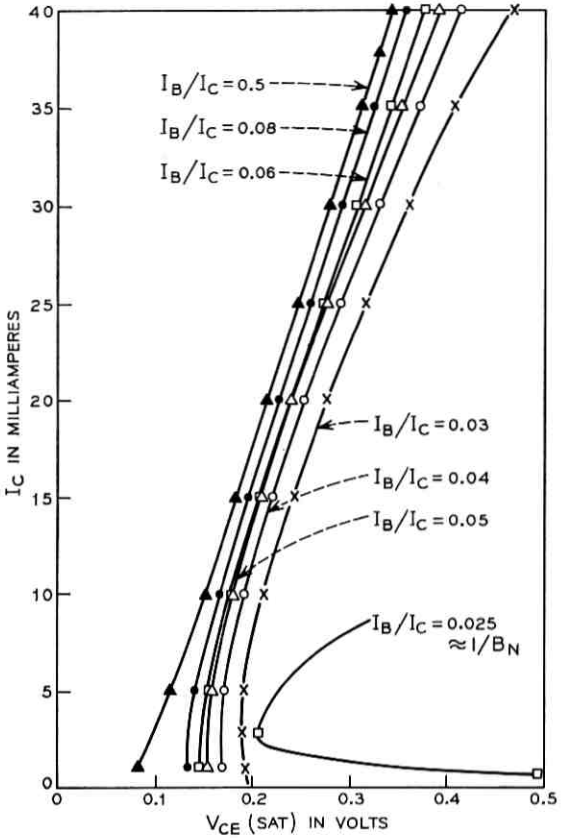

Fig. 16—I_C dependence on V_{CE} (SAT).

The parameters I_{ES} and θ_N are also estimated from Fig. 2(b) for the portion where equation (1) applies. The dc measurements* have to be made over a wide enough range and with sufficient accuracy particularly to resolve equation (20).

The current gain terms B_N and B_I and the voltage factor V_N are determined by dc measurements and evaluated as outlined in Section 3.3.2. To minimize the data reduction, a tabular format is used for the current gain terms in analysis programs[7,10] with interpolation for inter-

* An EAI 680 analog computer has been used to evaluate measurement techniques, since voltage and current sources are very easily programmed on such a machine and its digital voltmeter gives four-digit readout. The logic capability and sample and hold configuration enables pulsed measurements to be made and temperature monitored, where heating effects are significant.

mediate values.[10] As mentioned earlier, interpolation on a logarithmic current scale gives a very good estimation, minimizes the number of data points required and eliminates any curve fitting.

6.2.3 *Capacitance Measurements*

In reverse-bias, the capacitances C_{ej} and C_{cj} dominate and are measured on a capacitance bridge. In forward-bias, the shunt conductance of the junction makes bridge balance difficult and, in addition, the capacitances C_{de} and C_{dc} will become effective. A technique for estimating C_{ej} in forward-bias is given in Section 6.2.4. As with current gain terms, the measured capacitances C_{ej} and C_{cj} as functions of voltage are used in tabular format. With as few as three or four points and log-log interpolation, this gives an adequate representation and eliminates curve fitting difficulties.

6.2.4 *Frequency Domain Measurements*

Frequency domain measurements involve the small signal linearization of device behavior about some bias point. The model of Fig. 11 is then appropriate and it can be shown that the transistor cutoff frequency f_T is related to the collector current I_C in the active region by:

$$\frac{1}{2\pi f_T} = T_{CN} + \frac{1}{\theta_N I_C}(C_{ei} + C_{ci}) + R_C C_{ci} \,. \tag{21}$$

If f_T is measured at several values of I_c, then all the parameters in equation (21) are known except for T_{CN} and C_{ej}. These may be estimated from a plot of $1/2\pi f_T$ against $1/I_C$ as shown in Fig. 17 from which $T_{CN} + R_C C_{cj}$ is obtained as the intercept and C_{ej} in forward-bias can be calculated from the slope.

At high current levels, T_{CN} increases as shown by the curvature in Fig. 17. This is accounted for in the model by the tabulated function $T_{CN}(I_N)$.

Figure 18 shows the behavior of current gain $| h_{fe} |$ with frequency, indicating the cutoff frequency f_T at which the high-frequency asymptote extrapolates to unity. It is generally not possible to measure f_T directly since the actual curve deviates at high frequency as a result of capacitance effects. However, the characteristic of the asymptote is that the gain-frequency product is a constant from which

$$f_T = | h_{fe}(f) | \times [f]. \tag{22}$$

This measurement of $| h_{fe} |$ at a known frequency on the asymptote is sufficient to estimate f_T and such measurement is very quickly and

accurately done on computer-operated transmission measurement sets[22] which allow measurements up to 1 GHz.

6.2.5 *Storage Time Measurements*

If the transistor were symmetrical, T_{CI} could be estimated by the techniques of Section 6.2.4 for the inverted mode of operation. This approach does not work with planar diffused transistors on account of the charge storage mechanism, and a more satisfactory method is based on storage time measurements.

If t_s is the storage time for collector current I_C with base current drive I_{B1} and turn-off base current I_{B2}, then the storage time[23] in terms of the parameters of Fig. 4 is

$$t_s = \frac{B_N(B_I + 1)}{B_N + B_I + 1}\left[T_{CN} + \frac{B_I T_{CI}}{B_I + 1}\right] \ln\left\{\frac{|I_{B1}| + |I_{B2}|}{|I_C/B_N| + |I_{B2}|}\right\}. \quad (23)$$

Thus by measuring[13] storage time for a range of values of I_C and I_{B1} and knowing the other parameters in equation (23), the value of T_{CI} can be calculated.

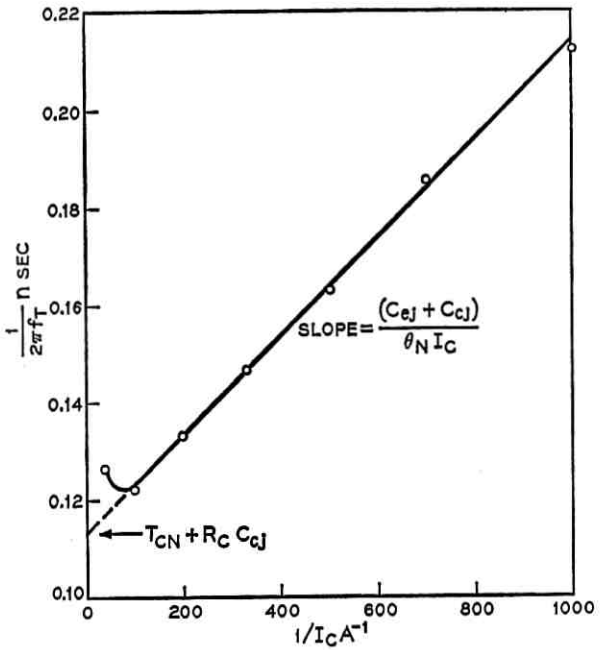

Fig. 17—Graphical solution for T_{CN}.

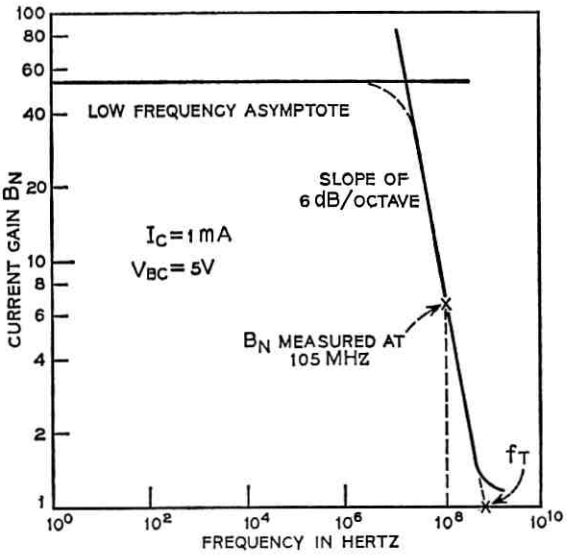

Fig. 18—Common emitter current gain B_N as a function of frequency.

6.2.6 *Parameter Verification*

The model of Fig. 4 is a simple model in which the parameters have to account for many second-order effects which were not considered in the simple one-dimensional analysis of transistor physics used to derive the model. Functional dependencies of the parameters on bias current or voltage provide the necessary degrees of freedom to match actual device performance. The continuing success of the model also depends on the measurement procedures used to estimate the parameters. These take account of the way the model behaves—which may not be the precise way microscopic effects in the physical device occur. The model, however, gives the same terminal performance, which is the most important consideration in circuit design.

For any specific device, it is essential to verify the adequacy of the measured parameter set and the most satisfactory approach is to simulate the test procedures. Just as these test procedures decoupled the parameters for measurement, so they give the maximum sensitivity to these same parameters in simulation.

6.3 *Statistical Analysis*

In this section, the problems encountered in "Monte Carlo" analysis of integrated circuits are considered. Nominal values, distribution

spreads and parameter interdependence have to be accounted for. The approach used to represent the production variability of parameters for transistor nonlinearities and resistor values is described and additional work to account for the statistical behavior of the dynamic parameters is outlined.

6.3.1 *Parameter Variation*

When many transistors of a given type are measured, one is usually asked for the parameters of a typical device. There is no simple answer to this request on account of possible interaction between parameters. For example, it would be meaningless to use some form of average for each of the transistor parameters as this could well result in a physically impossible combination of parameters.

With discrete passive elements, such as resistors described by a single parameter, the problem is much simpler, as the median of the distribution would probably be a good value to use. In integrated circuit work, resistor ratios are held within closer limits than nominal values on account of the common fabrication steps so that there are two variations to consider.

(*i*) Total variation in a component value for all the product, known as *global variation.*
(*ii*) Variation of the value of a component on an integrated circuit, given the value of another component, known as *local variation.*

Local variation results from the common dependence on processing steps and is the harder variation to characterize. In theory, parameter data for all components on many integrated circuit chips from a given process facility is desired. In practice, the statistical analysis required to pin down the exact form of interdependence would be prohibitive. Instead, the practical approach adopted was to develop a mathematical expression or statistical model for which the coefficients could be easily estimated. It will be shown that this expression yielded groups of parameters having the spreads and interdependence matching the little measurement data readily available.

The mathematical expression is:

$$P_{mn} = P_{on}(Y)\{1 + \lambda X_m + (1 - \lambda)X_n\}, \tag{24}$$

where

P_{mn} is a parameter of the nth device on the mth integrated circuit chip.

$P_{on}(Y)$ is the nominal parameter (having functional dependence on variables Y) for the nth device.

X_m is an independent random number whose selection amounts to picking a specific chip.

X_n is an independent random number whose selection accounts for picking a specific device on that chip.

λ is a tracking coefficient ($0 \leqq \lambda \leqq 1$) to account for the division between the free and dependent part of the permissible variation.

Two comments about equation (24) are in order. First, in the absence of better information, the numbers X_m and X_n are selected from the global distribution, normalized so that the median is zero. The effect, then, is for the selection of X_m to move the median value of parameter P away from nominal for the mth chip and narrow the range by the factor λ. The global distribution of P, normalized and narrowed by the factor $(1 - \lambda)$, is then placed about this new median and the selection of X_n determines the actual parameter value P_{mn}. It should be noted that the resultant distribution of P may differ from the global distribution since the distribution of the sum of two random variables is not necessarily of the same form as the distribution from which these random variables were selected. However, the mean and the variance of the resulting distribution are easily controlled.[10]

The second comment relates to the form of the expression. To obtain the relationship between two parameters, a visual technique was used in that a two-dimensional scatter plot of the measured values was compared with the scatter plot indicated by equation (24). Typical results are shown in Fig. 19. The coefficient λ was adjusted to get a good match and the summation form of equation (24) maintained the median value and range of the total distribution independent of λ.

An alternate method of estimating λ is to evaluate the correlation coefficient[10] for the parameter set $[P_{m_1n}, P_{m_2n}]$ in terms of λ and equate this to the measured correlation coefficient, solving for λ.

6.3.2 *The Nominal Device Parameters*

Returning to the question of the typical transistor, one approach has been to measure the dc properties of a number of devices and take the transistor having median current gain B_N. This device is then completely characterized and its parameter set used as nominal values for the transistor type. This is more meaningful than averaging and goes part way to solving the interdependence problem in that the parameter set is consistent. What it does not do is give any indication

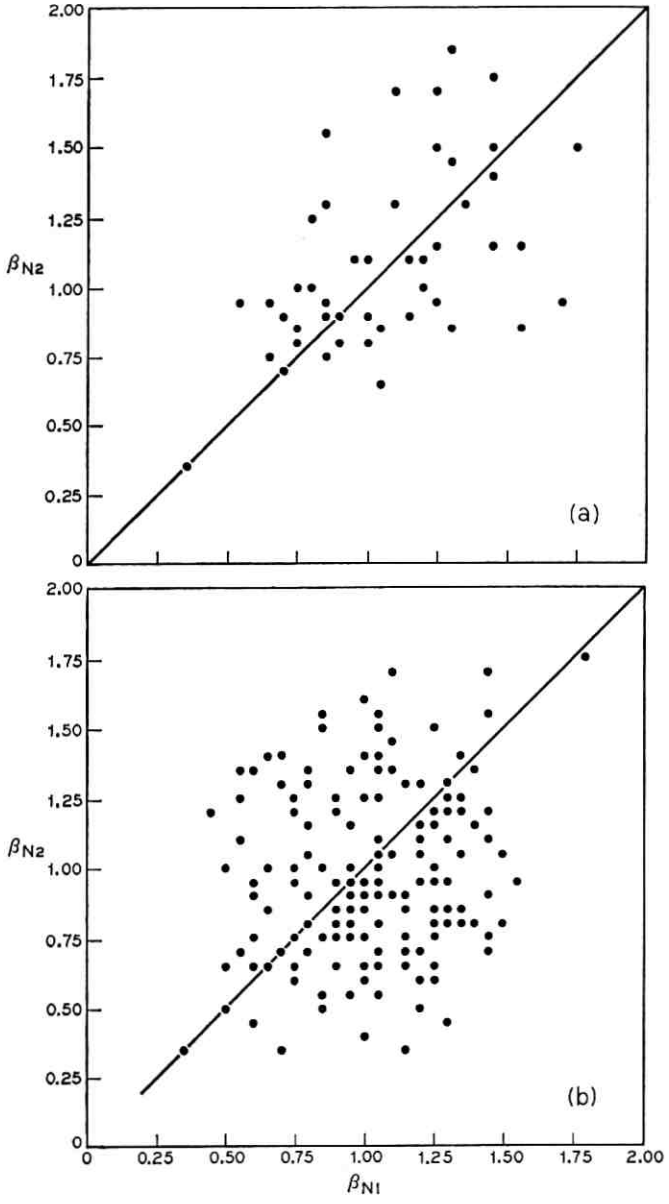

Fig. 19a—Normalized Beta scatter plot measured data.
Fig. 19b—Normalized Beta scatter plot computed data.

of the range of parameter sets to be expected. The technique could be expanded by characterizing the devices having maximum and minimum B_N values, but this would only give an indication of the range for situations where current gain is the controlling parameter. In addition, nonlinear combinations of device parameters may result in a "worst-case" circuit design for other than these types of limit values.

The only realistic solution is to gain some understanding of the transistor parameter combinations and interdependencies and characterize these in the format of equation (24). For a first attempt, it seemed reasonable to assume that the sheet resistance of the active base region would be a fairly basic entity affecting a number of the model parameters. It would certainly affect the current gain B_N and since this is a measurable parameter and one that is very significant in circuit design, B_N was chosen as the base parameter upon which to look for correlation.

6.3.3 *The Behavior of Current Gain* β_N

By equation (12), B_N depends on two coefficients, $\beta_N(I_N, T)$ and V_N. It was shown in Section 3.3.2 that V_N can be regarded as a constant and that variability is attributable to $\beta_N(I_N, T)$.

Figure 20 shows the measured dependence of β_N on current and temperature for the IC transistors used in the *Touch-Tone*® oscillator[17] which suggests a linear dependence on temperature. A good

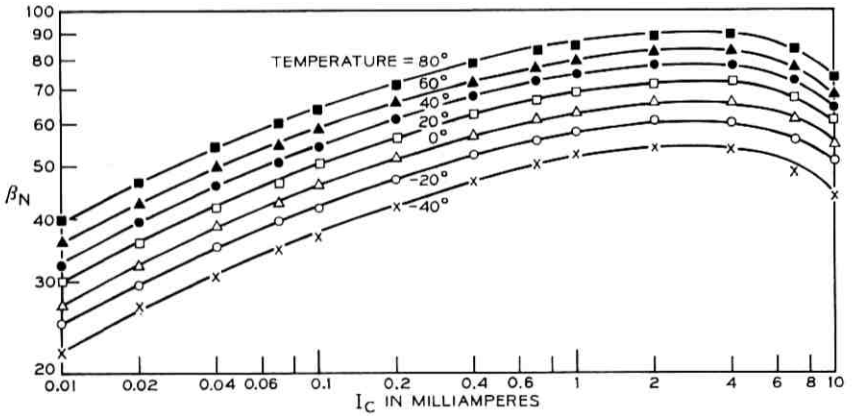

Fig. 20—β_N as a function of I_C and temperature for *Touch-Tone* transistor.

fit for this particular device is shown in Fig. 21 to result from the expression

$$\beta_N(I_N , T) = \beta_{N20}(I_N)[1 + 0.0039(T - 20)] \quad (25)$$

where β_{N20} is the value at 20°C and T is in °C.

The coefficient 0.0039 may well differ for different transistor structures depending on the dominant physical mechanism controlling β_N.

The distribution of values of $\beta_{N20}(I_N)$ to be expected in production results in percentiles shown in Fig. 22. Since the curves are essentially parallel, the same distribution function can be assumed for all current levels. The distribution function is obviously skewed toward the lower values and an important decision relates to the cutoff points for the tails. The lower tail is particularly significant since it is here that most marginal circuits may intuitively be expected to fail. Figure 22 shows that the 10th percentile and 90th percentile occur at 0.667 and 1.667 times the 50th percentile or median value. It seemed reasonable to use a lower limit of 0.2 times the median value and an upper limit of 2 times the median value. The form of the cumulative distribution is then as shown in Fig. 23. This completes the information necessary for the current gain form of equation (24) which is

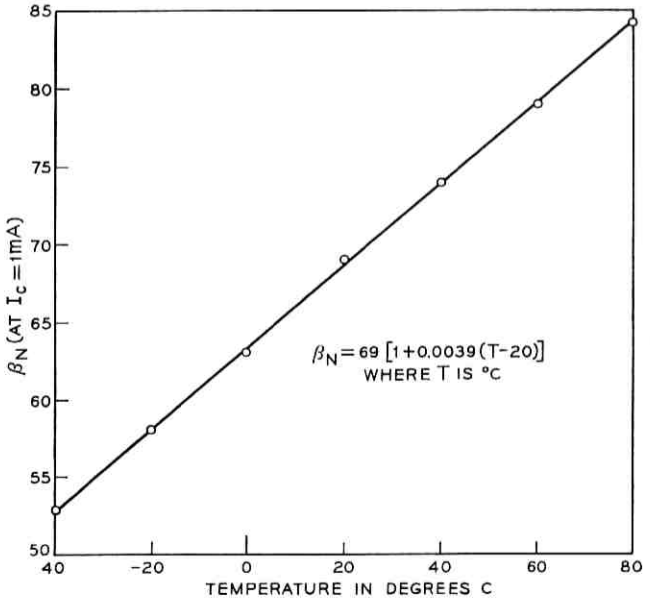

Fig. 21—Temperature variation of β_N for *Touch-Tone* transistor.

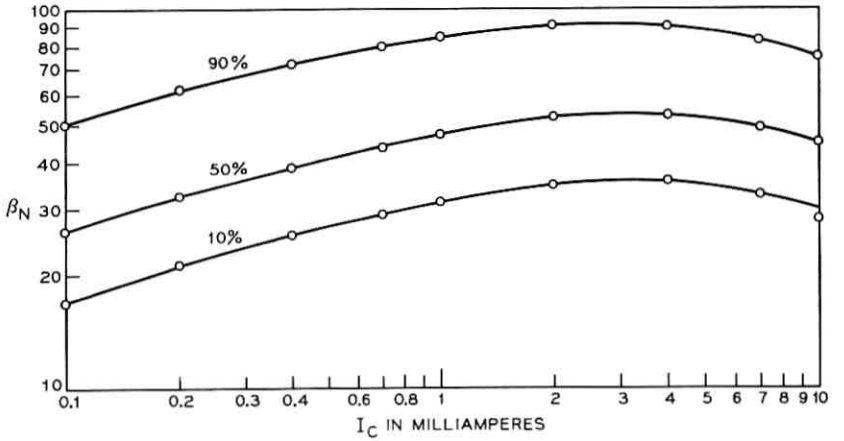

Fig. 22—Percentiles for distribution of β_N.

$$\beta_{Nmn} = \beta_{Non}(I_N, T)[1 + \lambda X_m + (1 - \lambda)X_n] \tag{26}$$

where the terms are as defined for equation (24) and X_m and X_n are selected from the distribution corresponding to Fig. 23, normalized such that the median is zero.

To determine the tracking coefficient λ, the β_N values for pairs of transistors on integrated circuit chips were plotted as shown in Fig. 19a from which $\lambda = 0.3$ was found to give a reasonable "match" as shown in Fig. 19b. This low value of λ means that the current gains for near neighbor transistors have fairly weak interdependence.

The current gain β_I for the inverted mode of operation is handled in the same way as β_N pending further measurements to evaluate the actual behavior of a statistically significant sample.

6.3.4 *The Behavior of Bulk Resistances*

Scatter plots were used to look for dependence of R_B on B_N and Fig. 24 shows an example for the *Touch-Tone* oscillator output transistor.[17] There is obviously, a strong relationship between the two parameters: In fact it almost appears to be a functional dependence. The resistance was measured by the technique outlined in Section 6.2.2 according to equation (19) which gives the clue to one possible interpretation. Equation (19) can be expanded to

$$\begin{aligned} \Delta V_{BE} &= I_B R_B + (B_N + 1) I_B R_E , \\ &= I_B[R_B + (B_N + 1)R_E]. \end{aligned} \tag{27}$$

So

$$R = R_B + (B_N + 1)R_E \,. \tag{28}$$

A technique to separate R_B and R_E can be developed from equation (28). Assume that integrated circuit transistors fabricated on a given slice may be expected to have values of R_B which are quite tightly distributed about some nominal value. Then on a scatter plot of R against B_N ; the "best" straight line drawn through points for devices from one slice will have an intercept which estimates the nominal value of R_B and a slope equal to the value of R_E. The plots in Fig. 24 are for three devices from a "low B_N slice" and two devices from a "high B_N slice." The parallel straight lines indicate a value for R_E of 0.45 ohm in both cases. It is reasonable to regard R_E as a constant since it is primarily a contact resistance and the value is consistent with the small emitter contact area in these devices.

The intercepts indicating the values for the nominal R_B for the two slices show a tracking between R_B and B_N in that devices with high B_N have high R_B . This might be expected from the common dependence on base impurity concentration. Unfortunately, data of the type shown in Fig. 24 on several devices from a number of different slices are not readily available and at this time it is not possible to estimate the

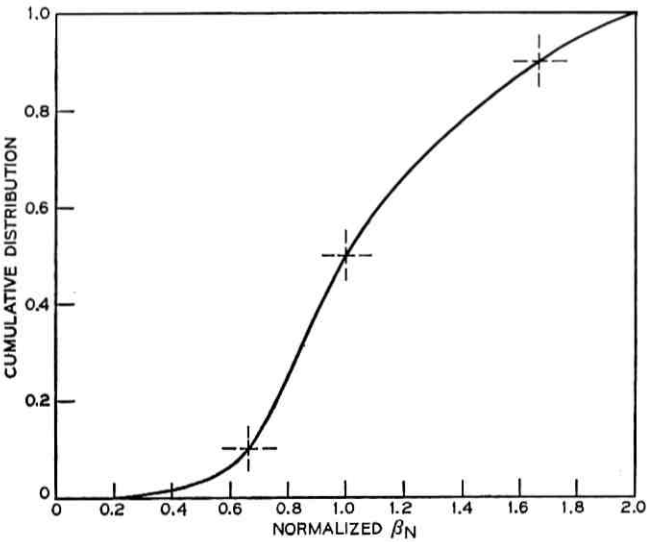

Fig. 23—Distribution for β_N.

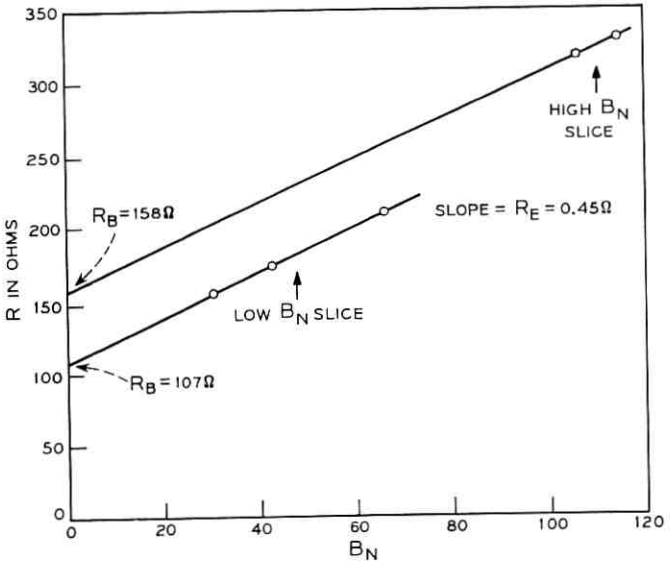

Fig. 24—Scatter plot for R and B_N.

value for the tracking coefficient. Until such information becomes available, it has been customary to treat R_B in exactly the same way as the silicon resistors described in Section 6.3.5.

This technique of resolving R_B and R_E from a scatter plot of R versus B_N requires further comment. First, the interpretation is well suited to statistical work since, as far as R_E is concerned, the regression lines in Fig. 24 perform the averaging required to specify the value to be used for R_E in simulations. Secondly, the loose interdependence of B_N for devices from one slice has been used to advantage since the spread in B_N at a given current level for different devices spreads the points out widely in Fig. 24. As the measurements are made at the same injection level on these devices, conductivity modulation and other second-order effects should not influence R_B, resulting in a realistic estimate for the nominal value of this parameter.

The collector resistance R_C is treated in the manner described in Section 6.3.5 with the appropriate temperature coefficient.

6.3.5 *Silicon Diffused Resistors*

It was expected that diffused resistors on the same chip as transistors would exhibit some correlation with B_N of the transistors because of

the common dependence on the base resistivity under the emitter. It was thought that chips with high B_N would have high resistance values, but in the limited measurement data available it was impossible to determine the nature of any such relationship and, pending further measurements, it was decided to assume independence.

The silicon resistors (base diffusion) are given a gaussian distribution truncated at $\pm 3\sigma$. The maximum total deviation of the resistors is $3\sigma = 15$ percent. The maximum deviation of resistors on one chip is only $3\sigma = \pm 5$ percent. The formula used for computation of resistors is

$$R_{mn} = R_{on}[1 + \alpha(T - T_0)][1 + \lambda X_m + (1 - \lambda)X_n] \tag{29}$$

where X_m and X_n are selected from a gaussian distribution with $3\sigma = \pm 0.15$, $\lambda = 0.667$, and $\alpha = 0.002/°C$ for nominal $200\Omega/\square$ base sheet resistance.

6.3.6 *The Intercept Current I_{ES} and Slope Factor θ_N*

Equation (1) and Fig. 2b give the basis for estimating the parameters I_{ES} and θ_N. Experience with integrated circuit devices has shown that if the junction temperature is known and controlled, then θ_N comes out very close to the theoretical value shown in equation (9). It has therefore been decided to use the theoretical values for θ_N (and θ_I) in simulations and attribute all the variability to I_{ES} (and I_{CS}).

From Fig. 4 and equation (27)

$$V_{BE} = V_{be} + I_B[R_B + (1 + B_N)R_E].$$

At low currents, as shown in Fig. 2b, the measured V_{BE} may be taken as V_{be}. Measurements of this V_{BE} on many devices shows a global distribution which is gaussian with $4\sigma = 36$ mV at 20°C. From equation (1), since $\exp(\theta_N V_{be}) \gg 1$, for transistors at the same current I it follows that

$$I = I_{ESO} \exp(\theta_N V_{beo}) = I_{ES} \exp(\theta_N V_{be})$$

where I_{ESO} is the reference intercept current (nominal value).

If $V_{beo} = V_{be} + \Delta V$, then

$$I_{ES} = I_{ESO} \exp(\theta_N \Delta V) \tag{30}$$

where ΔV is normally distributed with 4σ of 36 mV.

If N has a gaussian distribution with 4σ limits of ± 1, then equation (30) can be transformed to

$$I_{ES} = I_{ESO} K^N \tag{31}$$

where $K = e^{40 \times 0.036} = 4.2$.

The intercept currents are found to be highly correlated for transistors on an integrated circuit and the form of equation (24) for this situation is

$$I_{ESmn} = I_{ESon}(T)K^{[\lambda X_m + [1-\lambda] X_N]}, \tag{32}$$

where

$\lambda = 0.85$,
$K = 4.2$,
X_i = random number with a gaussian distribution truncated at $\pm 4\sigma$ normalized to $4\sigma = 1$.

Equation (32) results in transistors on a chip with V_{BE} match normally distributed with $4\sigma = 5.4$ mV at 20°C.

The temperature dependence of $I_{ES}(T)$ is evaluated from R. J. Widlar's[24] expression for V_{be}

$$V_{be} = \left(1 - \frac{T}{T_0}\right)V_{go} + \frac{T}{T_0} V_{BEO} + \frac{kT}{q} \ln \frac{T_0}{T} + (n - 1) \frac{kT}{q} \left(1 - \frac{T}{T_0}\right), \tag{33}$$

where

V_{go} is the extrapolated energy gap (1.205 for silicon),
n is a constant ($\approx$1.5 for double diffused silicon transistors).

$$V_{BEO} = \frac{kT_0}{q} \ln \frac{I_N}{I_{ES}(T_0)} \tag{34}$$

and $I_{ES}(T_0)$ is the intercept current at reference temperature T_0. When $V_{be} = 0$, $I_N = I_{ES}(T)$, the intercept current at temperature T. Substituting equation (34) in equation (33) for the above condition gives:

$$I_{ES}(T) = I_{ES}(T_0) \frac{T}{T_0} \exp \left[\left(\frac{T}{T_0} - 1\right)\left(\frac{qV_{go}}{kT} + n - 1\right)\right]. \tag{35}$$

This has been found to be in excellent agreement with experimental results. Equations (32) and (35) then give the statistical description for the intercept current including temperature effects.

6.3.7 *The Dynamic Parameters*

The preceding sections have described the techniques used to generate integrated circuit device parameters consistent with available measured data. These results can only be regarded as temporary. Not

only will processing techniques change but it is hoped that, as appropriate measured data become available, interdependencies will be observed which were expected but could not be detected with existing data.

Similar comments apply to the capacitance and characteristic time parameters which are also expected to show some correlation with each other and with other device parameters.

Referring to base resistivity as the controlling variable, it might be expected that base width variations would affect the current gains, the intercept current, the base resistance, and the transit times. Changes in base width arising from variations in emitter diffusion depths affect the profile slopes and hence the junction capacitances. It is not unreasonable, then, to expect some interrelationship at least between B_N, I_{ES}, R_B, T_{CN}, T_{CI} and C_{ej}. The nature of this can only be determined from measurements. C_{cj} on the other hand is determined by the base diffusion rather than the emitter diffusion and may be expected to show no dependence on the base width. Thus C_{cj} may be assumed to be independent of the above six interrelated parameters.

Although the interdependence is not known, the variability of the capacitance parameters is reasonably well documented. The space charge capacitances C_{ej} and C_{cj} are found to have global distributions which are gaussian with 3σ points of ± 20 percent. This figure presumably applies also to the substrate capacitance.

The temperature dependence of the junction capacitance results predominantly from the reduction in contact potential, which implies that temperature changes in capacitance are significant only in forward bias and for low reverse bias voltages. Even at zero applied voltage, the junction capacitance typically changes by ten percent or less over the temperature range—40°C to 80°C. To a first order, such a change can be ignored in comparison with the production variability.

The characteristic time parameters T_{CN} and T_{CI} have not been determined for a large enough sample of any one device type to be able to quote variational bounds at the present time. Likewise, the specific details of the temperature dependence have not been characterized. It is known,[23] however, that both parameters increase with temperature.

VII. CONCLUSIONS

The results of any Monte Carlo study are only as accurate as the characterization of the manufacturing and temperature variations of device model parameters. Thus, the objective in modeling for sta-

tistical design is to give an adequate description of the electrical behavior of devices, consistent with the accuracy of the available parameter data. In general, the availability of parameter data is directly proportional to the ease of measurements and the device model to be favored is one with parameters obtained directly from routine production measurements. The model must be sufficiently simple that parameters can be determined uniquely, since the alternative of optimization to find a "best fit" is impractical for large quantities of data from a production environment.

It was shown for transistors that one of the two forms of model in common use is to be preferred for both measurement simplicity and model accuracy. This model was expanded to account for output resistance by a simple yet efficient technique within the framework of existing computer analysis programs. At that point the important device effects were considered to have been taken into account.

The method of representing the variability of the "dc" model parameters for use in Monte Carlo analysis was outlined, with no pretense to mathematical rigor. Rather, forms were assumed and coefficients estimated such that the calculated parameters, spreads, and correlations "matched" existing measurement data and were consistent with the expectations of device designers. The same approach is being extended to the "dynamic" device parameters such that Monte Carlo techniques can be applied in a meaningful way to computer simulation at higher frequencies.

To determine statistical correlation, it is obviously essential to group measurement data for all parameters related to one device. This is not always possible in production where tests are performed on a go/no-go basis, or statistics on each individual test are recorded rather than data logging the information relating to identifiable devices. In planning for future statistical analysis support, every effort should be made to measure this type of consistent data.

The usual question in sensitivity analysis is to determine those items on which a given design may be particularly dependent. The studies for which the characterization of this article is intended, are sufficiently complicated that the question has to be turned around; given certain parameter spreads and correlations in production, what will be the yield of a circuit design in terms of some performance criteria? This is a very real problem faced in practice and simulation should be able to predict the performance. At the same time, analysis of the results should indicate paths to take to improve any given situation.

It should be noted that all the comments made in this article regarding modeling and characterization for statistical design apply to devices made by the Bell System standard process. Behavior of other devices is expected to be qualitatively the same but obviously the specifics will have to be verified before the techniques are widely applied.

VIII. ACKNOWLEDGMENTS

Acknowledgment is due to J. Chernak who, through his insight into the problems faced by circuit designers, directed the author to the study of practical characterization for simulation. The author is also grateful to L. A. Walter for providing information on certain semiconductor devices and to R. J. Bernard and M. M. Markus for transistor measurements.

APPENDIX A

A.1 *Estimation of Incremental Current Gain β from Tabular Data of B_N vs I_N*

For transistors, linear interpolation of B_N as a function of $\ln I_N$ generally gives reasonable estimates of B_N at intermediate values of I_N.

If B_{Ni} and $B_{N(i+1)}$ are the values of current gain at I_{Ni} and $I_{N(i+1)}$ where $I_{Ni} < I_N < I_{N(i+1)}$, then

$$B_N = R + S \ln I_N$$

where R is a constant, and

$$S = [B_{N(i+1)} - B_{Ni}]/\ln (I_{N(i+1)}/I_{Ni}). \tag{36}$$

The incremental current gain is

$$\beta = \frac{dI_N}{dI_B} = \frac{d}{dI_B}(B_N I_B) = B_N + I_B \frac{dB_N}{dI_B},$$

$$= B_N + I_B \frac{d}{dI_N}(R + S \ln I_N) \frac{dI_N}{dI_B}.$$

So

$$\beta = \frac{B_N}{1 - \dfrac{SI_B}{I_N}},$$

$$= \frac{B_N}{1 - \dfrac{S}{B_N}}.$$

APPENDIX B

B.1 *Estimation of* R_{be}

From Section 4.2,

$$\frac{1}{R_{be}} = \frac{dI_B}{dV_{be}} = \frac{d}{dV_{be}}(I_N/B_N),$$

$$= \frac{1}{B_N}\frac{dI_N}{dV_{be}} - \frac{I_N}{(B_N)^2}\frac{dB_N}{dV_{be}},$$

$$\frac{dI_N}{dV_{be}} = \theta_N I_{ES} \exp(\theta_N V_{be}),$$

$$\approx \theta_N I_N .$$

(dB_N/dV_{be}) may be estimated from $(\Delta B_N/\Delta V_{be})$ where,

$$\frac{\Delta B_N}{\Delta V_{be}} = [B_{N(i+1)} - B_{Ni}]/[V_{be(i+1)} - V_{bei}],$$

$$= \theta_N[B_{N(i+1)} - B_{Ni}]/\ln(I_{(i+1)}/I_i),$$

$$= \theta_N S, \qquad \text{where } S \text{ is defined in equation (36).}$$

So

$$\frac{1}{R_{be}} = \frac{\theta_N I_N}{B_N} - \frac{I_N}{(B_N)^2}\theta_N S,$$

$$= \frac{\theta_N I_N}{B_N}\left(1 - \frac{S}{B_N}\right) = \frac{\theta_N I_N}{\beta}.$$

Thus

$$R_{be} = \frac{\beta}{\theta_N I_N}.$$

APPENDIX C

C.1 *Derivation of Output Resistance* R_o

At low frequencies

$$R_0 = \left.\frac{dV_{ce}}{dI_N}\right|_{I_N/B_N = I_B,\ a\ \text{constant}}$$

So

$$I_N = B_N I_B = [\beta_N + V_{cb}/V_N]I_B$$

and

$$\frac{dI_N}{dV_{ce}} = \frac{d}{dV_{ce}}\{[\beta_N + (V_{ce} - V_{be})/V_N]I_B\},$$

$$= \frac{I_B}{V_N}, \quad \text{neglecting any small changes in } V_{be} \text{ which may result from changes in } V_{ce}.$$

So

$$R_0 = \frac{V_N}{I_B},$$

$$= \frac{B_N V_N}{I_N}.$$

REFERENCES

1. Hamilton, D. J., Lindholm, F. A., and Narud, J. A., "Comparison of Large Signal Models for Junction Transistors," Proc. IEEE, *52,* No. 3 (March 1964), pp. 239–248.
2. Koehler, D., "The Charge Control Concept in the Form of Equivalent Circuits Representing a Link Between the Classic Large Signal Diode and Transistor Models," B.S.T.J., *46,* No. 3 (March 1967), pp. 523–576.
3. Macnee, A. B., "Computational Utility of Nonlinear Transistor Models," Cooley Electronics Laboratory, Ann Arbor, Michigan, November 1967. AD824308. Contract No. DA 28-043-AMC-01870(E).
4. Calahan, D. A., *Computer Aided Network Design,* Chapter 5, New York: McGraw-Hill, 1968.
5. Gummel, H. K., and Poon, H. C., "An Integral Charge Control Model of Bipolar Transistors," B.S.T.J., *49,* No. 5 (May–June 1970), pp. 827–850.
6. Malmberg, A. F., and Cornwell, F. L., "NET 1 Network Analysis Program," Los Alamos Scientific Laboratory of the University of California, T1D-4500 (19th Ed.), April 30, 1963.
7. Milliman, L. D., Massena, W. A., and Dickhaut, R. H., "CIRCUS, A Digital Computer Program for Transient Analysis of Electronic Circuits," Harry Diamond Laboratory User's Guide, HDL 346-1, Program Manual HDL 346-2, January 1967.
8. Iwersen, J. E., Bray, A. R., and Kleimack, J. J., "Low Current Alpha in Silicon Transistors," IRE Trans. E.D., *9,* No. 6 (November 1962), pp. 474–478.
9. Gummel, H. K., "Measurement of the Number of Impurities in the Base Layer of a Transistor," Proc. IRE, *49,* No. 4 (April 1961), p. 834.
10. Cermak, I. A., and Kirby, Mrs. D. B., "Nonlinear Circuits and Statistical Design," B.S.T.J., this issue, pp. 1173–1195.
11. Buckingham, M. J., and Faulkner, E. A., "Saturation in Bipolar Transistors," Electronics Letters, *6,* No. 6 (March 1970), pp. 167–169.
12. Beaufoy, R., and Sparkes, J. J., "The Junction Transistor as a Charge-Controlled Device," ATEJ (London), *13,* No. 4 (October 1957), pp. 310–324.
13. Gray, P. E., DeWitt, D., Boothroyd, A. R., and Gibbons, J. F., "Physical Electronics and Circuit Models of Transistors," S.E.E.C., *2,* John Wiley & Sons, 1964, Chapter 10.
14. Pritchard, R. L., "Electric-Network Representation of Transistors—A Survey," IRE Trans. Circuit Theory, *CT-3,* No. 1 (March 1956), pp. 5–21.
15. Semmelman, C. L., Walsh, E. D., and Daryanani, G. T., "Linear Circuits and Statistical Design," B.S.T.J., this issue, pp. 1149–1171.

16. Warner, R. M., and Fordemwalt, J., *Integrated Circuits, Design Principles and Fabrication,* New York: McGraw-Hill, 1965, Chapter 10.
17. Balaban, P., Karafin, B. J., and Snyder, Mrs. D. B., "A Monte Carlo Tolerance Analysis of the Integrated, Single-Substrate, RC, *Touch-Tone®* Oscillator," B.S.T.J., this issue, pp. 1263–1291.
18. Steele, E. L., "A Computer Model for Integrated Circuit Transistors Including Substrate Interaction," Solid-State Electronics, *12,* No. 1 (1969), p. 41–53.
19. Kennedy, D. P., Murley, P. C., and O'Brien, R. R., "A Statistical Approach to the Design of Diffused Junction Transistors," IBM Journal, *8,* No. 5 (November 1964), pp. 482–495.
20. Berry, R., "Correlation of Diffusion Process Variations with Variations in Electrical Parameters of Bipolar Transistors," Proc. IEEE, *57,* No. 9 (September 1969), pp. 1513–1517.
21. Ashar, K. G., Ghosh, H. N., Aldridge, A. W., and Patterson, L. J., "Transient Analysis and Device Characterization of ACP Circuits," IBM Journal, *1,* No. 3 (July 1963), pp. 207–223.
22. Evans, J. G., "Measuring Frequency Characteristics of Linear Two-Port Networks Automatically," B.S.T.J., *48,* No. 5 (May–June 1969), pp. 1313–1338.
23. Searle, C. L., Boothroyd, A. R., Angelo, E. J., Gray, P. E., and Pederson, D. O., "Elementary Circuit Properties of Transistors," Chapter 9, S.E.E.C., *3,* New York: John Wiley & Sons, 1964.
24. Widlar, R. J., "An Exact Expression for the Thermal Variation of the Emitter-Base Voltage of Bipolar Transistors," Proc. IEEE, *55,* No. 1 (January 1967), pp. 96–97.

THE BELL SYSTEM TECHNICAL JOURNAL
Vol. 50, No. 4, April, 1971
Printed in U.S.A.

Statistical Circuit Design:

Linear Circuits and Statistical Design

By C. L. SEMMELMAN, E. D. WALSH and G. T. DARYANANI §

(Manuscript received November 17, 1970)

The design of linear circuits requires the designer to consider element tolerances, distributions and correlations and how they interact with proposed manufacturing test limits and service conditions such as temperature and aging. Analytical methods can be used in a limited number of cases; simulation methods using large modern computers permit study of more complex design problems. The principal themes of this paper are the designer's needs for computational assistance and the ways in which computer programs may be organized to meet these needs. Two computer programs for this purpose are described. One is a general-purpose analysis program for large networks having any topology. The other is a more specialized program suitable for "biquad" networks which may be used as building blocks to form a variety of filter and equalizer networks.

I. INTRODUCTION

In the Bell System, the origin of interest in the statistical design of linear circuits is lost in history. It could have been no later than the earliest planning for repeaters and filters for carrier systems, as no such system is possible without precise control of frequency and loss characteristics. As the total installed cost of a carrier system is always much greater than the cost of the design effort, use of the most advanced design procedures and techniques known, including statistical methods, has always been justified.

The selection of tolerances for component parts is one of the many topics which is under the control of the designer. He must select values and specify manufacturing tests so as not to increase costs either by paying a premium for unnecessarily precise elements or by rejecting correctly assembled networks in production. In the past, the tools that have been available to the designer to assist in the determination of tolerance limits have ranged from primitive to highly sophis-

ticated and mathematical. In the present era, which is dominated by electronic computers, simulation methods may prove the most valuable of all. The purpose of this paper is to review some of the basic methods of calculating and combining deviation characteristics, pointing out the powers and limitations of these methods, and to describe additional capabilities obtainable from two general purpose computer programs. These enable the designer to determine the result, in production and in service, of specifying a given set of tolerances, distributions, correlations, tuning and testing procedures and service conditions. All the material is confined to linear networks, such as filters, equalizers and feedback amplifiers, which are designed and built to frequency domain specifications.

1.1 *Analytical Methods*

Engineers engaged in designing electrical networks and selecting tolerances for their components have traditionally used the classical design technique which consists of making a first approximation, computing or measuring its performance and refining the approximation. That this procedure worked well and converged rapidly when applied to network design can be seen from the following. The image parameter design process for filters and comparable methods for other networks gave the engineer an understanding of the sensitivity of the various components, i.e., which component has its greatest effect in what part of the frequency spectrum. This led intuitively to both the specification of the tests that would be sufficient to assure accurate manufacture and to the knowledge of which few components need careful scrutiny at any frequency, in order to select appropriate tolerances. A few calculations or laboratory measurements followed by some experimental arithmetic would then produce the necessary tolerance limits. As the element tolerances being used were small, the resulting network deviations were proportional and could be combined by simple addition. Adding the absolute values of the maximum permissible deviations would produce worst-case behavior and if system performance limits were met the job was done.

Mathematicians came to the assistance of the design engineers and devised clever labor-saving methods of determining the deviation effects and of combining them linearly. For example, the rate of change of the driving point impedance of a reciprocal network with respect to a branch impedance is given by

$$\frac{\partial Z}{\partial Z_x} = \left(\frac{I_x}{I}\right)^2$$

and the rate of change of a transfer impedance is

$$\frac{\partial Z_T}{\partial Z_x} = \left(\frac{I_x}{I_2}\right)\left(\frac{I_x'}{I_1'}\right)$$

where the symbols all represent complex quantities and are defined in Fig. 1.* One or two solutions for all the branch currents then permit each individual driving point or transfer impedance deviation to be calculated and scaled to represent the assumed element tolerances. As stated above, these scaled deviations may be added to evaluate the behavior of a network with any one set of element values.

More insight, however, may be obtained by drawing a polygon in the complex plane within which the impedance must lie. This may be done in the following manner: Select a plus or minus sign for the departure of each element from its nominal, as required to make the real component of each scaled deviation positive. Adding the scaled deviations with these signs will give the rightmost point of the polygon. Successive corners are obtained by reversing the signs of the scaled deviations, one at a time, in the sequence of their increasing angles. When all signs have been reversed, the leftmost point is obtained and a second reversal in the same sequence generates the other half of the convex polygon and returns to the first point.

Still more may be learned by superimposing a family of ellipses each of which contains a specified percent of the universe of networks which would be manufactured from elements having the assumed tolerances. This may be done if the distribution of each element value is gaussian and its standard deviation is known.[1,2]

Figure 2 illustrates both the impedance polygon and ellipses for a

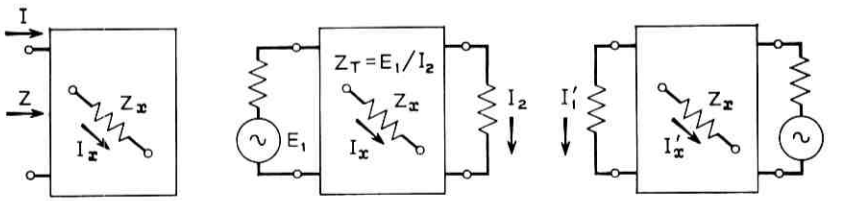

Fig. 1—Definition of symbols for driving point and transfer impedance deviations.

* The origin of these equations cannot be determined. They were in use in 1933 in the design of passive networks. They may be derived in a number of ways, including the use of network theorems and differentiating familiar expressions and identifying terms.

simple filter where the standard deviation is taken as 40 percent of the tolerance limit assumed for the polygon.

1.2 *Limitations to These Methods*

The first limitations are the facts that large tolerances do not permit linear extrapolation to large deviation shapes and that these do not combine linearly. Other difficulties arise when sophisticated design techniques such as filter synthesis by insertion loss design techniques[3] are used. The designer develops no "feel" for his design and the network performance becomes more sensitive to every element. Further, the elements may not have gaussian distributions. For example, 10 percent components may have a bimodal distribution resulting from a supplier's sorting the product and selling the 5 percent elements elsewhere. It may be impossible to determine whether high or low values of the elements should be used to evaluate worst-case behavior because a large change in one element's value may reverse the sign of the sensitivity for another element. Finally, the worst case may be so bad that system performance requirements are not met and tighter tolerances, factory adjustments, selective assembly, or reduced yield must be considered. Any of these increases the cost of manufacture, complicates the designer's task, and requires more powerful methods of determining the tolerances, adjustments and tests for production.

From the above discussion, it is apparent that only in rare cases will the selection of tolerances be a straightforward process where linear extrapolation and simple addition of deviation shapes will suffice. Frequently, the mathematical and engineering complexities put the designer's task beyond the limits of analytic methods available today.

II. MONTE CARLO TECHNIQUES

"Monte Carlo" computer techniques permit simulating the statistical behavior of random variables and imitating the tuning and testing actions performed in the factory. Such computer programs can take the place of a pilot production run, and furnish comparable information in a much shorter time and at a fraction of the cost.

In these methods the computer is programmed to generate a sequence of numbers which appear to a casual observer to be random, although their distribution and periodicities are known and carefully controlled. By mathematical transformations, these numbers are modified to represent possible values for each network element and to display the appropriate nominal value, tolerance, distribution shape and correlation with other elements. Further explanation of the

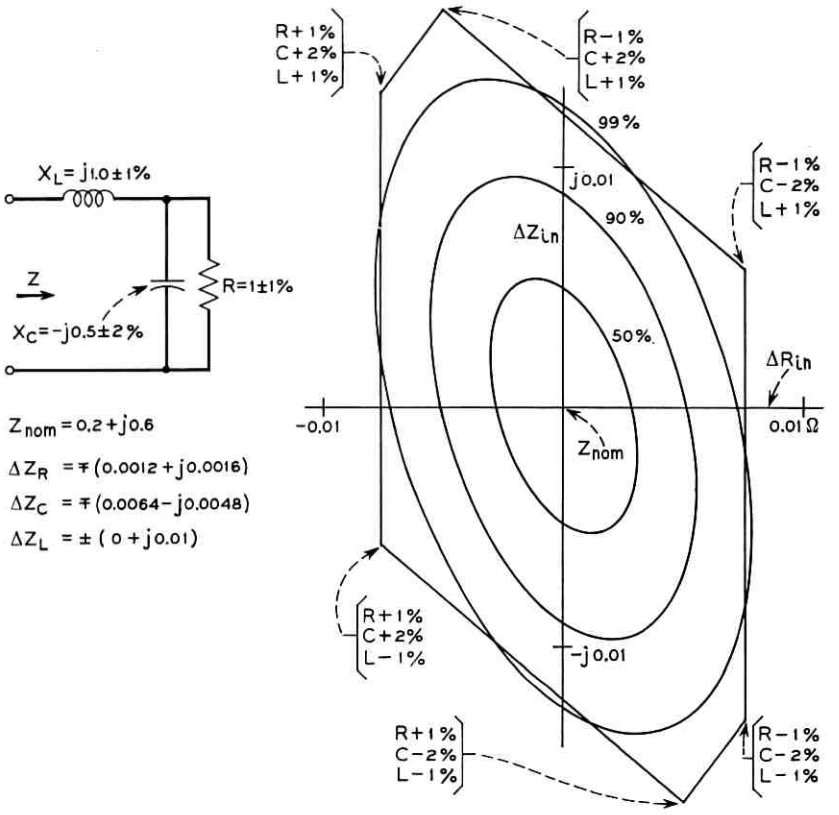

Fig. 2—Simple filter driving point impedance polygon and ellipses.

methods will be found in Appendix A. Many networks composed of such simulated elements are computed and the results compared with proposed test limits. A study of the computer output will enable the designer to determine the suitability of the nominal values, tolerances and tests.

The remainder of this article describes two computer programs, BELTAP and BITAP, which perform this simulation. The programs are addressed to different needs, but within its own area of application each is a general-purpose program.

BELTAP is a program for simulating and analyzing networks such as filters, equalizers, feed-back amplifiers, etc., having many elements and arbitrary topology. It computes insertion loss and return losses at both ends of the network. With it, the designer can obtain informa-

tion on test yields, the similarity between tests in this respect, element sensitivities, and selected scatter plots and histograms. This information should help him understand the complex interrelationships among element values, tolerances, distributions and tests which are not obvious from the network topology.

BITAP, on the other hand, can deal only with networks of a fixed topology, whose transfer function is restricted to a biquadratic function of frequency [defined in equation (1)]. By varying the element values used and connecting a number of such sections in tandem lowpass, highpass, bandpass filters and various types of equalizers can be constructed. BITAP facilitates specifying correlation among element values, factory tuning procedures, service conditions such as high or low temperature exposure and aging, and performance tests such as gain, phase and delay. If the service conditions are omitted, the tests become factory production tests; if included, end-of-life system performance checks.

III. DESCRIPTION OF BELTAP OPERATION

BELTAP is capable of performing tolerance analysis computations on a vast majority of the transmission networks in production today. The networks may consist of both lumped elements, having specified nominal values, tolerances and distributions, and fixed subnetworks, described by admittance matrices which are obtained either by calculation or measurement. BELTAP builds perturbed circuits by deviating each lumped element by a random amount within the specified tolerance and having a uniform, gaussian or arbitrary distribution shape. If correlation of deviations or tuning is required, special subroutines may be inserted. The perturbed circuits are then analyzed and insertion loss and input and output return losses are computed at each specified frequency. Special subroutines may be prepared to compute other quantities. For each perturbed network the complete set of elements and all measures of circuit performance are recorded on a disk file for later review by a postprocessor. The computed performance values are compared to the circuit requirements, to determine if the network passes or fails, and to calculate the production yields. The data on disk are then reviewed to collect other standard outputs and the listings, scatter plots and histograms requested by the designer. The output will be described more fully below. The variety of outputs available from BELTAP should be of great assistance to a designer who has little insight into the sensitivities of the elements, the interaction of their deviations and the relationship of both to the test limits.

3.1 *Specification of the Network*

A variety of types of information can be used to specify the network to be analyzed. It can contain resistors, inductors, capacitors and controlled current sources. Also, a quality factor, or Q, may be specified for the inductors and capacitors. Parallel and series resonant circuits may be specified by supplying only one of the reactive components and the resonant frequency. All the above items may be assigned tolerance limits and distribution shapes as required. Uniform and gaussian shapes are built-in; other special shapes may be read in at execution time. If correlations or factory tuning operations must be simulated, special subroutines can be written for this purpose.

BELTAP can allow fixed subnetworks to be included in the overall network. These subnetworks are specified by supplying their definite admittance matrices. The matrix data are generally obtained from an analysis of the subnetwork by a general-purpose linear network analysis program but may also be obtained from measurements.

The subnetwork feature allows BELTAP to perform a tolerance analysis on the critical components of a large network in a feasible amount of time. Consider, for example, the wideband amplifier shown in Fig. 3. The complete amplifier contains 80 nodes and 111 components. By blocking the circuit into two four-port subnetworks, as shown, the network to be computed is reduced to 24 nodes and 36 elements. The 36 elements are the critical components in the feedback paths and in sensitive positions in the forward path. The complete circuit contains

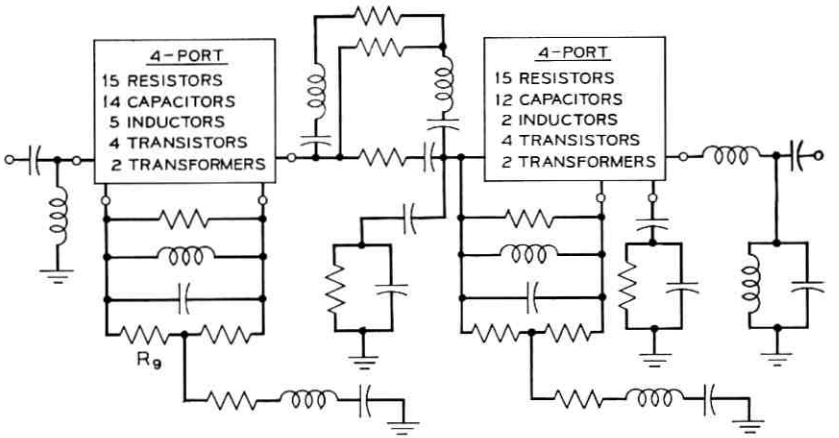

Fig. 3—Network for analysis by BELTAP, reduced to subnetworks.

four-port transformers, two-port transformers, and high-frequency transistors. Accurate lumped element models for these devices, particularly the transformers, do not exist. However, they can be easily incorporated into a BELTAP analysis by supplying their measured Y-matrix data (or, more likely, measured data reduced and transformed to give Y-matrix data).

3.2 BELTAP *Output*

A Monte Carlo analysis can produce such vast quantities of data that the designer, confronted with the complete results, might have difficulty identifying and extracting significant facts. It is the task of a postprocessor program to read the disk files and organize these data into brief comprehensible forms.

The postprocessor has two general classes of output, default output which is always produced and optional output which is produced only as specified. The default output is of a general nature and not of great detail or length. The requested output can be as voluminous as the engineer desires.

3.2.1 *Default Output*

The default output consists of four sections. The first section gives a summary of the test statistics. This includes the percent yield, average value, standard deviation, maximum value and minimum value for each test. It also gives the overall percent yield, combining all tests.

The second section of default output is a pseudo-correlation among pairs of tests. The pseudo-correlation is defined as the fraction of the networks for which the pass-fail result of the two tests agreed. For example, suppose ten networks were produced, the first seven passed test 1, the first nine passed test 2, and the remainder failed in both cases. The pseudo-correlation would then be 0.8 as networks 1 through 7 and 10 gave identical pass-fail results on the two tests. This output can be useful in reducing the number of tests performed without sacrificing reliability of performance. It may also be useful in determining an optimal sequence in which to perform the tests.

The third section of default output tabulates each parameter's name, nominal value, average value and standard deviation. This information is useful as a check on the random distributions and on the adequacy of the sample size. For example, the nominal value and the average value should be the same for all the parameters with a symmetrical density function.

The final section of default output gives the correlation among test

values and parameters. An approximation to the sensitivity of each test value to each parameter is also printed.

From these correlations and sensitivity estimates, the engineer is given insight into how individual circuit components affect his circuit's overall performance. More important, they give him a direction to follow in choosing those elements that may require tighter tolerances and those which may have broader tolerances.

3.2.2 *Optional Output*

The optional output has three sections: tabular output, scatter plots and histograms. Tabular output is merely a listing of the random element values and test values for each circuit. Circuits which failed tests are flagged for easy identification. Test results and element values may be intermixed so that the results of a test may be listed in a column adjacent to the values of an element to which the test is very sensitive.

There are three types of scatter plots available: test vs. test, element vs. test, and element vs. element. Figure 4 shows a scatter plot

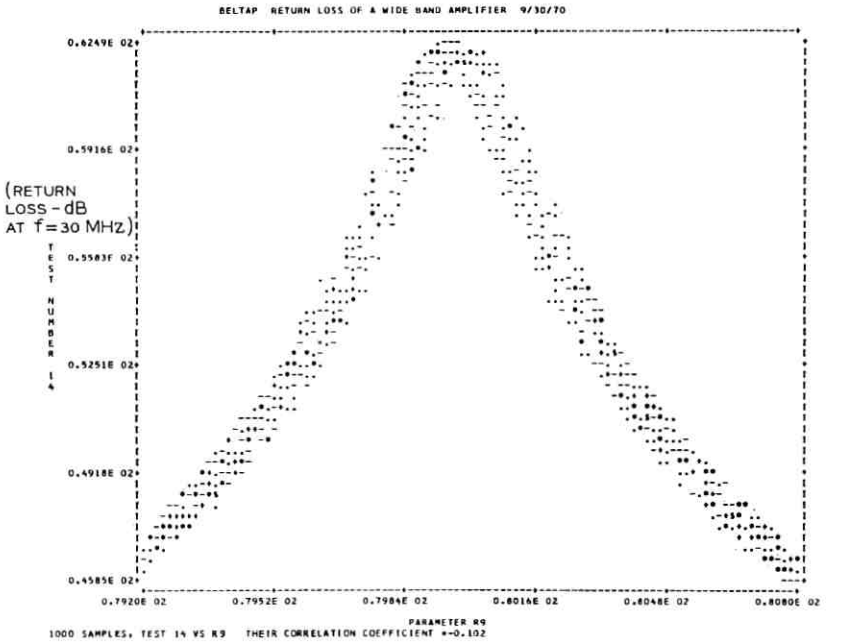

Fig. 4—Scatter plot of return loss vs. an element value.

of a test result vs. an element value. The various symbols printed on a scatter plot indicate the number of points that fell into a particular rectangular cell, the more points the blacker the symbol.

The scatter plots give an engineer more insight into how quantities in his circuit interact. They provide him with a type of pictorial information that is not available from correlation coefficients or sensitivity numbers. In Fig. 4, for example, the nominal value of the element occurs in the center of the plot, and at this point the slope of the test curve is near zero. Hence the partial derivative of the test result with respect to the element value and the correlation coefficient would be small. However, the test result is greatly influenced by the element value.

BELTAP can produce histograms of any number of element values and test values. Histograms of element values can be used as a check on the random number distributions and the density function routine in BELTAP. Histograms of the test values give the approximate shape of the probability density for the test.

3.3 *Summary of* BELTAP *Characteristics*

BELTAP provides a user with considerable flexibility in several respects. The network description language permits any configuration. The numbers of distribution types, branches, nodes and subnetworks are essentially unlimited as dynamic storage methods are used. As a result the size and number of networks computed will probably be restricted by computer running time, cost and numerical precision, rather than by array dimensions. Experience has indicated that when a very large network is encountered, the most sensitive elements can be selected by preliminary computer runs on portions of the entire structure. One or more additional runs can then be made with only these elements varying to obtain final data.

In addition to insertion loss and return loss calculations, which are provided by the program, users may write subroutines to evaluate other measures of network performance. Subroutines for simulating tuning adjustments, for introducing correlation effects, and for computing other measures of the network performance may also be written. The standard and optional outputs are designed to cover a broad range of types of data and methods of presentation. This variety should be helpful in discovering unsuspected interrelationships among tests and between tests and parameter values. For this reason, it is probably desirable to investigate considerably more tests than will actually be used in production.

IV. BITAP

The BITAP program has a very different purpose from that of BELNAP. BITAP can compute the behavior of only one kind of network, the "biquad." This network derives its name from the fact that its transfer function is a biquadratic function of frequency. It is an active network and has a fixed topology. The values of the resistors and capacitors used determine whether the biquad will be a lowpass, highpass, bandpass, loss equalizer or delay equalizer type of network. A number of biquad networks can be connected in tandem without interaction, so their gain and phase characteristics can be combined by simple addition and more complex structures realized. BITAP facilitates the investigation of realistic manufacturing conditions and environmental effects for biquad networks.

4.1 *Area of Application*

A common approach used in designing active filters is to build them with cascadable network sections. After the required transfer function has been determined, it is decomposed into a product of biquadratic functions of the form

$$\frac{V_{out}}{V_{in}} = \prod_{i=1}^{k} \frac{m_i s^2 + c_i s + d_i}{n_i s^2 + a_i s + b_i} \tag{1}$$

where m_i, c_i, d_i, n_i, a_i and b_i are real coefficients and $s = j\omega$.This decomposition may be done for any lumped, linear time-invariant network. The synthesis procedure consists of realizing each biquadratic function with an active network, which may be connected in tandem with other sections and will not interact with them. Examples of biquads are the state variable four amplifier biquad,[4] Moschytz's FENs[5] and the Sallen and Key networks.[6]

One of the aims in the realization of biquads is to make them isotopic, that is, to maintain the same network topology for all values of the coefficients m, c, d, n, a and b. If this can be done, the manufacturing process can be standardized, with obvious economic advantages. The state variable four amplifier biquad is completely isotopic; the FEN and Sallen and Key networks need a small number of topologies to realize all forms of the general biquadratic function. A circuit diagram of the four-amplifier biquad is shown in Fig. 5. By selecting the proper element values and making the right connections this network can be made to produce all the various filter functions—lowpass, high-

pass, bandpass, band-reject, notches and equalizers and delay shapes. The advantages of the realization justify writing the BITAP program.

We are concerned with the analysis of biquad networks under realistic manufacturing conditions and with environmental changes such as temperature, humidity and aging with time. Manufacturing conditions must include correlations, which will be present in thin-film and integrated circuit realizations and tuning adjustments needed to realize high-precision networks. Environmental factors must be taken into account as new manufacturing methods and materials are to be used and extensive experience with them is not available.

4.2 *Description of* BITAP

The basic approach is similar to that described above for BELTAP. For each element a nominal value, a tolerance and a distribution type are specified. The program generates random numbers which are transformed to become deviated element values. These are combined to form the six biquad coefficients, which then permit evaluation of the gain, phase or delay of each biquad at each frequency. These quantities are summed, the total is compared to the network requirements, and performance statistics are accumulated.

A number of additional considerations arise immediately. Because of the variety of types of biquad sections, a section type number is required to designate which set of formulas is to be used to calculate the biquad coefficients. The need to introduce correlation effects re-

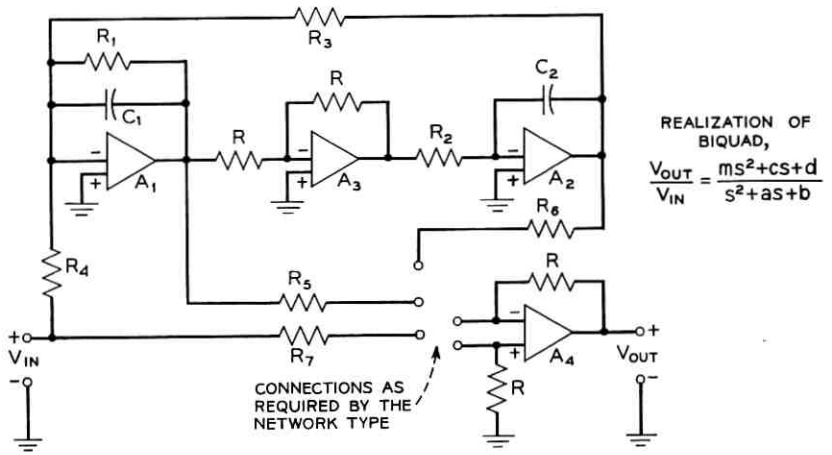

Fig. 5—Four-amplifier biquad circuit.

quires that every element value have an identifying serial number to permit cross-referencing. These serial numbers will also be useful in specifying tuning operations and in introducing environmental effects. Because of the limited number of section types, it has been possible to develop and include quite general methods of producing correlation, tuning, environmental effects and tests. More information on the methods of accomplishing these objectives will be given below. Where the standard methods are inadequate, new subroutines can be written and included in the program.

4.2.1 *Simulation of Manufacturing Conditions*

Due to the production process, parameters such as resistors, capacitors and amplifier gains have an actual value spread about the nominal value. This production tolerance on a parameter such as a resistor is represented by:

$$R_1 = R_0(1 + n_1) \tag{2}$$

where R_0 is the nominal value and n_1 is a random number whose range is the production tolerance on R_0. The distribution of n_1 could be gaussian, uniform, or any of several special shapes. The algorithm used to generate random numbers on the computers is discussed in Appendix A.

In integrated circuits, where all the elements are on the same chip, the values of the resistors track each other to some extent. Consider k resistors whose initial tolerances track. It has been found empirically that their values may be represented by:

$$\begin{aligned} R_1 &= R_{01}(1 + \rho n + (1 - \rho)n_1), \\ R_2 &= R_{02}(1 + \rho n + (1 - \rho)n_2), \\ &\vdots \quad\quad \vdots \\ R_k &= R_{0k}(1 + \rho n + (1 - \rho)n_k). \end{aligned} \tag{3}$$

The same random number n is used to perturb all k resistors. Each resistor $R_1, R_2, \cdots R_k$ is also perturbed by a separate random number $n_1, n_2, \cdots n_k$, respectively. ρ is a correlation factor which determines how closely the resistors track. The range of ρ is from 0 to 1. Complete correlation can be simulated by $\rho = 1$, and no correlation by $\rho = 0$. This correlation factor is different from the correlation coefficient used in statistics but has proven useful in the present application. The coding has been arranged so that the serial numbers mentioned earlier

effectively refer to both R and n values in equation (3), so that multiple correlations may be specified.

A practical problem in using the above sets of formulas, equations (2) and (3), is that of obtaining data on the distributions of the parameter values in production and on the correlation factor, ρ. The need for accurate statistical information may require that a major effort be made to obtain such data and keep it up-to-date. A companion paper, "Characterization and Modeling for Statistical Design," describes transistor characterization activities.

4.2.2 *Tuning*

The deviations from the nominal performance caused by the initial tolerances of components can be totally or partially corrected by tuning some of the network elements. The elements are tuned during the manufacture of the filter, at room temperature. Two types of tuning steps have been simulated on BITAP. In the first type, an element is adjusted so that a transmission requirement such as loss or phase is met at a given frequency. This type of tuning is used in adjusting for the bandwidth of a biquad section. In the second type of tuning, an element is adjusted for a peak (of gain or loss) at a given frequency. This is used in adjusting the resonant frequency of a pole or a zero. In both these tuning methods the variable element is changed continuously over a range. An additional subroutine could be written to simulate tuning in discrete steps, i.e., using a finite supply of element values close to the nominal, as this is an economical production method of adjusting the network performance. In production, the accuracy with which the element can be tuned depends on the sensitivity of the network to that element and on the precision of the measuring equipment. This is simulated by specifying a given nominal value for the tuning with a tolerance and a distribution.

4.2.3 *Simulation of Field Conditions*

The factors that caused the filter response to deviate from the nominal during manufacture were the initial tolerances of the components and inaccuracy in the tuning step. The environmental conditions that were assumed to exist during manufacture were room temperature and humidity. In the field, any change from these environmental conditions will cause the filter characteristics to change to some extent. The filter response will also change with time due to the chemical processes associated with aging. The temperature, aging and humidity effects in the field are modeled in the following way:

The value of a resistor (R_2) at T°C above room temperature is given by

$$R_2 = R_{02}(1 + \alpha T)$$

where R_{02} is the nominal value. The temperature coefficient (T.C.), α, is

$$\alpha = \alpha_0 + n_2$$

where α_0 is the nominal T.C. and n_2 the randomly distributed part of the T.C. The distribution function describing n_2 is usually gaussian.

The change in the value of a resistor or capacitor (R_3) with time is represented by

$$R_3 = R_{03}(1 + n_3) \tag{4}$$

where R_{03} is the nominal and n_3 simulates the random part.

The change due to humidity is represented by an equation similar to equation (4).

The combined effects of initial tolerance, temperature, aging and humidity is given by

$$R = R_0(1 + n_1)(1 + (\alpha_0 + n_2)T)(1 + n_3)(1 + n_4). \tag{5}$$

The random numbers associated with temperature coefficients (n_2), for components on an integrated circuit, are correlated. The same is true for the aging coefficient (n_3) and the humidity coefficients (n_4). These correlations are simulated just as in equation (3).

4.2.4 *Testing*

The values of the deviated parameters are used in the equations describing the biquad to evaluate the performance of the network. The biquad is analyzed several times using different sets of random numbers to simulate environmental and manufacturing conditions. The performance tests are spelled out in the form of filter function requirements (loss, phase or delay) at various frequencies. Three standard forms have been built into the program. These are:

(*i*) loss (phase, delay) at a frequency f_1 is between two limits, dB_1 and dB_2 ,

(*ii*) loss at a frequency f_1 is bounded below (or above) by dB_1 , and

(*iii*) loss at a frequency f_1 is greater (less) than the measured loss at a reference frequency f_2 plus the amount dB_1 .

More than one performance requirement may be specified at a frequency. It is expected that special subroutines will be written for

more sophisticated tests such as a resonant frequency, Q, and in-band ripple. It should be noted that if environmental conditions are included, the tests become service condition or end-of-life tests. If they are omitted, the tests may be interpreted as factory production tests.

4.2.5 *Output*

If, for a particular set of deviated elements, the network fails the required specifications, the complete network performance is stored. The output consists of a table which details the failed networks. If a test was failed, the performance function for that test is printed; otherwise, a blank is printed for the test.

The overall yield is computed as the ratio of the number of networks passing all tests to the total number of networks tested. Yields are also calculated for individual tests. The exact form of the output is illustrated by the example in the next section.

4.3 *Example*

The four amplifier biquad circuit of Fig. 5 will be used to illustrate the main features of BITAP. Its transfer function, in terms of the elements, is

$$\frac{V_{out}}{V_{in}} = \frac{+\frac{R}{R_7}\cdot S^2 + \frac{R}{R_7}\cdot\frac{1}{C_1}\left[\frac{1}{R_1} - \frac{R_7}{R_4R_5}\right]\cdot S + \frac{R}{R_7R_2C_1C_2}\left[\frac{1}{R_3} + \frac{R(R_5+R_7)+R_5R_7}{R_4R_5(R+R_6)}\right]}{S^2 + \frac{1}{R_1C_1}S + \frac{1}{R_2R_3C_1C_2}}.$$

The complete network contains two such sections connected in tandem as shown in Fig. 6, which also gives the element values. The resistors have a one percent manufacturing tolerance with a gaussian distribution. The capacitors are one percent elements with a flat distribution. The correlation factors, ρ, are 50 percent for both resistors and capacitors. The pole frequency of the first section is at 5 kHz, and R_3 is tuned to obtain this frequency within ± 1 Hz. This ± 1 Hz represents the accuracy of tuning and it is assumed to be distributed uniformly around the nominal 5 kHz. The bandwidth of the first section is tuned by R_1 to 100 Hz ± 1 Hz. Section 2 is not tuned. These initial tolerances and the tuning steps describe the manufacturing conditions. It is assumed that a BITAP run simulating the above conditions and manufacturing tests has already been made and 100 percent of the network passed. The filter performance is now to be tested at $+50°$C and at a time 20 years from manufacture. The T.C. of resistors is 130 ± 30 parts per million (ρ = 80 percent) and that of capacitors -135 ± 10

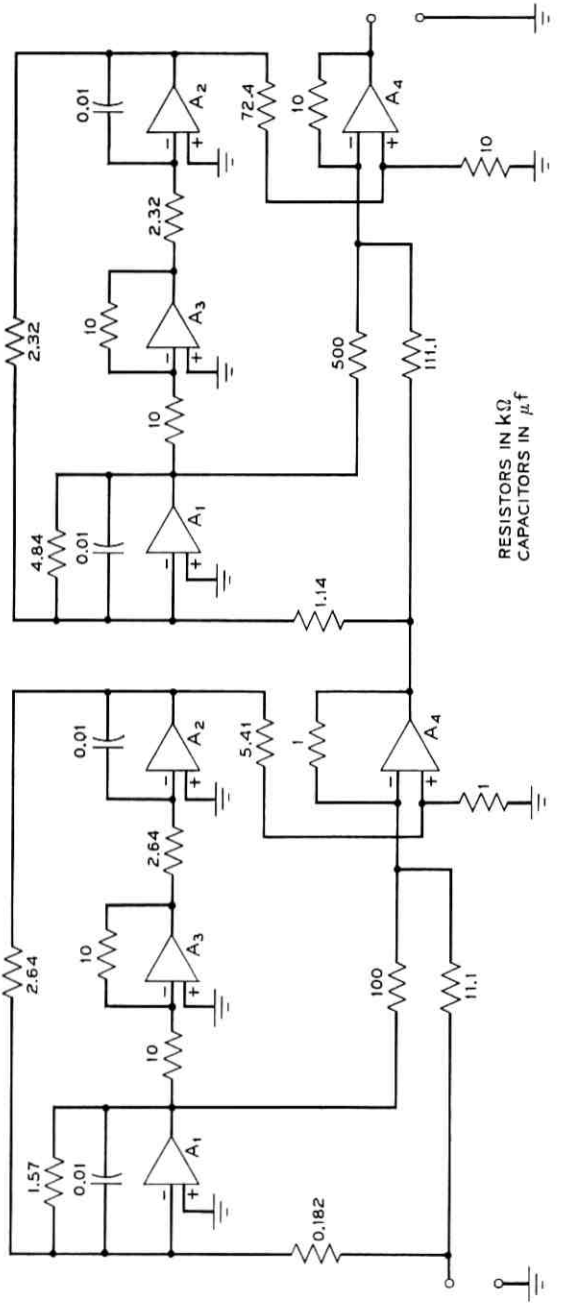

Fig. 6—Lowpass filter network for BITAP analysis.

ppm ($\rho = 50$ percent). The random parts (± 30 ppm and ± 10 ppm) are distributed normally about the nominal. The aging coefficient for the resistors and the capacitors in 20 years is ± 2 percent, uniformly distributed ($\rho = 50$ percent).

The nominal performance and the test requirements to be met at end-of-life are shown in Fig. 7. Figure 8 shows the results of a BITAP analysis of 100 filters and indicates that 82 percent will meet these service condition requirements. Figure 8 indicates both the frequencies where improvements are needed and the magnitude of the changes required. With the biquad type of realization and such data, the designer usually has no difficulty deciding which elements or tuning adjustments are responsible.

In order to improve the performance in the 1000- to 4000-Hz passband, the designer might examine several alternatives. A new nominal design with a smaller ripple or a better centered nominal loss would

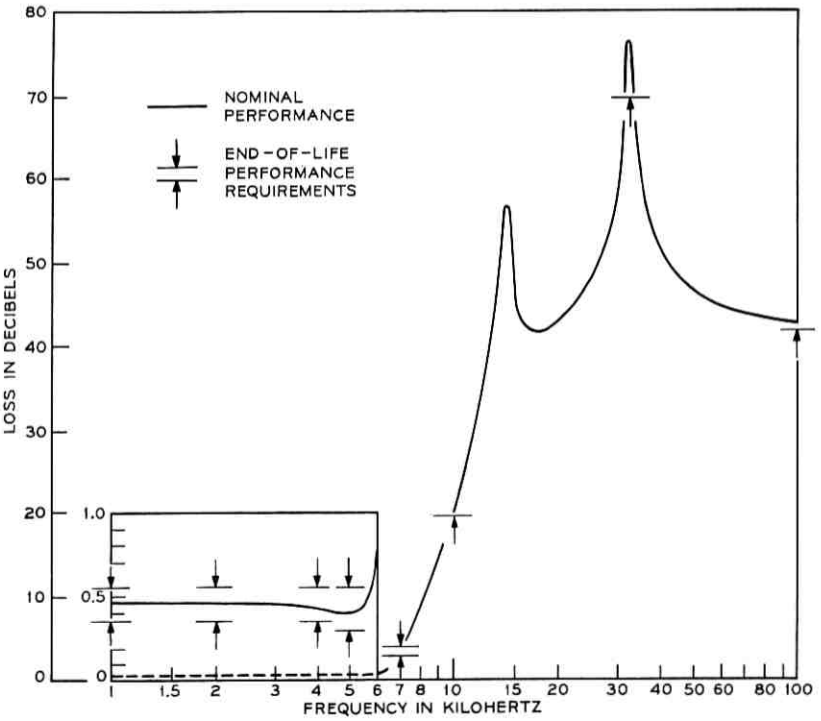

Fig. 7—Nominal performance and end-of-life requirement.

FREQ	1000.00	2000.00	4000.00	5000.00	7000.00	10000.0	32000.0	100000.
MEAS	LOSS	LOSS	LOSS	LOSS	LOSS	LOSS	LOSS	LOSS
BELOW	0.5500	0.5500	0.5500	0.5500	4.000	—	—	—
ABOVE	0.3500	0.3500	0.3500	0.3000	3.000	20.40	70.00	42.00
NOM	0.4845	0.4738	0.4468	0.3947	3.391	20.83	76.70	42.93
NET. NO.								
8	0.5569	0.5535	—	—	—	—	—	—
10	—	—	—	—	—	20.21	—	—
13	—	—	—	—	—	20.17	—	—
32	—	—	—	0.2998	—	20.32	—	—
36	—	—	—	—	—	20.39	—	—
45	—	—	—	0.2829	—	—	—	—
46	—	—	—	—	—	20.40	—	—
49	0.5506	—	—	—	—	—	—	—
50	—	—	—	—	—	20.21	—	—
51	—	—	—	—	—	20.16	—	—
57	—	—	0.3375	0.2819	—	—	—	—
60	—	—	—	0.2937	—	—	—	—
67	—	—	0.3364	0.2770	—	—	—	—
73	0.6009	0.6018	0.5891	—	—	—	—	—
76	0.5584	0.5641	0.5606	—	—	—	—	—
78	0.5657	0.5544	—	—	—	—	—	—
85	—	—	—	—	2.961	20.13	—	—
93	0.5620	0.5637	0.5564	—	—	—	—	—
NO. FAIL	6	5	5	5	1	8	0	0

FINAL YIELD = 82.000 PERCENT

Fig. 8—BITAP yield analysis.

entail no added cost. Use of closer tolerances for some components or more precise tuning might also provide sufficient improvement, but at some added expense. If none of these works, addition of a third section should be evaluated.

4.4 *Appraisal of* BITAP

BITAP is capable of analyzing up to 20 biquad sections. The number of performance tests is limited to 30. Ten types of biquad sections are currently included in BITAP. The addition of more biquad sections merely involves describing the biquad coefficients (m, c, d, n, a, b) in terms of the elements of the biquad and providing equations for the tuning steps. The rest of the program is identical for all biquads.

BITAP is an exact analysis package and as such it can be used in other steps of the design process. For instance, it could be used to determine whether or not a filter needs to be tuned, and to decide on the number of tuning steps needed. BITAP could also be used in determining the best (cheapest) components that could be used in a circuit while meeting all requirements.[7]

It has been shown how BITAP can be used to evaluate the performance of networks of the biquad family at the time of manufacture and under (end-of-life) field conditions. The information obtained here can be used to decide on the tests to specify during manufacture. The analysis under end-of-life conditions gives a measure of the adequacy of the design under extreme conditions.

V. CONCLUSIONS

We have described some simple analytic methods of calculating and combining deviation shapes and have discussed the areas in which they are useful and the respects in which they are limited. We have also presented two simulation procedures, which rely on the speed and large storage capacity of modern digital computers. Each is a general-purpose program in that it can be used to analyze statistically a large number of networks of an appropriate type. Although the BITAP networks form a subset of those analyzable by BELTAP, the two programs provide entirely different facilities for their users. BELTAP provides complete freedom in the network topology; BITAP uses a functional input form, which reduces computing time. BELTAP facilitates exploration of concealed interactions among component values and test results; in BITAP it is assumed that the few simple network functions allowed are completely understood in this respect. BELTAP provides no built-in cor-

relation, tuning, environmental exposure, or phase or delay evaluation but does include return losses; BITAP includes all of these except return losses which are of no interest.

Under certain conditions, the least expensive manufacturing method may require discarding some of the product. The simulation programs should be capable of demonstrating this, if it is true. They may also provide information that is useful in correcting troubles in the manufactured product. Their usefulness will, of course, depend on the availability of accurate statistical information.

Clearly, useful as they are, neither of these programs can be termed completely general purpose. Much work remains to be done in both areas of application. It is considered that the two programs make a very worthwhile contribution to a designer's repertoire and may point the way for still more comprehensive tools in the future.

VI. ACKNOWLEDGMENTS

The authors wish to express their appreciation to F. P. Sansone and Mrs. H. D. Reinecke for their work leading to BITAP.

APPENDIX A

Both BELTAP and BITAP use a congruential random number generator in which the modulus is an integral power of a prime number and the multiplier is a primitive root.[8] This method permits generating a sequence of numbers which has a flat distribution and a period which is made just large enough to produce the number of random numbers required. The modulus, M, is obtained by raising three to a power, n, such that the period, $2 \cdot 3^{n-1}$, exceeds the required value. The multiplier used is $2 + 9 \cdot k$, where k is an integer chosen to make the multiplier approximately equal to the square root of the modulus. It was found empirically that this function of k produces a primitive root, that is, a multiplier having the period given above, which is the longest that can be obtained for the assumed modulus.

A simple example using small numbers will illustrate the process. Suppose five networks are to be calculated and each contains three elements with distributions. Fifteen random numbers will be required. A value of three for n will produce a sequence of $2 \cdot 3^2 = 18$ numbers before repetition begins. The modulus M is $3^3 = 27$ and multipliers of 2, 11 or 20 are possible. Suppose the sequence begins with 1 and a multiplier of 11 is used. The second number is $1 \cdot 11 = 11$. The third is obtained by multiplying the second by 11, dividing by 27 and using

the remainder, 13. The fourth is 13 times 11 modulo 27 = 8, etc. The complete sequence is: 1, 11, 13, 8, 7, 23, 10, 2, 22, 26, 16, 14, 19, 20, 4, 17, 25, 5, 1. It should be noted that the nineteenth number, 1, is a repetition of the first and that all numbers less than 27 are present except multiples of three. The first three numbers will be used for the three random elements in the first network, the next three for the second network, etc.

The random numbers are shaped to become element values having the desired tolerance and distribution in the following manner. The first transformation is to put them into a range from -1 to $+1$ by dividing by half the modulus and subtracting 1.

$$n_b = \frac{n_a \cdot 2}{M} - 1. \tag{6}$$

The smallest random number, 1, yields $-0.925925 \cdots$, while the largest gives $+0.925925 \cdots$. With a larger modulus the numbers will approach -1 and $+1$ more closely. If an element has a flat distribution, the random value may be produced as follows:

$$R = R_0(1 + t \cdot n_b/100) \tag{7}$$

where R is the random value, R_0 is the nominal value for that element, and t is its (symmetrical) tolerance in percent. If the distribution is not flat, the values of n_b are transformed as shown in Fig. 9. For each value of n_b the proper line segment is identified and a value of n_c is calculated by interpolation. n_c is then used in place of n_b in equation

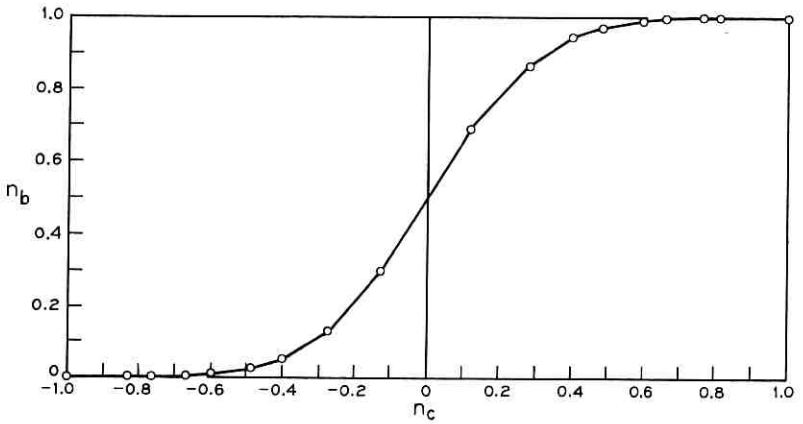

Fig. 9—Cumulative gaussian probability distribution approximated by straight-line segments.

(7) to calculate R. The coordinates for the gaussian distribution are permanently stored in the program. Other distributions can be used by reading in the appropriate sets of breakpoints.

If correlation is required, values of n_b and/or n_c may be combined as follows:

$$n_d = \rho n_x + (1 - \rho) n_y . \tag{8}$$

Here ρ is a correlation factor and n_d, n_x and n_y all represent random numbers in the -1 to $+1$ range, associated with selected elements, parameters, field conditions, and/or tuning tolerances. It is to be noted that n_d may be used to evaluate an R, using equation (7), or it may be used as an n_x or n_y in additional equations of the same form as (8). If the latter is done, the result will be partially correlated to three other parameters.

When equation (8) is used to introduce partial correlation and n_x and n_y have average values of zero and are uncorrelated, it can be shown that the variance of n_d is given by

$$\sigma_d^2 = \rho^2 \sigma_x^2 + (1 - \rho)^2 \sigma_y^2 . \tag{9}$$

It may also be shown that the tracking coefficient between n_d and n_x is given by

$$r = \sum_1^N n_d n_x / N \sigma_d \sigma_x = \rho \sigma_x / \sigma_d . \tag{10}$$

The tracking between two different distributions n_d formed using the same n_x and different n_y is discussed in the following paper.

REFERENCES

1. Hoyt, R. S., "Probability Theory and Telephone Transmission Engineering," B.S.T.J., *12*, No. 1 (January 1933), pp. 35–75.
2. Boghosian, W. H., unpublished memorandum, May 3, 1938.
3. Darlington, S., "Synthesis of Reactance 4-Poles," J. Math. and Phys., XVIII, (September 1939), pp. 257–353.
4. Tow, J., "A Step-by-Step Active Filter Design," Spectrum, *6*, No. 12 (December 1969), pp. 64–68.
5. Moschytz, G. S., "Active RC Filter Building Blocks using Frequency Emphasizing Networks," IEEE J. Solid State Circuits, *SC-2*, No. 2 (June 1967), pp. 59–62.
6. Sallen, R. P., and Key, E. L., "A Practical Method of Designing RC Active Filters," I.R.E. Trans. Circuit Theory, *CT-2* (March 1965), pp. 74–85.
7. Karafin, B. J., "The Optimum Assignment of Component Tolerances for Electrical Networks," B.S.T.J., this issue, pp. 1225–1242.
8. Hutchison, D. W., "A New Uniform Pseudo-Random Number Generator," N66-32469, Stat. Dept., U. of Calif., Berkeley, April 27, 1965.

THE BELL SYSTEM TECHNICAL JOURNAL
Vol. 50, No. 4, April, 1971
Printed in U.S.A.

Statistical Circuit Design:

Nonlinear Circuits and Statistical Design

By I. A. CERMAK and MRS. D. B. KIRBY §

(Manuscript received November 25, 1970)

Despite recent advances in the speed of digital computers and in numerical algorithms for the solution of differential equations, the evaluation of the dynamic response of nonlinear circuits is still too slow to permit Monte Carlo tolerance analysis. However, the performance of many nonlinear circuits can be evaluated on a static basis. One example is a D/A converter built with devices much faster than the converter's cycle time. Algorithms now exist that produce the static or equilibrium solution of such networks in seconds. This paper deals with these algorithms and the associated techniques that have been embodied in a program for the Monte Carlo tolerance analysis of nonlinear, "dc," circuits.

I. INTRODUCTION

To date, most tolerance analysis of circuits has been in the frequency domain, as this series of articles indicates. The need for nonlinear analysis arises not only for large signal circuits but also for small signal ac circuits where device model parameters vary with bias. Recent advances in the speed of digital computers and numerical algorithms have made possible the analysis of circuits with nonlinear behavior. Large signal, or time domain analysis of nonlinear circuits, however, is still such a comparatively slow process that Monte Carlo methods are out of the question. Enough algorithmic innovations have been achieved in the static analysis of nonlinear circuits that Monte Carlo methods can be applied to a wide class of nonlinear problems. DC in the sense used in this paper implies that the dynamic behavior of the nonlinear devices is fast in relation to the response of the rest of the circuit. There are, in general, three types of circuits that fall into this class.

(*i*) Circuits that are essentially dc, such as operational amplifiers, power supplies, and those circuits used as examples in this paper.

(*ii*) Circuits that can be subdivided into dc and ac blocks where the nonlinear behavior of the circuit is present essentially only in the dc part. An example of this type of circuit is the *Touch-Tone*® oscillator, the analysis of which is described in this series.[1] This class of circuits is very similar to the first.

(*iii*) Circuits designed for small signal applications may be analyzed in the frequency domain. Realistic modeling of devices, however, introduces changes in the small signal model parameters for different bias points. If the bias circuits vary randomly, then nonlinear dc analysis is required in the ac tolerance analysis loop.

This paper deals with some of the methods required for the efficient analysis of nonlinear circuits in a dc sense. The techniques and algorithms to be described have been embodied in a computer program which performs Monte Carlo tolerance analysis of nonlinear dc circuits as well as dc and transient analysis. Some of the more critical implementation aspects are described.

II. DESIGN OF A NONLINEAR TOLERANCE ANALYSIS PROGRAM

2.1 *Problems Involved*

Until recently tolerance analysis, even nonlinear tolerance analysis, has been simple in concept. Circuits were manufactured using *discrete* components which generally had independent statistical behavior; transistors and diodes were expensive items and were used sparingly. Hence, a large amount of analysis could be done without a complex software package.

Integrated circuits have opened a whole host of new problems in this area. Circuits designed today typically employ large numbers of transistors (since transistors are as cheap as resistors), posing many problems in their modeling, simulation, and solution. Probably the biggest dilemma in the design of a nonlinear tolerance analysis program is the minuscule past experience to draw upon as to what analysis is required, what to do with the analysis results once they are obtained, and how to interpret them.

Some of the special problems that arise in nonlinear tolerance analysis are:

(*i*) Parameters tend to be statistically correlated. This implies that many new output features have to be present in the software.

(*ii*) There is a very wide range of circuit problems that will have to be solved. This poses special difficulties and restrictions on the methods of analysis, as will be seen in the following sections.

(*iii*) Statistical data for circuits manufactured today are not yet available or are available in limited quantities;[2] manufacturing processes vary from day to day and parameter correlations, aging data, etc., are all important to the analysis.

2.2 *Criteria To Be Met*

One of the most important criteria to be met in the design of a nonlinear tolerance analysis program is that it be easy to use. Some of the characteristics implied by this, both for the users of the program and for the writers of it, are:

(*i*) The program must be humanly engineered to have a simple, clear, and easily learned input language. This applies not only to the network description but also to the description of statistical data and to the command structure. The trend has been for engineers to personally use available computer tools rather than work through intermediaries, and the program itself should present as few obstacles as possible. In addition, the output capabilities must include data reduction schemes so that insight is gained at a glance.

(*ii*) The program must be designed to be flexible enough so that it can be changed easily. Past experience has shown that a general-purpose analysis program will undergo many changes and, in fact, will probably never reach a static condition. This means the program must be written in modular form, a characteristic that very often degrades efficiency. Modularity, however, implies ease of maintenance, upgrading, and debugging.

(*iii*) The program must be portable because of wide demand. This implies that it be written in some high level language, such as FORTRAN, with possibly a very small number of critical routines written in Assembly language for efficiency.

In addition to ease of use, an important criterion is, of course, economy and reliability. The program must be very efficient if it is to be useful. Solution times for each statistical design must be measured in seconds to make the analysis practical at all, and possibly in milliseconds if sophisticated features such as performance contours and large scale sensitivities are to be included.[3] Until recently, one would have been happy to get one solution to a nonlinear circuit; today

we are faced with obtaining hundreds and perhaps thousands of these solutions in a reasonable time.

Various algorithms for solution of the nonlinear equations that arise from circuit simulations have been described in the literature; however, they are all basically variations on the Newton-Raphson scheme and are in general not suitable as they stand. The majority of the schemes converge in the order of tens of iterations, if they converge at all. Since solution times for each iteration are generally proportional to the cube of the number of variables, many iterations for each statistical solution preclude their use in a program such as this. Recent breakthroughs, however, in the Newton-Raphson solution of nonlinear circuits and careful implementation of these methods permit solution times short enough (of the order of one second) so that meaningful tolerance analysis is possible.

III. NUMERICAL ALGORITHMS AND THEIR IMPLEMENTATION

3.1 *Problem Formulation*

Given a network topology, there are various ways to write equations describing the behavior of the network. Some examples are nodal equations, loop equations, Branin's[4] mixed mesh/cut-set equations and the state-space formulation, which in the dc case has come to be known as the "normal form."[5] We have adopted the normal equation formulation for the following reasons:

(*i*) The reduced set of equations produces, in general, a small system that has to be solved iteratively, by effectively separating the linear and nonlinear aspects of the problem.

(*ii*) Implementation of various analysis techniques for equations in their normal form is straightforward.

(*iii*) The normal form of the equations can be generated extremely fast (see below) in a manner competitive with the most efficient sparse matrix techniques available today.

Some other formulation (such as nodal equations), coupled with sparse matrix techniques may be more efficient for circuits containing a large number of junctions compared with the number of linear resistors. The formulation employed here, however, allows straight forward implementation of various convergence schemes such as the nonlinear transformation described in Section 3.3.3. In addition, it is felt that the normal formulation is the most practical for small-to-medium size circuits with a significant number of linear resistors (including those in the device models). The operational amplifier

example in this paper probably represents the limiting practical size of circuit for this formulation. Most of the methods described here are also applicable to any other equation formulation.

3.2 *Generation of Equations in the Normal Form*

Consider any circuit consisting of current and voltage sources, diodes, transistors and resistors. From the network topology and network parameters, the large signal behavior of the network is characterized by a system of equations in the "normal form," viz.,

$$[A][\mathbf{V}] + [B][\mathbf{U}] + [N(\mathbf{V})] = 0 \tag{1}$$

where

- $[\mathbf{V}]$ is the vector of all device junction voltages and is the set of independent variables to be found;
- $[\mathbf{U}]$ is the vector of independent voltage and current sources in the network;
- $[A]$ and $[B]$ are coefficient matrices dependent on the network resistances; and
- $[N(\mathbf{V})]$ is a vector of functions dependent on the nonlinear properties of the network.

For computer simulation, the network devices are characterized by the Ebers–Moll model[6] where the functional form of $N(V)$ is

$$N(V) = I_D = I_S\,[\exp\,(\theta V) - 1]$$

where I_S is intercept current, and θ is dependent on temperature. Notice that the formulation (1) isolates the linear part of the network from the nonlinear part and that the nonlinear behavior can be characterized by a *vector* quantity.

The set of equations given by (1) must be generated for each statistical design, since the $[A]$ and $[B]$ matrices are dependent on resistor values. The implication of this, of course, is that a very fast algorithm is needed for equation generation.

To completely characterize network behavior, another set of equations is required which relates any requested network currents or voltages to the junction voltages found from (1). If $[\mathbf{Z}]$ is the vector of user-requested outputs (element currents and voltages), then

$$[\mathbf{Z}] = [C][\mathbf{V}] + [D][\mathbf{U}] \tag{2}$$

where again $[C]$ and $[D]$ are coefficient matrices dependent on resistor values and must be recalculated for each statistical design.

The basis for the formulation of the A, B, C and D matrices is

mainly topological in nature. From the network incidence matrix, $[T]$, and the choice of a network tree as described below, the fundamental loop and cut-set matrices ($[F]$ and $[-F]^T$, respectively) are derived.[4]

The incidence matrix, T, has elements 0 and ± 1 and dimensions $n \times b$ for a network with $(n + 1)$ nodes and b elements. Let $\mathbf{I}$ be a vector of element currents which is partitioned into tree branch currents, $\mathbf{I}_t$, and link currents, $\mathbf{I}_l$. Then,

$$[T][\mathbf{I}] = [-\mathcal{g}, F]\begin{bmatrix}\mathbf{I}_t \\ \mathbf{I}_l\end{bmatrix} = 0, \tag{3}$$

$$\mathbf{I}_t = F\mathbf{I}_l \quad \text{and} \quad \mathbf{V}_l = -F^T\mathbf{V}_t\,. \tag{4}$$

Equations (3) and (4) are expressions of Kirchoff's Current and Voltage Laws where $\mathcal{g}$ is the identity matrix and the vector of element voltages, $\mathbf{V}$, is partitioned like $\mathbf{I}$ into $\mathbf{V}_t$ and $\mathbf{V}_l$. $[F]$ has dimensions $n \times (b - n)$, and its elements are 0 and ± 1.

It is desired to place all voltage sources and device junctions in the tree and all current sources in links. Assuming this is possible, the columns of $[T]$ are arranged in the following preference order (given also is the notation to be used for tree and link current and voltage):

	I	V
voltage sources	I_E	E
device junctions	I_D	V_D
resistors—tree	I_R	V_R
—link	I_G	V_G
current sources	J	V_J

The incidence matrix, $[T]$, can be quickly reduced to the form $[-I, F]$ by gaussian elimination, from which the fundamental loop matrix is defined. The reduction process favors the above top elements for inclusion in the tree.

Now partition $[F]$ as follows:

	G	J
E	F_{11}	F_{12}
D	F_{21}	F_{22}
R	F_{31}	F_{32}

and from equation (4) write

$$\mathbf{I}_D = F_{21}I_G + F_{22}\mathbf{J}, \tag{5}$$

$$I_R = F_{31}\mathbf{I}_G + F_{32}\mathbf{J}, \tag{6}$$

$$\mathbf{V}_G = -F_{11}^T\mathbf{E} - F_{21}^T\mathbf{V}_D - F_{31}^T\mathbf{V}_R. \tag{7}$$

Let $[R]$ and $[G]$ be defined as diagonal matrices whose elements are tree resistor values and link conductance values, respectively. Then, from equations (6) and (7),

$$\begin{bmatrix}\mathbf{I}_R\\ \mathbf{V}_G\end{bmatrix} = \begin{bmatrix}R^{-1} & 0\\ 0 & G^{-1}\end{bmatrix}\begin{bmatrix}\mathbf{V}_R\\ \mathbf{I}_G\end{bmatrix}$$

$$= \begin{bmatrix}0\\ -F_{21}^T\end{bmatrix}[\mathbf{V}_D] + \begin{bmatrix}0 & F_{32}\\ -F_{11}^T & 0\end{bmatrix}\begin{bmatrix}\mathbf{E}\\ \mathbf{J}\end{bmatrix} + \begin{bmatrix}0 & F_{31}\\ -F_{31}^T & 0\end{bmatrix}\begin{bmatrix}\mathbf{V}_R\\ \mathbf{I}_G\end{bmatrix}$$

or

$$\begin{bmatrix}R^{-1} & -F_{31}\\ F_{31}^T & G^{-1}\end{bmatrix}\begin{bmatrix}\mathbf{V}_R\\ \mathbf{I}_G\end{bmatrix} = \begin{bmatrix}0\\ -F_{21}^T\end{bmatrix}[\mathbf{V}_D] + \begin{bmatrix}0 & F_{32}\\ -F_{11}^T & 0\end{bmatrix}\begin{bmatrix}\mathbf{E}\\ \mathbf{J}\end{bmatrix}. \tag{8}$$

Define

$$\begin{bmatrix}R^{-1} & -F_{31}\\ F_{31}^T & G^{-1}\end{bmatrix}^{-1} = \begin{bmatrix}H_{11} & H_{12}\\ H_{21} & H_{22}\end{bmatrix} = [H]. \tag{9}$$

Then

$$\begin{bmatrix}\mathbf{V}_R\\ \mathbf{I}_G\end{bmatrix} = [H]\begin{bmatrix}0\\ -F_{21}^T\end{bmatrix}[\mathbf{V}_D] + [H]\begin{bmatrix}0 & F_{32}\\ -F_{11}^T & 0\end{bmatrix}\begin{bmatrix}\mathbf{E}\\ \mathbf{J}\end{bmatrix}. \tag{10}$$

Substituting $\mathbf{I}_G$ into equation (5) results in equation (1), namely

$$\mathbf{I}_D = N(\mathbf{V}_D) = [A][\mathbf{V}_D] + [B][\mathbf{U}]$$

or

$$A\mathbf{V} + B\mathbf{U} - N(\mathbf{V}) = 0.$$

Also, from F and $-F^T$, any network current or voltage can be extracted and the $[\mathbf{Z}]$ vector of equation (2) calculated. In general,

$$[\mathbf{Z}] = [C'][\mathbf{V}] + [D'][\mathbf{U}] + [P]\begin{bmatrix}\mathbf{V}_R\\ \mathbf{I}_G\end{bmatrix} \tag{11}$$

where C', D' and P are matrices whose elements are 0, ± 1 obtained from selective rows and columns of F and $-F^T$. Substituting equation (10) into equation (11) yields equation (2).

The time-consuming task in the calculation of the A, B, C, D matrices is in finding $\begin{bmatrix} \mathbf{V}_R \\ \mathbf{I}_G \end{bmatrix}$ as expressed by equation (10). This calculation requires one matrix inversion and two matrix multiplications.

The number of rows and columns of H^{-1}, as seen by equation (9), is equal to the number of resistors in the network. For a completely characterized network, including parasitics, this number can easily approach 80 or 100. The number of multiplications required to invert an nth order matrix is n^3, or 10^6 for our example! Clearly, the implementation of generating the equations of (1) and (2) is critical.

Fortunately, the matrices that evolve from this formulation have special properties which can be advantageous. These are:

(*i*) The fundamental loop matrix, F, contains only 0, ± 1 entries and is sparse. From experience with a wide range of problems, this matrix is 20 to 50 percent dense (ratio of nonzero entries to total number of entries). Because of these properties, any matrix multiplication involving F or its partitions can be performed by additions and subtractions rather than by multiplications. The operation of addition is at least 3 to 4 times faster than multiplication on most digital computers. Also, the number of additions and subtractions to be performed in multiplying F by A, where A is an $n_1 \times n_2$ matrix, is equal to the product of n_2 and the number of nonzero entries of the F matrix involved.

(*ii*) In addition to F being sparse, other matrices as in equation (10), are sparse with predictably placed submatrices being identically 0.

(*iii*) The special form of H^{-1} of equation (9) allows profitable application of block inversion methods. This warrants further discussion. Consider equation (9):

$$\begin{bmatrix} R^{-1} & -F_{31} \\ F_{31}^T & G^{-1} \end{bmatrix}^{-1} = \begin{bmatrix} H_{11} & H_{12} \\ H_{21} & H_{22} \end{bmatrix}.$$

Both R^{-1} and G^{-1} are *diagonal* matrices and the dimension of H is $n \times n = (n_R + n_G)^2$ where n_R is the number of tree resistors in the network and n_G is the number of link resistances. A method of block inversion is chosen based on the min (n_R, n_G).

Case 1: $n_R \leqq n_G$	Case 2: $n_G > n_R$
$H_{11} = [R^{-1} + F_{31}GF_{31}^T]^{-1}$,	$H_{22} = [G^{-1} + F_{31}^T RF_{31}]^{-1}$,

$$H_{12} = H_{11}F_{31}G, \qquad H_{21} = -H_{22}F_{31}^T R,$$
$$H_{21} = -GF_{31}^T H_{11}, \qquad H_{12} = RF_{31}H_{22},$$
$$H_{22} = G - GF_{31}H_{12}. \qquad H_{11} = R + RF_{31}H_{21}.$$

In case 1, the inversion of an $n_R \times n_R$ matrix (H_{11}) is required; for case 2 the matrix to be inverted is of order n_G (H_{22}). To invert H could take n^3 multiplications. The worst case for this formulation is $n_R = n_G = n/2$, requiring $n^3/8$ multiplications. The calculation of the remaining submatrices of H involve additions, subtractions or, at worst, multiplication by diagonal matrices.

3.3 *Solution of the dc Equations*

3.3.1 *The Newton–Raphson Method and Its Limitations*

The standard Newton–Raphson solution of equation (1) is obtained as follows: For an arbitrary estimate of $\mathbf{V}$, say $\mathbf{V}^k$, equation (1) is not satisfied exactly, and there results:

$$[A][\mathbf{V}^k] + [B][\mathbf{U}] + [N(\mathbf{V}^k)] = [\mathbf{R}^k] \tag{12}$$

where the vector $[\mathbf{R}^k]$ is termed the residual vector and is, in this case, a measure of the current imbalances in the circuit that result from insisting that $[\mathbf{V}] = [\mathbf{V}^k]$. The superscript k refers to the iteration number. Successive estimates of $[\mathbf{V}]$ are formed as:

$$[\mathbf{V}^{k+1}] = [\mathbf{V}^k] + [\mathbf{P}^k] \tag{13}$$

where the step vector $[\mathbf{P}^k]$ is obtained by solution of

$$-[J(\mathbf{V}^k)][\mathbf{P}^k] = [\mathbf{R}^k]. \tag{14}$$

In equation (14), $[J(\mathbf{V}^k)]$ is the Jacobian of the system (1), viz.,

$$[J(\mathbf{V}^k)] = [A] + [N'(\mathbf{V}^k)]. \tag{15}$$

The iterations are terminated whenever either the step vector $[\mathbf{P}]$ and/or the residual vector $[\mathbf{R}]$ is sufficiently close to zero.

Straightforward application of the above iterative method to the system (1) results in several difficulties:

(*i*) If the starting guess $[\mathbf{V}^0]$ is not close to the solution, then there typically results exponential overflow in the nonlinear terms $I_S(e^{\theta V} - 1)$, since the full Newton–Raphson step may be too large in the positive direction. This may be overcome in several ways, the simplest probably being to reduce the step,[7] viz.,

$$[\mathbf{V}^{k+1}] = [\mathbf{V}^k] + S[\mathbf{P}^k] \tag{16}$$

where S is a step size, $0 < S \leqq 1$ and is chosen so that

$$\sum_i (R_i^{k+1})^2 < \sum_i (R_i^k)^2. \tag{17}$$

(*ii*) The method does not necessarily converge. Reliability can be greatly increased by the use of parameter-stepping techniques,[8] as described in the next section.

3.3.2 *Increasing Reliability Through Source-Stepping*

Newton–Raphson methods typically converge whenever the starting guess is close to the solution point. This fact was first utilized by D. F. Davidenko[9] and subsequently by various authors.[10–12] Implementation of the method in nonlinear circuit analysis can be accomplished as follows[7]: For any system (1), one accurate solution is always known, namely, $[\mathbf{V}] = 0$ if $[\mathbf{U}] = 0$. Hence, if the sources $[\mathbf{U}]$ are brought to their full value in small increments, convergence to each intermediate point is more likely.

The strategy for stepping can take on various forms (see, for example, Ref. 12); the approach taken here involves source-stepping only when necessary. If no convergence is obtained after a fixed number of iterations with the sources on full, the sources are reduced to one-half their value and solution is again attempted. If necessary, the sources are progressively reduced until convergence is obtained at some intermediate source value, whereupon solution is again attempted with the sources on full. If convergence is not obtained, the sources are again reduced to a value midway between full and the last point at which convergence was obtained. The process is repeated until convergence at the full source value is obtained.

3.3.3 *Nonlinear Scalar Transformation*

Reliability and speed of the Newton-Raphson method can also be greatly increased through the use of a nonlinear scalar transformation of variables. The transformation is an extension[13] of the notion of "charge-state-variables"[14,15] based on a suitable definition of the "capacitance" of a junction, viz.,

$$q = \int_0^v [1 + \theta K I_s \exp(\theta V)]\, dV \tag{18}$$

where (18) is a *scalar* equation. The potentials are considered to be

a function of q, i.e., $V = V(q)$, and the Newton-Raphson iteration is performed in the q-space rather than the V-space.

This is accomplished by noting that

$$[\mathbf{R}(q)] = [\mathbf{R}(V)] \tag{19}$$

and

$$[J(q)] = [J(V)][S(V)]^{-1} \tag{20}$$

where $S(V)$ is a diagonal matrix with elements of the form,

$$S_{ii} = 1 + \theta K_i I_S \exp(\theta V_i). \tag{21}$$

The Newton–Raphson step vector may be written in terms of q as

$$[\mathbf{P}(q)] = -[J(q)]^{-1}[\mathbf{R}] \tag{22}$$

which results in

$$[\mathbf{P}(q^k)] = [S(V^k)][\mathbf{P}(V^k)]. \tag{23}$$

What is required, then, is to transform the usual Newton–Raphson step vector, where now

$$[\mathbf{q}^{k+1}] = [\mathbf{q}^k] + [\mathbf{P}(q^k)]. \tag{24}$$

Since equation (23) represents a *scalar* transformation on the individual q_i , equation (24) may be written in terms of the individual elements V_i of the vector [**V**] as

$$V_i^{k+1} + K_i I_{S_i} \exp(\theta V_i^{k+1}) = V_i^k + K_i I_{S_i} \exp(\theta V_i^k) + S_i(V_i^k) P_i(V_i^k) \tag{25}$$

where

$$S_i(V_i^k) \equiv 1 + \theta K_i I_{S_i} \exp(\theta V_i^k)$$

and $P_i(V_i^k)$ is the ith element of the usual Newton–Raphson step in V. The transform parameter K_i remains to be determined.

Solution of equation (25) for each V_i^{k+1} gives the new estimate of the vector [**V**], given the standard Newton–Raphson step vector [$\mathbf{P}(V)$], which may be obtained in the usual manner. Note that (25) is a scalar equation which may be solved very simply by Newton's method, as discussed further below.

Empirical studies have shown that the speed of the iterative process is dependent on the value of K, which has the effect of "straightening out" the exponential characteristics at the expense of "warping" the linear parts of the solution space. It was determined that a good

choice for K is

$$K_i = \frac{10}{\theta I_{S_i} \exp(\theta V_i^k)}, \qquad 10^2 \leq K \leq 10^4 \tag{26}$$

which, it is believed, results in a near-optimum solution sequence.[13] The value of K varies from iteration to iteration and is different for every variable.

Once the value of K_i is determined, solution of (25) is accomplished as follows:

Set

$$D_i = V_i^k + K_i I_{S_i} \exp(\theta V_i^k) + [1 + \theta K_i I_{S_i} \exp(\theta V_i^k)] P_i(V_i^k) \tag{27}$$

where K_i is picked according to equation (26). To obtain the new estimate, V_i^{k+1}, set

$$Y_i \equiv V_i^{k+1} \tag{28}$$

and establish an iterative procedure for solution of Y as

$$Y_i^{n+1} = Y_i^n - \frac{Y_i^n + K_i I_{S_i} \exp(\theta Y^n) - D_i}{1 + \theta K_i I_{S_i} \exp(\theta Y_i^n)} \tag{29}$$

where the superscript n indicates the iteration number in the *scalar* Newton–Raphson subloop. This is done for each element of [**V**].

A first estimate, Y^0, is formed as follows.

Set

$$Z_i = -\frac{1}{\theta} \ln [K_i I_{S_i}]; \tag{30}$$

then

$$\left.\begin{aligned} &\text{if} \quad D_i \leqq Z_i + 0.08, \quad Y_i^0 = D_i, \\ &\text{and if} \quad D_i > Z_i + 0.08, \quad Y_i^0 = \frac{1}{\theta} \ln D_i + Z_i. \end{aligned}\right\} \tag{31}$$

The iterative procedure in Y_i is terminated whenever

$$\frac{|Y_i^{n+1} - Y_i^n|}{|Y_i^n|} < \epsilon \tag{32}$$

where ϵ is some suitably small constant, such as 10^{-6}.

The procedure outlined above, combined with the source stepping described in Section 3.3.2, provides an extremely powerful and rapid algorithm for solution of circuits with exponential nonlinearities. Solution for most circuits is accomplished in very few iterations (fewer than 10), so that in combination with the efficient generation of the

equations, the overall method is competitive with analysis of *linear* systems.

There is, however, one main limitation that must be dealt with as a special case. It arises from the formulation of the circuit equations and is discussed below.

3.3.4 *Treatment of Junction Cut-sets*

Whenever the circuit under consideration contains cut-sets of junctions, the matrix $[A]$ of the system (1) becomes singular. This causes severe instability problems in the solution whenever the junctions in the cut-set are not (or barely) conducting. The problem, and its solution, are best illustrated by an example.

Consider the simple circuit in Fig. 1. The system of equations describing this circuit is:

$$\begin{bmatrix} -\frac{1}{R} & -\frac{1}{R} \\ -\frac{1}{R} & -\frac{1}{R} \end{bmatrix} \begin{bmatrix} V_{D1} \\ V_{D2} \end{bmatrix} + \begin{bmatrix} -\frac{1}{R} \\ -\frac{1}{R} \end{bmatrix} [E] - \begin{bmatrix} I_{S1}[\exp(\theta V_{D1}) - 1] \\ I_{S2}[\exp(\theta V_{D2}) - 1] \end{bmatrix} = 0, \tag{33}$$

for which the Jacobian is

$$[J] = \begin{bmatrix} -\frac{1}{R} - \theta I_{S1} \exp(\theta V_{D1}) & -\frac{1}{R} \\ -\frac{1}{R} & -\frac{1}{R} - \theta I_{S2} \exp(\theta V_{D2}) \end{bmatrix} \tag{34}$$

which, by inspection, is seen to be extremely ill-conditioned whenever $\theta I_{S2} \exp(\theta V_{D2}) \ll 1/R$. The conditioning of the system can be improved by subtracting the second equation from the first in (33) to yield:

$$\begin{bmatrix} -\frac{1}{R} & -\frac{1}{R} \\ 0 & 0 \end{bmatrix} \begin{bmatrix} V_{D1} \\ V_{D2} \end{bmatrix} + \begin{bmatrix} -\frac{1}{R} \\ 0 \end{bmatrix} [E] + \begin{bmatrix} I_{S1}[\exp(\theta V_{D1}) - 1] \\ I_{S2}[\exp(\theta V_{D2}) - 1] - I_{S1}[\exp(\theta V_{D1}) - 1] \end{bmatrix} = 0, \tag{35}$$

for which the Jacobian is

$$J = \begin{bmatrix} -\frac{1}{R} - \theta I_{S1} \exp(\theta V_{D1}) & -\frac{1}{R} \\ \theta I_{S1} \exp(\theta V_{D1}) & -\theta I_{S2} \exp(\theta V_{D2}) \end{bmatrix}. \tag{36}$$

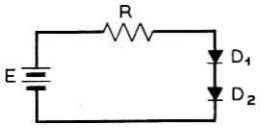

Fig. 1—Junction cut-set example.

The Jacobian shown in (36) can be scaled very simply to produce a well-behaved system.

In the above example, the treatment of the cut-set problem was determined by inspection. Junction cut-sets can be found in any network by forming the so-called "L-tree"[16] of the network and forming the fundamental loop (or cut-set) matrix. The L-tree preference order dictates that junctions be made links with all other types of elements retaining their order. The treatment is simple, once junction/ current source cut-sets are found. For each cut-set, one row of the $[A]$ and $[B]$ matrices corresponding to one of the offending junctions is set to zero. The appropriate additions and subtractions in the vector $[N(V)]$ are performed, and the system scaled. A similar procedure is used by Shichman.[14]

3.4 *Parameter Perturbation and Monte Carlo Analysis*

In addition to methods of solution of the nonlinear circuit equations, a method of statistically perturbing circuit parameters is required. The two are then combined in an overall strategy.

3.4.1 *Parameter Perturbation*

It is desired to generate correlated random variables with a fixed range, corresponding to the tolerance set by the user. Since large arrays of correlated numbers have to be generated, a parametric representation is used that correlates random variables by the use of "pivots."[1] In addition, a linear additive statistical model is used which ensures that parameters stay within tolerance. Generation of fixed interval correlated random numbers can be illustrated by a simple example:

Assume x_0, x_1 and x_2 independent, each from a distribution of mean m and variance $\sigma_{x_i}^2$. Two correlated random variables, y_1 and y_2 can be generated as

$$\begin{aligned} y_1 &= (1 - |\lambda_1|)x_1 + \lambda_1 x_0, \\ y_2 &= (1 - |\lambda_2|)x_2 + \lambda_2 x_0, \end{aligned} \tag{37}$$

where λ_1, λ_2 are tracking coefficients and x_0 is serving as a "pivot." Note that if the x_i are in the interval $(-1, 1)$, then the y_i will be in this interval also. The correlation factor ρ_{12} is easily determined,

$$\rho_{12} = \frac{E(y_1y_2) - E(y_1)E(y_2)}{\sigma y_1 \sigma y_2} \tag{38}$$

resulting in

$$\rho_{12} = \frac{\lambda_1\lambda_2\sigma_{x_0}^2 - \lambda_1\lambda_2 m_0^2}{\{[(1 - |\lambda_1|)^2\sigma_{x_1}^2 + \lambda_1^2\sigma_{x_0}^2][(1 - |\lambda_2|)^2\sigma_{x_2}^2 + \lambda_2^2\sigma_{x_0}^2]\}^{\frac{1}{2}}} \tag{39}$$

with

$$\begin{aligned} E(y_1) &= (1 - |\lambda_1|)m_1 + \lambda_1 m_0, \\ E(y_2) &= (1 - |\lambda_2|)m_2 + \lambda_2 m_0, \\ \sigma_{y_1}^2 &= (1 - |\lambda_1|)^2\sigma_{x_1}^2 - \lambda_1^2\sigma_{x_0}, \\ \sigma_{y_2}^2 &= (1 - |\lambda_2|)^2\sigma_{x_2}^2 + \lambda_2^2\sigma_{x_0}^2. \end{aligned}$$

For the special case of $\lambda_1 = \lambda_2 = \lambda$, $\sigma_{x_0}^2 = \sigma_{x_1}^2 = \sigma_{x_2}^2 = \sigma^2$ and $m_0^2 = 0$.

$$\rho_{12} = \frac{\lambda^2}{1 - 2|\lambda| + 2\lambda^2}. \tag{40}$$

The model actually used allows correlation to two pivots (or other parameters) as

$$y_i = (1 - |\lambda_i| - |\eta_i|)x_i + \lambda_i x_{01} + \eta_i x_{02} \tag{41}$$

and normalized random factors for the various parameters generated as

$$r_i = 1 + ty_i \tag{42}$$

where t is the tolerance.

The independent variables, x_i, are generated as follows: A piecewise-linear probability density *shape* is supplied by the user in the form of a table in arbitrary units for distributions other than uniform, normal or log normal which are "built in." This table is scaled and extended to include the cumulative density function which is a piecewise-quadratic on the interval $(-1, 1)$. A random variable from a uniform distribution is generated by a Tausworthe random number generator[17] and transformed to the desired distribution by quadratic interpolation from the cumulative density function. Parameter perturbations are then calculated according to equations (41) and (42). Nominal (design) values of parameters are taken to be the *median* value of their corresponding distributions.

3.4.2 *Monte Carlo Analysis*

Parameter perturbations and analysis are combined in a standard tolerance analysis loop. The nominal solution is taken as the starting guess for each random design and the solutions along with the parameter values stored on disk for later post-processing. Work is in progress to allow various other procedures (such as tuning or adjustment) in the loop.

IV. IMPLEMENTATION

The techniques and methods described in the preceding section allow fairly efficient nonlinear statistical design. The details of their implementation can, however, spell the difference between success and failure in a general-purpose program, as well as the input/output features and structure of the program. Described below are some of the more critical aspects of the design and structure of a general-purpose nonlinear tolerance analysis program for IBM series 360 computers.

4.1 *Memory Allocation*

As in any large program, there exists a conflict between efficient use of memory and speed of execution. In addition to the program itself, memory is required for the various coefficient matrices, the variables and outputs, as well as the various circuit parameters such as element values, model parameters, statistical data and topological information.

The program itself, written largely in FORTRAN-IV, is overlayed with major divisions separating (*i*) input and initial handling of data, (*ii*) generation of the various topological matrices, (*iii*) generation of the equations, (*iv*) analysis, and (*v*) output. Communication among the various overlays is via a labeled common structure. Data at input time is handled largely via fixed-dimension arrays which are then partly overwritten by run-time data during execution. Run-time data is stored in a dynamic linear array with pointers used for addressing. This data includes such arrays as the A, B, C and D matrices, the variables, the Jacobian, various tabled quantities, and so on. In this way, efficient use is made of fast-access memory in that only data that is needed is stored. At the same time, this structure does not degrade the speed of execution.

4.2 *Algorithms*

The IBM 360 series is not well suited for applications such as described

here and special care is required in the implementation of the various algorithms in addition to standard good programming practices. All floating-point computation in the program is done in double precision (8 bytes). It was found that some of the matrix-handling subroutines had to be written in Assembly language in order to achieve any efficiency at all. For example, one routine that multiplies two matrices one of which has only 0, ± 1 entries could be speeded up by a *factor* of 5–10 by direct coding in Assembly language. Assembly language coding is also required for the equation solution and matrix inversion routines.

Matrix sparsity is used to advantage in the solution of simultaneous equations as in equation (14) by column reordering[18] and stability is preserved by row-pivoting. Ill-conditioning is detected by monitoring the magnitude of the smallest pivot used in the gaussian elimination process.

Other small details in the programming are equally critical. It is of utmost importance in an application such as this to preserve as much numerical precision as possible since many mathematical steps are required before a solution is attained. For example, the analysis requires evaluation of quantities such as $I_S[\exp(\theta V) - 1]$. For values of V close to zero, a call to the exponential routine and subsequent subtraction of the constant 1 can yield an inaccurate result. For this situation, a series evaluation of the function is used.

4.3 *Data Reduction and Display*

Some care has to be taken in handling the voluminous data produced by the program. Experience has shown that it is almost impossible to determine beforehand how to analyze and display the output data, at least until a preliminary investigation of the results is available. In addition, any extensive Monte Carlo analysis of most circuits is likely to be expensive (despite the efficient algorithms) so that it becomes worthwhile developing a flexible post-processing scheme. For these reasons, the philosophy adopted here is the following:

(*i*) All output data, including parameter values of every "important" or expensive analysis, is stored in a permanent disk file for later access. This raw data may be later reduced or displayed in whatever way the user sees fit.

(*ii*) Extensive post-processing capability is available immediately following the analysis, accessed via the input language to the program. This facility allows scatter plots and histograms of any outputs or parameters to be produced on-line, including the printing out of extremal cases and various statistics. The

facility also allows separation of the data by temperature or any other parameter.

(*iii*) Hard-copy printout of *all* data is produced whether or not the user requires it. In this way an expensive run is not lost even if the disk file is destroyed. Experience has also shown that sometimes it is desired to inspect the raw data weeks after initial analysis. The hard-copy output provides this facility.

V. SAMPLE PROBLEMS

Two sample problems are presented, both of which Monte Carlo analysis has verified to be good designs. The transistor model[2] used in both examples is shown in Fig. 2. In both problems silicon resistors (including the base and collector resistances of the transistor model) were allowed to vary $\pm 15\%$ within a normal distribution truncated at $\pm 3\sigma$, with resistor values tracking to $\pm 5\%$. This is illustrated in the scatter diagram shown in Fig. 3. The intercept currents were picked from a log-normal distribution ranging from $1/4I_{S_0}$ to $4I_{S_0}$ and correlated by a factor of 0.85. The βs of the devices were picked from a triangular distribution, typically ranging from $1/2\beta_0$ to $2\beta_0$ and correlated by a factor of 0.3.

The first example, a constant current source, used in a D/A converter, is shown in Fig. 4. Resistors R1 through R4 are thin film tantalum resistors with a tolerance of $\pm 2\%$, with the exception of R4 which was assigned a tolerance of $\pm 0.5\%$. R5 represents the load and was allowed to vary $\pm 25\%$. Analysis of this circuit verified that the output current is essentially insensitive to all parameters except the power supplies and R4. A scatter plot of the output current versus the value of R4 is shown in Fig. 5 for the case where the power supplies are held fixed. Figure 6 shows a histogram of the values of output current with all parameters varying. For this case, the twelve-volt supply was assigned

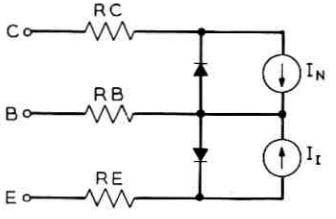

Fig. 2—Transistor model.

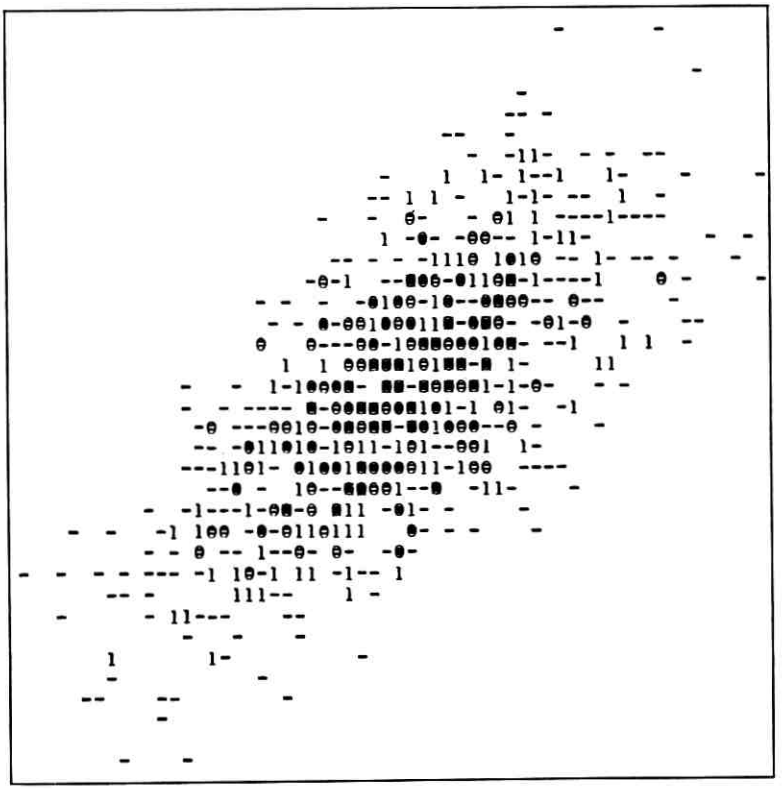

Fig. 3—Resistor correlation, range of each axis ±15%.

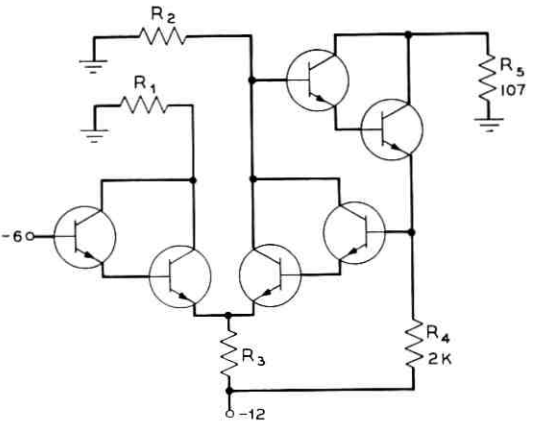

Fig. 4—Constant current source.

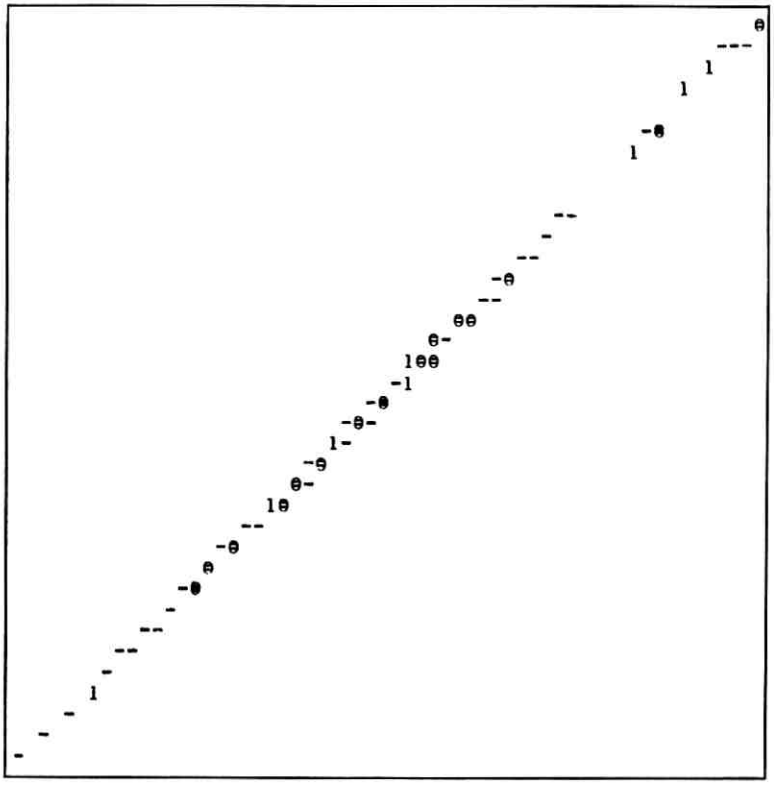

Fig. 5—Current source output (vertical axis) versus R4 (normalized).

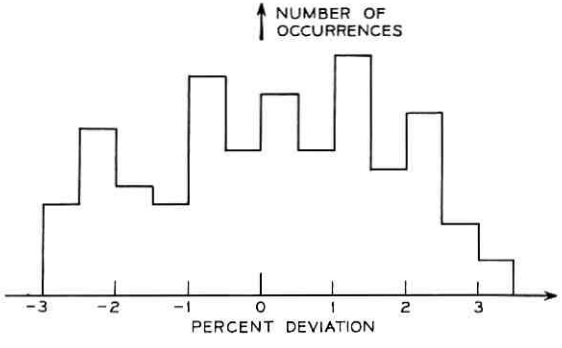

Fig. 6—Current source output with all parameters varying.

to a tolerance of $\pm 2\%$, with the six-volt supply tracking to $\pm 1\%$. Analysis time for this example was approximately one second CPU time per random design on an IBM 360/65 computer. The great majority of this time represents overhead in the form of subroutine calls, various bookkeeping operations and writing data on disk and the printer. Solutions were carried to approximately seven digits of accuracy with each random design requiring typically 3–5 iterations.

The second example shown in Fig. 7 is a silicon integrated operational amplifier designed at Bell Laboratories. Of interest in this example is the output offset voltage with the inputs grounded. In addition, minimum and maximum (worst case) currents in the collectors of T13, T14 and T16, as well as dc gain were sought. This circuit represents a rather large simulation with 48 junctions, 76 resistors, 79 nodes and 127 branches. Figure 8 shows a histogram of the output voltage at room temperature with the power supplies held fixed. The range of offsets for this circuit was found to be slightly higher than predicted by approximate hand analysis. Analysis time for this

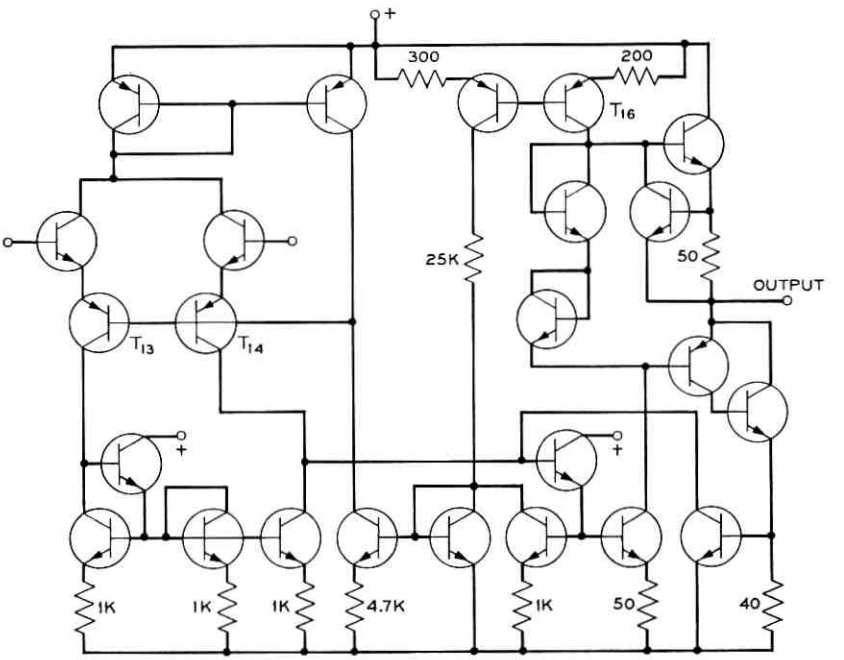

Fig. 7—Operational amplifier.

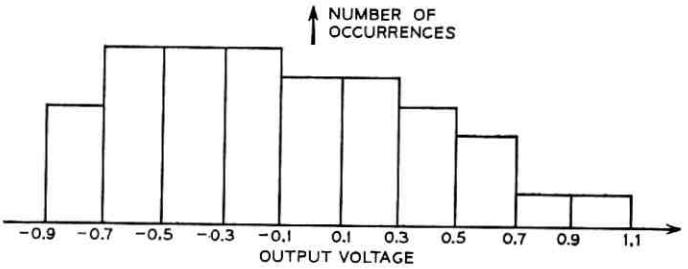

Fig. 8—Operational amplifier output offset voltage.

example was 8 seconds CPU time per statistical design, some of this time being bookkeeping overhead. It is expected that this time will be cut down considerably with some reprogramming. As in the previous example, typically 3-5 iterations were required per statistical design for a seven-digit accuracy in junction voltages.

VI. CONCLUSIONS

Analysis techniques and programming considerations have been presented that allow reasonably economical tolerance analysis of nonlinear "dc" circuits of reasonable size. Many of the ideas presented have evolved from past experience with ac tolerance analysis and will most probably be modified as experience with nonlinear statistical design becomes more plentiful. It is already apparent, however, that the trend in the near future will be to larger scale integration of circuits for which some of the present analysis techniques will likely be inadequate. Research is in progress in analysis methods capable of coping with large and complex circuits, as well as methods to make the present techniques even more efficient.

VII. ACKNOWLEDGMENTS

The authors are indebted to Mrs. H. D. Rovegno for her programming efforts in the postprocessor, and to Messrs. B. J. Karafin and R. G. Olsen for their helpful discussions.

REFERENCES

1. Balaban, P., Karafin, B. J., and Snyder, Mrs. D. B., "A Monte Carlo Tolerance Analysis of the Integrated, Single-Substrate, RC, *Touch-Tone*® Oscillator," B.S.T.J., this issue, pp. 1263–1291.

2. Logan, J., "Characterization and Modeling for Statistical Design," B.S.T.J., this issue, pp. 1105–1147.
3. Butler, E. M., "Large Change Sensitivities for Statistical Design," B.S.T.J., this issue, pp. 1209–1224.
4. Branin, F. H. Jr., "Computer Methods of Network Analysis," Proc. IEEE, *55*, No. 11 (November 1967), pp. 1787-1801.
5. Sandberg, I. W., "Theorems on the Analysis of Nonlinear Transistor Networks," B.S.T.J., *59*, No. 1 (January 1970), pp. 95–114.
6. Ebers, J. J., and Moll, J. L., "Large Signal Behavior of Junction Transistors," Proc. IRE, *42*, No. 12 (December 1954), pp. 1761–1772.
7. Broyden, C. G., "A Class of Methods for Solving Nonlinear Simultaneous Equations," Math. Comp., *19*, No. 92 (October 1965), pp. 577–93.
8. Cermak, I. A., "DC Solution of Nonlinear State-Space Equations in Circuit Analysis," IEEE Trans. on Circuit Theory, *CT 18*, No. 2 (March 1971).
9. Davidenko, D. F., "On a New Method of Numerical Solution of Systems of Nonlinear Equations," Doklady Akad. Nauk. SSSR (N.S.), *88*, No. 4 (1953), pp. 601-602.
10. Freudenstein, F., and Roth, B., "Numerical Solution of Systems of Nonlinear Equations," J. ACM, *10*, No. 4 (1963), pp. 550–556.
11. Kizner, W., "A Numerical Method for Finding Solutions of Nonlinear Equations," SIAM Journal, *12*, No. 2 (June 1964), pp. 424–428.
12. Broyden, C. G., "A New Method of Solving Simultaneous Equations," Computer Journal, *12*, No. 1 (1969), pp. 94–99.
13. Cermak, I. A., to be published.
14. Sandberg, I. W., "Some Theorems on the Dynamic Response of Nonlinear Transistor Networks," B.S.T.J., *48*, No. 1 (January 1969), pp. 35–54.
15. Shichman, H. "The Analysis of a Class of Nonlinear Networks," Ph.D. Thesis, Stevens Institute of Technology, Hobroken, N. J., September 1970.
16. Sedore, S. R., "SCEPTRE: A Program for Automatic Network Analysis," IBM Journal of Research and Development, November 1967, p. 627.
17. Payne, W. H., "FORTRAN Tausworthe Pseudorandom Number Generator," Comm. ACM, *13*, No. 1 (January 1970), p. 57.
18. Tewarson, R. P., "On the Product Form of Inverses of Sparse Matrices," SIAM Rev., *8*, No. 3 (July 1966), pp. 336–342.

THE BELL SYSTEM TECHNICAL JOURNAL
Vol. 50, No. 4, April, 1971
Printed in U.S.A.

Statistical Circuit Design:

Confirmation of Design Using Computer-Controlled Test Sets

By G. D. HAYNIE and S. YANG

(Manuscript received December 1, 1970)

The ability to evaluate the performance of linear network elements used in complex systems is vital to effective optimization and verification of the system design.

Measuring systems controlled by digital computers provide a new capability for linking the steps of network design, breadboard development and characterization, and factory test in such a way that the networks produced will more nearly meet the requirements of the systems in which they are used. This linkage is effected by incorporating in the measuring system the algorithms relating the measured quantities to the system performance parameters used during the design stage.

Output of the system performance parameters in real time provides a powerful aid for debugging development models and a more valid basis for accepting or rejecting product in factory tests. Statistical analysis is used as an aid in setting test limits by evaluating the relationships between component tolerances, measurement errors and the calculated system performance parameter.

I. INTRODUCTION

Communication systems, both analog and digital, often use linear networks to which system performance is highly sensitive. In cases where the relationship between network characteristics and system performance are complex, computers are being increasingly used for network and systems design. Examples of such designs are given in other papers in this issue. The design process is not completed until the design intent is verified, first by measurements of the breadboard models and finally by measurements of the manufactured networks.

When a physical network is to be evaluated, direct measurement of its effect on system performance requires having a system available

as a test instrument. To be a satisfactory test, one would also require that the physical system represent all necessary worst cases. This approach has been used, but it has inherent difficulties such as the difficulty in obtaining a nominal or worst-case system, the difficulty in maintaining the system, and the lack of information on a network that has failed a test.

These difficulties are largely overcome with the test method described in this paper. Using this method, the network is measured on a general purpose test set controlled by a computer. From these measurements of the network, parameters are calculated which predict the performance of the network in a system and which provide direct information about the network. The sections which follow give examples of such tests and the steps necessary to implement the tests and establish their validity.

II. IMPLEMENTATION OF TESTS

With the general purpose computer operated test set, we evaluate the linear network parameters from insertion loss and phase data produced by the network when measured in a suitable connection. In many cases, the linear parameter used for network synthesis can be directly measured. In other cases, a transformation of the insertion loss and phase data is required.[1]

As suggested in the introduction, the relationship between loss and phase measurements and system performance with the network inserted can be quite complex. In fact, examples exist where setting limits on insertion loss and phase (based on component tolerances) rather than system performance causes "good" networks to be rejected and "bad" networks to be accepted. Output of the system performance in real time provides a more valid basis for accepting or rejecting networks in factory tests and provides a powerful aid for debugging breadboard models during development.

What is needed to implement the system performance test then is a computational link between system performance and network loss and phase. Fortunately, this link has essentially been established in those cases where network synthesis, optimization, or tolerance analysis were done on a computer using system performance as the design goal. What remains is to extract the required computation section of the design program, put it on the test set computer, and couple it to the measurement program through a common set of parameters.

After the system performance test is implemented, we must establish

its validity. A lack of exact correspondence between the on-line measurements and actual system performance with the network inserted is caused by:

(*i*) uncertainties in the linear measurement, and
(*ii*) error multiplication in the system parameter calculation.

Uncertainties in the linear measurement are a function of such quantities as test frequency, insertion loss, and measurement averaging time. These uncertainties can be reliably predicted. Errors in the system parameter calculation could in theory be determined by experiment (measurement) but this would be very time consuming and worst-case values would be difficult to obtain. The framework used in the Tolerance Analysis Program is a convenient tool for providing a statistical model of the relationship between measured system performance and actual system performance. This is discussed in more detail in Section V.

The next section will describe, in some detail, the implementation of a test for digital (D2) channel bank filter.

III. D2 CHANNEL BANK FILTER TEST

The D2 Channel Bank is used for time division multiplexing and demultiplexing in a pulse code modulation transmission system.[2] The two filters being tested are linear networks operating in series with a periodically operated switch. In the design stage, filter component values were optimized to meet requirements imposed on the tandem combination of filter and switch, i.e., "switched transfer function." Historically, acceptance of the filter would be based on measurements of insertion loss under continuous excitation. However, computer studies by E. M. Butler[3] point to the possibility of passing bad product (i.e., failed STF test) and rejecting good product (i.e., passed STF test) when using the insertion loss test. Figure 1 shows the results

INSERTION LOSS:	SWITCHED TRANSFER FUNCTION	
	PASS	FAIL
PASS	88.5%	0
FAIL	9.5%	2.0%

2% TOLERANCES

INSERTION LOSS:	SWITCHED TRANSFER FUNCTION	
	PASS	FAIL
PASS	66.5%	1%
FAIL	19.5%	13%

3% TOLERANCES

Fig. 1—Comparisons between switched transfer function and insertion loss tests.

of Butler's studies for the demultiplex filter when all network elements are deviated from nominal with uniform distributions of ±2 percent and ±3 percent. Note that in the 2 percent case, 9.5 percent of the good product fails the insertion loss test. In the 3 percent case, 1 percent of the bad product passes the insertion loss test. Even though the correspondence between the two tests improves for the tighter tolerances actually used in the system, the conclusion is reached that a proper filter acceptance test must be based directly on the switched transfer function (STF).

3.1 *General Approach*

Figure 2 shows the configuration of the switched filters used in the D2 system. Two different approaches are available for calculating the STF of the filters. The state variable method of F. R. Mastromonaco and M. L. Liou[4,5] can give us exact solutions but require exact knowledge of the network topology and element values including all parasitic elements. The other approach, used by W. R. Bennett,[6] C. A. Desoer,[7] T. H. Crowley,[8] M. R. Aaron,[9] and P. E. Fleischer,[10] expresses the STF as a function of z parameters of the network. Z parameters can be easily derived from loss and phase measurements at the terminals of the network. The value of a capacitor in the network is also required, but this too is readily obtained.

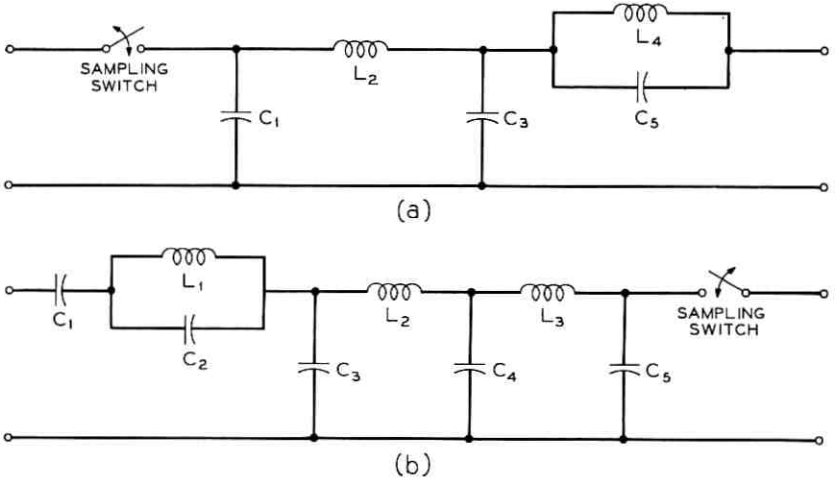

Fig. 2—Switched filters for pulse code modulation transmission system. (a) Demultiplex network. (b) Multiplex network.

The STF of the demultiplex filter, $H_d(j\omega)$, and the STF of the multiplex filter, $H_m(j\omega)$, are expressed by Fleischer as:

$$H_d(j\omega) = \frac{H_m(j\omega)}{\frac{T}{RC}} = \frac{z_{12}(j\omega)}{\frac{T}{2C} + \sum_{k=-\infty}^{+\infty} z_{11}\left(j\omega + jk\frac{2\pi}{T}\right)} \tag{1}$$

where: T = period of switching frequency,
C = input capacitance, and
R = source impedance of multiplexer.

An approximation to the equation above is given by Fleischer as:

$$H_d(j\omega) = \frac{H_m(j\omega)}{\frac{T}{RC}}$$

$$\doteq \frac{z_{12}(j\omega)}{\frac{T}{2C} + \sum_{k=-1}^{+1} z_{11}\left(j\omega + jk\frac{2\pi}{T}\right) + j\frac{0.645T}{\pi C}\left(\frac{\omega T}{2\pi}\right)\left[1+0.127\left(\frac{\omega T}{2\pi}\right)^2\right]}. \tag{2}$$

Since the STF formulation used for the filter test [equation (2)] gives only approximate results, it was important to confirm the accuracy of the approximation. Results from equations (1) and (2) were compared with results of calculations using the state variable method of M. L. Liou. This comparison between the three methods showed a maximum discrepancy of 0.0049 dB in the passband and 0.029 dB in the reject band.

3.2 *Measurement Method*

To perform the calculation indicated by equation (2), three values of z_{11} and one value of z_{12} are required for each frequency at which STF is to be calculated. Referring to Fig. 3 and for the case where $I_2 = 0$,

$$V_1 = z_{11}I_1 ,$$

$$V_2 = z_{12}I_1 .$$

Hence:

$$z_{12} = \frac{V_2}{V_1} z_{11} ,$$

also,

$$\frac{V_1}{E_0} = \frac{z_{11}}{z_{11} + R_1}$$

and

$$z_{11} = R_1 \frac{V_1/E_0}{1 - V_1/E_0}.$$

The value of capacitance C_1 (Fig. 2a) must also be known. This is determined by measuring z_{11} as just described at a frequency where the series inductance L2 is in resonance with its distributed capacity so that the remainder of the circuit is virtually disconnected. At the resonant frequency, ω_r,

$$C_1 = \frac{1}{j\omega_r z_{11}(\omega_r)} = \frac{1 - (V_1/E_0)}{j\omega_r R_1 V_1/E_0}.$$

The measurements of C_1, z_{12}, and z_{11} are implemented by automatically switching a high impedance probe to measure V_1/E_0 and V_2/V_1 at the appropriate frequencies.

3.3 *Validation of STF Test*

The STF test is validated by reviewing the factors contributing to error in the STF measurement and performing tests to gain assurance that the net error is small.

3.3.1 *Determination of Capacitance*

The value of capacitance obtained by measuring $z_{11}(\omega)$ is shown on Fig. 4 together with the values obtained from measurements on an admittance bridge. The discrepancy in the two values was less than 0.2 percent and perturbs the STF by less than 0.008 dB in the passband. The reproducibility of the measurement of C_1 is better than 0.5 percent.

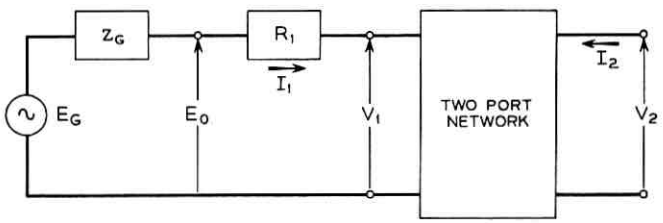

Fig. 3—Basic test configuration.

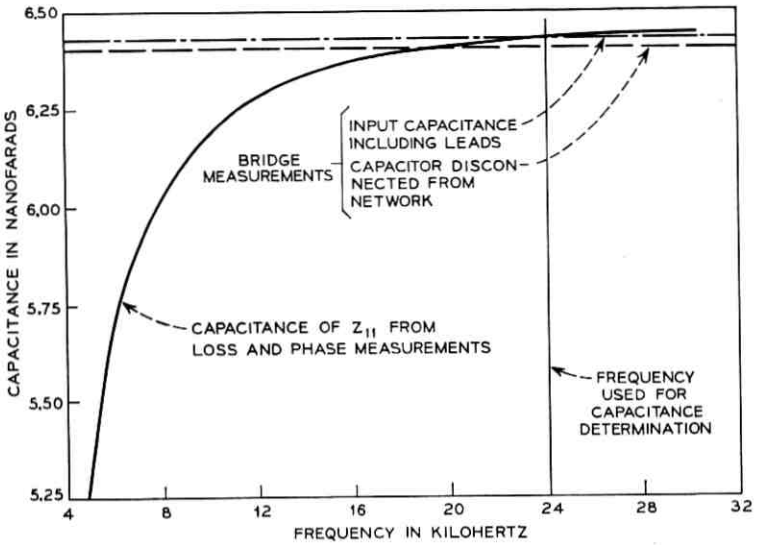

Fig. 4—Determination of filter input capacitance.

3.3.2 *Probe Errors*

After optimizing levels for the best tradeoff between probe noise and linearity, the linearity errors in the probe were measured to be less than 0.01 dB and errors from probe noise were less than 0.1 dB in the STF reject band. Loading errors from the finite probe input impedance were considered and were estimated to introduce less than 0.01 dB error in the STF passband.

3.3.3 *Accuracy of z_{11} and z_{12} Measurements*

Admittance measurements were made on a demultiplex filter using an admittance bridge capable of ±0.1 percent accuracy. From these measurements z_{11} and z_{12} were evaluated and compared with values obtained from loss and phase measurements and agreement is within 0.4 percent. When bridge measurements are made directly on the individual components of the filter and STF is calculated, the discrepancy with the STF obtained from loss and phase measurements is as large as 0.05 dB in the passband. Much of this difference is due to errors in the circuit model used in calculating z parameters.

3.4 *Sensitivity of STF to Loss and Phase Measurement Errors*

The Tolerance Analysis Program (TAP)[11] was used to determine the "amplification" of measurement errors inherent in the computation of STF from loss and phase data. Figure 5 gives the results for a

demultiplex filter in which errors in each measurement (V_1/E_0, V_2/V_1 in Fig. 3) were assumed to be 0.03 dB and 0.2° with the sign of the error randomly chosen. This run included 17,500 cases and virtually 100 percent of the STF loss values lie within ±0.1 dB of the correct value. We also note that a 0.3 percent error in loss and phase (0.03 dB, 0.2°) has been amplified to a 1 percent error in STF. In a second run, loss and phase errors 1/3 as great produced errors in STF 1/3 as great. Similar results were obtained at other passband frequencies where TAP runs were made. Slightly greater spreads were observed in the filter reject region, but the differences were not significant.

3.5 *Summary of D2 Test*

The STF test on the computer operated test set provides a more valid acceptance test of the D2 multiplex and demultiplex filters than the insertion loss tests commonly used for filters of this type. The STF

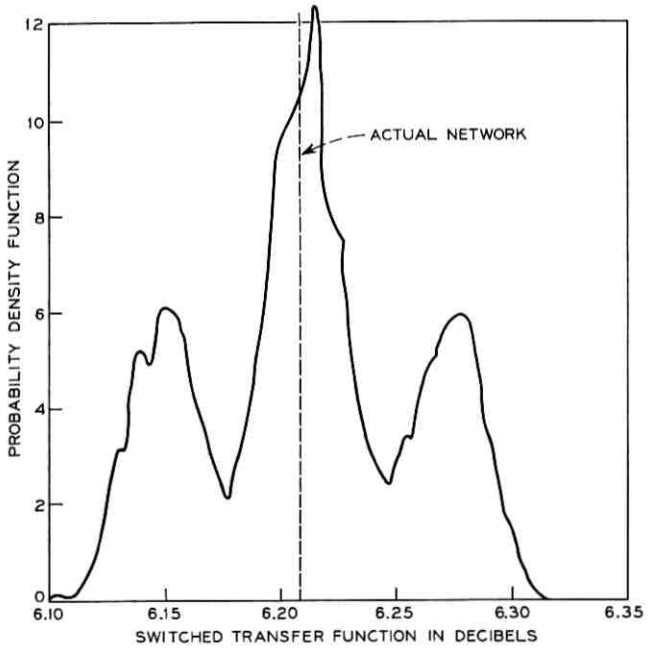

Fig. 5—Distribution of STF loss measurements for 0.3 percent errors in loss and phase. (17,500 samples; measurement error, ±0.03 dB and ±0.2°; frequency, 2.2 kHz.)

is measured with a passband error of less than 0.05 dB and an error of less than 0.2 dB in the reject band. Using computer controlled relays for switching the measuring probe, the STF measurement at 1, 2, 3, 4, and 5 kHz is obtained in 14 seconds.

IV. T2 DIGITAL SYSTEM EQUALIZER TEST

The design evolution of the T2 equalizer is covered elsewhere in this issue.[12] This digital system network provides a potent example of design criteria having a very complex relationship to loss and phase measurements. In the T2 equalizer test used during development, insertion loss and phase measurements were transformed to pulse response, eye opening, and error rate for a system section having varying cable lengths and varying cable temperature. The program to effect this transformation was essentially the same program used for the equalizer design. In the T2 factory test, eye opening was chosen as the test parameter, and the original program was modified somewhat to reduce the program size and running time.

The results of a TAP analysis on the eye opening measurement and some verification by analytical techniques show that, for a nominal network, errors of ± 0.1 percent in loss and phase cause a variation of ± 0.3 percent in the eye pattern. In the test program used, measurement precision is controlled to ± 0.1 percent or better and the eye pattern is evaluated for 3 cases of cable length and temperature in about 1.5 minutes.

V. SETTING LIMITS ON FACTORY TESTS

In the two TAP analyses previously described, the effects of measurement errors on the calculated STF and eye opening were considered for the nominal network only. In the actual factory environment, we also have the statistical variation of the networks themselves resulting from component variations. To establish the limits of acceptance in the factory test, a two-stage TAP analysis is used.

In the first step, network components are varied according to expected statistical distributions and the maximum and minimum of the system performance parameter is determined. The output from this step is the loss and phase values associated with the nominal network and with the networks producing the upper and lower limits of the system performance parameter.

In the second step, 3 TAP runs are made using the appropriate statistical variations in measured loss and phase (these depend on net-

work loss). The output here is three distributions of system performance parameter. Figure 6 gives the results for the D2 demultiplex filter. This analysis provides a model of the distribution of measurements to be expected in the factory with the assumed design and shows the relationship between design limits and test limits. Note that a requirement of 100 percent yield on the network would mean that these limits must lie within the system requirements.

There is one tradeoff that should be mentioned. If one is concerned with a minimum cost network, the cost of testing with higher or lower accuracy must be compared with the cost of decreasing or increasing the component tolerances. Two possible conditions are indicated in Fig. 7.

VI. DISCUSSION AND SUMMARY

In the past, test requirements on networks used in systems have not necessarily been optimum from the standpoint of system per-

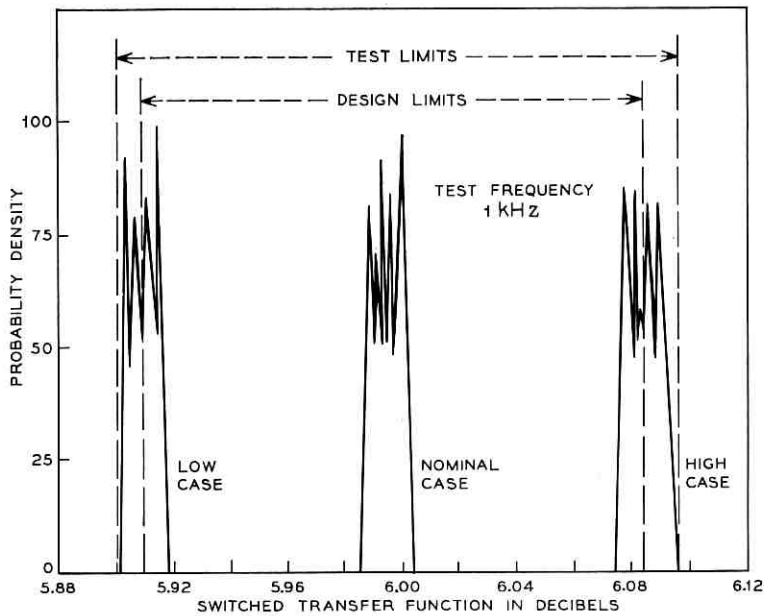

Fig. 6—Distribution of STF loss measurements for D2 filters with lowest loss, nominal loss, and highest loss.

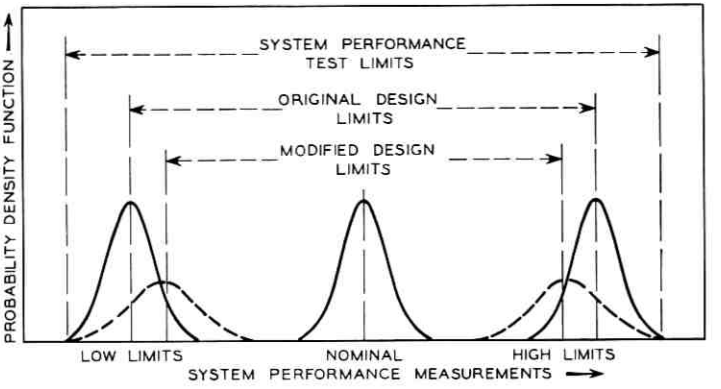

Fig. 7—Relation between measurement accuracy and design limits. (_____ original measurement accuracy; _ _ _ _ lower measurement accuracy.)

formance or network cost. The test requirements have depended on such things as the availability of test equipment and the confidence in the knowledge of relationships between network characteristics and system performance. Analysis tools to determine yield or tradeoffs between component and test costs were not available. If special test equipment was needed, delays for development of test equipment were incurred and development tests and factory tests were often different.

The test method described in this paper provides a flexible and accurate method of evaluating linear networks on general purpose test sets in terms of parameters that are meaningful to the system designer. The approach fits in conveniently with techniques used during the design phase and makes use of software developed in that phase. This makes possible, in cases where the designer and the manufacturer have compatible measuring sets, very rapid startup of factory tests and convenient intercomparison of data. The TAP analysis used to set test set limits provides an analytical tool for use in comparing costs related to components, testing, and yield.

VII. ACKNOWLEDGMENT

The authors are indebted to Mr. E. M. Butler whose work in statistical design techniques pinpointed the shortcomings of insertion loss tests for characterizing switched filters and whose TAP computer program greatly expedited the task of verifying the filter tests described in Section III.

REFERENCES

1. Evans, J. G., "Measuring Frequency Characteristics of Linear Two-Port Networks Automatically," B.S.T.J., *48,* No. 5 (May–June 1969), pp. 1313–1338.
2. Saal, F. A., "D-2; Another Step Toward Nationwide Digital Transmission," Bell Laboratories Record, *47,* No. 10 (November 1969), pp. 327–329.
3. Butler, E. M., unpublished work.
4. Liou, M. L., and Mastromonoco, F. R., unpublished work.
5. Liou, M. L., McDonald, Mrs. P. H., and Phelen, W., "Computer Optimization of Active and Passive Switched Low Pass Filters for PCM Systems," Proc. 20th Elec. Component Conf., May 13–15, 1970, Washington, D. C., pp. 301–306.
6. Bennett, W. R., "Steady-State Transmission Through Network Containing Periodically Operated Switches," IRE Trans., *PGCT-2,* No. 1 (March 1955), pp. 17–22.
7. Desoer, C. A., "A Network Containing a Periodically Operated Switch Solved by Successive Approximations," B.S.T.J., *36,* No. 6 (November 1957), pp. 1403–1438.
8. Crowley, T. H., unpublished work.
9. Aaron, M. R., unpublished work.
10. Fleischer, P. E., unpublished work.
11. Bohling, D. M., and O'Neill, L. A., "An Interactive Computer Approach to Tolerance Analysis," IEEE Trans. Computers, *C-19,* No. 1 (January 1970), pp. 10–16.
12. O'Neill, L. A., "A Case Study of the Use of Computer Aids in Circuit Design—Pulse Equalizers for the T2 Digital Transmission Line," B.S.T.J., this issue, pp. 1243–1262.

THE BELL SYSTEM TECHNICAL JOURNAL
Vol. 50, No. 4, April, 1971
Printed in U.S.A.

Statistical Circuit Design:

Large Change Sensitivities for Statistical Design

By E. M. BUTLER §

(Manuscript received November 25, 1970)

A Monte Carlo study is an analysis in the sense that for specified tolerances, correlations, etc., empiric distributions of measures of performance are obtained. An approach is presented which addresses itself to the inverse problem, that of determining the tolerances, correlations, etc., necessary to realize acceptable performance distributions. The approach is based on the concept of large change sensitivities which are proposed as a measure of sensitivity for statistical design. The approach specifically addresses design problems such as specifying tolerances, desensitizing a nominal design, recognizing the possibilities for and specifying tuning and/or matching procedures, and verifying that a design is consistent with expected statistical correlation between parameters. We present an example illustrating several of these applications.

I. INTRODUCTION

Realistic system and circuit design must account for the fact that exact realizations of paper designs are seldom achieved. The Bell System is particularly sensitive to this problem not only because of physical and economic constraints in manufacture, but also because of the varied field environments in which the system must operate. The effects of variations in design parameters, which are usually modeled as random variables, can be investigated via a Monte Carlo study. However, a Monte Carlo study is an analysis in the sense that for specified probability density functions of design parameters (specified by "nominal" value, tolerance, correlation, etc.) an empirical distribution for various outputs or performance measures is found. The inverse problem, that of finding nominal values, tolerances, and correlation in order to obtain an acceptable performance distribution, has received

relatively little attention. This paper describes an approach addressed to this problem of "closing the loop around tolerance analysis." *

There are three significant points about this approach. First, the approach does not rely on first- or second-order approximations.† Like Monte Carlo, no attempt is made to approximate measures of performance. Second, the approach can accommodate multiple-specifications. Third, the implementation of the approach is feasible with a computer and so the techniques may be thought of as computer aids to statistical design.

The approach is based on four assumptions.

(*i*) There exists a designer-specified scalar performance criterion, J, which adequately reflects the goodness of a design and which is a continuous function of the design parameters. A method for forming a single criterion from many criteria is illustrated in the examples.

(*ii*) There is a designer-specified value of this criterion beyond which designs are not acceptable.

(*iii*) There is a known nominal design which is acceptable in terms of the performance criterion.

Definition: The region of acceptability, R_A, is defined to be a connected region in parameter space such that the nominal design is in R_A and such that for all realizations in R_A the corresponding performance is acceptable.

Finally, we make a fourth assumption.

(*iv*) All realizations inside R_A are equally good; i.e., a pass/fail decision can be made for each realization.

These ideas are illustrated in the one parameter, two criterion example in Fig. 1 where J_i is the scalar value of the ith performance criterion, p^0 is the nominal design parameter value, J_i^0 is the ith performance at nominal and ϵ_i is the allowable degradation in J_i from J_i^0.‡ Since there is more than one specification which must be met, the region of acceptability, R_A, is the intersection of the individual regions of acceptability for each J_i. In this example, R_A is $[p \mid a \leqq p \leqq b]$.

---

* Some of the information in this paper has appeared elsewhere.[1] It is included here in the interest of completeness.

† There have been suggestions in control theory to eschew first-order sensitivities, but the proposed concepts have been difficult to realize.[2–4]

‡ The superscript ^{0} denotes nominal value. A method for forming a single criterion from many criteria is illustrated in the examples.

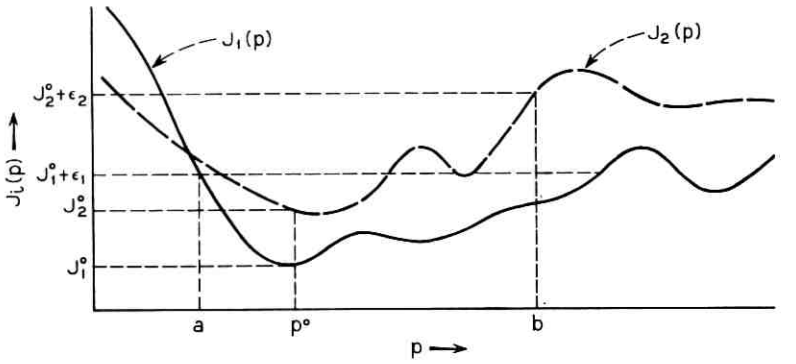

Fig. 1—A one-dimensional example.

Under the above assumptions, the region of acceptability is clearly important in the context of statistical design, that is, in specifying nominal values, tolerances, etc. In fact, it is the shape of this region and the placement of the nominal in it rather than the value of the performance at nominal that is important. For example, if the random deviations in the realization of p in the above example were uniformly distributed and symmetric about the nominal, then a nominal design located half way between points a and b would be better than p^0 in terms of yield and/or allowable tolerance. Furthermore, in this context of statistical design the concept of sensitivity takes on a new meaning which is introduced in Section II. Applications of this sensitivity information to closing the loop in tolerance analysis are discussed in Section III and an example is given in Section IV.

II. LARGE CHANGE SENSITIVITY

2.1 *Intercepts*

Suppose that we hold all parameters fixed at nominal except the kth. We define the upper (lower) intercept of parameter k to be the value in percent deviation from nominal of parameter k for which the performance is unacceptable for the first time as parameter k is increased (decreased) from nominal. Parameter values are expressed in percent deviation from nominal for reasonable scaling. Points b and a are the upper and lower intercepts for the one parameter example of Fig. 1. We denote these intercepts by

$I_k^+(J, \mathbf{p}^0, \epsilon) \equiv I_k^+ \equiv$ upper intercept of parameter k with respect to performance criterion J, nominal design $\mathbf{p}^0$, and allowable performance degradation ϵ.*

Similar notation holds for I_k^-.

The intercepts are simply a measure of how far a single parameter can deviate within the region of acceptability. If the kth intercepts are small, then being in R_A is very "sensitive" to the kth parameter, and vice versa. Using this observation as motivation, the following measure of sensitivity is proposed.

$L_k^+(J, \mathbf{p}^0, \epsilon) = L_k^+ =$ upper large change sensitivity of parameter k with respect to J, $\mathbf{p}^0$ and ϵ.

$$\triangleq \frac{1}{I_k^+}.$$

Similarly,

$$L_k^- \triangleq \frac{-1}{I_k^-}.$$

A single large change sensitivity for parameter k can be defined as the maximum of $[L_k^+, L_k^-]$.

2.2 *Performance Contours*

The intercepts provide information about how far a single parameter can vary while all others are fixed at nominal before the specifications are not met. This idea can be extended to two parameters. For a pair of design parameters, a line (or lines) of constant, just acceptable performance provides an indication about how the two parameters can vary simultaneously around nominal before specifications are not met. In fact, a *performance contour* for a pair of parameters is defined to be this line (or lines) which describes the edge of R_A restricted to the two-dimensional subspace defined by these parameters, while all other parameters are held fixed at nominal. Again, each parameter value is specified in terms of percent deviation from its nominal value.

The concept of a performance contour can be illustrated with a simple example. Consider the two parameter voltage divider shown in Fig. 2 where $R_1^0 = R_2^0 = 1$. The transfer function, T, is given by

$$T = 1/(R_1/R_2 + 1), \qquad T^0 = 0.5;$$

the input resistance, R, is given by $R = R_1 + R_2$, $R^0 = 2$.

* Bold face letters denote vector quantities.

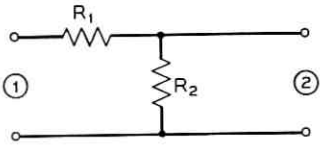

Fig. 2—A voltage divider example.

Suppose the design specifications call for $0.49 \leqq T \leqq 0.51$ and $1.8 \leqq R \leqq 2.2$. The region around nominal where the first specification is met is the shaded area in Fig. 3 and the region where the second specification is met is the cross-hatched area. The region where both specifications are met is the intersection of these regions. The edge of this acceptable region is the performance contour. The points where the contour crosses the axes are the intercepts.

Notice that the performance contour has sharp corners because of the multiple design specifications. The particular specification which determines an intercept or a section of a performance contour is said to be dominant at that point or points. For example, the upper left part of the contour in Fig. 3 is determined by the $T \leqq 0.51$ specification.

A performance contour can be interpreted as providing "second-

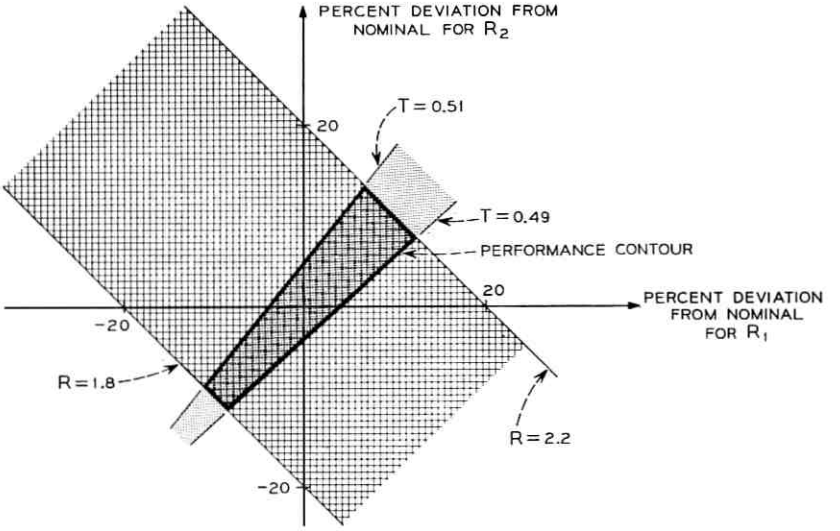

Fig. 3—Performance contour for the voltage divider example.

order" large change sensitivity information since it indicates how L^+ and L^- for one parameter will change for a change in the nominal value of the second parameter.

2.3 *Comparison with Classical Sensitivities*

One can argue that large change sensitivities are similar to first-order sensitivities in the sense that only one parameter is varied while others are held fixed. There is, however, a fundamental difference in approach. The latter sensitivities are proportional to the change in performance due to similar changes in the individual parameters. The large change sensitivities, on the other hand, are based on the change necessary in each parameter to bring about a particular (but similar) change in performance. Finally, it should be noted that if J is a linear function of the parameters, the two sensitivities are similar. This lends credence to the definition of large change sensitivity as proportional to the inverse of the intercepts.

It is interesting to note that large change and classical sensitivities each provide a characterization. The intercepts and performance contours (first- and second-order large change sensitivities) provide a characterization of R_A in one and two dimensions in parameter space, while the first two terms in a Taylor series of performance about nominal (first- and second-order classical sensitivities) provide a characterization of the performance near nominal. In statistical design, attention is (or should be) focused on R_A rather than on the performance at nominal. The large change sensitivities provide a characterization of R_A, and hence, a measure of parameter sensitivity for statistical design.

III. APPLICATIONS

3.1 *Preliminary Remarks*

Information provided by large change sensitivities can enhance a designer's insight into a problem. This can be especially important when complicated specifications exist and intuition becomes hard pressed. One might question the amount of useful information derivable from performance contours since they represent R_A for only pairs of parameters. It should be pointed out, however, that electrical properties tend to depend on parameters in pairs such as RC products and resistor ratios.

In this section, several specific applications of large change sensitivity information to design problems are discussed. The problems

which are addressed include desensitizing a nominal design, specifying tolerances, recognizing the need for and specifying tuning and/or matching, and verifying that a design is consistent with known statistical correlation or tracking.

3.2 *Desensitizing a Design*

3.2.1 *The Problem*

We have seen in the example of Fig. 1 that the design could tolerate larger parameter variations from nominal if the nominal were centered in R_A. That is, we could desensitize (in a large change sense) the design by placing the nominal half-way between the intercepts rather than at p^0. We extend this notion to N dimensions and base our measure of being centered in R_A on the intercepts, or equivalently, on the large change sensitivities.

We have investigated an algorithm to automatically desensitize an initial design which satisfies the performance specifications but is not necessarily centered. Two pertinent observations which influenced the formulation of our algorithm are:

(*i*) If we change the nominal values of more than one parameter simultaneously in an attempt to center based only on intercept information, it is possible to move outside of R_A inadvertently. Consider the hypothetical two-parameter example described by its performance contour in Fig. 4. If we center both p_1 and p_2

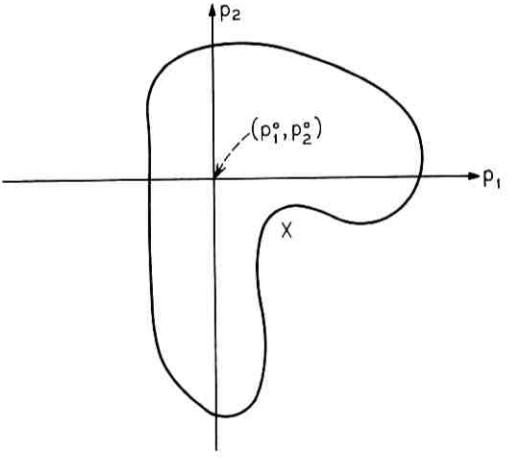

Fig. 4—Performance contour for a hypothetical two-parameter example.

simultaneously based on the intercepts at point (p_1^0, p_2^0), we move to point X which is outside R_A.

(*ii*) The intercepts for a particular parameter are simple functions of that parameter's nominal value, but they can be complicated, even noncontinuous functions of the nominal values of other parameters. For example, in Fig. 4 the upper intercept of parameter 1 (for $p_1 = p_1^0$) is not a continuous function of p_2.

3.2.2 *An Algorithm for Desensitizing*

In view of the above comments, it was decided to iterate towards a desensitized design by changing only one nominal at a time using a simple algorithm. We have taken as our measure of being centered,

$$E(\mathbf{p}) \equiv \max_i |I_i^+(J, \mathbf{p}, \epsilon) + I_i^-(J, \mathbf{p}, \epsilon)| \equiv \max_i e_i ,$$

$$\equiv | I_M^+ + I_M^- | .*$$

Suppose we start at $\mathbf{p}$ and that the error, $E(\mathbf{p}) = E$, is attributable to parameter k, i.e., $M = k$. Let us call p_k the "worst offender." First, we center parameter k and compute the new error $E(\mathbf{p}') = E'$. Note that centering p_k insures $e_k = 0$, but the intercepts for the other parameters can, and probably will, change. If E' is less than E, $\mathbf{p}'$ becomes our new starting point with error E', and we then center that parameter which is the current worst offender. (It cannot be p_k since p_k is centered.) If E' is not less than E, it means that centering p_k has altered the other intercepts enough to cause a larger error. We thus step p_k back half-way between its present value and its original value, and again compute the error. This process continues until a lower error has been found or until p_k has been stepped back seven times at which point the error is accepted and the algorithm starts over. Note that if this happens the worst offender will not be parameter k.

This algorithm has been implemented in a computer program called XCENTRIC (Experimental Centering Program) and some results will be given in Section IV. No claims are made about convergence of the algorithm; rather, its strength lies in its simplicity.

3.3 *Specifying Tolerances*

Typical approaches to specifying tolerances in the past have been either to set tolerances roughly inversely proportional to first-order

* We have assumed symmetry in the probability density function for p_i. This is not necessary since one can weight the intercepts accordingly. For example, if the density function for p_i were rectangular with twice as much probability above nominal as below, one could set e_i proportional to $(I_i^+ + 2I_i^-)$.

sensitivities or to set them to the tightest available. The former approach requires linear approximations while the latter can be unnecessarily expensive. The intercepts and performance contours provide a designer with information about how far parameters can deviate and stay within R_A. This is what a designer really needs to better specify tolerances. Furthermore, if 100 percent yield is desired, the intercepts and contours provide upper bounds and pairwise constraints respectively on feasible parameter tolerances. This fact has been utilized to help solve a version of the minimum cost tolerance specification problem; the method and results are presented in another paper in this issue.[5]

3.4 *Parameter Correlation with Respect to the Performance Specifications*

Consider again the performance contour shown in Fig. 3 for the voltage divider example. The shape is an indication that the two resistors are "correlated" with respect to the design specifications. Two parameters are qualitatively defined to be correlated with respect to the performance specification if the region of acceptability for one parameter (specified by its intercepts) depends strongly on the value of the second parameter. If the contour were rectangular and parallel to the axes, the two parameters would be uncorrelated. This correlation information can be useful in two ways.

First, a design may be evaluated by determining whether parameter correlation with respect to the performance specifications is consistent with statistical parameter correlations. A design should be insensitive to, and in fact, it should take advantage of known statistical correlation. For example, it would be desirable if R_1 and R_2 in the voltage divider example tracked each other (or could be chosen to track) because of manufacture and/or environment. In addition, it is suggested that if one is investigating a design with statistical correlation between many parameters, it might be advantageous to find intercepts and contours for the independent and correlation determining random variables since they are really the design parameters.

Second, problems of specifying tuning or matching are inherently linked to the tolerance specification problem; parameter correlation with respect to performance specifications is an indication that tuning or matching might be desirable. In addition, the contour information can indicate how to match parameters and/or the specification to which to tune. In the case of tuning, the constraint which is dominant along the "long" side of the contour is the criterion to which to tune. In the voltage divider example this would be the transfer function specifica-

tion. For the case of matching, correlation can indicate that the performance specifications depend strongly on, or are most sensitive to, a particular combination of the two parameters such as their ratio. Properties of performance contours which relate certain correlated contour shapes to particular combinations of the two parameters are given elsewhere.[1] However, two of the more important properties are stated in the Appendix. Design parameters presumably would be matched according to the particular combination. For example, the contour for the voltage divider lies along and contains the 45° line and so one should consider matching the ratio of the two resistors to their nominal ratio (see Section A.2). Finally, it should be pointed out that the contour information can be used to suggest sequential tuning or matching procedures since contours for a tuned or matched design might suggest further tuning or matching.

3.5 *Computation of Performance Contours*

A program, CONTOUR, has been written to compute intercepts and performance contours for user supplied subroutines which compute design performance. The program has been written for an interactive CDC 3500 facility. On-line scope displays of the contours as well as Calcomp plots are options which complement printer output. A Monte Carlo program to estimate yield is also part of the entire package. Thus, a user can verify immediately whether any changes made based on contours or intercepts did, in fact, increase the yield. The choice of parameter pairs for which performance contours are to be computed is up to the user.

The intercepts are found via a search and the contours are found via a performance contour following algorithm. Since many performance evaluations are necessary, the speed of computation depends strongly on the time required for a circuit analysis. For the example to be presented, a general purpose analysis routine for ladder networks was used to analyze the circuit and the computation of a performance contour typically took on the order of a few seconds. No advantage was taken of the fact that during the search for intercepts or computation of a contour, only one or two circuit parameter values are changed between each analysis.

IV. AN EXAMPLE

4.1 *Preliminary Remarks*

In the last section we indicated that large change sensitivity information could be used to desensitize an initial design, to help specify

tolerances, and to indicate parameter correlation with respect to the specifications. In this section we present an example which illustrates the insight provided by intercepts and contours as well as their utility in suggesting matching and in desensitizing an initial design. CONTOUR was used to compute the intercepts and contours, and XCENTRIC was used to desensitize the initial design. The yields were estimated using TAP[6] with components assumed to be independent, uniformly distributed random variables. This example is not contrived; it was a recent B.T.L. design.

4.2 *The Problem*

The circuit is a low frequency bandpass filter with insertion loss specifications shown in Fig. 5. This is an example of the multicriteria case. We obtain a single criterion by defining

$$J_i \triangleq \frac{IL_i - IL_i^0}{IL_i^{\text{limit}} - IL_i^0},$$

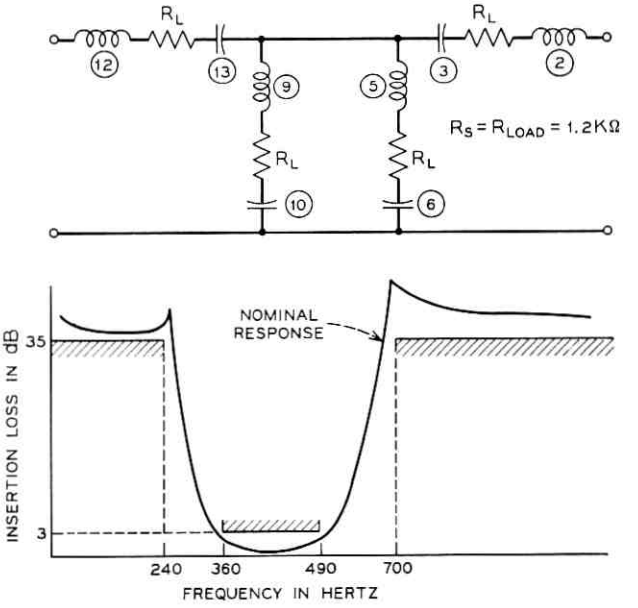

Fig. 5—The circuit and specifications for the example. (Parameters 5 and 6 correspond to the loss peak at 700 Hz. Parameters 9 and 10 correspond to the loss peak at 240 Hz. Parameters 2, 3, 12, and 13 correspond to the bandpass loss minimum at 420 Hz.)

where IL_i is the insertion loss at the ith frequency (for this example there were 30 different frequencies of interest), and

$$J \triangleq \max_{i=1,30} \{J_i\}.$$

Thus, $J^0 = 0$ and $\epsilon = 1$.

4.3 *Results*

Two of the performance contours for this example are shown in Fig. 6. The numbers which are written alongside the contours indicate the frequency at which the insertion loss specifications failed first, i.e., which criterion determined or was dominant along that edge of the region of acceptability.

The insight gained from the contours agrees with one's intuitive feel for the circuit. Consider the transmission zeroes which we know depend on LC products and in particular consider parameters 5 and 6, which determine the loss peak at 700 Hz. If both 5 and 6 increase (first quadrant in 5, 6 contour), the loss peak moves down in frequency and a specification is in trouble at 490 Hz, the upper edge of the passband. If both 5 and 6 decrease, the loss peak moves up in frequency and the 35-dB insertion loss at 700-Hz criterion is the first to be violated. Similar observations can be made by looking at the 9, 10 contour.

Let us now consider possible component matching to increase yield or to permit loosening tolerances. It turns out that the shape of the contour for parameters 5 and 6 is an indication that the specifications are sensitive to the product of these parameters. With tolerances of

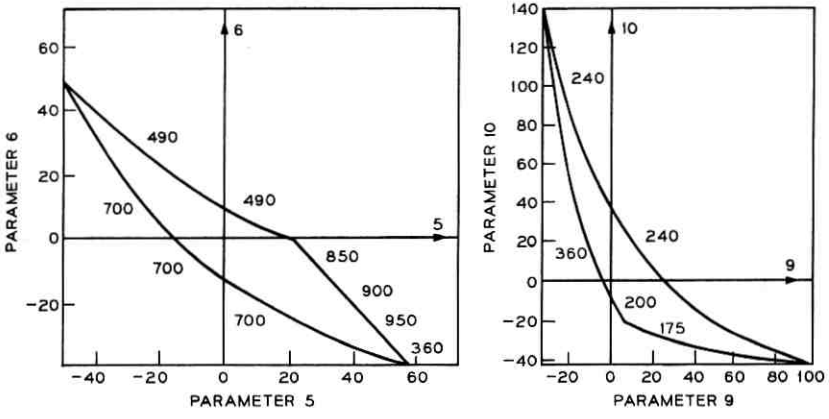

Fig. 6—Two performance contours for the example.

30 percent on the Rs, 5 percent on parameters 2, 3, 12, and 13, 1 percent on 9, 2 percent on 10, and 10 percent on 5 and 6, *the yield went from 85 percent with no matching to 99 percent with matching* 5 and 6 to their nominal product. The contour for parameters 9 and 10 also indicates that their product is important. With tolerances of 30 percent on the Rs, 10 percent on parameters 5, 6, 9, and 10, and 5 percent on parameters 2, 3, 12, and 13, *the yield went from 67 percent (no matching) to 94 percent with matching* 5, 6 and 9, 10 to their respective nominal products. It is true that in this sample example, the desirability of matching might be intuitively obvious to a designer. The purpose, however, was to illustrate how matching based on contour information can dramatically affect the yield.*

Finally, let us consider desensitizing this design since it is not centered as is obvious from the contour for parameters 9 and 10. The centering would hopefully effect an increase in yield for a particular set of tolerances or an increase in tolerances for a particular yield. XCENTRIC was run for two cases: centering only the inductors, and centering both inductors and capacitors. Yields for various tolerances were estimated for the original and both of the centered designs. The results are shown in Table I. (30 percent tolerances were used for the Rs.)

The following comments are pertinent:

(*i*) The tolerances for the original design were 1 percent Ls and 2 percent Cs which gave the desired 100 percent yield.

(*ii*) The error function for XCENTRIC as defined in Section 3.2.2 went from 21 to 0.6 for centering only the inductors and from 25 to 2.5 for centering all Ls and Cs. The changes from original nominal parameter values to centered values were typically on the order of a few percent.

(*iii*) For any of the tolerance combinations shown, the yield increased significantly as a result of "centering."

(*iv*) The original tolerances on the inductors could have been loosened to virtually 5 percent if the centered nominals had been used. This would have been physically feasible since the inductors were wound to desired values for this particular circuit.

(*v*) Ignoring the problem of preferred capacitor values, the tolerances for both Ls and Cs could have been loosened to 5 percent as a result of applying XCENTRIC.

* For other examples of this, see Ref. 1.

TABLE I—YIELDS FOR VARIOUS TOLERANCES FOR ORIGINAL AND CENTERED NOMINAL VALUES.

Tolerances	Original Nominal Values	Centered L Original C Nominal Values	Centered L and C Nominal Values
1% L 2% C	100	—	—
5% L 2% C	95	99.9	—
10% L 2% C	75	89.0	—
5% L 5% C	92	97.5	100

V. CONCLUSION

In this paper we have discussed an approach to "closing the loop" in tolerance analysis. The approach specifically addresses design problems such as specifying tolerances, desensitizing a nominal design, specifying adjustment procedures, and verifying that a design is consistent with manufacturing and environmental component tracking. The approach is particularly applicable to Bell System designs not only because in such designs deviations from nominal must be anticipated, but also because the designs many times have complicated, multiple specifications. The approach does not rely on first- or second-order approximations. In addition, since they are feasible via computer implementation, the techniques may be thought of as computer aids to (statistical) design.

Under the reasonable and realistic assumptions stated in Section I and in the context of statistical design, it was seen that the shape of the region of acceptability and the placement of the nominal design in it are more important than the performance of the nominal design. Furthermore, in view of this the concept of sensitivity has a meaning different from the classical first-order one, and so large change sensitivity was introduced. Intercepts and performance contours were seen to provide "first- and second-order" large change sensitivity information. In fact, they provide a characterization of the region of acceptability in somewhat the same way that classical first- and second-order sensitivities provide a characterization of performance near nominal. Thus, because of the attention focused on the region of acceptability in statistical design, the large change sensitivities provide a measure of sensitivity for statistical design.

Two computer programs, CONTOUR and XCENTRIC, have been written to compute and utilize large change sensitivity information. An example was presented to illustrate the utility of the approach in providing insight, in suggesting possible adjustment procedures, and in desensitizing a nominal design. In the two latter applications the yield increased significantly when adjustments and changes were made based on large change sensitivity information.

In short, for the realistic design problem, attention is (or should be) focused on the region of acceptability. Large change sensitivities provide a measure of parameter sensitivity for this region and design techniques based on them are addressed to the problem of "closing the loop" in tolerance analysis.

VI. ACKNOWLEDGMENT

The author would like to express his appreciation to B. J. Karafin and L. A. O'Neill for many valuable discussions and suggestions, and to Mrs. L. H. Hott and Mrs. H. D. Rovegno for their programming efforts and suggestions.

APPENDIX

Properties of Performance Contours

The notation used is p_i for the value of parameter i, p_i^0 for nominal value, v_i for percent deviation from p_i^0, and $\Gamma(v_i, v_j)$ or Γ_{ij} for the contour of the i, j parameters.

A.1 *Product Property*

If J depends only on the product of two parameters p_i, p_j, then

(*i*) $\Gamma(v_i, v_j)$ contains the curve shown in Fig. 7 and is not bounded at either end;

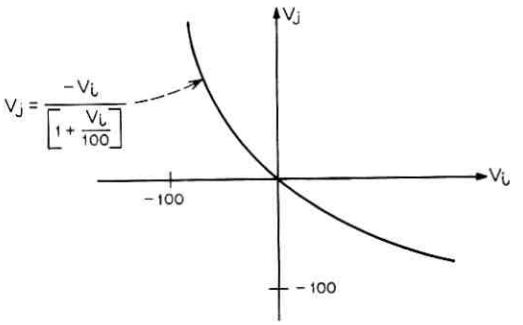

Fig. 7—The constant parameter product curve in percent deviation space.

(*ii*) $\Gamma(v_i, v_k) = \Gamma(v_j, v_k)$, for all v_k.

One could qualitatively relax this exact property into the following corollary.

A.2 *Product Property Corollary*

If J as a function of p_i and p_j is most sensitive (in a large change sense) to the product of p_i and p_j, then Γ_{ij} will roughly follow the curve in Fig. 7 and $\Gamma_{ik} \approx \Gamma_{jk}$, for all k.

A.3 *Ratio Property*

If J depends only on the ratio of two parameters p_i, p_j, then

(*i*) $\Gamma(v_i, v_j)$ contains the 45° line in the v_i, v_j plane and is unbounded;

(*ii*) for v_i and $v_j \ll 100$, $\Gamma(v_i, v_k)$ looks like $\Gamma(-v_j, v_k)$, for all v_k.

A.4 *Ratio Property Corollary*

If J is most sensitive to the ratio of two parameters p_i, p_j, then Γ_{ij} will roughly follow the 45° line, and $\Gamma(v_i, v_k) \approx \Gamma(-v_j, v_k)$ for all k, for $v_i, v_j \ll 100$.

The motivation behind parts (*i*) of these two properties is simply that the hyperbola in Fig. 7 and the 45° line are loci in percent deviation space of constant parameter product and ratio, respectively.

REFERENCES

1. Butler, E. M., "Realistic Design Using Large Change Sensitivities and Performance Contours," IEEE Trans. Circuit Theory (Special Issue on Computer-Aided Design), *18*, No. 1 (January 1971), pp. 58–66.
2. Rohrer, R. A., and Sobral, M., "Sensitivity Considerations in Optimal Control Systems," IEEE Trans. on Automatic Control, *AC-10*, No. 1 (January 1965), pp. 43–48.
3. Butler, E. M., and Rohrer, R. A., "On Relative Sensitivity For Certain Linear Optimal Control Problems," Proc. Second Asilomar Conference on Circuits and Systems, Pacific Grove, California, October 30–November 1, 1968.
4. Medanic, J., and Chen, Chang-I, *Segment Method for the Control of Systems in the Presence of Uncertainty*, Report R-442, Coordinated Science Laboratory, University of Illinois, Urbana, Illinois, November 1969.
5. Karafin, B. J., "The Optimum Assignment of Component Tolerances for Electrical Networks," B.S.T.J., this issue, pp. 1225–1242.
6. Bohling, D. M., and O'Neill, L. A., "An Interactive Computer Approach to Tolerance Analysis," IEEE Trans. on Computers, *C-19*, No. 1 (January 1970), pp. 10–16.

THE BELL SYSTEM TECHNICAL JOURNAL
Vol. 50, No. 4, April, 1971
Printed in U.S.A.

Statistical Circuit Design:

The Optimum Assignment of Component Tolerances for Electrical Networks

By B. J. KARAFIN

(Manuscript received December 18, 1970)

The prediction of manufacturing yield of an electric circuit, given the tolerances and statistics of the components, is a straightforward procedure using Monte Carlo tolerance analysis. The inverse problem, namely, specifying the component tolerances that produce the cheapest network, is more difficult and has received little attention in the literature. In this paper an algorithm is presented that solves this problem for a significant class of networks.

The algorithm is limited to circuits for which one hundred percent yield is sought and whose components are statistically independent, i.e., discrete circuits. The one hundred percent yield assumption is used to reduce the number of possible tolerance choices. A variation of the branch and bound strategy that is shown to be particularly efficient is then used to make an optimum selection. Two-dimensional performance contours, worst-case, and Monte Carlo computations are also used as part of the procedure.

An example circuit is demonstrated for which the algorithm produced a tolerance assignment substantially cheaper than that projected by the designer.

I. INTRODUCTION

Monte Carlo tolerance analysis has proven to be a useful tool in evaluating the effects of component tolerances and environmental variations on electrical circuit performance. The method involves "constructing" samples of the circuit inside the computer using element values that obey the manufacturing statistics, analyzing these samples, and forming empirical distributions of performance. One common outcome of the process is the prediction of yield.

Monte Carlo tolerance analysis, henceforth referred to as TAP

(Tolerance Analysis Procedure), is an open-loop structure. If we examine the way in which it is used, we find that for discrete circuits the designer supplies the TAP program with a set of component tolerances he has chosen based on breadboard measurements, linear sensitivity or worst-case analysis, or some other approximate technique. At the conclusion of the TAP run, he observes yield and is faced with one of two situations:

(*i*) Yield is too low. With this result the designer knows he must change his tolerances. Unfortunately, TAP gives him little information as to which tolerances to change and by how much.

(*ii*) Yield is adequate. Here the designer may be satisfied by the design but he obtains little help in determining whether a cheaper (looser) set of tolerances might not give equally satisfactory yield.

TAP, then, is open-loop in that it is a tool for predicting yield given a set of tolerances; both the initial set of tolerances or any changes to that set must be provided by the designer without assistance from TAP. (It is interesting to note that for integrated circuits the designer has little freedom in specifying tolerances or tracking. In this case TAP is used to check that designs themselves are adequate, *given* the component tracking that can be achieved in integrated production.)

This paper discusses an algorithm for closing the TAP loop. The program embodying this algorithm will accept a circuit topology, nominal element values, a figure of merit for circuit performance and data relating element cost to element tolerance, and specify the set of tolerances that will produce the cheapest manufactured network that has 100 percent *a priori* yield. (By *a priori* yield we mean the percentage of those manufactured circuits all of whose components are within tolerance limits and which are wired correctly that meet specifications. 100 percent *a priori* yield implies that any manufactured circuit that fails to meet specifications has either a component outside of tolerance or a wiring error.) The techniques described are applicable at present only to discrete circuits, i.e., circuits where the parameters are statistically independent. Work is in progress to treat circuits with correlated parameters.

The method described below is a combination of two-dimensional performance contours,[1] a method the author has since learned is a variation on the branch and bound technique,[2] quasi-worst-case computations and repetitive TAP computations.

II. THE CHEAPEST NETWORK

In this paper the cheapest network is defined as the network with 100 percent *a priori* yield such that the sum of the costs of the components comprising that network is not greater than the sum of costs for every other network with 100 percent *a priori* yield. We are concerned with a network of fixed topology and fixed nominal element values for which we want to choose a tolerance vector, τ, each of whose elements, τ_i, is the tolerance chosen for circuit parameter, p_i. Associated with each parameter tolerance, τ_i, is a cost, $C_i(\tau_i)$, where $C_i(\cdot)$ is the cost function of the ith circuit parameter.

For each parameter the designer has a limited number of discrete tolerances from which to choose. Therefore, we will consider a finite universe of possible realizations, each realization being characterized by a unique tolerance vector. We will number the realizations in the universe 1, 2, $\cdots$, l, and refer to each realization by its associated tolerance vector τ^k. We next define the set,

$$\mathfrak{A} = \{k \mid \text{realization } k \text{ has 100 percent } a \textit{ priori} \text{ yield}\}$$

and the associated set,

$$\mathfrak{A}_\tau = \{\tau^k \mid k \in \mathfrak{A}\}.$$

Then *a* cheapest network has tolerance vector τ^* satisfying the conditions:

(*i*) $\tau^* \in \mathfrak{A}_\tau$,

(*ii*) $$\sum_{i=1}^{n} C_i(\tau_i^*) \leqq \sum_{i=1}^{n} C_i(\tau_i^k); \qquad \text{for all } k \in \mathfrak{A},$$

where the circuit under study has n components.

One could imagine other criteria by which the cheapest network might be defined. In particular, one might find a network cost function that traded off yield against cost of repairing, component salvaging, or discarding networks. However, consideration of such tradeoffs raises serious questions about manufacturing practices, not to mention the question of allowing sub-marginal circuits to be installed in the field. Because of these questions, the following discussion is limited to circuits for which 100 percent *a priori* yield is required. As we shall see, this assumption is central to the proposed tolerance specification method.

III. REGIONS OF ACCEPTABILITY AND POSSIBILITY

It is assumed that the circuits with which we are dealing have a scalar performance, J, that is a computable function of the circuit parameter values; a nominal design with performance measure, J_0; and an allowable degradation from nominal, ϵ, such that $(J_0 + \epsilon)$ marks a boundary separating acceptable circuits from unacceptable ones.*

We now examine the n-dimensional parameter deviation space, i.e., a space whose origin is defined as the nominal parameter vector and each of whose axes is the percent deviation of one parameter from its nominal value. We postulate the existence of a connected region, including the origin, such that all circuits built with parameter values represented by points inside the region are acceptable and those outside the region are unacceptable. We call this the Region of Acceptability, R_A.[1] We now notice that in this same space, each tolerance vector, τ^k, is associated with an n-dimensional parallelepiped that we call the Region of Possibility.† In other words, all circuits built of components with tolerances specified by τ^k have parameter deviation vectors inside the parallelepiped we are calling the Region of Possibility, R_P.

To clarify these ideas we extend an example presented in Ref. 1. Figure 1a shows a simple voltage divider. Its transfer function is given by $T = 1/(1 + R_1/R_2)$, and its input resistance is $R = R_1 + R_2$. With nominal one-ohm resistors, the nominal transfer function and input resistance are 0.5 and 2.0 respectively. Suppose the design specifications call for $0.46 \leqq T \leqq 0.53$ and $1.85 \leqq R \leqq 2.15$. Then the Region of Acceptability (R_A) shown in Fig. 1b is bounded by four lines, each of which is the locus of all points producing networks exactly satisfying one of the four specification limits. Figure 1b also shows the Region of Possibility (R_P) when the voltage divider is built with 5 percent components. Notice that R_P intersects the parameter deviation axes at ± 5 percent. Notice further that all possible networks are acceptable, i.e., R_P is totally contained within R_A. In Fig. 1c, a new R_P that is the result of using a 10 percent resistor for R_1 and a 3 percent resistor

* See Ref. 1 for examples of transcribing classical loss, phase, frequency specifications into J, ϵ representation.

† Here we are assuming that all components are 100 percent tested, i.e., a batch of 15 percent components has *all* components within ± 15 percent of nominal value. We are further assuming that tolerances place symmetric limits on component values. The asymmetric case can be handled but it makes the argument obtuse. Lastly, we are assuming all components are statistically independent.

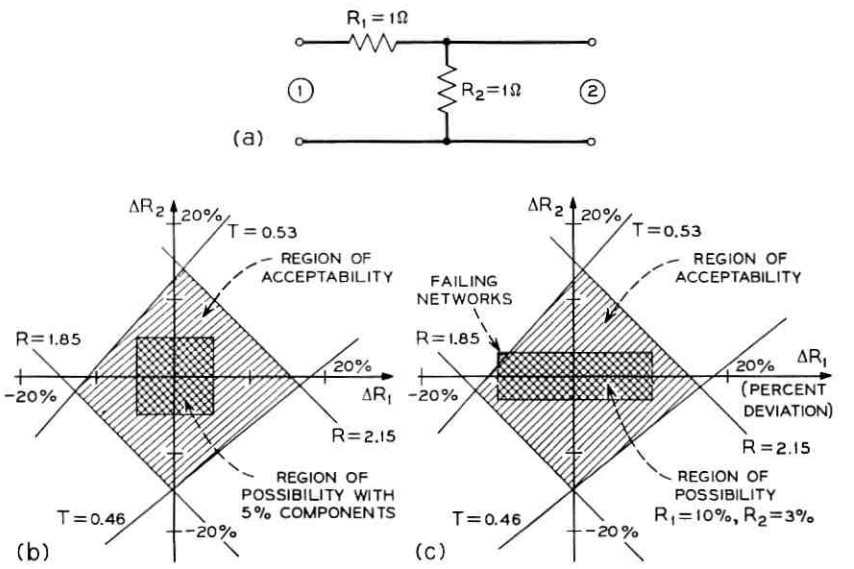

Fig. 1a—Voltage divider example.
Fig. 1b—Regions of acceptability and possibility for voltage divider (5 percent components).
Fig. 1c—Regions of acceptability and possibility for voltage divider (R_1 a 10 percent resistor, R_2 a 3 percent resistor).

for R_2 is superimposed over R_A. Notice that some networks in the second quadrant fail, i.e., they are inside R_P but outside R_A. Hence, the tolerance vector (10, 3) is not a member of $\mathfrak{A}_\tau$ and cannot be used for the example network.

The conclusion we may now reach is that in order for a network to have 100 percent *a priori* yield we must have $R_P \subseteq R_A$. Further, because we are restricting our attention to networks that have 100 percent *a priori* yield, our task is to choose the cheapest tolerance vector that will satisfy the condition, $R_P \subseteq R_A$.

If we could characterize the Region of Acceptability, the task of choosing a tolerance vector that produces the cheapest network would be reduced to the problem of finding the "largest" parallelepiped (R_P) that is contained within R_A. (Notice that our assumptions of 100 percent *a priori* yield and 100 percent component testing obviate the need to consider component distributions. All we are concerned with are the limits of component deviation.) Unfortunately, characterization of R_A is an impractical task; we are trapped by "the curse of dimensionality." Even if R_A were as simple a region as a hypercube, it would, for a net-

work of say 15 parameters, have over 32,000 vertices. The number of function evaluations required to locate these vertices would be exceedingly large. When one considers that the $(n - 1)$ dimensional surfaces bounding R_A are likely to be quite complex, the magnitude of the problem becomes staggering.

The algorithm that is used to select the tolerance vector that will produce the cheapest network, τ^*, begins with a consideration of two-dimensional subspaces of R_A.[1] We will require that two-dimensional subspaces of R_P be inside the corresponding subspaces of R_A. We will then use a series of techniques to insure that $R_P \subseteq R_A$.

IV. FINDING THE CHEAPEST NETWORK

The algorithm for finding a cheapest network is broadly outlined in Fig. 2. Below we take up each of the major blocks in detail.

4.1 *Pairwise Constraints*

The first step in obtaining pairwise constraints on component tolerances is to compute the minimum intercept[1] for each parameter. Call this L_i for the ith parameter. Briefly, this is the minimum deviation each parameter can undergo, keeping all other parameters fixed at nominal value, before the network specifications are violated.

Next we consider the $\binom{n}{2}$ performance contours[1] for the n parameter network. These contours are the boundaries of the two-dimensional subspaces of R_A, holding $(n - 2)$ parameters fixed at nominal. Each contour determines what tolerance pairs are allowable for the variable parameters. In short, each tolerance pair defines a rectangle. The pair is allowable if that rectangle is within the performance contour.

The designer is presumed to have specified a discrete set of obtainable tolerances for each component. Call this set S_i for the ith component. We will number the members of S_i in descending order and refer to them as $\tau_{i1}, \tau_{i2}, \cdots, \tau_{im_i}$, where m_i is the number of obtainable tolerances for the ith component. We will form a table for each pair of parameters, say (r, s), of the form:

p_r	p_s
$\tau_{r,i}$	$\tau_{s,\alpha}$
⋮	
τ_{r,m_r}	$\tau_{s,\gamma}$.

For ease of subsequent computation, the parameter on the left will be the one with the smaller minimum intercept. Not all m_r entries neces-

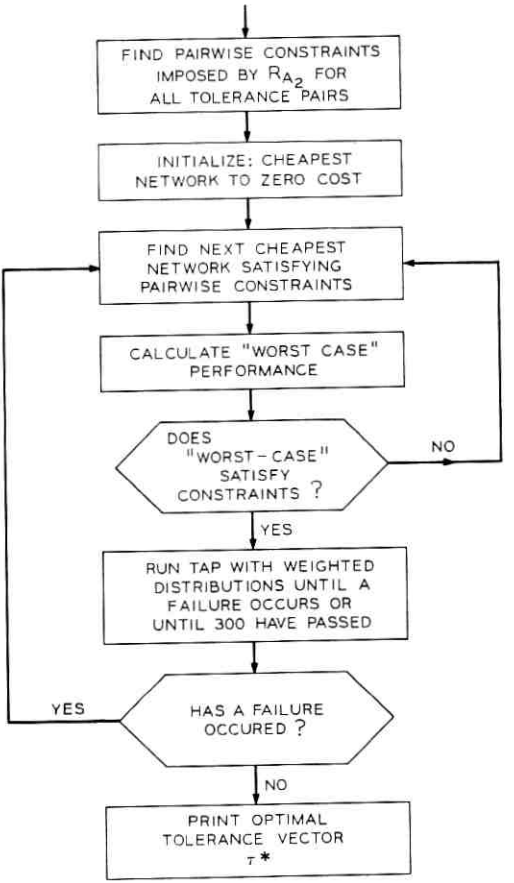

Fig. 2—Tolerance specification algorithm.

sarily exist in the table. First we eliminate those tolerances that are larger than the minimum intercept, since they will clearly produce rectangles not contained within the (r,s) contour $(\Gamma_{r,s})$. Then for the first $\tau_{r,j} \leqq |L_r|$, we find the largest element of S_s that produces a rectangle inside $\Gamma_{r,s}$, and this tolerance is entered into the table opposite $\tau_{r,j}$. If a line of the table reads

$$\tau_{r,j} \qquad \tau_{s,k}$$

and if parameter r has tolerance $\tau_{r,j}$, parameter s may have $\tau_{s,k}$ or any smaller tolerance. We proceed through the elements of S_r finding the corresponding largest allowable tolerance within S_s until we have entered τ_{r,m_r} and its companion in the table.

An example should clarify these ideas. R_A for the voltage divider of Fig. la is reproduced in Fig. 3. Since the voltage divider has only two parameters, only one performance contour exists and this is identical to R_A. Suppose that R_1 and R_2 have the same set of obtainable tolerances,

$$S_1 = S_2 = \{15, 10, 5, 3, 1\}.$$

Figure 3 indicates $L_1 \simeq -11$ percent $L_2 \simeq 13$ percent. We will therefore consider p_1 to be the left side of the table. To begin to fill the table we notice $\tau_{11} = 15$ percent $> |L_1|$ and is therefore eliminated from consideration. $\tau_{12} = 10$ percent is entered as the first entry in the left-hand column. Starting at the points in Fig. 3 (10 percent, 0) and (−10 percent, 0), the vertical directions are explored to determine how far R_2 may be varied before specifications are exceeded. In the second quadrant, specifications are exceeded before $\Delta R_2 = 2$ percent. Therefore, $\tau_{2,5} = 1$ percent is made the first right-hand entry in the table. Computationally we alternate between $\Delta R_1 = 10$ percent and $\Delta R_1 = -10$ percent and take small steps in ΔR_2 both positively and negatively until the specifications are violated (shown as step 1 on Fig. 3). The horizontal lines of the (10, 1) rectangle are then explored until ΔR_1 has been reduced to $\tau_{1,3} = 5$ percent. Since no specification failures are detected, the entry (10,1) is certified (step 2 in Fig. 3). (Notice we are assuming that performance contours are simply connected.) We then explore vertically from the four points on which step 2 ended and find that the next entry in the table is (5, 5). We continue in this way until

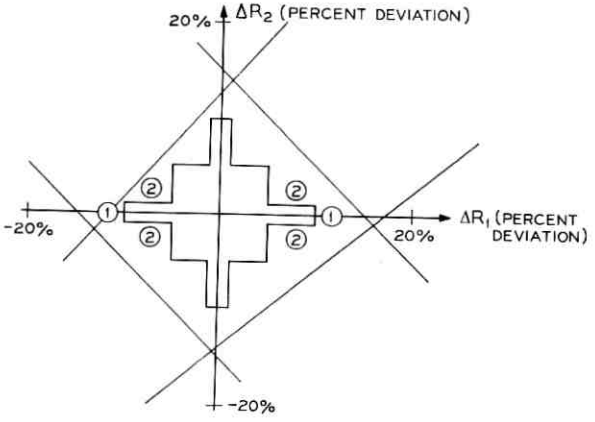

p_1	p_2
10%	1%
5%	5%
3%	5%
1%	10%

Fig. 3—Allowable tolerance rectangles for voltage divider.

the table shown in Fig. 3 is complete, and we have explored the combined perimeter of all allowable tolerance rectangles. Notice that tightening ΔR_1 from 5 percent to 3 percent resulted in no increased allowable tolerance for R_2.

This process is repeated for each of the $\binom{n}{2}$ parameter pairs. The table for each parameter pair (r, s) is denoted $T_{r,s}$. Each table gives us a pairwise constraint on tolerances. The next step in our effort to find τ^* is to find the cheapest network satisfying the pairwise constraints, i.e., to find a tolerance vector, $\tau^\#$, whose elements satisfy the table constraints pairwise and is the cheapest of all such tolerance vectors. Having found $\tau^\#$, we will then try to discover if $\tau^\# \in \mathfrak{A}_\tau$, i.e., if $\tau^\# = \tau^*$. If $\tau^\# \notin \mathfrak{A}_\tau$, we will find the next cheapest tolerance vector satisfying the pairwise constraints, etc., until we find one that is a member of $\mathfrak{A}_\tau$. If we define a set,

$$\mathfrak{B}_\tau = \{\tau \mid \tau \text{ satisfies pairwise constraints}\},$$

then it is clear that $\mathfrak{B}_\tau \supseteq \mathfrak{A}_\tau$ and by choosing elements of $\mathfrak{B}_\tau$ in order of increasing cost, the first chosen element of $\mathfrak{B}_\tau$ that is also an element of $\mathfrak{A}_\tau$ is in fact τ^*.

4.2 *Branch and Bound Technique for Finding the Cheapest Network*

In this section we describe a variation on the branch and bound technique that is used to find the cheapest element of $\mathfrak{B}_\tau$, $\tau^\#$. Consider the multi-root tree structure shown in Fig. 4. The nodes in the first column represent the elements of S_1, the obtainable tolerances for p_1. From each node in the first column we have branches leading to all the elements of S_2, the obtainable tolerances for p_2, etc. Finally, the last column has all the elements of S_n repeated for every choice of the $(n - 1)$ preceding element tolerances. There are $\prod_{i=1}^{n} m_i$ nodes in the last column and an identical number of paths from the left side of the tree to the right. Each path is associated with a choice of tolerance vector and hence has an associated cost, $C = \sum_{i=1}^{n} C_i(\tau_i^k)$. The task of finding $\tau^\#$ is then the task of finding a path through the tree from left to right such that:

(*i*) The tolerance pair associated with every node pair of the path is consistent with the tabled constraints.

(*ii*) C is minimized.

With each node we can associate a partial cost. For a node selected in column k, we have a partial cost $C^k = \sum_{i=1}^{k} C_i(\tau_i)$ where τ_k is the tolerance selected in column k and τ_i, $i < k$, are the tolerances selected for the initial part of the path.

A flowchart for selecting the cheapest path whose associated $\tau \in \mathcal{B}_\tau$ is shown in Fig. 5. In words, we begin at the left and choose for τ_1 the largest (cheapest) tolerance not greater than L_1. We then move across the tree picking the kth element's tolerance using

$$\tau_k = \underset{i<k}{\text{Min}}\, T_{i,k}(\tau_i),$$

where the function $T_{i,k}(\tau_i)$ picks the right-hand entry opposite τ_i in the table, $T_{i,k}$. After each such selection we compute a partial cost, C^k, for the portion of the path chosen so far. Two occurrences will allow us to eliminate that part of the tree with initial path $\tau_1, \cdots, \tau_{k-1}$, viz.:

(*i*) At column k, one or more $T_{i,k}(\tau_i)$ does not exist. This indicates that any τ with the first $(k-1)$ components, $\tau_1, \cdots, \tau_{k-1}$ is not a member of $\mathcal{B}_\tau$.

(*ii*) The partial cost $C^k \geqq C^T$, a target cost. The target cost, initially set at ∞, is replaced by the cost of the first complete path found, and is updated as cheaper tolerance vectors emerge from the process.

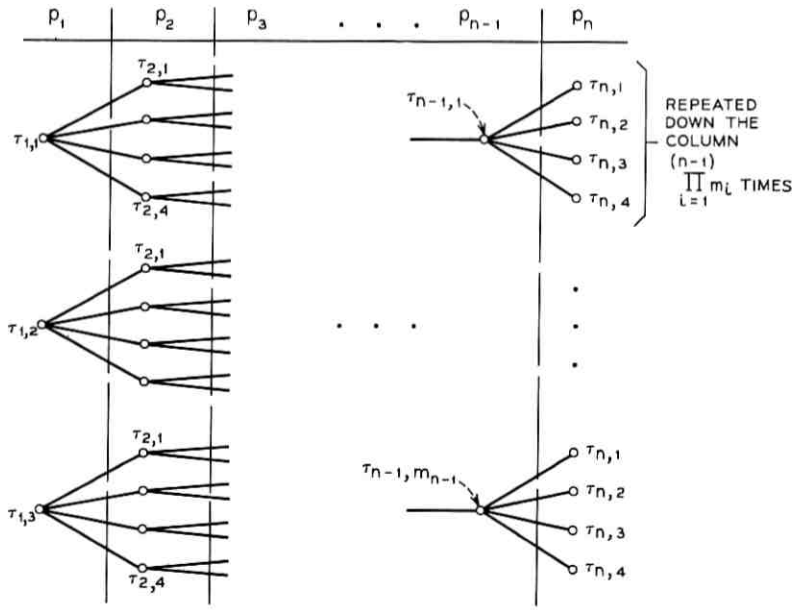

Fig. 4—Tolerance choice tree.

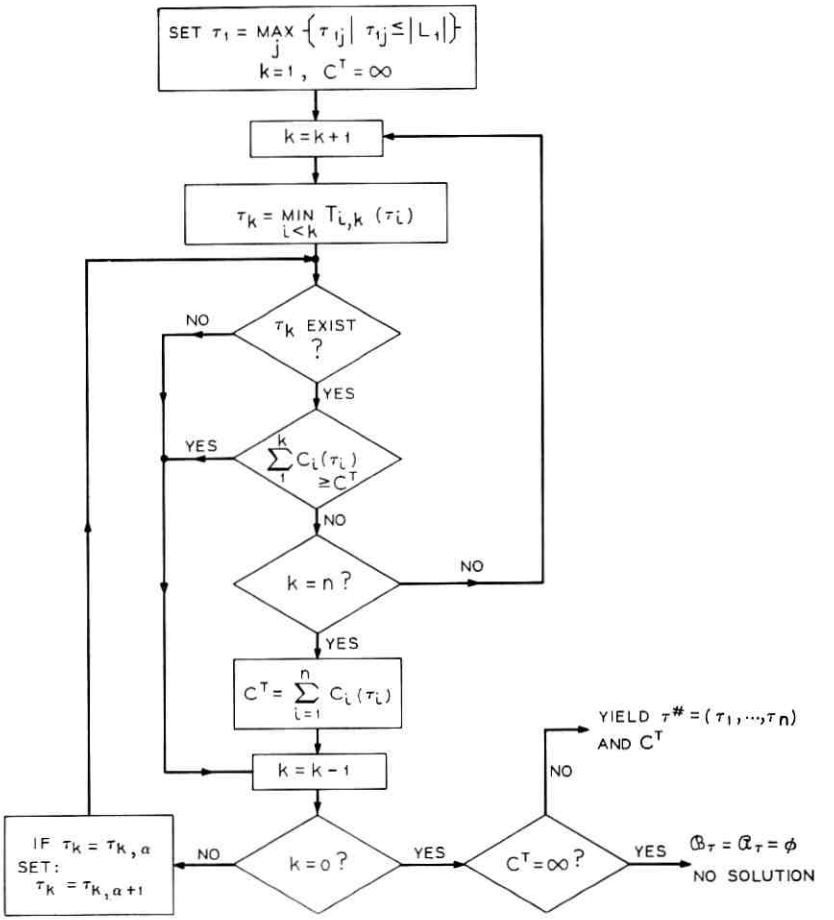

Fig. 5—Algorithm to find $\tau^\#$.

In either case, we return to the $(k-1)$st column and choose the next tighter allowable tolerance. If we are already at the tightest allowable tolerance in the $(k-1)$st column, we return to the $(k-2)$nd column, etc. If neither event occurs, a path reaches the right side of the tree. The associated cost of this path then becomes the target cost. We then back up to the $(n-1)$st column and choose the next tighter tolerance, etc.

The efficiency of the algorithm derives from the fact that the vast majority of paths are never explored to completion, but rather are eliminated by one of the two terminating rules.

The algorithm terminates when all paths have either been explored or terminated. The final target cost is the cost associated with $\tau^{\#}$. Having found $\tau^{\#}$, we must now determine whether $\tau^{\#} \in \mathcal{A}_\tau$.

4.3 *Yield Checks Using Worst-Case and Tolerance Analysis*

A circuit built with the tolerance vector $\tau^{\#}$ determined by the branch and bound optimization has the property that if any two parameters are allowed to vary within their tolerance limits while all other parameters are held constant at their nominal values, design specifications will be satisfied. In other words, this circuit is the cheapest realization that meets all two-at-a-time constraints. Having determined that $\tau^{\#} \in \mathcal{B}_\tau$, we must now verify that $\tau^{\#} \in \mathcal{A}_\tau$, or that the circuit with tolerance vector $\tau^{\#}$ has 100 percent *a priori* yield.

If it happens that $\tau^{\#} \notin \mathcal{A}_\tau$, we will return to the branch and bound algorithm, delete $\tau^{\#}$ from the tree, and find the next cheapest network. We can thus view the branch and bound as a technique for ordering the elements of $\mathcal{B}_\tau$ by cost. At each call to the algorithm we obtain the next element in the nondecreasing cost sequence, $\tau^{\#}, \tau^{\#2}, \cdots, \tau^{\#q}, \cdots$. The first element of this sequence that is an element of $\mathcal{A}_\tau$ is τ^*.

Tolerance vectors that satisfy the two-at-a-time constraints but that have less than 100 percent yield are easy to visualize. Figure 6 is a

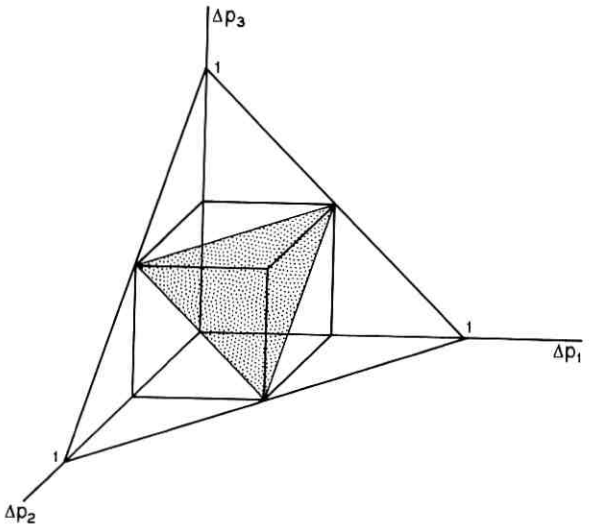

Fig. 6—R_A and R_P for a circuit that meets pairwise constraints but has less than 100 percent *a priori* yield.

three-dimensional perspective of a circuit that meets the two-at-a-time constraints but has less than 100 percent yield. Considering only the positive octant, we see that each of the three performance contours is a triangle. After inscribing rectangles in each triangle, we have a cubic R_P in three dimensions. Now if R_A is a tetrahedron, we see that the shaded plane of intersection of R_A and R_P in Fig. 6 separates the possible circuits into acceptable and unacceptable classes, and despite the fact that the pairwise constraints are met in each of the planes that includes the origin, we have a tetrahedron of failing circuits extending out of the drawing.

Since we have not characterized R_A, we go through two approximate steps to determine if $\tau^* \in \mathcal{A}_\tau$. The first step is a quasi-worst-case computation. We use the signs of L_i to extend each parameter to the limit defined by τ_i. In other words, we compute the circuit's performance with parameters

$$p_i = p_{i0}[1 + \tau_i \operatorname{sgn}(L_i)]$$

where p_{i0} is the nominal value of p_i. If this performance does not meet specifications, we know that the realization with tolerance vector τ^* cannot have 100 percent yield. If the worst-case circuit fails, we eliminate τ^* from the tree, go back to the branch and bound algorithm, and find the next cheapest circuit.

Since even a linear circuit normally has a performance measure that is a nonlinear function of its parameters, the true worst-case performance need not occur at an extreme point of R_P. Hence neither the preceding nor any other classical "worst-case" computation is sufficient to determine if $R_P \subseteq R_A$. The technique that has been chosen is to run Monte Carlo samples of the circuit using the tolerances of τ^* until either a sample fails, in which case we again return to branch and bound for the next cheapest network, or until 300 sample networks have passed specification. The probability distributions used for the Monte Carlo analysis are the triangular shapes shown in Fig. 7. This shape is chosen to emphasize the regions near the parameter extremes; satisfaction of the specifications when the parameters are near nominal has been assured by compliance with the pairwise constraints.

After successful completion of 300 Monte Carlo samples, we claim that $\tau^{*a} \in \mathcal{A}_\tau$. We then replace the distributions of Fig. 7 with the actual distributions to be expected in manufacture and continue to run Monte Carlo samples as a further check. The latter process is continued to whatever extent is desired. It has been found in practice that some failing samples show up if the Monte Carlo analysis is run long enough. In this event we content ourselves with the notion that 99+ percent is an acceptable yield.

V. AN EXAMPLE

The techniques described above were tested on the bandpass filter whose schematic and requirements appear as Figs. 8a and b respectively. In our computation, 30 discrete frequencies were used to define the specification. The network designer's first guess at a tolerance assignment used all 2 percent components. In fact, such a choice does insure 100 percent yield, but it is not the optimum choice.

The set of obtainable tolerances were given as:

$$S_i = \{20, 15, 10, 5, 3, 2, 1, \tfrac{1}{2}\}; \; i = 1, \cdots, 8.$$

Absolute costs, of course, are of no importance to the algorithm; all computations are performed on the basis of relative cost. Therefore, for this example we used

$$C_i(\tau_i) = 1/\tau_i; \; i = 1, \cdots, 8.$$

It is interesting to consider the dimensionality of this example. We have eight parameters, each with eight obtainable tolerances. Hence, we have $8^8 = 16{,}777{,}216$ conceivable tolerance vectors. Many of these vectors can be eliminated by not considering tolerances greater than the minimum intercept of the associated parameters. For example, the inductor labeled p_5 had $L_5 = -5.7$ percent. If this is done, the number of conceivable tolerance vectors falls to just under 3×10^6 —still a rather formidable number.

Two examples of the tolerance-pair tables are shown below:

p_5	p_6
5%	½%
3%	3%
2%	5%
1%	5%
½%	5%

p_1	p_4
20%	½%
15%	5%
10%	10%
5%	15%
3%	15%
2%	15%
1%	20%
½%	20%

The cheapest network that the branch and bound algorithm located, i.e., that satisfied the pairwise constraints, was

$$\tau^* = \{10, 5, 5, 10, 3, 3, 10, 5\},$$

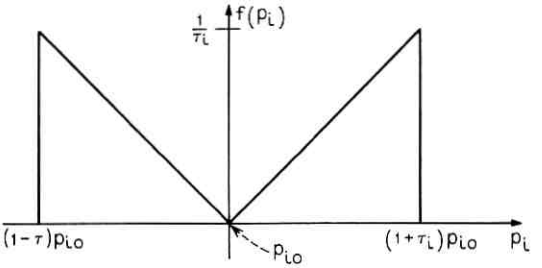

Fig. 7—Probability density function used in Monte Carlo analysis.

with a cost, $C(\tau^*) = 1.57$. The efficiency of branch and bound is demonstrated by the fact that although there are almost 3×10^6 paths through the tree, τ^* is found in 200 ms of computer time on a CDC 3500. To understand this efficiency we note that the number of tolerance vectors satisfying the pairwise constraints is under 700,000. This is 4 percent of the original sixteen million realizations and less than a quarter of those remaining after each S_i is diminished by $\{\tau_i \mid \tau_i > \mid L_i \mid\}$. Perhaps more important to note is that the optimum realization has cost 1.5

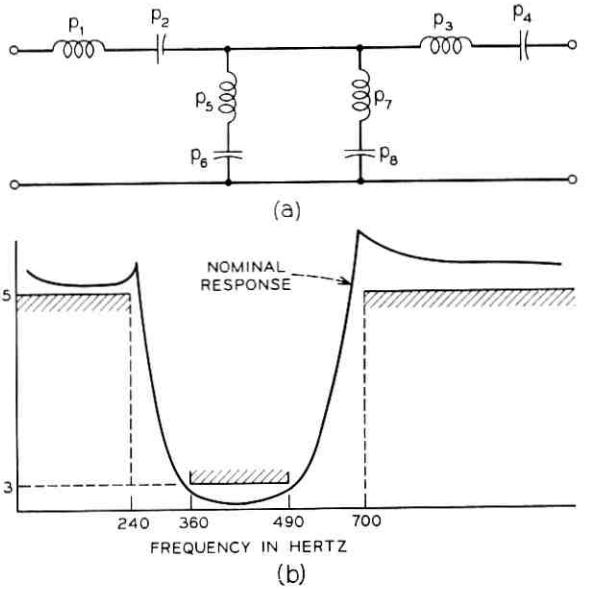

Fig. 8a—Example bandpass filter.
Fig. 8b—Example circuit specifications.

while any path that reaches a node of tolerance $\frac{1}{2}$ percent has a cost greater than 2. Clearly, a great number of paths are eliminated quickly because of the cost constraint.

Examination of the algorithm's operation reveals that τ^* with cost 1.57 failed the "worst-case" test. The branch and bound routine was then re-entered 2167 times to produce tolerance vectors of 25 different costs each of which failed the "worst-case" test. At a cost level of 2.47, 362 tolerance vectors were produced of which three passed worst-case. However, each of these three failed during the TAP analysis. Costs of 2.50, 2.53, and 2.57 were then obtained with a total of 1124 vectors of which 12 passed worst-case but again failed during TAP. Finally, the tenth vector with a cost of 2.60 passed both worst-case, the initial 300 TAP samples and a subsequent 500 TAP samples. The solution vector was:

$$\tau^* = \{3, 3, 5, 3, 2, 2, 5, 5\}.$$

The final cost of 2.60 compares favorably with the designer's first assignment, using 2 percent components, that has a cost of 4.0.

The total time to execute the entire algorithm was 20 minutes on a CDC 3500. There were 8124 circuit evaluations: 121 to compute the L_i, 5659 to form the tables $T_{r,s}$, and 2024 total TAP samples.

VI. CONCLUSION

In this paper we have described an algorithm that will assign network element tolerances in a manner that minimizes network cost. The tolerance for each element is chosen from a list of obtainable values, which, together with associated costs, is supplied by the designer. The set of tolerances chosen by the algorithm satisfies two conditions, namely:

(*i*) All sample networks built with components whose values are within the limits imposed by the tolerances meet circuit performance specifications.

(*ii*) The sum of element costs associated with the chosen tolerances is a minimum.

The number of circuit evaluations required by the algorithm is relatively large and can be expected to grow as the square of the number of elements. An example circuit with eight parameters required just over eight thousand circuit evaluations. The feasibility of the algorithm is thus tied to the efficiency of our circuit analysis techniques. Linear networks, nonlinear static networks,[3] and a limited class of

nonlinear dynamic circuits are presently analyzed in a few seconds or less and hence are acceptable candidates for tolerance prediction. On the other hand, it is not unusual for the time-domain analysis of a nonlinear circuit to require several minutes of large scale computer time. The application of the tolerance prediction algorithm to such circuits must await algorithmic or hardware advances that bring the cost of circuit analysis down by at least an order of magnitude.

The efficiency of the techniques is also influenced by the nature of the Region of Acceptability, R_A, the shape of which is determined by the equations describing the network and by the performance objectives. More specifically, the algorithm depends on the adequacy of the characterization of R_A by the performance contours. For the example circuit we noted that there were approximately 700,000 tolerance vectors satisfying the pairwise constraints. However, only 3663 of these vectors had to be tested before one was found that was a member of $\mathfrak{A}_\tau$, i.e., before a vector guaranteeing 100 percent *a priori* yield was found. We deduce then that the performance contours were, for our purposes, a good characterization of R_A. It is possible to imagine an R_A for which this is not the case. In such a situation, where the number of vectors that are not members of $\mathfrak{A}_\tau$ but which still satisfy the pairwise constraints is very large, the number of circuit evaluations for both "worst-case" and TAP computations can become large enough to render the entire technique unfeasible. Fortunately, our experience indicates that in a large class of circuits, element pairs, e.g., LC and RC products and quotients, are dominant influences on circuit response, and that for this class of circuits the performance contours are an acceptable characterization of R_A.

All of this is to say that application of the tolerance specification algorithm is not cheap, and moreover may become quite expensive in some pathological situations. Hence, the algorithm should only be applied to networks whose anticipated production rate is large. In other words, one must balance out expected savings resulting from optimum tolerance assignment against the computational cost of achieving such an assignment. In any case, the variation of component cost with tolerance selection is seldom an issue for limited production networks.

One final point should be mentioned, namely, the designer's ability to obtain accurate component cost data is essential to the success of the process. The generation of such data has often proved more difficult than it might seem. For example, choice of a component of given tolerance for a large production circuit may in itself cause a pricing

change for that component. Further, when one is dealing with adjustable elements for which an adjustment accuracy is sought from the algorithm, one is faced with obtaining costs on a process before it is implemented. The solution of this problem, of course, lies in the close cooperation between design and production engineering.

It should be clear that the algorithm depends strongly on the assumption that only tolerance choices that allow 100 percent yield are acceptable. This assumption eliminates consideration of component probability distributions and the necessity of performing multi-dimensional integration. It allowed us to use the performance contours, "worst-case," and TAP computations to eliminate large numbers of tolerance vectors and bring the problem within manageable proportions.

The assumption of statistical independence of the components is less vital. In the algorithm as presented above, it meant only that the Regions of Possibility in two dimensions were assumed to be rectangular. Techniques that allow component correlation are subjects of future work.

VII. ACKNOWLEDGMENT

The author is indebted to E. M. Butler whose work formed a basis for much of the above, to Mrs. J. M. Schilling who designed and wrote the tolerance specification programs, and to J. Chernak who suggested the project.

REFERENCES

1. Butler, E. M., "Large Change Sensitivities for Statistical Design," B.S.T.J., this issue, pp. 1209–1224.
2. Lawler, E. L., and Wood, D. E., "Branch and Bound Methods: A Survey," J. Operations Res., *14*, No. 4 (July–August 1966), pp. 699–719.
3. Cermak, I. A., and Kirby, Mrs. D. B., "Nonlinear Circuits and Statistical Design," B.S.T.J., this issue, pp. 1173–1195.

THE BELL SYSTEM TECHNICAL JOURNAL
Vol. 50, No. 4, April, 1971
Printed in U.S.A.

Statistical Circuit Design:

A Case Study of the Use of Computer Aids in Circuit Design—Pulse Equalizers for the T2 Digital Transmission Line

By L. A. O'NEILL

(Manuscript received December 1, 1970)

Computer simulation makes it economically feasible to analyze competing circuit configurations and optimize the circuit parameters using complicated criteria related to system performance. Furthermore, the influence of manufacturing tolerances on optimized performance can be statistically investigated to establish component specifications before production is started. Thus, the designer can predict more easily whether or not a circuit will perform adequately in the field.

In addition, computer operated test sets can provide accurate measurements of circuit performance during manufacture to insure that the product will be satisfactory. These test facilities can be programmed to provide a factory evaluation of the individual circuits based on worst-case system performance.

To illustrate these concepts, it is shown how computer aids were utilized in the design of the pulse equalizers for the T2 digital transmission line. The discussion of the equalizer design is intended to illustrate why and in what manner the various functions were implemented. The statistical tolerance analysis and manufacturing test phases receive the greatest emphasis as they are the most recent developments.

I. INTRODUCTION

Tolerance analysis is the most recent development in a continuing effort to design circuits and systems realistically. Realism requires that you model as closely as possible the complex environment in which the requisite functions must be accomplished. As computers evolved, it has become economically feasible to take more and more factors into account. The objective of this effort is to anticipate potential prob-

lems so that they may be eliminated in the design phase rather than unexpectedly to discover them when the unit is put into service. Standard design practice is to progress through several test phases, first using breadboards and prototypes of individual circuits, then using complete systems in the field trials and limited service trials. If computer simulation is also employed during the design process, it is frequently possible to detect design deficiencies at an earlier stage, and the earlier the problem is detected the less expensive is the corrective action.

The impact that the computer has had on this quest for realism is most readily illustrated with a specific example. The design of the pulse equalizers for the T2 digital transmission line evolved during the era discussed in the introduction to this issue. Thus the improvements in computers and computer-aided design techniques made it possible to introduce more and more realism into the design process. Initially, the computer was used for analysis (by simulation) of the equalizer and the evaluation of complicated performance measures so that the engineer could make design decisions. Subsequently, when more powerful computers became available, the function of the computer was increased to provide automatic optimization of the circuit parameters. Next, the influence of manufacturing tolerances on optimized performance was statistically investigated to establish component specifications. When the prototypes were constructed, detailed measurements made on a Computer Operated Transmission Measurement Set (COTMS) were used to insure that the equalizers performed as predicted. Finally, the equalizers were tested at WECo on COTMS using a criterion that was representative of the one used in the design phase. This insured that the manufactured units would also provide the predicted performance.

The subsequent discussion is intended to illustrate why and how the various operations are implemented in order to obtain realistic predictions of performance. Since this is not intended as a history of the project, only those developments directly related to computer simulation are discussed. Although it is a specific example, the discussion can serve as a guide so that designers of other systems can profit from the experience gained with T2.

II. ANALYSIS AND OPTIMIZATION

2.1 *Design Requirements*

A set of pulse equalizers was designed for the T2 digital transmis-

sion line which operates at 6.3 million bits per second.[1,2] The equalizer is a basic part of the repeater shown in Fig. 1. Its function is to reshape the pulses dispersed by the cable into a shape suitable for deciding what level was transmitted. These pulses are then sampled and regenerated for retransmission. The input and output of a typical equalizer are shown in Fig. 2. The upper trace is an individual pulse after dispersion by the cable as received at point A in Fig. 1 and the lower is the same pulse at the output of the equalizer, point B.

An actual transmission consists of a sequence of these pulses spaced one signaling interval apart. Since this interval corresponds to one division in Fig. 2, it is evident that equalized as well as unequalized pulses would overlap. Even if the equalizer output pulse was sampled exactly at its peak, the typical pulse has nonzero values at adjacent sampling times separated by the signaling interval. These nonzero values interfere with the decision made at the neighboring sampling times; this is referred to as intersymbol interference. Thus, the equalizer design will be influenced both by variations in sampling time and intersymbol interference caused by adjacent pulses.

The performance measure for equalizer design should reflect the influence of as many factors as it is feasible to include that might affect the correct regeneration of the transmitted information. Thus, the design criterion was error rate, the rate at which errors are made in regeneration. Since, for example, the design requirement for each regenerator may be less than one error in 10^7 transmitted pulses, excessive computer time is required for accurate estimation by accumulating errors; instead, the probability of occurrence is calculated. This calculation includes most sources of interference, for example, intersymbol interference, sampling jitter, thermal noise, and crosstalk due to neighboring transmission paths. The probability of errors

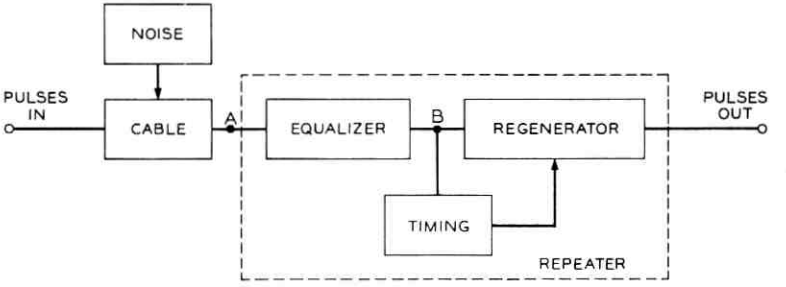

Fig. 1—A pulse repeater and its environment.

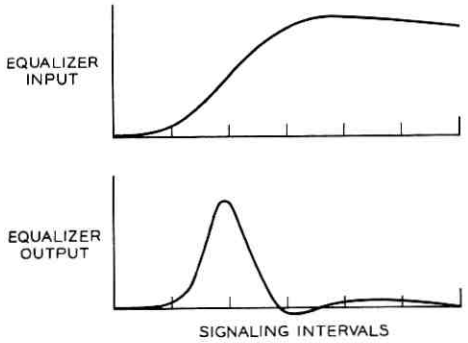

Fig. 2—Pulse interference caused by cable dispersion may not be entirely removed by equalization.

caused by noise can be kept low by maximizing the worst-case separation between adjacent signal levels; this separation is referred to as the eye opening.[1] The error rate will be a minimum if the eye opening which is inversely proportional to intersymbol interference is sampled at its largest point. It is the need to include all these factors in the criterion that makes it necessary to use a computer to obtain a realistic prediction of performance.

2.2 *Characterization of Transmission Medium*

In T2, the transmission medium is a twisted pair of insulated wires within a multi-pair cable. The dispersion produced by a cable pair depends on physical properties such as wire gauge, conductivity of the wire, capacitance, dielectric material and length of cable between regenerators; some of which are affected by temperature. To design an equalizer that compensates for dispersion, it is necessary that the medium be correctly modeled. This characterization requires that many individual cable pairs be accurately measured so that an average representation can be chosen that will reflect the proper dispersion of the pulses as cable length and temperature are varied. The averaging operation also smooths the data, thus minimizing the effect of measurement errors. Polynominals are then fitted to both the average loss and phase characterization. Thus, any required cable can be simulated by a proper choice of coefficients for the polynominals.

2.3 *Equalizer Configuration*

An adaptive configuration for the equalizer was selected to reduce the number of designs needed to cover the entire loss range, that is,

allowable cable lengths. The basic configuration contains up to three constant-R shaping networks and an automatic line build out (ALBO) network. A bridged-T, constant-R section, as shown in Fig. 3, produces a real zero and a pair of complex poles in the transmission path for reshaping the dispersed pulses. The ALBO is two simple RL sections whose singularities are adjusted to keep the output amplitude and shape constant. The variable elements in the ALBO are resistances whose values are determined by the forward resistance of diodes in a feedback control loop. This brief description is adequate for the present; for additional details see Ref. 2.

To summarize, the analysis objective was to simulate how the equalizers respond to various cable lengths, temperatures, and input pulse shapes so that the probability of error could be calculated. This analysis followed two paths, a digital simulation for calculating the error rate of a specific equalized transmission channel, and an analog simulation for investigating the influence of equalizer parameters on pulse shape. These two approaches were combined in a hybrid simulation that was used for iterative optimization.

2.4 *Pulse Transmission Program (PTP)*

This digital program can be used for calculating the pulse shape, eye opening, and error rate of a particular equalizer attached to a specified cable. The representation of the equalizer may consist of models, experimental measurements, or a combination of both. With this flexible program, it is possible to investigate the effect on equalizer performance produced by changing the cable characteristics and input pulse shape, as well as many arbitrary factors that influence the error rate calculation.

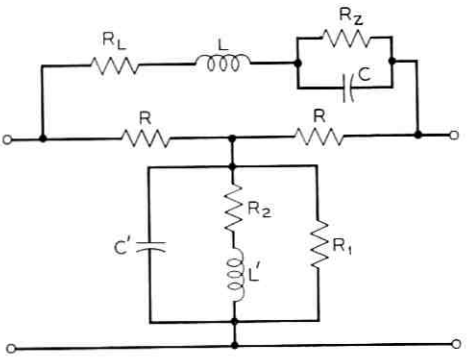

Fig. 3—Bridged-T equalizer section.

This program was the principal tool used in the initial design phase and it is still used for all investigations other than iterative optmization. The computational approach is to combine all the individual representations of the various sections into a single set of loss and phase data. An inverse Fourier transform is then evaluated to determine the equalizer pulse shape. From this pulse shape the eye opening and error rate are calculated. The ability to easily change representations is particularly valuable in allocating the design margins among the various sections of the system.

2.5 *Hybrid Simulation*

The equalizer was simulated initially on an analog computer because the time required for a digital calculation of the pulse response was too long for effective human interaction. The parallel operation of the analog components provides a rapid evaluation of the time response of continuous systems. Thus, the designer can modify equalizer parameters or circuit configurations while watching the effect on the pulse response. This ability to rapidly interact with the simulation enables the designer to develop intuition about the circuit operation and apply this knowledge to improve the design. This interactive capability was unique on the analog computer at the start of the design phase. Today, faster digital computers with graphic display devices can also provide some of this interactive capability.

The digital computer was first connected to the analog in a hybrid simulation to generate realistic dispersed pulse shapes for equalization so that the designer could observe immediately the influence of parameter variations on equalized pulse shape. This simulation was limited in its application because a more representative criterion, such as error rate, was required to properly weight all factors influencing the design. When more powerful digital computers became available, they were used to process the data from the analog computer in order to compute the error rate. Finally, a more modern hybrid made it possible to implement an automatic optimization strategy.

Since optimization was of prime importance, it was necessary to keep to a minimum the number of parameters to be adjusted. If this was not done, the time required for convergence to an optimum could become excessive, thus again making the human interaction ineffective. The bridged-T sections were represented by a single zero, two pole network rather than simulation of the actual configuration. This approximation assumes that the series and shunt arms are correctly matched. The use of a simplified representation, of course, requires

that the optimized parameters later be converted into the component values for the bridged-T networks. A digital program was written that selected from standard parts lists the component values nearest the values computed from the optimized parameters. The sections of the equalizer that were not to be optimized were simulated by considering the actual network configuration. This was done so that the models used could be made to conform to the measured device parameters, particularly, the diodes in the ALBO.

The program used for optimization was based on the general-purpose Hybrid Optimization Program (HOP)[3] that was modified specifically for T2. For each equalizer, an ALBO was designed manually and then the fixed equalizer sections were optimized automatically. The block diagram of the hybrid simulation of the equalizer is shown in Fig. 4. The optimization program allows for up to eight different cable lengths (that are representative of the range of application of the equalizer) to be used in designing the fixed equalizer. The Pulse Transmission Program described in Section 2.4 is used to generate the unequalized pulses that would occur with each cable. Each input is used to drive the equalizer simulated on the analog computer with the adaptive section properly adjusted for that cable. To evaluate the effect of thermal noise on each equalizer design, an impulse is used as an additional input. The equalized pulses are sampled and the thermal noise computed from the sampled impulse response; these are used to compute error rate on the digital computer. The worst of the eight individual error rates is used as the measure of performance for each equalizer.

An initial equalizer design is determined manually because the engineer must provide a reasonable starting point for the optimization strategy. The Simplex[3] strategy is used to select the next parameter set specifying an equalizer, and the entire process is repeated until the relative improvement in performance is below a pre-selected limit. The strategy requires only a scalar performance measure for each design and does not require that derivatives be computed as in a gradient search procedure. Thus, it is much less sensitive to measure-

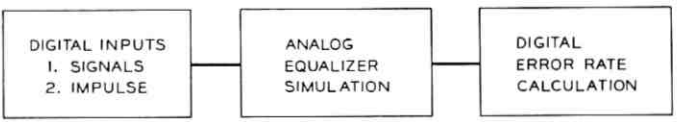

Fig. 4—Hybrid equalizer simulation used for optimization and tolerance analysis.

ment errors inherent in analog simulation. For an n parameter optimization, $n + 1$ designs must be evaluated initially. The procedure iteratively replaces the worst of the $n + 1$ designs by another design which is chosen along the line connecting the worst point with the center of gravity of the other designs in the n-dimensional parameter space. The best position along the line is determined by iteratively evaluating designs found by operations such as "reflection" about the center of gravity, "contraction" toward it, or "expansion" away from it.

This design strategy resulted in a set of equalizers that satisfied all requirements for the field trials. A final design phase will be necessary after the information gained in the field trials is taken into account. For this final phase a digital optimization program has just been written that provides data that is accurate and precise. A flexible simulation was no longer required for human interaction as the configuration has been chosen. Thus, it was possible to write a fast, digital analysis algorithm for this restricted application.

III. VARIABILITY ANALYSIS

Throughout the design phase, the engineer has been concerned with the realizability of the configuration and its sensitivity to parameter variations. Once the design has been optimized, it is necessary to verify that the performance will still be adequate when manufacturing limitations are considered and that the component tolerances are correct.

Tolerance analysis[4,5] is required because the optimized parameter values cannot be exactly realized in manufacture. The parameter values are not exact because components are usually available only in discrete ranges with a statistical spread in each range that is dependent upon the manufacturing process and the component's age.

Even after extensive analysis, it is still necessary to measure the performance of the actual circuits. First, prototype circuits must be tested to be sure that the predicted performance has been obtained. Each manufactured circuit must then be tested to ensure that it has been properly assembled. The computer can aid in diagnosing if predictions are not realized and also in automating the factory test procedures.

3.1 *Tolerance Analysis*

The Monte Carlo approach to tolerance analysis consists of simulating the system under investigation, randomly perturbing the param-

eter values and displaying the distribution of a scalar performance measure. With this approach, the influence of component variations on the nonlinear, error rate performance measure could be investigated with fewer assumptions and approximations than required with more analytical approaches. The most severe shortcoming with this approach is the amount of computer time required to acquire statistically significant information. Since analysis time is as critical as in optimization, the same hybrid simulation was used. To reduce the number of analysis runs, the designer can interact with the computer while watching a graphic display of a histogram of the performance measure. Thus, he can quickly terminate unsatisfactory runs, and also recognize by the insensitivity of the display to new data when sufficient samples have been accumulated rather than always accumulating the amount of data required by a pre-selected confidence limit.

The influence of parameter tolerances on the error rate to be expected from a pulse equalizer was investigated to aid in establishing the manufacturing specifications for both the bridged-T sections and the adaptive sections. The computer program repeats the following sequence of operations and accumulates the distributions under the user's control. A set of perturbed component values for each design is selected from the random distribution specified by the nominal values and tolerances with the relationship:

$$X_{\text{perturbed}} = X_{\text{nominal}}(1 + \text{Tolerance} \times \text{Random Number})$$

where the random number in the range ± 1 is selected from a scaled distribution. The component distributions used in the subsequent investigation are described in Section 3.1.1. Simulation parameter values are computed from the perturbed sets—on the hybrid computer these are potentiometer values. Both an unequalized pulse and an impulse are applied to the analog simulation to determine error rate, as during the optimization phase. It is possible to evaluate the error rate for one design every five seconds with this simulation.

The discussion of the information obtained from tolerance analysis is divided into three parts. In Section 3.1.2 only the bridged-T sections are perturbed, with the adaptive loop open, to determine an acceptable set of nominal tolerances for the passive components. In Section 3.1.3 the adaptive section operating closed loop is used to determine how closely the ALBO diodes must be matched. Finally, in Section 3.1.4 a closed loop simulation is used with all components perturbed to determine anticipated yield and establish limits for a factory acceptance test.

3.1.1 *Component Distributions*[6]

One of the most difficult problems in tolerance analysis is to obtain meaningful component data. If only a relative comparison is required, it is sufficient to use crude approximations to the actual distributions; but when one attempts to accurately predict yields, exact data is required with temperature effects and aging taken into account. Since only relative comparisons between various sets of tolerances were required for the analysis described in Section 3.1.2, all passive component values were assumed normally distributed with the nominal values as the mean. The standard deviation of the distribution was set equal to one-half the specified tolerance.

For proper closed loop operation of the ALBO, it is important that both sections act together to provide the correct pulse shaping. Unless the dynamic resistance of the individual diodes, used to provide the variable resistance, is approximately the same function of the control current, this tracking cannot be maintained. To provide adequate tracking, it was decided to select a set of matched diodes. The cost of matching a set will, of course, depend on the allowable resistance range within a set. Tolerance analysis was used to determine whether unusually tight control had to be established or standard production line techniques would be adequate.

The diodes are to be matched based on their measured resistance at two values near the upper and lower limits of control loop current. The matching operation was simulated in two steps. The first diode in each set was specified by choosing a pair of resistance values from measured distributions for that diode type. The two values could be selected independently because the resistance at the high current level depended primarily on the bulk resistance of the material while the bulk resistance is swamped by the normal diode resistance at the low level. The remainder of the set was obtained using two uniform distributions, having the specified matching limits, centered on the first pair of resistances.

The diode matching limits were chosen to reflect not only the original matching but also the changes that would occur with temperature and aging. For example, if the original match is assumed to be two ohms, the range may broaden to six ohms because of these effects. The tolerances on the passive components were the same as those used in Section 3.1.2.

After all tolerances had been specified for the components, additional investigations were performed to determine anticipated yield and performance variations that could be expected with a typical set

of tolerances. The component types were chosen after discussions with the potential manufacturers, and then distributions were selected based on the data available for these types. Since the inductors are the most expensive component, it is desirable to use the widest tolerance possible. With wider tolerances, it is important to carefully model the limiting distributions. Since the worst-case limits for aging are large, the inductor tolerance model included separate nominal and aging distributions.

3.1.2 *Bridged-T Tolerance*

First, the component tolerance in the bridged-T sections were investigated to determine the relationship between various sets of passive tolerances and variations in error rate. It was assumed that these sections are correctly terminated and that all other circuit parameters are set to their nominal values and the control loop is not active. All the components in the basic bridged-T equalizer section shown in Fig. 3 may have tolerances applied to them except the resistors labeled R, which set the characteristic impedance. To simplify the analog simulation, these resistor values were equated to the termination resistances that were not to be perturbed. In a tolerance analysis simulation, it is important to avoid programming simplifications that, although correct when nominal values are used, may not be valid when components are perturbed. For example, the bridged-T section can be analyzed as a second-order system if it is assumed that the series and shunt arms are properly matched. Since this match would be destroyed by the perturbations, a fourth-order simulation is required.

Let us consider the influence of the parameters on the error rate for one bridged-T section. Several sets of passive tolerances were investigated and the resulting histograms are replotted on probability paper in Fig. 5. On this paper, a normal distribution appears as a straight line with the standard deviation (σ) inversely proportional to the slope. The histograms with finite tolerances are clearly not normally distributed; thus, the sets cannot be compared on the basis of their standard deviations. The relative influence of the tolerance sets can be compared based on the yield at a selected error rate. If the threshold of acceptability for this equalizer were, for example, an error rate less than 10^{-10}, then with one percent tolerance on the Rs and Cs and three percent on the Ls, approximately 98 percent of the designs would be acceptable. With the low number of samples used to obtain this data, the absolute yields may not be accurate but a relative comparison is valid. In examining these data, it is observed

that a finite σ exists with no perturbations applied to the components; this is caused by the limited reproducibility of the analog simulation. This measure of reproducibility is valuable in determining whether the observed variability is produced by the programmed perturbations or machine errors. Since the equalizer was not optimized for this cable alone but for eight different cables, some designs with perturbed components produce error rates better than the nominal design.

The nonlinear nature of the error rate makes it difficult to estimate the effect of several bridged-T sections from single section histograms. This is illustrated in Fig. 6 which compares the histograms for each of the three bridged-T sections perturbed separately and all three simultaneously perturbed. The simultaneous perturbation of all three did not produce performance appreciably different from the worst of the individual sections (each section had different nominal component values). If one attempts to combine the individual section data to obtain a worst-case estimate of the overall three-section performance,

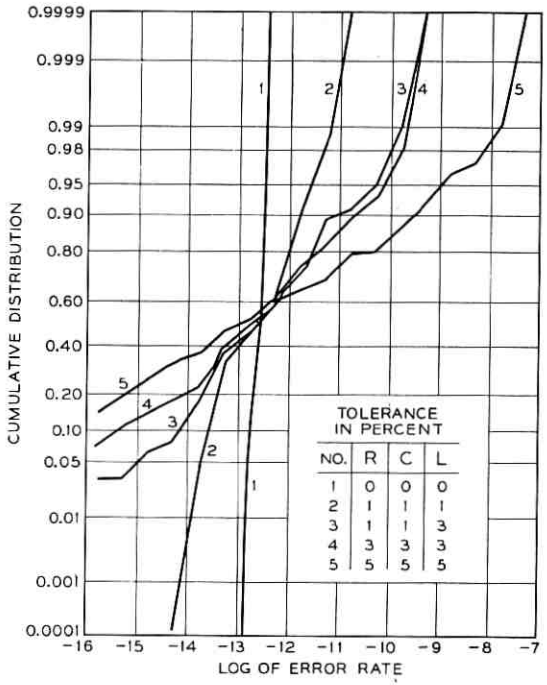

Fig. 5—Variation in error rate produced by applying component tolerances to one bridged-T section of a pulse equalizer.

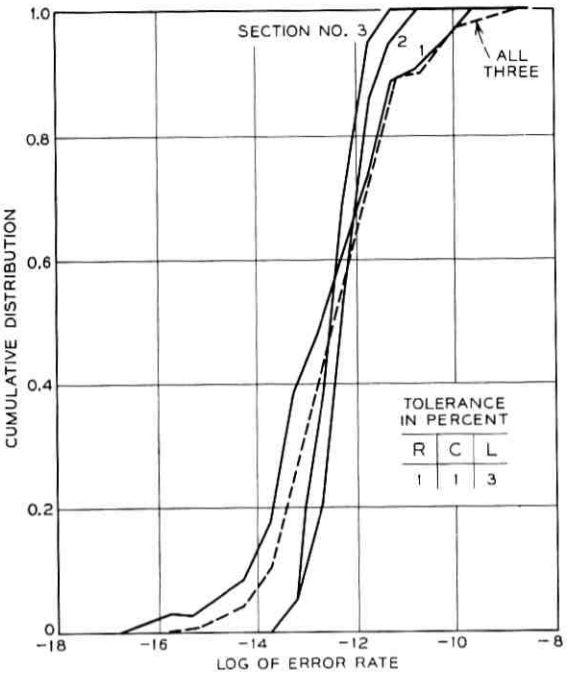

Fig. 6—Comparison of error rate variations produced by applying component tolerances to each of three bridged-T sections separately and to all three simultaneously.

a much more pessimistic estimate would result than the performance actually measured. If acceptable yields can be obtained with worst-case estimates, there is no need for measuring the distributions; but typically with "state of the art" designs, this is not the case and the use of actual distributions may allow the designer to relax some specifications and still obtain adequate performance.

As a result of these investigations, a set of tolerances were specified for the passive components in the bridged-T sections. The decision was based on allocation of margin, relative yields, and cost of various tolerances. It was verified that adequate performance could be obtained with commercially available components.

3.1.3 *Adaptive Equalizer*

The simulation was modified to include the effect of the adjustment loop before investigation of the parameter tolerances in the adaptive section. The adjustment of this loop will essentially compensate for

variations in the average value of diode resistance; thus, only diode mismatch would affect the error rate. For each perturbed design, a simple iterative procedure was used to determine a value of control current that would change the diode ac resistance and thus return the pulse peak to a reference level. The diode ac resistance is related to the control current by the model:

$$R = K_1 + \frac{K_2}{I}.$$

The coefficients K_1 and K_2 were calculated from each pair of resistance values specifying a diode. Then the resistance in the ALBO could be calculated for any value of control current.

The adjustment procedure consists of first determining a nominal current level for the unperturbed design that produces a reference pulse height. After the components are perturbed, the pulse amplitude is measured at the nominal current. The control current is then perturbed and the peak amplitude is measured again. The value of the control current to readjust the peak to the reference level can then be calculated. Since the relationship between control current and diode resistance is approximately linear in the region of adjustment, this iterative procedure produced satisfactory results. The iterative procedure lengthens the time to evaluate each design because several analog runs are required but the time is still less than ten seconds per design.

The results of a typical set of runs are summarized in Table I. Normal distributions were used on the passive components in the adaptive section with the standard deviation equal to one half the specified tolerance. From this data it is evident that the effect of diode mismatch is of secondary importance when compared to the effect of passive component tolerances. Additional runs verified that diodes matched to standard manufacturing limits would produce satisfactory

TABLE I—INFLUENCE OF ADAPTIVE SECTION TOLERANCES ON ERROR RATE

Diode Mismatch Ohms		Passive Tolerances %		Range of Variation in Log of Error Rate
R(20 μa)	R(1 ma)	R	L	
±100	±3	0	0	0.36
0	0	2	4	1.54
±100	±3	2	4	1.55

performance. Therefore, the cost of tightening the matching procedure was not justified.

3.1.4 *Entire Equalizer*

A complete simulation consisting of three bridged-T and two adaptive networks operating closed loop was used to estimate the error rate and eye opening to be expected with manufactured units. Component distributions that reflect the manufacturers' specifications were applied to a typical equalizer design and some of the results are shown in Figs. 7 and 8. The passive tolerances used were R—1.5 percent, C—2.0 percent and L—nominal 2.0 percent with 0.2 percent aging. The diodes were matched within six ohms at the high current level and within 200 ohms at the low level. Figure 7 reveals that for this equalizer connected to a specific length of reference cable, the error rate would never be worse than 10^{-27}. In Fig. 8, it is observed that the eye opening can be reduced from a nominal 77.5 percent to a 75.9

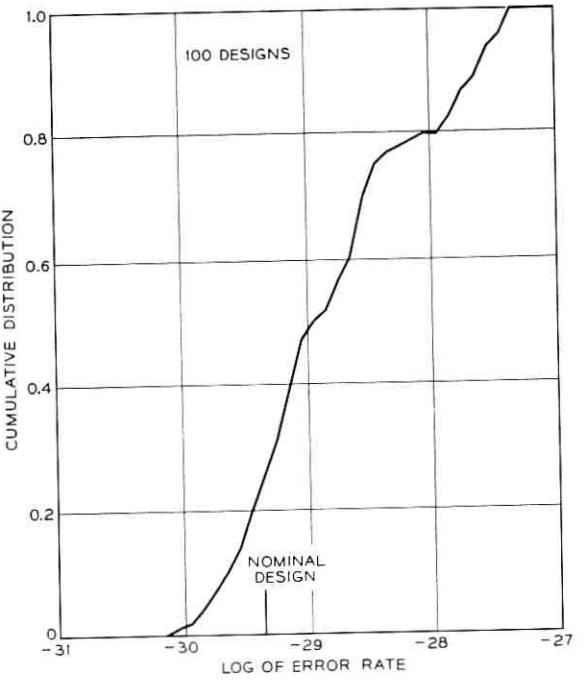

Fig. 7—Distribution of error rate resulting from application of typical manufacturing tolerances to all equalizer components.

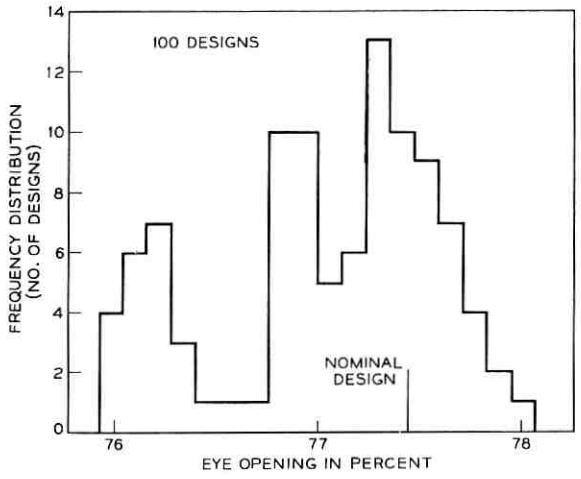

Fig. 8—Distribution of eye opening resulting from application of typical manufacturing tolerances to all equalizer component.

percent opening by component variations. Both these curves indicate satisfactory performance.

3.2 *Verification of Design*

Next we consider the computer aids available for verifying that the physical networks provide satisfactory performance. The approximations made in a simulation for computational efficiency are usually the reasons that disagreements between predicted and actual performance occur. For example, simplified device models and idealized network topologies are used to reduce the dimensionality of the system of equations being solved and thus save time. However, the real world may not be adequately represented because all the variability in the device is not included and effects such as spurious coupling are either ignored or crudely approximated.

When prototype equalizers were constructed, the performance was significantly worse than predicted and thus the cause and corrective action had to be determined. To determine the cause of poorer prototype performance, the circuits were measured and their performance compared to predictions. The computer can greatly alleviate the tedium of this task by automatically reducing the comparison data to a form suitable for evaluation by the engineer. The isolation of problem areas usually requires a degree of engineering judgment that is difficult, if not impossible, to implement in a general sense on the

computer. The engineer can often test the validity of his diagnosis, however, by modifying the computer models and determining if the predictions now correspond to the measurements.

In addition to making detailed comparisons of time domain waveshapes measured with an oscilloscope in the laboratory and computer predictions, computer-aided procedures were also used. The Computer Operated Transmission Measuring Set (COTMS)[7] was used to measure the insertion loss and phase of the entire equalizer and the individual bridged-T sections. These data were inserted in PTP, Section 2.4, to calculate the pulse shapes. For comparison the pole-zero configurations used in the design were also inserted in PTP. For example, it was determined by a comparison of the pulse waveforms from PTP that the data from an equalizer measured as a complete unit produced 20 percent more undershoot at the first sample point following the peak than was produced by its pole-zero configuration. However, the measurements of the individual sections when combined produced an undershoot only four percent larger than that produced by the poles and zeros. It was evident that individual section measurements when combined did not produce the same pulse shape either as an equalizer measured as a complete unit or as actually obtained in the laboratory. This indicated that some of the discrepancy might be due to spurious coupling paths between the sections of the equalizer. Similar combinations of measurements, computations, and laboratory results uncovered other problem areas. Improvement in computer models, rearrangement of component layout, and the introduction of shields resulted in pulse waveforms that agreed very closely with computer predictions.

3.3 *Manufacturing Test*[8]

A fundamental difference normally exists between the techniques used to evaluate the performance of a circuit during the design phase and during manufacture. One strives for reality at all cost during design but wants an inexpensive test in the factory. For computer-aided design, one selects a performance measure, such as error rate or eye opening, that reflects how the circuit will function when installed in a system. For economic reasons, however, normally only a few simple tests on individual circuits are performed during manufacture. Since it is usually difficult to devise a simple test that will be indicative of system performance, the factory test may not detect all units that would fail in service and/or may cause a rejection of units that would be acceptable in the field.

To insure that proper selection is made, it is desirable to use similar performance measures in the design phase and in manufacturing test. The cost of maintaining and using complete systems to test individual circuits and the difficulty in simulating worst-case field conditions has made this approach unacceptable in the past. Now in some cases it is feasible to use the design measure and test under worst-case conditions using computer-operated test facilities (COTMS). The computer that controls the measurements can also contain a program that converts the measurements into the system performance measure. This is accomplished by storing in the computer a representation of the remainder of the system that corresponds to the worst case. This stored data is combined with data measured for a particular circuit and the performance measure calculated. The stored representation makes it possible not only to simulate worst-case field conditions at the manufacturing level, but also to take system modifications that occur into account by simple software changes.

To efficiently run the test procedure on the small computer in COTMS, it was necessary to develop a fast algorithm that required limited storage. The PTP program served as a basis for the eventual algorithm. To improve the run time, the generality in the input structure was removed and all data except for the equalizer were precalculated. The computation of the complete pulse shape was replaced with a search algorithm that located the pulse peak. Then only those samples of the pulses needed in the computation of the performance measure were calculated. It was possible to develop a fast search algorithm because the approximate peak height and location are known from the prototype measurements. If the waveshape deviated significantly from the prototype, the equalizer must produce unacceptable performance. Additional time was saved by basing the test on eye opening rather than error rate.

This procedure has been used to measure manufactured equalizers. The acceptability limits on eye opening to satisfy system requirements were determined after considering the effect of the component tolerances, as displayed in Fig. 8, and performing a tolerance study of the influence of measurement precision.[9] The running of the test procedure for each equalizer requires approximately $1\frac{1}{2}$ minutes. The program also provides an interpretive dialogue that tells the COTMS operator what to do and when; thus, the operator requires little specialized training. Furthermore, the measured data for each equalizer is recorded on tape so that subsequent field failures can be related to the performance at manufacture.

IV. CONCLUSIONS

A complete computer-aided design procedure has been used on the T2 equalizer. Initially the computer was used only for analyzing the circuit performance. As more powerful computers became available, they were used to optimize the parameters and measure the influence of component tolerances. Finally, a manufacturing test that evaluated the equalizers based on worst-case system performance was developed. The procedure appears to be applicable to other systems.

When integrated circuits are used, it becomes increasingly important to accurately predict performance and perform optimization and tolerance analysis before construction. The cost of constructing experimental circuits and the time required for the construction make it unrealistic for the designer to use standard laboratory procedures. Rather than construct breadboards, the designer can use the computer to obtain similar information. Thus, the computer approach to designing realizable circuits may prove to be the most economical way to build equalizers and other complex circuitry.

V. ACKNOWLEDGMENTS

In the discussion of the various computer aids that have been applied to the T2 equalizer design, I have summarized the work of others in addition to my own work. Many members of the Digital Transmission Laboratory and Transmission Technology Laboratory have participated in this effort. I would like to acknowledge some of the major contributors and list a few of their specific contributions. A. J. Osofsky and Mrs. D. B. Kirby developed the original digital transmission analysis program that pre-dated the T2 project. Miss N. K. Shellenberger greatly expanded the capabilities of this program and adapted it specificially for T2. P. E. Rubin and R. L. Ferch developed the original analog simulation. K. R. Swaminathan extended the analog simulation and used it to design the first set of fixed equalizers. P. E. Fleischer and R. P. Snicer wrote the hybrid optimization program and designed the first adaptive equalizers. E. M. Underwood, W. G. Leeman and R. A. Hunter had the major responsibility for the difficult task of physically realizing the designs. D. R. Smith optimized the present set of equalizers, verified the correctness of the simulation, and wrote the new digital optimization program. Mrs. D. B. Snyder wrote the tolerance analysis program. Mrs. R. M. Allgair and R. G. Schleich wrote the manufacturing test program. The author is personally in-

debted to J. Chernak, J. M. Sipress, J. R. Davis and J. H. Davis for their guidance and encouragement.

REFERENCES

1. *Transmission Systems for Communication,* Bell Telephone Laboratories, Incorporated, Fourth Edition, 1970, Chapter 27, pp. 626–676.
2. Davis, J. H., "T2: A 6.3 Mb/s Digital Repeatered Line," IEEE Int. Conf. Commun. Record, 1969, pp. 34.9–34.16.
3. Fleischer, P. E., "A General-Purpose Hybrid Optimization Program," IEEE Conf. Computerized Elec. Proc., August 1969, pp. 187–204.
4. O'Neill, L. A., "Interactive Tolerance Analysis with Graphic Display," Proc. Spring Joint Computer Conference, 1969, pp. 207–213.
5. Bohling, D. M., and O'Neill, L. A., "An Interactive Computer Approach to Tolerance Analysis," IEEE Trans. Computers, *C-19,* No. 1 (January 1970), pp. 10–16.
6. Logan, J., "Characterization and Modeling for Statistical Design," B.S.T.J., this issue, pp. 1105–1147.
7. Geldart, W. J., Haynie, G. D., and Schleisch, R. G., "A 50 Hz—250 MHz Computer-Operated Transmission Measuring Set," B.S.T.J., *48,* No. 5 (May–June 1969), pp. 1339–1381.
8. O'Neill, L. A., "Extending Computer-Aided Design into the Manufacture of Pulse Equalizers," Proc. Fall Joint Computer Conference, 1970, pp. 471–475.
9. Haynie, G. D., and Yang, S., "Confirmation of Design Using Computer-Controlled Test Sets," B.S.T.J., this issue, pp. 1197–1208.

THE BELL SYSTEM TECHNICAL JOURNAL
Vol. 50, No. 4, April, 1971
Printed in U.S.A.

Statistical Circuit Design:

A Monte Carlo Tolerance Analysis of the Integrated, Single-Substrate, RC, *Touch-Tone*® Oscillator

By P. BALABAN, B. J. KARAFIN and MRS. D. B. SNYDER

(Manuscript received November 30, 1970)

Monte Carlo tolerance analysis has proven to be an effective tool in evaluating the sensitivity of a circuit design to manufacturing tolerances and environmental changes. Such an analysis involves repetitively "constructing" samples of the design in the computer, randomly selecting parameters that obey the manufacturing statistics; "tuning" the samples; and analyzing their operation under "field conditions." At the conclusion of this process one is able to form empirical distributions of circuit performance, to predict yield, evaluate tuning procedures, etc.

This paper describes a Monte Carlo study of two proposed designs for an integrated, single-substrate, RC, Touch-Tone® *oscillator. Difficulties arise in perfoming this study because (i) the statistics of integrated circuit components are closely correlated, and (ii) the inherent nonlinearity of oscillators coupled with tight circuit performance specifications require tailored analysis techniques.*

The study shows one of the two designs to be superior. A lower bound of 55 percent yield is predicted for this design, and a simple test for eliminating oscillators that fail to meet requirements is presented. Low transistor current gain is shown to be a dominant cause of failure. Lastly, asymmetry in the effects of impairments on circuit performance suggest a modification in adjustment strategy.

I. INTRODUCTION

The effective design of a circuit that will be mass-produced and subjected to a wide range of environmental conditions must go beyond the specification of a nominal circuit. It must include consideration of performance deviations due to parameter variations stemming

from manufacturing tolerances and environmental changes. Bounding these performance deviations is often the most difficult part of the design process.[1]

Monte Carlo tolerance analysis has proven to be a useful tool in dealing with these broader design questions. The approach, which is depicted in Fig. 1, simulates on a computer the process of picking a random sample of manufactured circuits, following these circuits through factory adjustment, monitoring their operation under field conditions, and compiling statistics on circuit performance.[2,3] Note that the Monte Carlo approach obviates the need for linearizing assumptions that characterize many other techniques for viewing product performance (worst-case, first-order sensitivities, etc.). It should be remembered that the response of even a linear circuit is a nonlinear function of its parameters.[2]

This paper contains the results of a computer tolerance analysis of two integrated, single-substrate, *Touch-Tone* oscillators. Section II describes the two designs and lists the performance specifications that must be met. The study produces distributions of oscillator frequency, amplitude and other measures for the various modes of circuit operation at several values of temperature. When these distributions are considered in the light of allowable degradations, several questions can be answered:

(*i*) Yield can be predicted. By yield we mean the ratio of circuits that will meet all field requirements to the total number produced without catastrophic failure. Computer simulation cannot include, for example, those cases where chips are damaged in handling or where silicon imperfections result in circuits being discarded.

(*ii*) Factory tests can be devised to insure that factory yield matches true yield. In other words, tests are devised such that the factory neither ships circuits that will fail in the field, nor discards those that would be acceptable. In the case where extremes of tem-

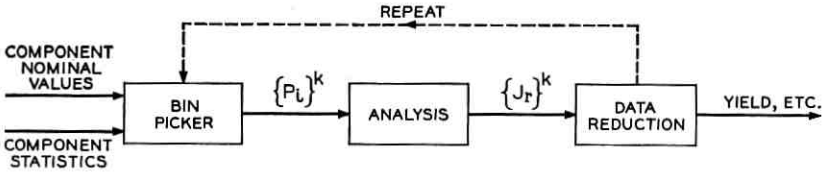

Fig. 1—Monte Carlo tolerance analysis. $\{P_i\}^k$, set of parameters for kth sample circuit; $\{J_r\}^k$, set of performance indices for kth sample circuit.

perature are encountered in the field, an effective but expensive factory test facility would involve a temperature chamber. The results of the study presented below indicate that a test on a secondary criterion (dc feedback current) at room temperature is an acceptable test of circuit performance over the full temperature range.

(*iii*) The parameter deviations that cause circuit failure can be identified. This information indicates where efforts to improve fabrication techniques should be concentrated.

Integrated circuits in general accentuate the need for automated tolerance analysis. The long turnaround time for masks and models and the expense associated with design changes make the ability to study such changes on the computer attractive, especially when one is interested in the implications of a change on manufacturing yield and field performance. In the particular case of a *Touch-Tone* oscillator whose production rate might exceed a million per year, accurate prediction of yield is vital in determining the economic feasibility of a design.

Unfortunately, while integrated technology increases the need for automated tolerance analysis, it also makes that analysis more difficult to perform. At each iteration of the Monte Carlo loop shown in Fig. 1, the block labeled "Bin Picker" must produce a set of parameters from which one sample circuit can be "built." Implementation of the "Bin Picker" is straightforward for discrete circuits. In that case, parameters are independent and the box is implemented by using random number generators to select element values from their individual distributions. By contrast, the parameters of a silicon integrated circuit are *not* independent. In fact, every element on the chip is correlated with at least every other element of the same kind, e.g., the βs of all transistors on the same chip are correlated with one another. It is a familiar fact that while a given resistor on a chip may vary by ± 15 percent from nominal, the ratio of any two resistors will vary by only ± 5 percent from nominal. It would not do, therefore, for the Bin Picker to select silicon resistors from distributions with limits of ± 15 percent. The Bin Picker must be concerned with both global statistics (the distribution of parameter values across the population of manufactured circuits) and chip statistics (the relationship of parameter values on any given chip).

A comprehensive treatment of the statistical characterization of integrated circuits appears in Ref. 4; comments particular to the *Touch-Tone* oscillator are contained in Section III below.

While the fact that the *Touch-Tone* oscillator is an integrated circuit complicates the Bin Picker, its nonlinear character presents difficulties in the implementation of the Analysis box of Fig. 1.* The analysis of linear circuits is accomplished by algebraic manipulations, a task at which the digital computer is fast.[2] Nonlinear circuits, on the other hand, require the integration of the differential equations describing the circuit. Unfortunately, the digital computer is slow at this task.[3] The problem is complicated further by the fact that the system of differential equations describing the *Touch-Tone* oscillator is stiff, i.e., has eigenvalues differing by several orders of magnitude. This is not surprising since we have a kHz oscillator built with MHz transistors. Although efficient algorithms have recently been developed to handle stiff systems of differential equations,[5] analysis of a single oscillator at a single temperature that provides sufficient accuracy to determine whether or not the rather stringent design requirements (e.g., ± 0.1 percent frequency deviation due to amplifier variations) are met requires in excess of *ten hours* of computer time on a CDC 3300. Since several hundred oscillators will have to be analyzed at a number of temperatures, such an analysis time for a single oscillator is unacceptable. Special analysis techniques, therefore, had to be developed for the *Touch-Tone* oscillator study. These techniques, which are described in Section IV, reduce the analysis time for a single oscillator to about 3 minutes.

The results of the tolerance study are presented in Section V. Histograms of oscillator frequency and amplitude are presented at $-40°C$ and $+60°C$, the temperature extremes expected in the field. Further, the change in amplitude with frequency selection is discussed. The oscillator is designed to generate four tones, corresponding to different user selection of dial digits. The change in amplitude with "button-selection" is significantly different from what one might expect by looking at the oscillator as a quasi-linear system. Finally, the implications of using a dc feedback current measurement at room temperature as an oscillator acceptance test is discussed.

It should be kept in mind that while this paper is concerned primarily with the computer study of the single-substrate, *Touch-Tone* dial, that study has been carried on in parallel with laboratory testing of breadboards and models. The extent to which these two approaches—laboratory and computer—have complemented one another cannot

* Oscillators are inherently nonlinear; some phenomenon must be present to limit the amplitude of oscillation.

be overemphasized. In many instances the direction of the computer study was influenced by effects observed in the laboratory, and vice versa. Further, the assumptions and many of the qualitative results detailed below have been corroborated experimentally.

II. THE OSCILLATORS AND THEIR REQUIREMENTS

The dial incorporated in the Bell System *Touch-Tone* telephone contains two multifrequency audio oscillators to perform the dialing function. These oscillators and the associated switching are used to generate appropriate frequencies (a unique pair for each button on the dial) for dial switching information.

In this paper we study two RC, single-substrate, integrated oscillators that have been proposed as replacements for oscillators currently in use.

Each RC oscillator contains a nonlinear active device, a Twin-T feedback network and a buffer stage for connection to the telephone line (Fig. 2). The Twin-T portion of the oscillator is a tantalum, thin-film circuit whose schematic and voltage transfer ratio are shown in Figs. 3a and b, respectively. The notch depth of the voltage transfer characteristic is adjusted to −37 dB. The oscillator is designed to produce tones of four separate frequencies. The switches, S1 to S4, in Fig. 3a are used to select the different frequencies by changing the value of R_2. The Twin-T is so designed that the changes in R_2 have only a small effect on notch depth.

The nonlinear active device is an integrated silicon dc-coupled amplifier with a built-in limiter. Figure 4 shows the voltage transfer characteristic of such an amplifier. To sustain an oscillation, the

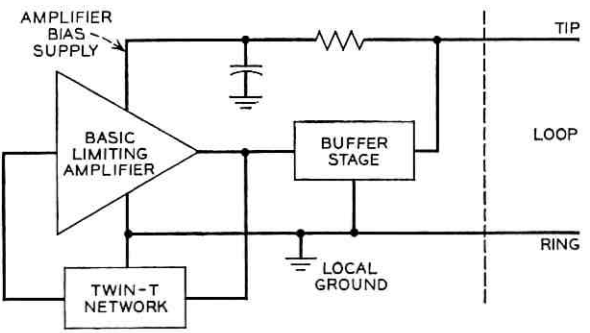

Fig. 2—Basic oscillator configuration.

slope of the amplifier transfer characteristic (gain) in the vicinity of the steady-state operating point must exceed 37 dB—the loss of the Twin-T network. The limiting voltage (E_{LIM}) of the amplifier must be controlled so that oscillator amplitude can be controlled. E_{LIM} is controlled by a tantalum resistor on the same substrate as the Twin-T network that is anodized during oscillator adjustment.

After an amplifier chip is bonded to the thin-film circuit, each component of R_2 in the Twin-T circuit is adjusted at room temperature so that each of the four tones is within ±0.2 percent of its nominal frequency. Once the frequencies have been adjusted, deviations in each of the four frequencies from their tuned values due to amplifier changes over a temperature range of −40°C to +60°C must be within ±0.1 percent.

Amplitude of oscillation at one of the four tones is also adjusted at room temperature to within ±0.5 dB of its nominal value. The deviation in the amplitude of the adjusted tone must be less than ±1.0 dB due to temperature-induced changes in the amplifier. Further, the range of amplitudes of the four tones must be within ±1.0 dB at any temperature. One way of viewing these requirements is to say that oscillator amplitude must be within ±2.5 dB from nominal over the full temperature and tone frequency ranges.

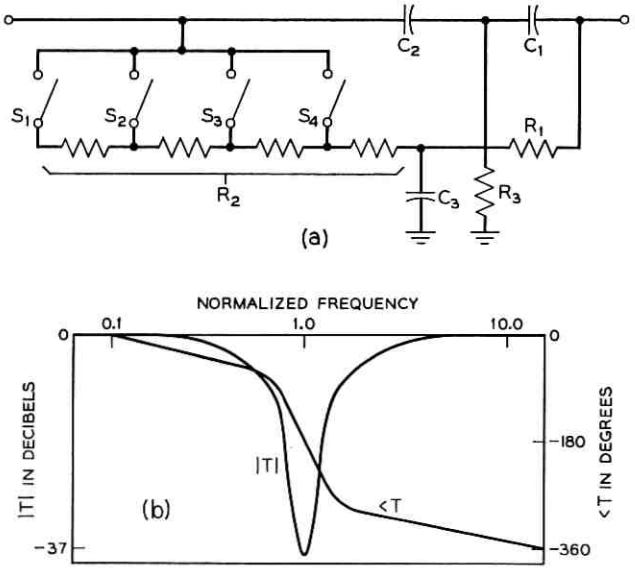

Fig. 3—(a) Twin-T schematic, (b) Twin-T no-load transfer ratio.

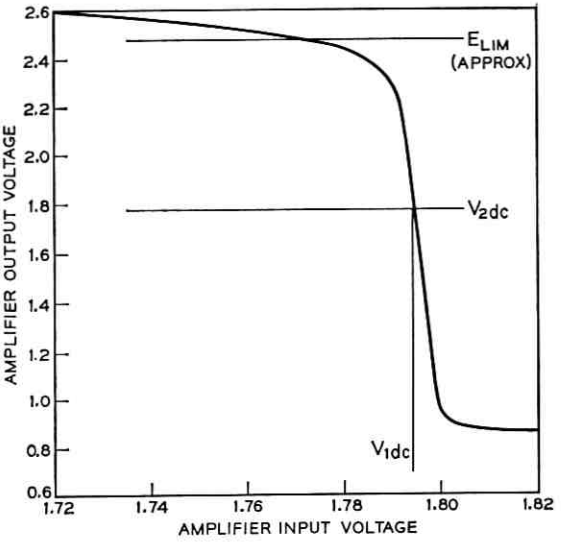

Fig. 4—Typical amplifier static transfer curve.

Requirements are quoted in terms of temperature effects on the amplifiers since the two designs under study differ only in the amplifiers used. It is possible, therefore, using the computer, to hold the Twin-T at nominal temperature while subjecting the amplifier to the full temperature range and thus separate out deviations due to amplifier sensitivity.

To achieve the required amplitude and frequency stability (as well as low distortion), the amplifier should exhibit: (*i*) high ac input impedance, (*ii*) low ac output impedance, (*iii*) small dc input current, and (*iv*) constant gain in the linear region.

Schematics of the two amplifiers (henceforth called A and B) are shown in Figs. 5 and 6. Both amplifiers achieve limiting via nonlinear feedback: In Amplifier A, transistor Q_3 is cut off until the output voltage divided by the R_1R_2 voltage divider is sufficient to turn it on. In other words, Q_3 is cut off in the high gain region, but provides limiting when it goes active. R_2 is a tantalum resistor that can be adjusted to control the limiting point and hence the oscillator amplitude. In Amplifier B, transistor Q_6 is cut off in the high gain region and is turned on when the output voltage divided by the $R_8R_{91}R_{92}$ voltage divider is high. R_{92} is tantalum and is used to adjust oscillator amplitude. The basic differences in the amplifiers are that B has substan-

tially higher input and lower output impedances than A. Furthermore, while the input impedance of A degenerates in the limiting region, the input impedance of B is held at a high level by the feedback provided by R_5. The input impedance of B drops off only when Q_4 goes into cutoff, a condition that is avoided by keeping the oscillator gain margin relatively low.

It should be clear that the above discussion is qualitative. For example, it is difficult to make precise statements about the effects of low input impedance of Amplifier A in the limiting mode. Furthermore, both amplifiers are satisfactory when built with nominal device parameters. It is left to the computer tolerance analysis to supply data with which to compare the two designs when subjected to manufacturing tolerances and temperature extremes.

III. THE VARIATION OF PARAMETERS

In the simulation each iteration of the Monte Carlo loop shown in Fig. 1 represents the "building" of one sample oscillator. The circuit's nominal parameters at 20°C are altered by techniques described in Ref. 4 using appropriately shaped random number generators and the device fabrication statistics. The circuit "built" with these altered parameters is then put through a simulation of the adjustment procedure to arrive at values for the adjustable elements. At this point

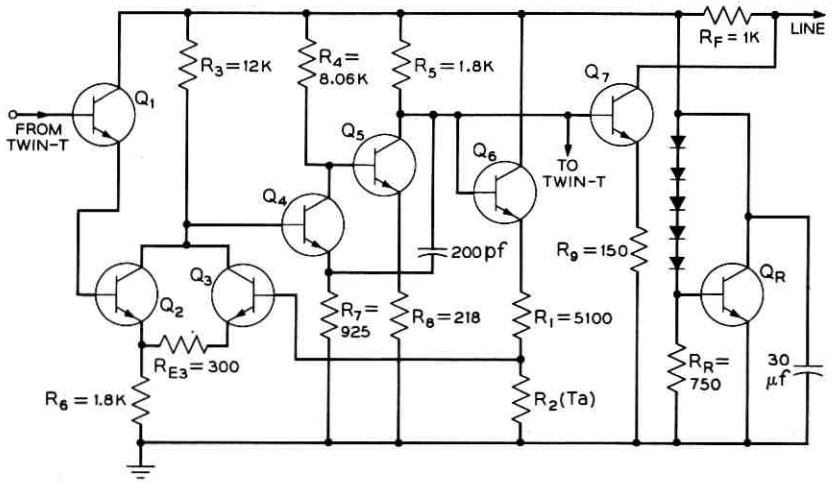

Fig. 5—Amplifier A schematic.

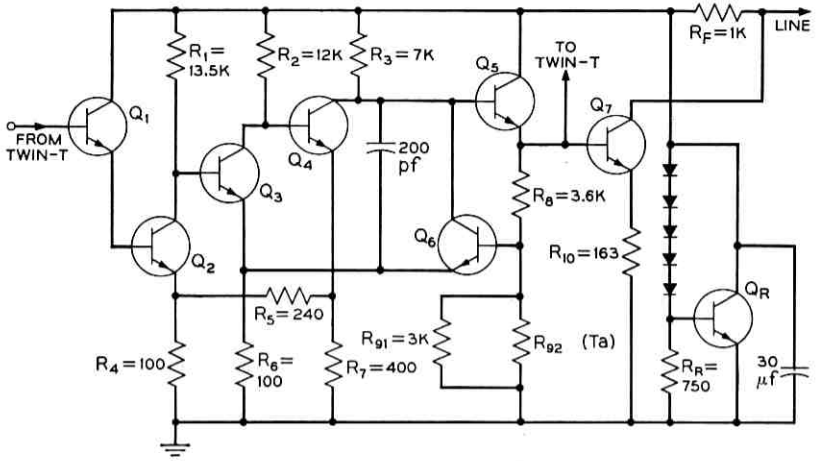

Fig. 6—Amplifier B schematic.

we have a realistic sample circuit that is ready for "installation in the field." Its operation at 20°C is analyzed; frequency, amplitude, loop current, etc., are noted. The parameters are then again altered in accordance with their temperature behavior to simulate circuit operation at other temperatures of interest. Further, at each temperature, the variable arm resistor of the Twin-T is stepped through four values to allow simulation of the production of the oscillator's four tones.

In the *Touch-Tone* oscillator study, the parameters of the tantalum Twin-T network are held fixed at their nominal values at 20°C, while the parameters of the amplifier are chosen in accordance with expected statistical manufacturing variations and subjected to temperatures of −40°C, +20°C and +60°C. (The change in performance of a given realization of either of the oscillators is expected to be monotonic with temperature. Therefore, the oscillators are tested at nominal and at the extremes of the temperature range of interest.) This line of attack is taken so that oscillator degradations due to the amplifier imperfections can be isolated; performance and influence of the Twin-T components are relatively well understood. With the exception, then, of the tantalum adjustment resistor, the parameters that the Bin Picker is concerned with are those of the silicon, integrated amplifier.

Further, the silicon amplifiers are treated as infinite-bandwidth devices. The amplifier capacitors, both inside and outside the transistors, are ignored. Hence, the amplifiers are modeled as networks of

resistors and Ebers-Moll dc transistors.[4] The parameters that are subjected to Monte Carlo perturbations and vary with temperature are: (*i*) transistor forward current gain, β_N; (*ii*) silicon resistors, R_S; (*iii*) base resistors, R_B; and (*iv*) collector and emitter intercept currents, I_{CS} and I_{ES}. In normal operation of either amplifier, no transistor is in saturation. Therefore, it is assumed that effects of variation in the reverse current gain, β_I, are negligible, and so β_I is held constant for all transistors, $\beta_I = 1$.

It is clear that the results of the Monte Carlo study are only as accurate as the characterization of the manufacturing and temperature variations of the above parameters. Unfortunately, statistical data for silicon, integrated circuits is very sketchy. The data used for this study is a combination of (*i*) data on "similar" transistors, (*ii*) measurements of a limited number of *Touch-Tone* devices, and (*iii*) some educated guessing by the device designers and modelers. Because of the uncertainty in the data, no attempt has been made at rigorous statistical characterization of the silicon process. Instead, coefficients were estimated for the assumed mathematical model such that the silicon parameters, spreads, and correlations produced by the Bin Picker "match" what measurement data exist and are consistent with what is expected by the device designers.

The precise distributions, correlations, temperature coefficients, etc., that were used in this present study may be found in the more thorough discussion presented in Ref. 4.

IV. ANALYSIS

Both amplifiers under study are very broadband. Since the intended frequencies of the oscillators are below 2 kHz, the amplifiers are assumed to be of infinite bandwidth. The amplifiers are thus treated as nonlinear, memoryless, two ports; all capacitances, both those intrinsic to the transistors and those added to suppress high-frequency oscillations, are ignored. The amplifiers are then analyzed as networks of resistors and Ebers-Moll dc transistors.

The nonlinear two-port, Fig. 7, can be characterized by:

$$\begin{aligned} v_2 &= f_1(v_1, i_2), \\ i_1 &= f_2(v_1, i_2). \end{aligned} \tag{1}$$

Since the output current of both amplifiers is small, we can use a Taylor series expansion of (1) around $i_2 = 0$. Keeping the first two terms of the expansion of the first equation, we have

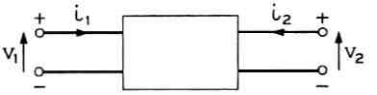

Fig. 7—Nonlinear two-port.

$$v_2 \approx f_1(v_1 , 0) + \left.\frac{\partial f_1}{\partial i_2}\right|_{i_2=0} i_2 . \tag{2}$$

The first term is the open circuit voltage gain of the amplifier, while the second term coefficient is the incremental output impedance.

The second equation of (1) is handled even more simply, since

$$\left.\frac{\partial i_1}{\partial i_2}\right|_{i_2=0}$$

the incremental reverse current gain, is near zero for most multistage amplifiers. Hence,

$$i_1 \approx f_2(v_1, 0).$$

To characterize the amplifiers it is, therefore, only necessary to compute three nonlinear functions:

$$v_{20} \equiv f_1(v_1 , 0) \quad \text{(the no-load gain function)} , \tag{3a}$$

$$i_1 = f_2(v_1 , 0), \tag{3b}$$

$$Z_0 \equiv \frac{\partial f_1(v_1 , 0)}{\partial i_2} \equiv f_3(v_1 , 0), \tag{3c}$$

each of the independent variable, v_1 .

Having computed these functions for each amplifier produced by the Bin Picker at each temperature, the analysis of the oscillator is carried out in a manner illustrated by Fig. 8. In words, the nonlinear

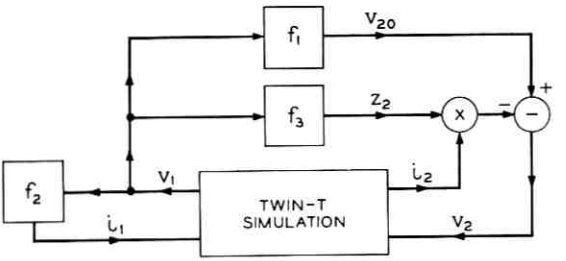

Fig. 8—Oscillator simulation.

functions describing the amplifier are used to supply the necessary port termination to the differential equations of the Twin-T. This set of differential equations, made nonlinear and implicit by the addition of the amplifier functions, are then solved using an implicit, numerical integration scheme to produce $v_2(t)$, the oscillation output, as a function of time from which oscillator frequency and amplitude can be measured.

To compute the three functions (v_{20}, i_1, Z_0), we proceed as follows: Fig. 9 is a block schematic of the oscillator and its environment. A fixed length is assumed for the loop (6 kft). The bypass capacitor, C_1, is assumed to be an ac short circuit, and hence V_0 is taken as a constant dc potential.* The first step is a computation of V_0 for each amplifier produced by the Bin Picker at each temperature. Since distortion is very low in the amplifier, the assumption is made that the dc current supplied to the amplifier in steady state is equivalent to the dc currrent supplied when the Twin-T is replaced by its series resistance.

The mesh equations of one amplifier with the dc resistance of the Twin-T in the feedback loop are written. V_0 is assumed an external source. The buffer transistor is added by assuming it always operates in the active region so that the collector current, I_C, is determined by the base-emitter junction operation. The linear equations of this set are solved leaving a set of nonlinear algebraic equations, one equation for each nonlinear junction. We will call this set of equations the basic set for the amplifier. To account for the remainder of the configuration of Fig. 9, we augment the basic set with equations that describe the regulator, the equalizer, and an equation that accounts for the second amplifier. This last equation is:

$$V_0 = E_B - (2I_S + I_R)(R_F + R_L) - (2I_C + I_H)R_L.$$

This augmented set of nonlinear algebraic equations is then solved by a norm-reducing, Newton–Raphson technique. The results of this analysis are: V_0 ; V_{1dc}, the voltage at the input of the amplifier; V_{2dc}, the output voltage of the amplifier or the input voltage to the buffer stage; and a quantity that turns out to be of special importance in analyzing the results, I_{dc}, the current through the dc resistance of the Twin-T, i.e., the current into the input of the amplifier when the Twin-T is replaced by its dc resistance. Since output distortion of the oscillator is expected to be low, V_{2dc} is the "center line," or average

* Consideration of the effects of variable loop length would require inclusion of the capacitor, C_1, in the simulation model.

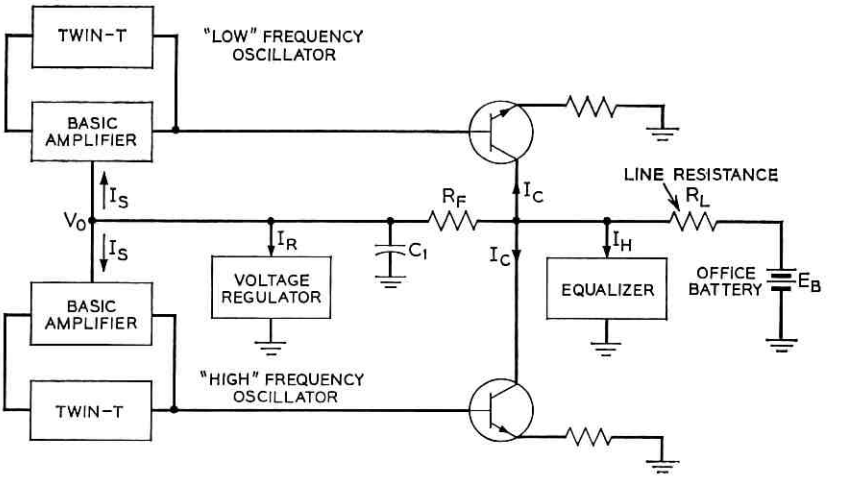

Fig. 9—Block-schematic of oscillator and related circuitry.

voltage of the oscillator output. Hence, crossings of V_{2dc} are used to measure frequency during the dynamic simulation. Further, we know that in calculating three functions (3a–c), we can restrict the range of v_1 to include and be slightly larger than the high gain region shown in Fig. 4. The value, V_{1dc} , gives us a point in the high gain region, fixing the position of that region in the range of v_1 . It should be noted that the high gain region shifts considerably over v_1 from amplifier to amplifier and from temperature to temperature. It is therefore important to fix the position of the region to minimize the necessary computation in building (3a–c).

Once V_0 , V_{1dc} and V_{2dc} are computed, we return to the basic set of equations. The dc resistance of the Twin-T is removed and a voltage source, V_1 , is connected between the input to the amplifier and ground. V_1 is then stepped in 1.5 mV increments and around V_{1dc} to cover a range of 150 mV, and v_{20} and i_1 are calculated. The process is repeated with the addition of a small current source at the output of the amplifier to compute Z_0 .

Once the functions (3a–c) are computed, we could proceed to the dynamic simulation of the oscillator as shown in Fig. 8, if it were not for the frequency and amplitude adjustments that must be made. These adjustments are accomplished in the following manner: Considering frequency tuning first, we realize that tuning is necessary because of manufacturing tolerances on the components of both the

tantalum and silicon circuits. Since our simulation has exact values for tantalum components, one cause of frequency deviation is removed. Further, because frequency deviations are expected to be small, we make the assumption that frequency deviations due to temperature in a given oscillator are independent of frequency tuning. In other words, for a given oscillator the frequency difference measured between +20°C (the tuning temperature) and any other temperature is independent of the actual frequency at +20°C, at least for the expected deviation between tuned and untuned +20°C frequencies. We further assume that frequency tuning has a negligible effect on oscillator amplitude. With these assumptions we eliminate the need for frequency tuning and proceed as follows. Each oscillator is simulated at +20°C. The frequency is measured; call it f_{20}. The difference

$$\Delta f = f_0 - f_{20}$$

is calculated, where f_0 is the nominal frequency. The oscillator is then simulated at other temperatures and the frequency measured to be f_T'. The frequency predicted for the oscillator at temperature T (again accounting only for effects in the amplifier) is then

$$f_T = f_T' - \Delta f.$$

Amplitude adjustment cannot be handled so simply. In our simulation, the tantalum tuning resistor in the amplifier is actually adjusted at +20°C and at one *Touch-Tone* frequency to produce an amplitude within the tuning specs, ±0.5 dB. This is accomplished by repetitively simulating, measuring, adjusting, simulating, etc. By using a sub-loop adjustment while (3a–c) are being calculated so that $E_{\text{LIM}} - V_{2\text{dc}}$ (see Fig. 4) is the desired peak amplitude, accurate adjustment can usually be made with one iteration of the full simulation. It should be remarked that if the amplifier and Twin-T were perfectly buffered from one another, $E_{\text{LIM}} - V_{2\text{dc}}$ would be an accurate prediction of amplitude. Hence, those amplifiers for which the prediction is poor and which require more than one or two iterations of the full simulation loop are precisely those amplifiers with poor performance.

Upon completion of amplitude adjustment, the resulting amplifier functions are used in the simulation shown in Fig. 8. This dynamic simulation is run for 30 cycles of the oscillator fundamental to obtain accurate measures of steady-state amplitude and frequency.

The separation of the oscillator into an infinite-bandwidth, nonlinear amplifier and a linear frequency selective network reduced the computation time for a single oscillator by at least two orders of magni-

tude from the time required by the most efficient nonlinear circuit analysis programs.

V. RESULTS

Monte Carlo studies were made on several versions of oscillator A, i.e., for several sets of suggested nominal parameter values. In every case the results were discouraging, i.e., only a small number of Monte Carlo samples passed the oscillator specification tests. On the other hand, the results of Monte Carlo studies on oscillator B are encouraging. The differences in the results of the studies of the two oscillators are so great that oscillator A has been abandoned as a contender for the next generation of RC *Touch-Tone* dials.

Figure 10 displays the histograms of oscillator A frequency at

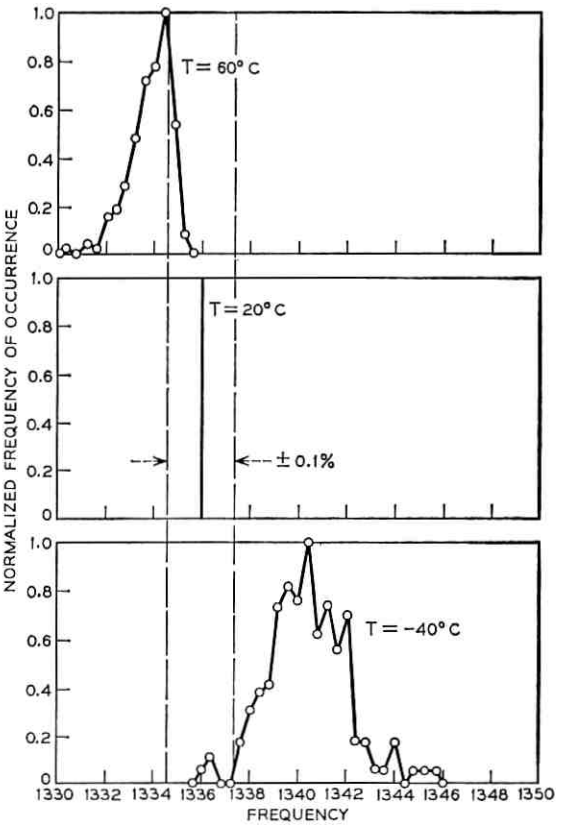

Fig. 10—Amplifier A normalized frequency histograms, $f_0 = 1336$ Hz.

60°C, 20°C, and −40°C. This histogram at +20°C is an impulse since the oscillators are tuned at this temperature. The histograms at the other two temperatures, however, show that the majority of oscillators fall outside the 0.1 percent frequency limits; only four sample oscillators, of 200 tested, were inside the frequency limits. With frequency stability this poor, further tests of the oscillator were not performed.

Poor frequency stability is explained by loading of the Twin-T by the amplifier,* loading that is largely eliminated in oscillator B. Both input and output impedances of the amplifiers under study are nonlinear, i.e., change during the oscillator cycle. Hence, no linear analysis of Twin-T loading is possible. However, by examining the extremes of these nonlinear impedances, we can make qualitative statements about frequency stability.

A typical sample of amplifier A has an input impedance that varies between 165 kΩ and 1.5 MΩ at +20°C and between 80 kΩ and 785 kΩ at −40°C. Even if these impedances were constant at their maximum values, i.e., if the input impedance of the amplifier were 1.5 MΩ at +20°C and 785 kΩ at −40°C, the change in the −180° phase point of the Twin-T is almost 0.1 percent. Changes of the −180° point at the low impedance level, i.e., between 80 and 165 kΩ, are very large. Since the −180° phase point determines the frequency of oscillation, we see that amplifier A has insufficient input impedance to provide an acceptable oscillator.

Typical samples of amplifier B, on the other hand, have input impedances varying between 900 kΩ and 19 MΩ at +20°C and between 700 kΩ and 14 MΩ at −40°C. At these impedance levels, shift in the Twin-T −180° phase point is negligible.

An additional factor is that amplifier A has output impedance as high as 1.6 kΩ while that of amplifier B is held below 250 Ω.

The preceding discussion intimates that oscillator B will be frequency stable. As we shall see below, this is correct, and although amplitude stability causes some difficulties, the Monte Carlo study predicts a lower bound of 55 percent yield for oscillator B.

5.1 *What is Yield?*

When dealing with integrated circuits, the word "yield" must be interpreted with caution. Tests are performed at many points in the

* This effect has been observed both with computer simulations and model tests at Bell Telephone Laboratories at Indianapolis. It has been observed further that increases in transistor β_N increase the frequency stability of oscillator A.

multistep fabrication process with some number of circuits rejected at each test. The actual yield, i.e., the ratio of satisfactory circuits to the total number of circuits for which fabrication was begun, may be quite low. Economically, however, the cost of rejecting circuits at an early fabrication step is much lower than rejecting a circuit that fails a final manufacturing test. Therefore, no single yield figure is a complete measure of the economics of a design.

The population from which yield is predicted in this paper is first a population of amplifiers; it is assumed that tantalum circuits to which the amplifiers are appliqued are perfect. Second, the amplifier population already has deleted from it those amplifiers, perhaps entire slices, that have been rejected in fabrication tests meant to insure the integrity of the circuits. Circuits with shorts, opens, etc., have been deleted, and components are within broad tolerance limits, i.e., resistivity measurements insure a ± 15 percent spread in resistance values and a variety of tests, including junction breakdown, impose limits on transistor parameters.

In short, the population from which we predict yield is a population of amplifiers each of whose circuits are topologically equivalent to the schematic of Fig. 6 and all of whose parameters are within the limits defined in Ref. 4. It is the population with which one would expect bonding to begin, and, most importantly, the population where failure to meet specification is costly. The yield figure we predict is the yield which is most indicative of the virtue of an electrical design, failures removed prior to construction of our population being process dependent and independent of electrical design.

The outlook for oscillator B is actually brighter than even the 55 percent yield prediction indicates. Four major factors should be considered, viz.,

(*i*) The statistics used to select amplifier parameters were, in general, pessimistic. In this sense, the 55 percent yield figure represents a lower bound. Further, processing improvements which might be expected once the circuit is in full production, especially improvements that increase transistor Betas, will increase yield.

(*ii*) Self-heating of the chip has been ignored in the study. As we shall see, low temperature operation is the limiting condition of the design. Because of self-heating, it is possible that the chip may never operate at $-40°C$, the lowest expected environmental temperature.

(*iii*) It should be noted that the temperature at which amplitude is adjusted ($+20°C$) is not centered in the temperature range over

which the oscillator must operate (−40°C to +60°C). Furthermore, amplitude is not a symmetric function of the impairments, e.g., the change in amplitude for negative temperature changes is larger than with positive changes. Hence, a gain in yield may be realized by adjusting amplitude off nominal.

(*iv*) Perhaps most important is that the results of the study show that a simple go/no-go test may be performed on the amplifiers before they are bonded to the tantalum circuits to weed out the 45 percent that fail.

Now to take a detailed look at the results.

5.2 *Frequency Stability*

Figure 11 shows the frequency histograms for oscillator B at the temperature extremes. Note that all the oscillators are well within the ±0.1 percent limit. In fact, the oscillators are within ±0.05 percent limits. Hence, as far as frequency is concerned, oscillator B has 100 percent yield. The tight stability has suggested that the notch depth of the Twin-T circuit can be relaxed from 37 dB to 36 dB to ease tantalum fabrication.

5.3 *Amplitude Stability*

Figure 12 shows the amplitude histograms at frequency f_2,* at the adjustment temperature and at the temperature extremes. Notice that the only failures occur at −40°C. These failures represent 25 percent of the sample amplifiers. Note that all the oscillators meet the adjustment specification by a safe margin.

5.4 *Amplitude Change with Tone Frequency*

To examine the change of amplitude with tone change, examine Fig. 13. This figure is a profile of one oscillator; it has 12 data points—four tones, each at three temperatures. Considering the design of the oscillator, one would possibly expect amplitude to increase monotonically with tone frequency. One might argue as follows: The amplifier limits on only one side, and the point of limiting is unaffected by tone change. On the other hand, the base line of oscillation is approximately given by the point on the gain curve where

$$V_2 - R_T I_{dc} = V_1 ,$$

* The oscillator is designed to generate tones of four different frequencies. Henceforth we denote the nominal values of these four frequencies by f_1 through f_4. f_1 = 1209 Hz, f_2 = 1336 Hz, f_3 = 1447 Hz, and f_4 = 1633 Hz. Amplitude is adjusted at f_2.

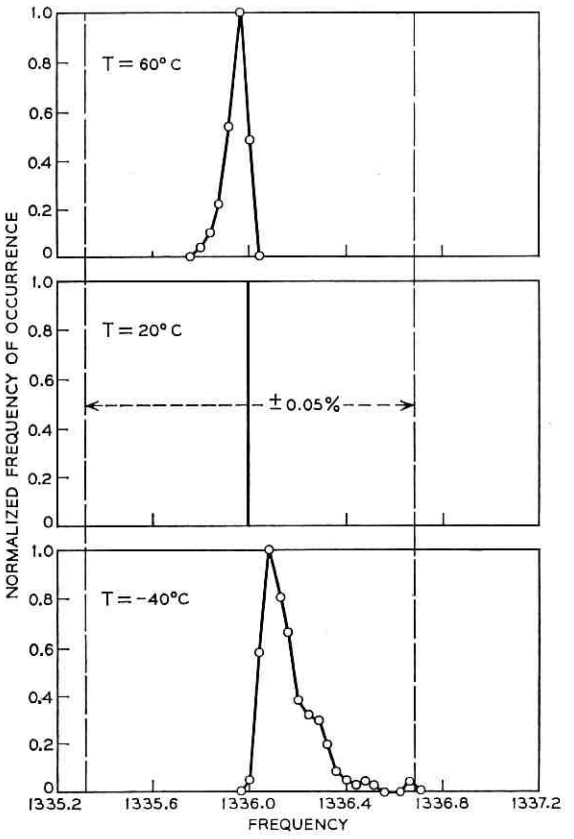

Fig. 11—Amplifier B normalized frequency histograms, $f_0 = 1336$ Hz.

where R_T is the dc resistance of the Twin-T network. V_2 and V_1 are connected via the amplifier gain, i.e.,

$$V_2 = V_A - KV_1$$

in the linear region, where V_A is some constant and K is the amplifier gain. Then,

$$V_{2dc} + \frac{V_{2dc} - V_A}{K} = R_T I_{dc} ,$$

$$V_{2dc} \approx V_\alpha + R_T I_{dc} ,$$

where V_α is the baseline voltage when $I_{dc} = 0$, the point on the amplifier gain curve where $V_2 = V_1$.

R_T varies inversely with tone frequency, and hence we would expect the center of oscillation to decrease with increasing tone frequency. Since the amplitude is given by the difference between the limiting voltage and the center line voltage, we would expect amplitude to increase monotonically with tone frequency and, assuming constant I_{dc}, to be linear at a slope of $-I_{dc}$ with R_T. Figure 14 is a plot of amplitude versus R_T with temperature as a parameter. Notice that for f_1 to f_3 the curves are almost linear but with slopes closer to $-2I_{dc}$. However, when we come to f_4, we notice that the curves change direction and violate the monotonicity assumption. One possible explanation for this "turndown" is that the notch of the Twin-T rises monotonically for f_1 to f_3 and deepens at f_4. While this phenomenon

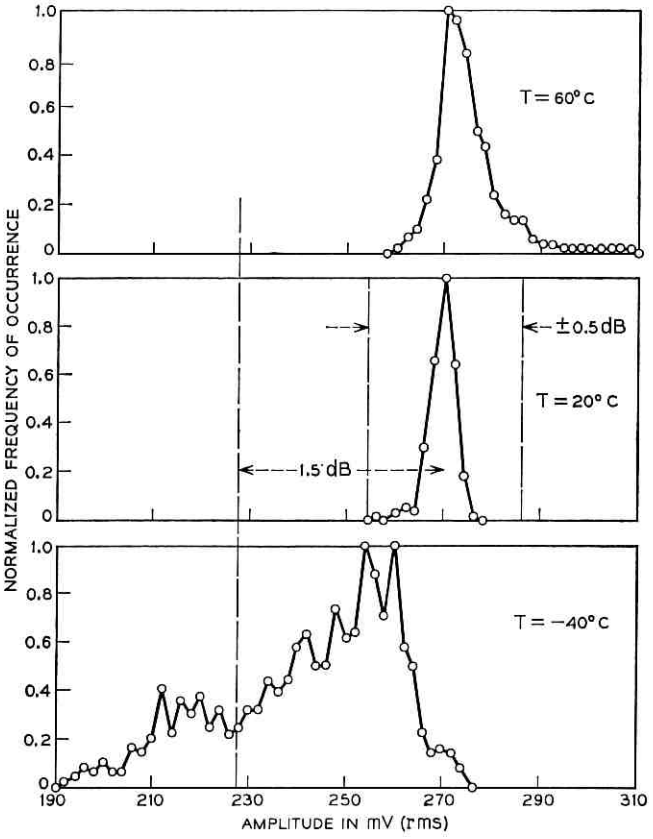

Fig. 12—Amplitude histograms at adjustment frequency.

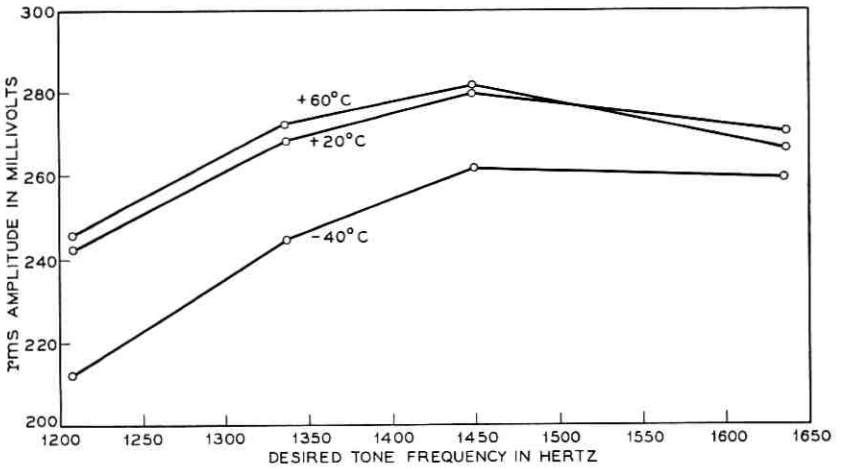

Fig. 13—Amplitude versus frequency profile of one oscillator.

would have a small effect if limiting were perfect, the amplifier under study has exponential limiting. The fact that the notch is deeper at f_4 implies that the oscillator does not have to go as far into the exponential limiting region to achieve a loop gain of 0 dB. This effect appears to more than compensate the amplitude growth due to I_{dc}. In any case, the amplitude "turndown" has been corroborated by breadboard experiments.

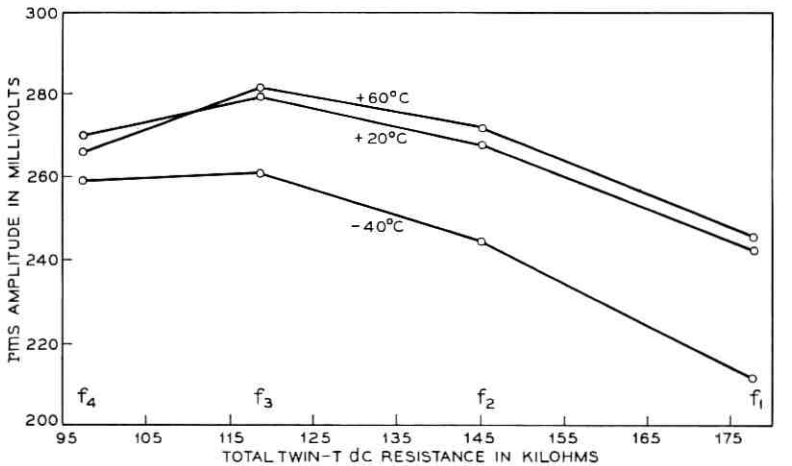

Fig. 14—Amplitude versus Twin-T dc resistance for one oscillator.

Two implications of the non-monotonic relation of amplitude with frequency should be mentioned. First, a linearized, first-order guess, indeed the design assumption, has been proven inaccurate by an analysis which maintains the nonlinear properties of the circuit. Second, since the design specifications place limits on the total amplitude deviation due to tone change, the lack of monotonicity is helpful in meeting specifications.

5.5 *Calculation of Yield*

Returning to Fig. 13, we see that the worst-case amplitude deviations due to all causes—adjustment, temperature, tone change—occur at f_1, $-40°C$ for negative deviations and f_3, $+60°C$ for positive deviations. If we ignore the causes of deviation and simply say that oscillators with amplitudes within ± 2.5 dB (see Section II) of the nominal amplitude for all modes are acceptable, then Fig. 15 allows us to quickly calculate yield. Figure 15 shows the amplitude histograms for f_1, $-40°C$ and f_3, $+60°C$, with the -2.5-dB limit drawn in. The normalized area under the curves outside the 2.5-dB limit represents the fraction of the total amplifiers that fail. Notice that all amplifiers that fail do so at f_1, $-40°C$—another indication of the asymmetry of the nominal design. The yield figure is 55 percent.

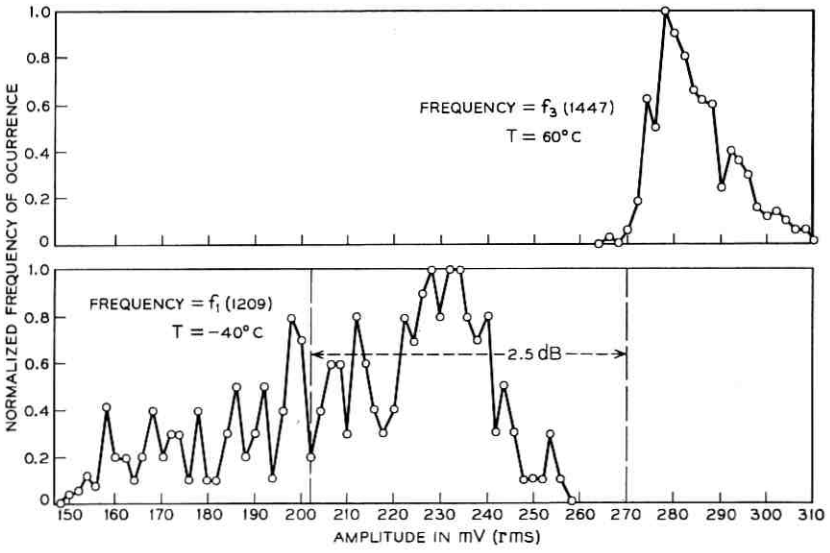

Fig. 15—Amplitude histograms at worst-case conditions. (f_3, $+60°C$), (f_1, $-40°C$).

5.6 *Production Screening Test*

Breadboard experiments and first-order computations had suggested that some level of dc feedback current (I_{dc}) could be used as a threshold for production screening of amplifiers. Figure 16 confirms that this is indeed the case and defines the threshold quantitatively. The figure shows maximum amplitude deviation (uniformly this deviation occurs at f_1, $-40°C$) versus I_{dc} at $+20°C$ and f_2. The close correlation is obvious. If amplifiers with $I_{dc} \geqq 0.4$ μA are rejected, all remaining amplifiers produce oscillators within design specifications. Note that no temperature tests need be made.

Figure 17 is a histogram of I_{dc}. The normalized area under the curve in the interval $[0.4, \infty]$ represents the fraction of amplifiers rejected by the test ($I_{dc} \geqq 0.4$ μA) and also predicts the same 55 percent yield.

After noting that amplifiers with high I_{dc} have large amplitude deviations, we then ask what causes high I_{dc}. Figures 18 and 19 show that low transistor Betas cause high I_{dc} and failures. Figure 18 plots maximum amplitude deviation versus $\beta_{N1} - \beta_N$ of the first transistor. The correlation is barely detectable. The argument here is that I_{dc} is a function of the β_Ns of both transistors one and two as well as other parameters and, although there is correlation between the transistor β_Ns on the same chip, that correlation is not strong enough

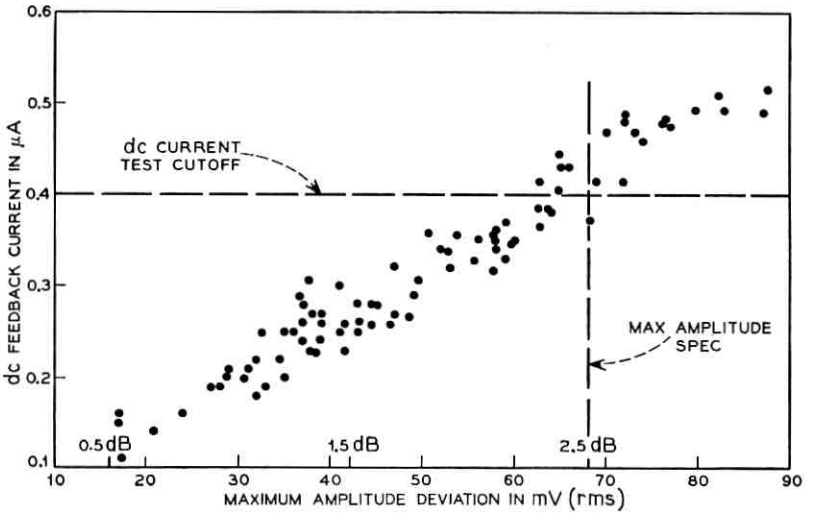

Fig. 16—DC feedback current versus maximum amplitude deviation.

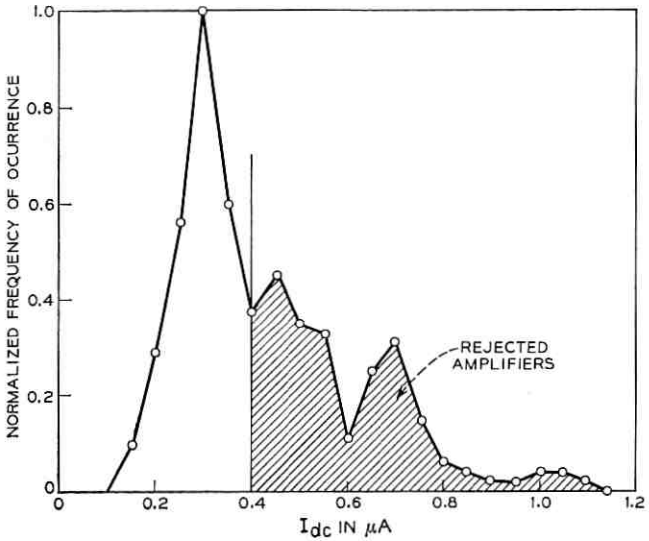

Fig. 17—I_{dc} histogram.

to permit prediction of performance based on measurement of a single transistor β_N. Figure 19 plots amplitude deviation versus $(\beta_{N1}\beta_{N2})^{\frac{1}{2}}$. Here we see the strong correlation that allows us to draw the conclusion about the dependency of I_{dc} on transistor β_N and to predict an improvement in yield if processing improvements result in increased β_N.

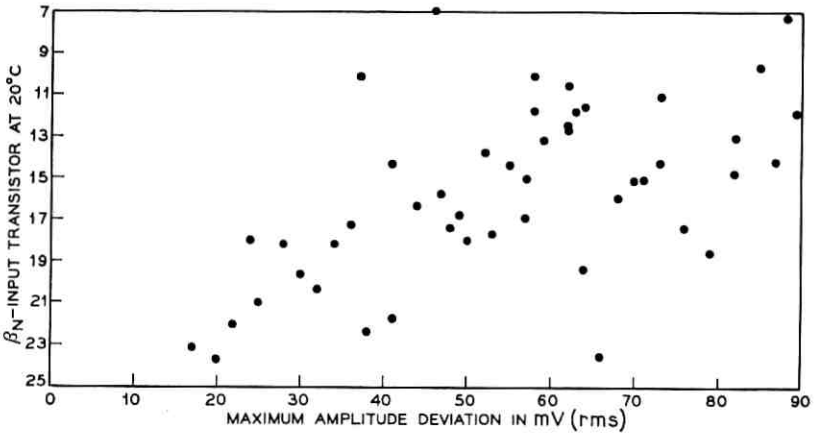

Fig. 18—Maximum amplitude deviation versus β_N of input transistor at +20°C.

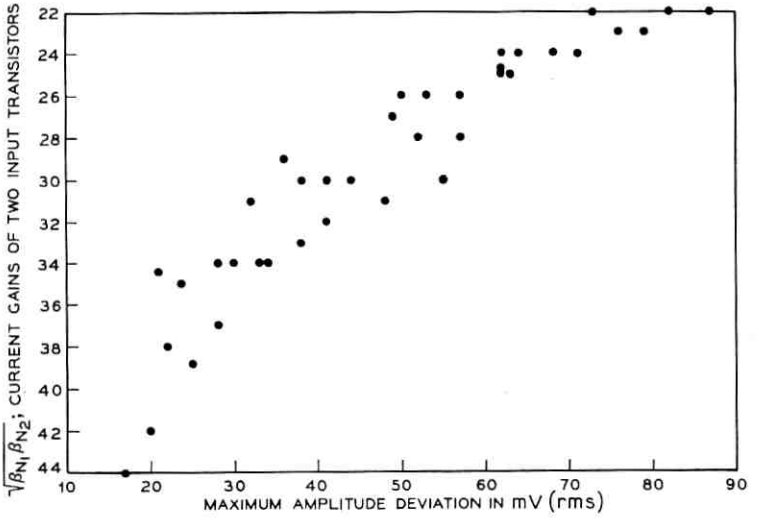

Fig. 19—Maximum amplitude deviation versus $(\beta_{N_1}\beta_{N_2})^{\frac{1}{2}}$. β_{N_1}, current gain first transistor; β_{N_2}, current gain second transistor.

Finally, Fig. 20 is a histogram of maximum amplitude deviation with all amplifiers having $I_{dc} \geqq 0.4$ μA removed. It is clear that all the oscillators in this reduced population are within the design specifications.

5.7 *Asymmetric Adjustment*

As a final word, let us return to a discussion of the asymmetry of the nominal design. For amplitude adjustment at 20°C and f_2, a first guess for the adjustment target was nominal amplitude. An adjustment temperature of 20°C is higher than the center of the operational temperature range (−40°C to +60°C), and for this reason one might consider adjusting amplitude at a higher value than nominal. However, f_2 is lower than the center of the frequency range, and if one accepted the notion of amplitude varying proportionally with frequency, one might consider adjusting to an amplitude below nominal. These two factors then tend to cancel one another.

The results presented previously, however, indicate that amplitude is not a monotonic function of frequency, and amplitude deviations due to both temperature and frequency changes are asymmetric. We have shown that larger variations in amplitude result from negative changes in temperature and frequency than from positive changes.

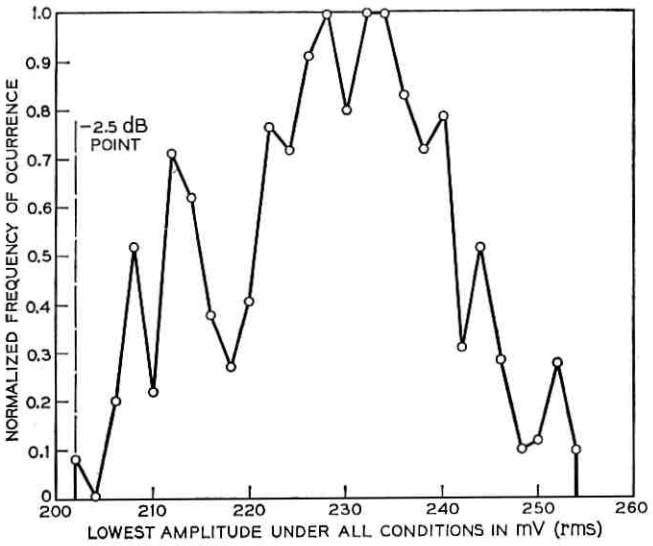

Fig. 20—Histogram of lowest amplitude from all conditions, amplifiers with $I_{dc} \geqq 0.4$ μA removed.

We have seen that the dominant failure condition is f_1, −40°C, i.e., low tone frequency, low temperature. This suggests that amplitude can be adjusted to take advantage of the asymmetry. If adjusting at f_2 and +20°C, an adjustment objective of 285 mV rather than 270 mV is likely to result in increased yield, i.e., it will be possible to accept amplifiers with I_{dc} greater than 0.4 μA. Although the exact adjustment figure must still be studied, our results suggest that taking advantage of the asymmetry of the design can result in not insignificant savings.

VI. CONCLUSIONS

In this paper we have described the application of Monte Carlo tolerance analysis to the integrated, single-substrate, RC, *Touch-Tone* oscillator. The conclusions to be drawn are pertinent not only to the specific oscillator designs studied, but also to the state-of-the-art of tolerance analysis itself.

We have examined two proposed oscillator designs. Both designs employ the same Twin-T as the frequency selective network, the difference appearing in the high-gain, limiting amplifier. The study, therefore, concentrated on the statistical variation of parameter values within the amplifier; the Twin-T was held fixed at design values.

Variations in oscillator performance, then, were judged against degradation limits allocated to the amplifier.

The first design was dismissed because of poor frequency stability stemming from loading effects of the amplifier on the Twin-T. The second design, on the other hand, seems promising; its production now seems likely.* The Monte Carlo analysis of this design revealed two significant properties:

First, the oscillator has excellent frequency stability. Frequency deviations over the full temperature range were less than 0.05 percent for all the sample oscillators in the Monte Carlo study.

Second, the amplitude stability is acceptable. Fifty-five percent of the oscillators in the study were within amplitude limits over the full temperature and tone frequency ranges. Forty-five percent of the oscillators failing specifications is less alarming than might appear at first glance for the following reasons:

(*i*) The results show that amplitude deviations are strongly correlated with the dc feedback current through the Twin-T, i.e., into the amplifier, at room temperature. Hence a test is easily performed on the amplifier chips before bonding takes place and without the need of a temperature chamber to weed out amplifiers that would result in unsatisfactory oscillators. This test reduces the cost penalties associated with a relatively low amplifier yield.

(*ii*) The statistical characterization of the parameters of the oscillator was purposely pessimistic. Hence, the yield figure should be taken as a lower bound. Further, the results indicate that amplifier failure is associated with low transistor current gain. Fabrication improvements that increase these gains will therefore improve yield.

(*iii*) The deviation of oscillator amplitude in response to both temperature and tone change is asymmetric, i.e., amplitude deviations due to both low temperature and lower frequency is larger than corresponding changes for high temperature and higher frequency. By changing the amplitude adjustment target to some value offset from the middle of the amplitude window (270 mV $\pm$ 2.5 dB), a significant increase in yield can be expected.

In summary, amplifier yield of 55 percent is lower than might be

* It should be noted that several potential problem areas have been ignored in the computer analysis and remain to be examined. Primary among these are the effects of variable loop length and the possibility of parasitic oscillation.

hoped for, but the cost penalties associated with this relatively low yield are minimized by a simple go/no-go test performed on the amplifiers before bonding. Furthermore, there are good prospects that yield can be increased by changes in silicon processing and adjustment strategy.

With regard to Monte Carlo tolerance analysis itself, two aspects of the present study should be noted. First, since the oscillator is nonlinear and requires factory adjustment, no standard circuit analysis program could reasonably be used as part of a Monte Carlo loop. Hence, a special program in which efficiency could be achieved by restricting its applicability to a small class of oscillators had to be written. To write this program required one man-year of effort—a not unsubstantial investment. The point is that while Monte Carlo tolerance analysis of circuits like the *Touch-Tone* oscillator cannot, at present, be performed using off-the-shelf computer programs, the analysis can be done using special techniques if the circuit's importance warrants the investment.

Secondly, since the oscillator's amplifier is fabricated on a single silicon chip, its parameters are not statistically independent. Unfortunately, almost no data exists with which to make a statistical characterization of silicon circuit parameters. On the other hand, it is obvious that the results of the Monte Carlo study are exactly as accurate as the assumed parameter statistics. It is clear, then, that if we are to exploit the possibilities Monte Carlo tolerance analysis presents, an effort must be made to structure the measurements of silicon circuits as they go into production, to clarify the statistical interrelation of silicon circuit parameters.

VII. ACKNOWLEDGMENT

The help of many people in providing device characterization, circuit expertise, and their insight into the problems of producing a single-substrate, *Touch-Tone* dial is gratefully asknowledged. Without being exhaustive, L. A. Walter supplied most of the device data from which J. Logan produced the statistical characterization and technique for parameter selection;[4] T. L. Powers, D. P. Borenstein, J. H. Hamm and R. A. Tice shared their experience with previous *Touch-Tone* dials and their insight into the problems of the new circuits, and coordinated their own laboratory work with the computer analysis; W. H. Orr and P. Zuk provided details of the fabrication process and their own views of the circuit operation; R. W. Wyndrum, Jr., and

T. N. Rao introduced us to the problem; and J. Chernak provided leadership that kept us excitedly at our task.

REFERENCES

1. Dickieson, A. C., and Chernak, J., "History and Introduction," B.S.T.J., this issue, pp. 1099–1103.
2. Semmelman, C. L., Walsh, E. D., and Daryanani, G. T., "Linear Circuits and Statistical Design," B.S.T.J., this issue, pp. 1149–1171.
3. Cermak, I. A., and Kirby, Mrs. D. B., "Nonlinear Circuits and Statistical Design," B.S.T.J., this issue, pp. 1173–1195.
4. Logan, J., "Characterization and Modeling for Statistical Design," B.S.T.J., this issue, pp. 1105–1147.
5. Shichman, H., "Integration System of a Nonlinear Network Analysis Program," IEEE Trans. Circuit Theory, *CT-17*, No. 3 (August 1970), pp. 378–385.

THE BELL SYSTEM TECHNICAL JOURNAL
Vol. 50, No. 4, April, 1971
Printed in U.S.A.

Statistical Circuit Design:

The Application of Monte Carlo Techniques to the Study of Impairments in the Waveguide Transmission System

By R. G. OLSEN

(Manuscript received December 3, 1970)

Monte Carlo techniques have proven to be useful in examining the effects of component variations in electronic circuits. These techniques can also be applied to the study of parameter variation in systems. As an example of this approach, this paper reports on the use of Monte Carlo techniques in the study of impairments in the waveguide transmission system, a high-capacity, long-haul communication facility now under development at Bell Laboratories. Two examples of the Monte Carlo analysis are discussed. These examples show how the Monte Carlo analysis can give the system designer insight into the effects of impairments on the system performance, and can aid the designer in setting requirements on the system components. It is expected that these techniques will find further application in other Bell System design efforts.

I. INTRODUCTION

1.1 *Monte Carlo Analysis in Circuit and System Design*

Monte Carlo tolerance analysis has proven to be a useful tool in the circuit design process. [1-3] Typically, the designer uses the statistical distributions and correlations of the circuit components in conjunction with random number generators to produce in the computer a large number of sample circuits. These circuits are then analyzed on the computer and empirical distributions of circuit performance are obtained. From these distributions, the designer can predict yield and can study the implications of altering component tolerances.

Monte Carlo techniques can also be used to analyze the effects of parameter variations in systems; in particular, these methods can be applied to the study of impairments in a transmission system. We shall

first discuss some of the steps involved in the system design and specification, and then show how Monte Carlo techniques can be applied.

1.2 *System Specification and Impairment Allocation*

An important part of the design of a transmission system is the specification of the system transmission characteristics. This specification is made in two steps:

(*i*) Specification of the nominal transmission characteristics of each block of the system.
(*ii*) Specification of the allowed deviations from the nominal transmission characteristics.

The first step involves the specification of the modulation type, nominal filter shapes and bandwidths, and the nominal characteristics of other blocks such as amplifiers and equalizers, so that the nominal system meets the performance objectives.

The second step involves the specification of the allowed range of impairments (such as delay and amplitude distortions) in each block of the system so that the performance will still be satisfactory with impairments present. This step is known as the *impairment allocation.*

These specifications translate into performance requirements for the individual circuits and components comprising each block of the system. There are several difficulties: First, these requirements must be consistent with the hardware capabilities; overly stringent requirements would result in a reduced manufacturing yield. Secondly, if realistic requirements are placed on each component, a repeater assembled at random from a number of separate components may not meet the overall impairment requirements. In this situation, alternatives such as tightening component requirements, component matching, or tuning must be considered.

1.3 *Using Monte Carlo Techniques in Impairment Analysis*

The impairment allocation requires a knowledge of the effects on the system performance of impairments in each block of the system. Determining the effects of impairments one at a time (by computer simulation) is useful, but does not provide the entire answer. If there are nonlinearities in the system, the effects of many simultaneous impairments cannot be found by the superposition of their individual effects. Similarly, the effects of a particular impairment (such as quadratic amplitude distortion) may depend on the block in which the impairment occurs.

Monte Carlo analysis, on the other hand, can provide valuable insight into the effects of multiple impairments. Each individual impairment is described by a probability distribution representing its range of possible values. The system is simulated for many sets of impairments chosen from the assumed distributions, and the resulting measures of system performance are tabulated in histograms.

This procedure can be used in preliminary impairment studies and impairment allocations, using hypothetical impairment distributions, to get a feeling for the way in which impairments combine, and what maximum and minimum degradations can be expected from impairments which are constrained to lie in a certain range.

Monte Carlo analysis can also be used to get quantitative results on repeater yield and component tolerance requirements if the actual impairment distributions in each block of the system are known. Typically, this information becomes available as the hardware design progresses. For example, the designer can trade off repeater failures for looser component requirements. The tolerances required to give 100 percent acceptable repeater performance may result in overly stringent requirements on the individual hardware components. Relaxing the component requirements to give, say, 99 percent acceptable repeater performance would increase the component yield, at the expense of having a one percent repeater rejection rate. Monte Carlo analysis can thus give the designer valuable information on the various tradeoffs involved in the system specification.

1.4 *Outline of Paper*

This paper reports on the use of Monte Carlo techniques in the study of impairments in the waveguide transmission system, a high-capacity, long-haul communication facility now under development at Bell Laboratories.

The outline of this paper is as follows: Section II describes the waveguide transmission system and the sources of impairments. Section III discusses the Monte Carlo analysis program; Section IV describes the case studies which have been made; and Section V gives the results of the Monte Carlo analysis. Section VI gives a summary and conclusions.

II. THE WAVEGUIDE TRANSMISSION SYSTEM

2.1 *System Description*

The waveguide transmission system will utilize the vast communication potential of millimeter waves to transmit voice, data, *Picture-*

phone® service, and other signals over the telephone network. A decade from now, it is expected to play a major role in meeting the increased demand for telecommunication services.

A simplified block diagram of one link of the system for one direction of transmission is shown in Fig. 1. Present plans call for 120 broadband channels (60 in each direction) to occupy the frequency band from 40 to 110 GHz, giving the system a capacity of about a quarter million voice circuits. The baseband input signal in each channel is two-level PCM at a bit rate of 282 MHz. The modulation technique used is differentially-coherent phase-shift-keying (DCPSK), in which information is transmitted in the relative phase of the carrier.

The oscillator frequencies for the carriers are spaced at 560-MHz intervals across the 40- to 110-GHz band. Tre modulator outputs are fed into a channel-combining network, and are then transmitted over a twenty-mile* section of buried two-inch circular waveguide. The channel-separation network separates the signals from the various channels at the waveguide output.

The signal in each channel then enters a regenerative repeater. The down converter shifts the signal to an IF frequency of about 1.4 GHz; the equalizers correct for delay and amplitude distortions; and the IF filter limits the noise power entering the detector. The regenerator samples the detector output every time slot, decides if a one or a zero was transmitted, and puts out a pulse of the appropriate polarity. The regenerated pulse stream is then modulated back to the millimeter band for transmission over the next link of the system.

2.2 *Design Objective*

The design objective in each channel is a 10^{-9} error rate per repeater with a twenty-mile repeater spacing. The probability of error can be reduced by raising the received carrier power. Thus the performance measure for each channel is based on the amount of carrier power required to obtain a 10^{-9} error rate. First we define the *relative carrier power* (RCP) by

$$\text{RCP} = \frac{C}{\mu f_b}$$

where C is the undeviated carrier power at the receiver input, μ is the thermal noise per unit bandwidth and f_b is the bit frequency. The RCP is thus the carrier power relative to the noise power in a band-

* The nominal repeater spacing is twenty miles.

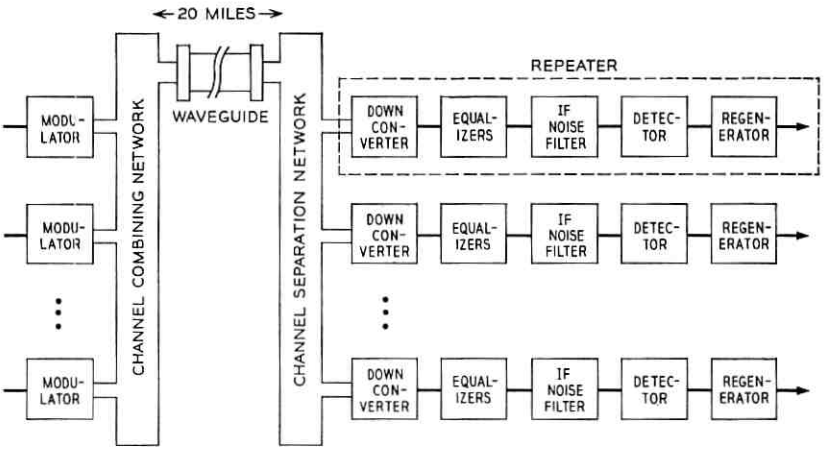

Fig. 1—Block diagram of the waveguide transmission system.

width equal to the bit frequency. The performance measure for a channel is the RCP required to obtain a 10^{-9} error rate (called the required RCP).

We now reformulate the design objective in terms of the required RCP. Taking into account the power output of millimeter wave sources, waveguide and network losses, thermal noise and amplifier noise figures, the RCP *available* for the worst channel (at 40 GHz) turns out to be 25 dB; other channels have a higher available RCP. The error rate in any channel is satisfactory if

$$\text{Required RCP} \leqq \text{Available RCP}.$$

The system is being designed to meet the worst channel requirement; thus the design objective for each channel is

$$\text{Required RCP} \leqq 25 \text{ dB}.$$

2.3 *Sources of Impairments*

There are two main causes of impairments in the system: imperfect equalization and variations in component characteristics. For example, the waveguide delay characteristic is such that in any one 560-MHz channel, the delay is almost linear with frequency. The IF delay equalizer should therefore have a linear delay characteristic with a slope which is the negative of that of the waveguide, so that their combined delay characteristic is flat.[4] However, the combined waveguide and equalizer delay characteristic typically contains some residual

distortions, which are adequately modeled as having linear, quadratic, cubic, and ripple terms.

Similarly, variations from the nominal waveguide delay characteristic will produce distortion even if the nominal is perfectly equalized. Another important source of impairments is the repeater, which consists of about fifteen separate components (such as amplifiers, isolators, filters), each with an inherent variability.

The above considerations also apply to *amplitude* distortions, which must also be included in an impairment analysis of the system.

III. COMPUTER ANALYSIS OF THE WAVEGUIDE TRANSMISSION SYSTEM

3.1 *Computer Simulation of the System*

In order to carry out a Monte Carlo study of impairments, we need a simulation program to evaluate the system performance (i.e., compute required RCPs) given a particular set of transmission characteristics. Such a program has been written by J. H. Mullins.[5] This program has many features and options; only the ones relevant to this discussion are described below. The program simulates the transmission of two periodic streams of sixteen pulses through one channel of the system, so that intersymbol interference from all combinations of five adjacent pulses is obtained. A calculation is made of the required RCP for each time slot in the transmitted pulse stream. The effects of timing jitter are included by computing the required RCP for various regenerator timing errors, typically $-\frac{1}{8}$, 0, and $+\frac{1}{8}$ of a time slot. A record is made of the worst (i.e., highest) required RCP for each timing error, taking all time slots into account.

The effects of an interfering signal in an adjacent channel can also be included in the simulation, in which case the relative time position of the adjacent channel signal is adjusted for each time slot to produce the worst effect (highest required RCP). Thus there are several required RCPs computed for a given channel. Characterizing the performance of the channel by a single number, we define the *computed* performance measure to be the maximum of the required RCP at $-\frac{1}{8}$ or $+\frac{1}{8}$ timing error, with adjacent channel interference included in the simulation (called the required RCP with $\pm\frac{1}{8}$ timing error).

3.2 *The Monte Carlo Analysis Program*

The waveguide simulation program described in the previous section has been embedded in a Monte Carlo analysis program which selects parameter values from probability distributions, passes them

to the simulation program, and forms histograms of the required RCPs computed by the simulation. The program was written for a Control Data 3500 computer. About 45 seconds of computation time is required for each run through the simulation program when adjacent channel interference is included in the simulation; and about 15 seconds when the interference is omitted. Generating histograms of 1000 samples, therefore, takes either four or 12½ hours of computer time.

IV. EXAMPLES OF MONTE CARLO IMPAIRMENT ANALYSIS

4.1 *The Monte Carlo Impairment Studies*

The Monte Carlo analysis program described in the previous section has been used to study the effects of delay and amplitude impairments on the waveguide transmission system and has aided in the setting of preliminary impairment allocations.

The nominal transmission characteristics of the system are shown in Table I; the system is assumed to be perfectly delay-and-amplitude equalized in the absence of impairments. The impairments are described in Section 4.2.

The worst-case required RCPs (with adjacent channel interference) for the nominal system are as follows:

Zero timing error: 15.20 dB,

$-\frac{1}{8}$ timing error: 16.37 dB, and

$+\frac{1}{8}$ timing error: 16.34 dB.

The computed performance measure for the nominal system is thus 16.37 dB.

TABLE I—NOMINAL TRANSMISSION CHARACTERISTICS FOR MONTE CARLO IMPAIRMENT STUDY

Modulation: DCPSK, path length modulator.
Symbol rate, polar binary PCM = 282 MBd = f_b.
Time slot = 3.5 ns = τ.
RF Channel Spacing = 560 MHz = 1.98 f_b.
RF Channel Filters:
  Two-pole, maximally flat, lossless
    3-dB bandwidth = 450 MHz = 1.6 f_b;
  In tandem with two-pole lossless rejection filter centered 560 MHz higher than passband filter.
Receiver IF Noise Filter:
  Four-pole, maximally flat
    3-dB bandwidth = 370 MHz = 1.31 f_b.
Detector: Ideal DCPSK.
Adjacent channel interference included in simulation.
System is delay and amplitude equalized.

Two Monte Carlo studies have been carried out. In the first, the distortions were assumed to originate in the waveguide section of the system (i.e., at an RF frequency in the 40- to 110-GHz range). In the second, the distortions were assumed to originate in the repeater (i.e., at the IF frequency of 1.4 GHz). The only difference between the two is that in the second case, the amplitude distortions affect the amount of noise power entering the detector, whereas in the first case the noise power is independent of the distortions. This difference is significant, as will be seen in the discussion of the results.

Adjacent channel interference was included in the simulation, and histograms of required RCPs were made for timing errors of $-\frac{1}{8}$, 0, and $+\frac{1}{8}$ of a time slot. An additional histogram was made of the required RCP with $\pm\frac{1}{8}$ timing error. One thousand samples were obtained in each histogram, and a record was made of the impairment parameter values causing the maximum and minimum entries in each histogram.

4.2 *Impairment Parameters and Distributions*

The impairments investigated in these studies are delay-and-amplitude distortions consisting of linear, quadratic, cubic and ripple components. The linear, quadratic and cubic terms are characterized by their values at the frequency $f = f_c + f_b/2$, where f_c is the carrier frequency and $f_b = 1/\tau$ is the bit frequency (282 MHz). The ripple terms are characterized by their peak-to-peak amplitude, period and phase.

In these preliminary studies, the impairments are assumed to originate in a single block (transfer function) of the system. The overall delay of this block is the sum of the four delay components, and is given by:

$$d(f) = d_1[2(f - f_c)/f_b] + d_2[2(f - f_c)/f_b]^2 + d_3[2(f - f_c)/f_b]^3 + (1/2)d_R \sin [2\pi(f - f_c)/P_D + \theta_D].$$

The distributions of the delay distortion parameters, d_1, d_2, d_3, d_R, P_D and θ_D assumed in this study are given in Table II.

The amplitude response of the impaired transfer function is unity plus the four amplitude distortions:

$$A(f) = 1 + A_1[2(f - f_c)/f_b] + A_2[2(f - f_c)/f_b]^2 + A_3[2(f - f_c)/f_b]^3 + (1/2)A_R \sin [2\pi(f - f_c)/P_A + \theta_A].$$

The distributions assumed in this study for the amplitude impairment

TABLE II—ASSUMED DELAY IMPAIRMENT DISTRIBUTIONS*

Impairment Type	Parameter	Distribution Limits
Linear Delay	d_1 = value at $f_c + f_b/2$	-0.2τ to 0.2τ
Quadratic Delay	d_2 = value at $f_c + f_b/2$	-0.2τ to 0.2τ
Cubic Delay	d_3 = value at $f_c + f_b/2$	-0.2τ to 0.2τ
Ripple Delay	d_R = peak-to-peak value	-0.3τ to 0.3τ
	P_D = period	$0.125 f_b$ to $1.0 f_b$
	θ_D = phase	0° to 90°

* All distributions are uniform and independent.

parameters A_1, A_2, A_3, A_R, P_A, and θ_A are given in Table III. All delay and amplitude distributions are assumed to be independent.

The impairment parameters are assumed to be uniformly distributed, since the actual distributions are not known. However, this is adequate for our purposes, since a primary goal of these preliminary studies is to determine the effects of multiple impairments which are constrained to lie within certain limits.

A few words are in order concerning the distribution limits specified in Tables II and III. These limits were arrived at after a study had been made of the effects of individual impairments on the system performance. From this study, a preliminary set of impairment limits was obtained for which it was felt that the overall required RCP with $\pm 1/8$ timing error would not exceed 22 dB or so, leaving a margin of about 3 dB for other types of impairments. It is these *preliminary* impairment limits which are tabulated in Tables II and III. These should not be construed as final requirements on the system, or as anything other than first estimates of the impairment levels which the system can tolerate. In fact, the Monte Carlo results in Section V indicate that these limits are probably too tight, and satisfactory performance can be achieved with somewhat larger impairment limits.

TABLE III—ASSUMED AMPLITUDE IMPAIRMENT DISTRIBUTIONS*

Impairment Type	Parameter	Distribution Limits
Linear Amplitude	A_1 = value at $f_c + f_b/2$	-0.15 to 0.15
Quadratic Amplitude	A_2 = value at $f_c + f_b/2$	-0.2 to 0.2
Cubic Amplitude	A_3 = value at $f_c + f_b/2$	-0.1 to 0.1
Ripple Amplitude	A_R = peak-to-peak value	-0.06 to 0.06
	P_A = period	$0.125 f_b$ to $1.0 f_b$
	θ_A = phase	0° to 90°

* All distributions are uniform and independent.

V. RESULTS OF THE MONTE CARLO ANALYSIS

5.1 *Case Study #1: Impairments at RF*

The histograms of required RCP resulting from the Monte Carlo analysis with the distortions occurring at RF are shown in Figs. 2 through 5. Also shown are the mean required RCP, the nominal (no distortion) value, the value which was exceeded in only one percent of the cases, and the percentage of cases in which the required RCP was lower than nominal.

Figure 2 shows the histogram of the required RCP for zero timing error. The mean required RCP is 1.1 dB higher than the nominal value. The highest value which occurred was 19.0 dB, but only one percent of the cases exceeded 17.55 dB, or 1.45 dB lower. There were three cases (0.3 percent) in which the required RCP was less than the nominal value, indicating that there are some combinations of dis-

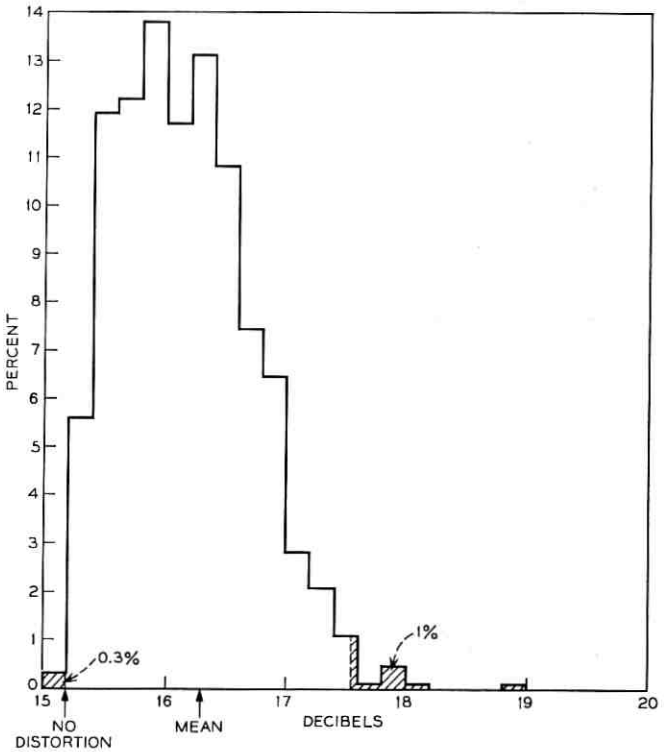

Fig. 2—Histogram of required RCP for zero timing error with impairments at RF.

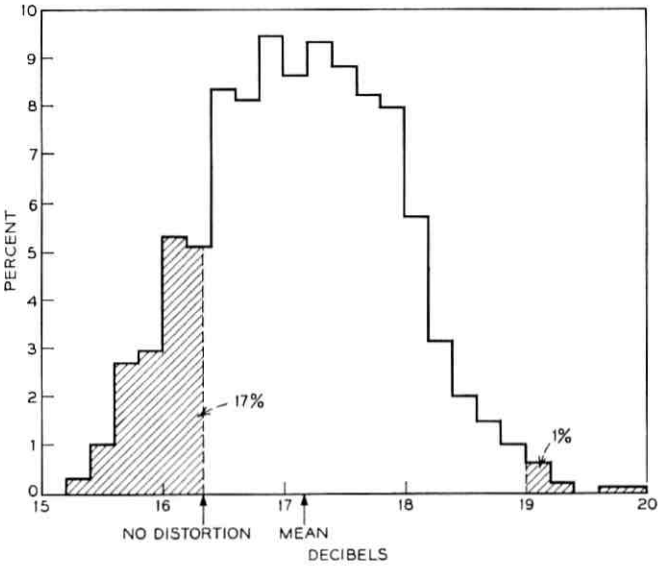

Fig. 3—Histogram of required RCP for −1/8 timing error with impairments at RF.

tortions which produce better results than no distortions at all. This is not too surprising, since the nominal transmission characteristics were not chosen to minimize the required RCP at zero timing error, but rather to minimize the required RCP with ±1/8 timing error.

Figure 3 shows the histogram of the required RCP for −1/8 timing error. The mean value is 0.75 dB higher than nominal. However, 17 percent of the distortion combinations reduced the required RCP below its no distortion value. This is primarily due to the effects of delay distortion. Large positive quadratic delay distortion shifts the pulse stream sufficiently so that better results are obtained by sampling with −1/8 timing error rather than with zero timing error. At the lowest value in the histogram in Fig. 3, the quadratic delay distortion is $d_2 = 0.16\ \tau$. However this distortion is not desirable, since it seriously degrades the required RCP at +1/8 timing error. The *highest* value in the histogram in Fig. 4 (+1/8 timing error) was obtained for $d_2 = +0.19\ \tau$. Similarly, large *negative* quadratic delay distortion improves the required RCP at +1/8 timing error, but degrades it at −1/8 timing error.

Figure 5 shows the histogram of the required RCP with ±1/8 timing error when the impairments occur at RF. The mean required

RCP in the impaired system is about 1.1 dB higher than nominal. The maximum value that occurred was 20.6 dB, or 4.2 dB higher than nominal. The impairment parameter values which resulted in this maximum degradation are given in Table IV. The linear and cubic delays are both negative and have about the same value (and hence are reinforcing) and the quadratic delay is almost at its maximum positive value. The delay ripple has a large period and a large peak-to-peak amplitude. Looking at the amplitude impairments in Table IV, we see that the quadratic amplitude has a large negative value, as does the peak-to-peak amplitude ripple.

The most interesting feature of the histogram in Fig. 5 is that four percent of the distortion combinations produce a lower required RCP than nominal, the lowest being 15.8 dB, 0.55 dB below nominal. The impairment values producing this minimum required RCP are also given in Table IV. All the distortions are quite small, except for the quadratic amplitude distortion which is almost at its maximum positive value. These results indicate that positive quadratic amplitude distortion occurring at RF improves the performance of the system.

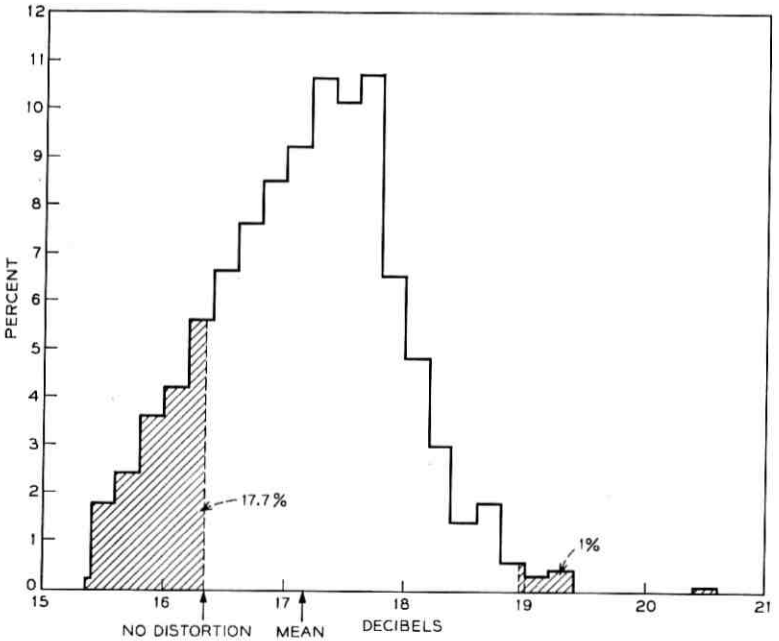

Fig. 4—Histogram of required RCP for +1/8 timing error with impairments at RF.

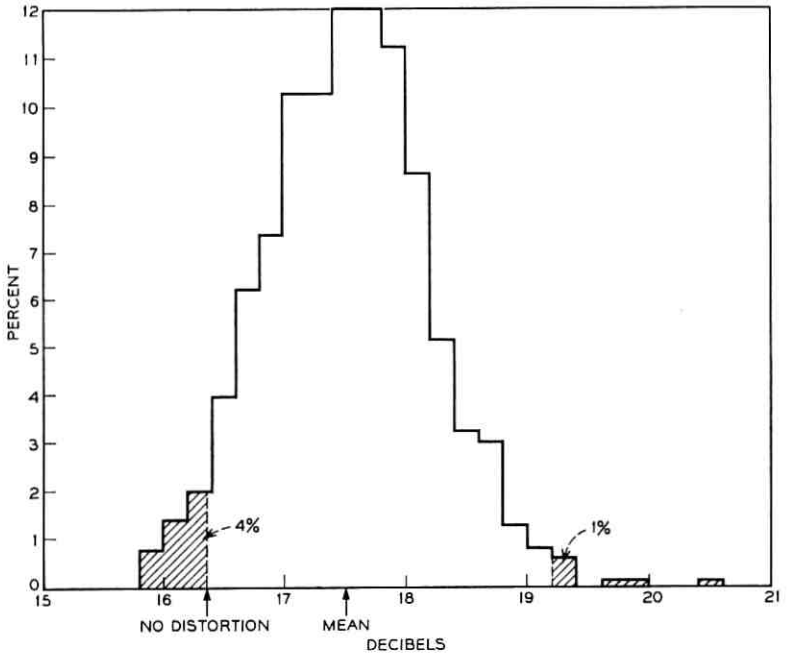

Fig. 5—Histogram of required RCP with ±1/8 timing error with impairments at RF.

This indication is quite true, as is shown by the graph of the required RCP with ±1/8 timing error versus quadratic amplitude at RF in Fig. 6. (All other impairments are set to zero.) A quadratic amplitude shaping at RF with parameter $A_2 = 0.3$ reduces the required RCP to 15.45 dB, 0.9 dB below the nominal.

It would seem desirable to build this amplitude shaping into the nominal system to take advantage of the improved performance. Yet any intentional amplitude shaping would have to be done in the IF strip, since it is extremely difficult to build filters and provide gain at RF. Unfortunately, the beneficial effect of quadratic amplitude shaping is lost when we apply it at the IF frequency. The shaping filter would follow the primary noise source in the system (the IF input amplifier), and would increase the amount of noise power entering the detector. The shaping filter would require gain,

$$A(f) = 1 + 0.3[2(f - f_c)/f_b]^2,$$

and hence increases the noise bandwidth of the system. The resulting degradation in the system performance from the increased noise power is greater than the improvement gained by amplitude shaping, as is shown in Fig. 6. The system performance is degraded by *any* quadratic amplitude distortion introduced at IF, but the effects of a negative distortion are relatively small. If quadratic shaping were introduced by a passive filter, there would be a decrease in signal power which would similarly raise the required RCP. Amplitude shaping introduced at IF degrades the system performance, and we are left in the position of having some "impairments" at RF which improve performance, but being unable to build the improvements into the system.

5.2 *Case Study #2: Impairments At IF*

Another Monte Carlo analysis was made with the impairments in the IF strip instead of at RF. This was the only difference between the two studies; the same sets of impairments were generated in both. The histogram of the required RCP with $\pm 1/8$ timing error for the impairments at IF is shown in Fig. 7. There were *no* combinations of distortions for which the system performance was better than nominal.

The impairment parameter values producing the maximum and

TABLE IV—IMPAIRMENT VALUES—MAXIMUM AND MINIMUM OBTAINED REQUIRED RCP WITH $\pm 1/8$ TIMING ERROR (IMPAIRMENTS AT RF)

	Maximum Obtained Required RCP = 20.6 dB	Minimum Obtained Required RCP = 15.8 dB
Impairment Parameter	Value at Maximum	Value at Minimum
Linear Delay d_1	-0.13τ	-0.06τ
Quadratic Delay d_2	0.19τ	0.01τ
Cubic Delay d_3	-0.12τ	0.03τ
Ripple Delay		
Peak-to-peak value d_R	-0.29τ	-0.18τ
Period P_D	$0.99 f_b$	$0.44 f_b$
Phase θ_D	29.4°	23.4°
Linear Amplitude A_1	−0.06	0.004
Quadratic Amplitude A_2	−0.18	0.19
Cubic Amplitude A_3	−0.02	0.06
Ripple Amplitude		
Peak-to-peak value A_R	−0.06	−0.01
Period P_A	$0.16 f_b$	$0.83 f_b$
Phase θ_A	58.6°	63.4°

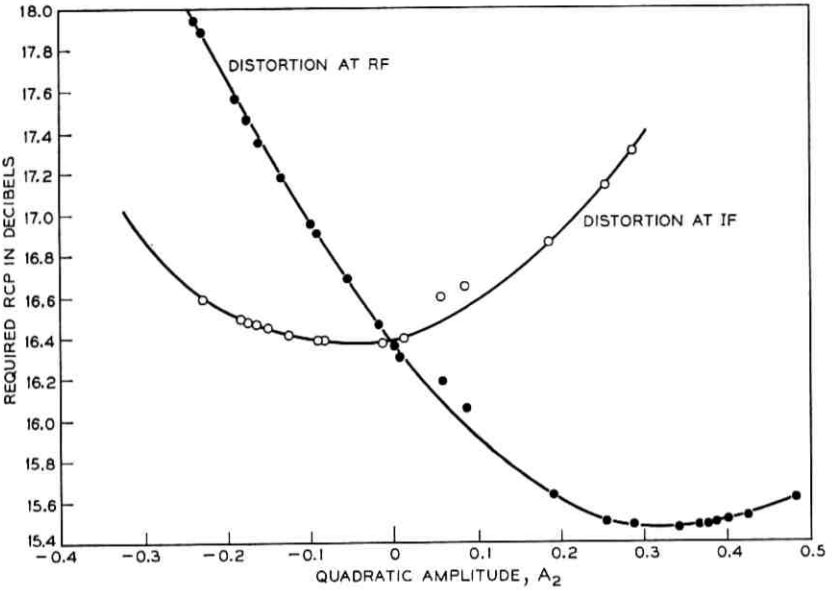

Fig. 6—Required RCP with ±1/8 timing error as a function of quadratic amplitude distortion.

minimum required RCP with ±1/8 timing error are given in Table V. The maximum required RCP obtained in the Monte Carlo analysis was caused by large negative linear, quadratic, and cubic delay components and a large slow delay ripple. The amplitude impairments, however, were quite small.

The impairments producing the minimum obtained required RCP of 16.4 dB are also tabulated in Table V. The quadratic and ripple delays are quite small, and the linear and cubic delays practically cancel each other out. The cubic and ripple amplitude distortions are very small, but the linear amplitude distortion is quite large and the quadratic amplitude is of moderate size.

Comparing the histograms in Figs. 5 and 7, we see that impairments at IF have, in general, a slightly worse effect on the system performance than those at RF: The mean of the distribution at IF is 0.1 dB higher than at RF, and the one percent point is 0.35 dB higher. Also, there were no distortions at IF for which the system performance was better than nominal, whereas four percent of the distortions at RF did improve the system performance.

The range of the distribution at RF was greater than that at IF

(15.8 dB—20.6 dB at RF, 16.4 dB—20.1 dB at IF). This is primarily due to the effects of quadratic amplitude distortion (Fig. 6). At RF, a quadratic distortion A_2 in the range -0.2 to 0.2 produces a required RCP ranging from about 15.6 dB to 17.7 dB; whereas at IF the range is from 16.4 dB to 16.9 dB.

In summary, the histograms in Figs. 5 and 7 show that the maximum required RCP observed in the two case studies was 20.6 dB, which is 1.4 dB below the 22-dB objective. Hence the eventual system impairment requirements could conceivably be less stringent than the distribution limits assumed in these Monte Carlo studies (Tables II and III).

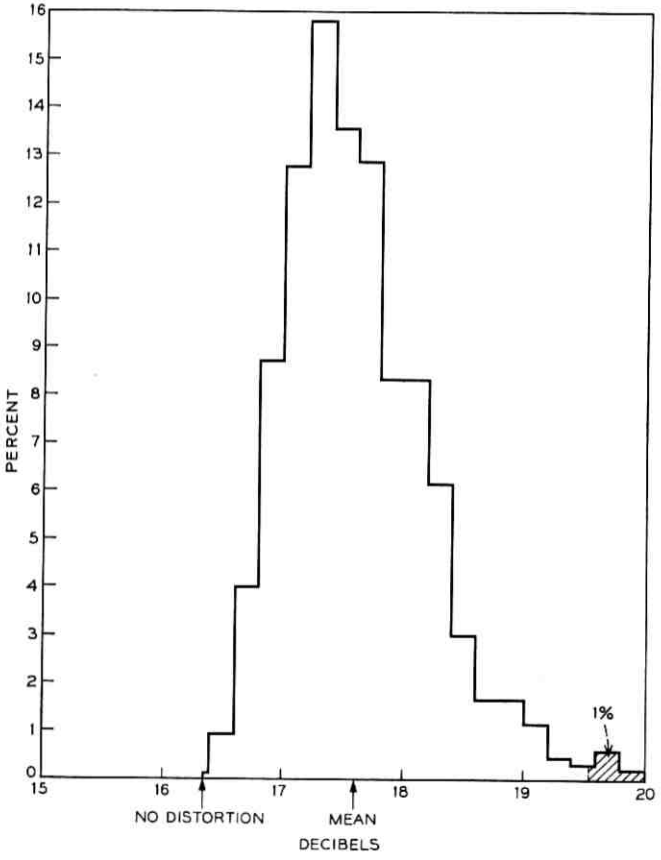

Fig. 7—Histogram of required RCP with ±1/8 timing error with impairments at IF.

TABLE V—IMPAIRMENT VALUES—MAXIMUM AND MINIMUM OBTAINED REQUIRED RCP WITH ±1/8 TIMING ERROR (IMPAIRMENTS AT IF)

	Maximum Obtained Required RCP = 20.6 dB	Minimum Obtained Required RCP = 16.4 dB
Impairment Parameter	Value at Maximum	Value at Minimum
Linear Delay d_1	-0.14τ	-0.08τ
Quadratic Delay d_2	-0.18τ	-0.002τ
Cubic Delay d_3	-0.15τ	0.12τ
Ripple Delay		
Peak-to-peak value d_R	0.28τ	0.003τ
Period P_D	$0.94\, f_b$	$0.40\, f_b$
Phase θ_D	82.8°	70.8°
Linear Amplitude A_1	0.008	−0.13
Quadratic Amplitude A_2	−0.003	−0.09
Cubic Amplitude A_3	0.07	0.006
Ripple Amplitude		
Peak-to-peak value A_R	0.03	−0.02
Period P_A	$0.41\, f_b$	$0.82\, f_b$
Phase θ_A	5.1°	84.0°

VI. SUMMARY AND CONCLUSIONS

Monte Carlo techniques can be used to study the effects of parameter variability in systems as well as circuits: Statistical distributions are used to model variations in system characteristics rather than tolerances on circuit components. In particular, this paper has shown how Monte Carlo methods can be applied to the analysis of impairments in the waveguide transmission system. Two examples of the Monte Carlo analysis have been presented. These examples show how the Monte Carlo technique provides insight into the effects of impairments on the system performance, and can aid in determining the system impairment allocations.

Monte Carlo analysis can be used in the solution of future waveguide system problems, such as the problems of component variability and tolerance allocation. The effects of a particular choice of component tolerance requirements and the percentage of randomly assembled repeaters which meet the RCP objectives can be determined by Monte Carlo analysis. The effects of tighter tolerances and the need for component matching or tuning can also be determined. As more information becomes available on component variability in manufacturing and aging, it can be incorporated into the Monte Carlo analysis and its effects can be readily evaluated. This capability for obtaining quick results from new information is expected to be of significant value to the waveguide system design effort.

Employing Monte Carlo methods at an early stage in the waveguide system design and development is expected to shorten the design interval and reduce the design effort. It is expected that Monte Carlo techniques will find further application in the study of parameter variability in other Bell System projects.

VII. ACKNOWLEDGMENTS

I have worked closely with Mark Bonomi, Joe Mullins and Peter Tu on this project and want to thank them for their many helpful discussions on the waveguide system and the waveguide system simulation program. I also want to thank Charlie Semmelman, John Logan, and Barry Karafin for their comments on and criticisms of earlier versions of this paper.

REFERENCES

1. Semmelman, C. L., Walsh, E. D., and Daryanani, G. T., "Linear Circuits and Statistical Design," B.S.T.J., this issue, pp. 1149–1171.
2. Cermak, I. A., and Kirby, Mrs. D. B., "Nonlinear Circuits and Statistical Design," B.S.T.J., this issue, pp. 1173–1195.
3. Balaban, P., Karafin, B. J., and Snyder, Mrs. D. B., "A Monte Carlo Tolerance Analysis of the Integrated, Single-Substrate, RC, *Touch-Tone*® Oscillator," B.S.T.J., this issue, pp. 1263–1291.
4. Tu, P. J., "New Equalizers Help Waveguide Communications," Bell Laboratories Record, *48,* No. 4 (May 1970), pp. 137–141.
5. Mullins, J. H., "Using Computers in Designing Millimeter Waveguide Systems," Bell Laboratories Record, *48,* No. 10 (November 1970), pp. 292–298.

THE BELL SYSTEM TECHNICAL JOURNAL
Vol. 50, No. 4, April, 1971
Printed in U.S.A.

1969-70 Connection Survey:

Analog Transmission Performance on the Switched Telecommunications Network

By F. P. DUFFY and T. W. THATCHER, JR.

(Manuscript received December 16, 1970)

To characterize the transmission performance of the Bell System switched telecommunications network, Bell Telephone Laboratories conducted a survey of toll connections during 1969 and 1970. Connections were established between Bell System end offices chosen by statistical sampling techniques. Both analog and data transmission tests were performed. A summary of analog transmission performance is presented in this paper. It contains estimates for noise, loss, attenuation distortion, envelope delay distortion, peak-to-average ratio, frequency offset, level tracking, nonlinear distortion, and phase jitter for toll calls within the Bell System. Accompanying papers discuss data transmission error performance at various speeds between 150 and 4800 bits per second.

I. INTRODUCTION

Information related to transmission performance of toll connections is essential to the evaluation of toll service quality, necessary for assessing the adequacy of present administrative and maintenance procedures, and important in establishing objectives for new transmission systems and equipment. Bell Telephone Laboratories has conducted a number of system-wide transmission surveys since 1959. Surveys made in 1959, 1962, and 1966[1-3] concentrated on the transmission performance of toll connections. Other surveys have examined the performance of specific equipments or portions of the telephone network.[4-6] This survey is based on a probability sample of telephone traffic. The use of probability sampling permits estimation of transmission performance parameters for the population of all toll calls and permits quantitative measure of the possible error in these estimates. The 1969–70 survey differs from previous surveys by including more measures of the transmission performance of the connection.

Frequency offset, peak-to-average ratio (P/AR), level tracking, and intermodulation and harmonic distortion for toll connections had not been measured previously on a system-wide basis.

This paper presents a statistical summary of analog transmission data. Measurements were made on toll connections from end office (local switching office) to end office over the switched telecommunications network. Due to alternate routing and diversity routing within trunk groups, connections between the same originating and terminating offices may differ. Information on the characteristics of loops, which are fixed entities connecting a subscriber to his local office, has been reported by P. A. Gresh.[7] Connection measurement results are presented on the basis of airline distance between the end offices. Results are separated into three mileage categories. The breakdown is short (0–180 airline miles), medium (180–725 airline miles), and long (725–2900 airline miles). Mileage categories are combined to provide results for the population of all toll connections. The transmission characteristics reported include noise, loss, attenuation distortion, envelope delay distortion, P/AR, frequency offset, level tracking, nonlinear distortion, and phase jitter. Accompanying papers[8,9] provide results for data transmission error performance at various speeds between 150 and 4800 bits per second (b/s).

II. SURVEY LOGISTICS

2.1 *General*

It was apparent that to achieve a valid measure of the switched telecommunications network performance, the survey would be a large-scale operation encompassing the measurement of a large number of transmission characteristics on many toll connections between many different pairs of offices. Standard test sets or equipment units used for circuit maintenance or characterization were available for making most of the measurements. The remaining test equipment was purchased, or designed and built. Considering the bulk of the test equipment required to perform both analog and data transmission measurements, the shipping involved, and the manpower required to make measurements at many different locations, several decisions were made to control the magnitude of the physical effort:

(*i*) Several measurements were made from each location to limit the amount of travel and provide opportunity for measuring alternate routes.

(*ii*) Measurements were made in one direction of transmission

for most characteristics. The receiving locations for these tests required a large quantity of equipment and were designated *primary* test sites. The transmitting ends required a much smaller amount of equipment and were designated *secondary* test sites. Message circuit noise and 1000-Hz loss, however, were measured for both directions of transmission.

(*iii*) Personnel and equipment remained at a primary site for a given time while a secondary team and equipment moved from location to location.

(*iv*) With several tests to be made, and different equipment required for each test, tests were run simultaneously on several connections and then rotated rather than being made sequentially on only one connection at a time.

(*v*) Testing at each secondary site continued for at least a full day, this being judged to be an appropriate compromise between time required to travel to a site and set up the equipment, and measurement time at the site.

(*vi*) Sufficient equipped secondary teams were provided so that one could travel while another tested, thus keeping the primary team busy every working day.

2.2 *Test Equipment*

Equipment used in making *Data-Phone*® transmission performance tests is described in companion papers.[8,9] Analog transmission measuring equipment is listed in Table I.

Packed for shipping, each set of secondary test gear (analog and data), consisted of nine cases totaling about 27.5 cubic feet and weighing 550 pounds. The primary equipment was about five times larger. Figure 1 shows a primary equipment arrangement.

2.3 *Test Lines*

Access to toll connections was the same as that of telephone subscribers. Subscriber line appearances were connected directly from the main frame to the test console; the distance to the main frame ranged from 20 to 100 feet. At secondary locations five lines were used, three for simultaneous tests, one for coordination of tests (order wire), and one to provide a reference path for envelope delay measurements. At primary locations five lines were used for connections to the secondary locations and three additional lines were provided: one line for teletypewriter access to a time-shared computer for analog data management; one line for *Data-Phone* service to transfer data transmission

test results from a small computer at the primary location to a similar computer at the Bell Laboratories Holmdel, N. J., location; and one line for normal telephone service, used for coordination purposes.

III. SAMPLE DESIGN

3.1 *Sampling Considerations*

In the concluding remarks of I. Näsell's report of the 1966 Connection Survey, he noted that the survey suffered from two limitations:

TABLE I—CONNECTION SURVEY ANALOG TRANSMISSION TESTING EQUIPMENT

Equipment	Function
BTL* Console. (Pri, Sec)	Terminate and connect up to 8 telephone lines to 12 test sets
WECo 3A Noise Measuring Set [10] (Pri, Sec)	Measure circuit noise
WECo 6F Voiceband Noise Measuring Set (Pri)	Count impulse noise peaks (four threshold levels)
BTL Noise Measuring Set Control Unit (Pri)	Switch control of weighting networks, notch filter, and narrow band filters for intermodulation and harmonic distortion product measurement
WECo 25B Voiceband Gain and Delay Measuring Set (Pri, Sec)	Measure loss, attenuation distortion, and envelope delay distortion
WECo KS-19260L1 Oscillator (Sec)	Resettable accurate voice-frequency source
WECo 27B P/AR Receiver[11] (Pri) WECo 27E P/AR Generator (Sec)	Measure compression of peak-to-average power ratio of test signal (P/AR)
BTL Phase Jitter Meter (Pri)	Measure peak-to-peak phase jitter
X-Y Plotter (Pri)	Associated with 25B for swept plots of gain and envelope delay distortion
Frequency Counter (Pri)	Measure frequency offset
Amplifier and BTL Attenuator (Pri)	Shift receiving sensitivity of 25B to desired range
WECo 71B Milliwatt Reference Generator (Pri, Sec)	Calibration of test set sending power and receiving sensitivity
Accessories (Pri, Sec): Power Supplies, Tools, Batteries, Interconnecting Cords, Instructions, Shipping Cases, etc.	
Teletypewriter (Pri)	Transfer analog measurement results to data management system in time-shared computer

* BTL indicates equipment designed and built for the survey.

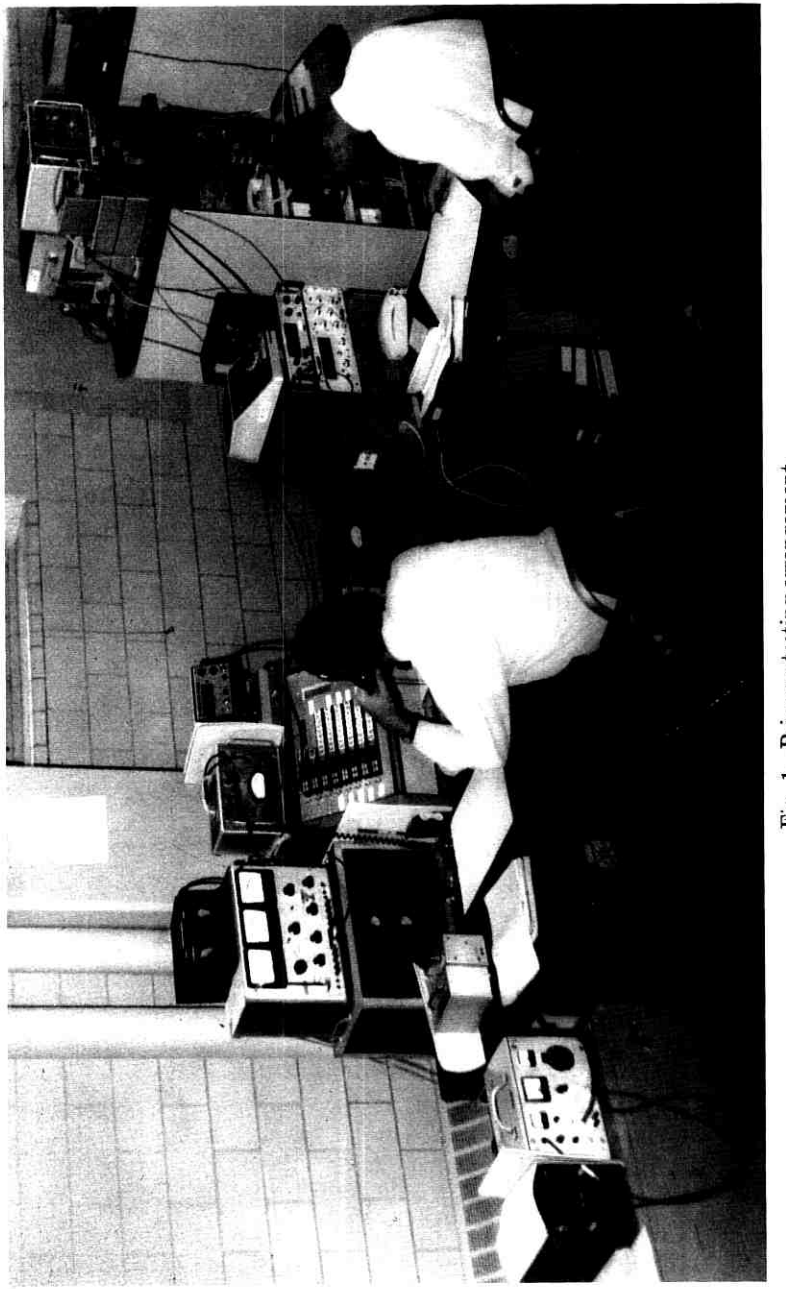

Fig. 1—Primary testing arrangement.

with test personnel only at one end of a connection, many tests could not be performed and calibration of far-end milliwatt supplies could not be verified.[3] Test personnel were assigned to both ends of the connections in the 1969–70 survey to overcome these limitations. This approach substantially increased the travel and overall time required to complete the survey. To bring these within manageable proportions, a three-stage sampling plan was adopted with 12 primary and 98 secondary test offices. Execution of this survey required at least seven persons in the field for a period of a year.

3.2 *Selection of the Samples*

A population for which information is desired must be defined prior to selecting a sample from that population. Characterization of analog transmission for toll connections was the criterion used to define a population for sampling purposes. The population was defined as all customer-dialed toll calls established between Bell System end offices via the switched telecommunications network during a normal business day. A call was classified as a toll call if the customer was detail billed, i.e., the customer incurred a specific, identified surcharge for placing the call. Calls originating or terminating in end offices not owned by the Bell System were excluded from the population. Calls originating in manual end offices also were excluded on the basis that they may not be placed without operator assistance. On January 1, 1970, 12 of the approximately 15,000 Bell System end offices were manual.

A three-stage sample with stratifications at the first and second stages of sampling was selected from the population defined above by established techniques.[12,13] First-stage sample units were selected with probabilities proportional to a measure of size. Second- and third-stage sample units were selected using stratified and simple random sampling respectively.

Prior to selecting the first-stage or primary sample units, a geographic stratification was imposed upon the population to achieve wide physical dispersion of the sample. Continental United States plus Ontario and Quebec (Bell Canada) were partitioned into twelve strata on the basis of annual outgoing toll messages (AOTM). Ideally, each stratum should have equal total AOTMs. Individual states were not subdivided in attempting to obtain equal size primary strata. This facilitated assembling the first-stage sampling frames.

One Bell System end office building was selected from each primary stratum. Selection took place independently in each primary

stratum and was based upon probabilities proportional to the number of annual outgoing toll messages. The primary units selected were in the 12 cities listed in Table II.

Units of the first-stage sample were designated as primary test sites for the analog transmission characterization of the voice network, i.e., buildings from which test calls originated and which served as receiving sites for transmission tests. The suitability of each primary for serving *Data-Phone* customers was verified. At two end office buildings it was noted that a *Data-Phone* customer normally would be served from an alternate or remote building because the offices within the sampled building were unacceptable with respect to impulse noise. Accordingly, test calls were originated from the alternate buildings for these primary locations. Tests were made from the selected building and from the alternate building in one of the instances. Tests were underway at the selected building when it was discovered that a *Data-Phone* customer indeed would not be served from that building. Tests scheduled for this site were completed. Another series of tests later was made at the alternate building. In the other case, tests were conducted only at the alternate building. The improvement in precision did not justify the effort required to visit the sampled building in addition to the alternate building. The sample for analog characterization does not include data collected at alternate buildings.

When an end office building contained offices with different types of switching, tests were performed on connections established through each type of office. One building contained offices having panel and crossbar switching. In this instance, the sample for analog characterization includes connections established through the panel and the crossbar offices. The sample for *Data-Phone* characterization includes connections established through the crossbar offices only.

In the second stage of sampling, from six to twelve calls were selected from originating traffic printouts compiled at the primary test sites composing the first-stage sample. These calls were used to determine secondary test offices, i.e., offices in which the test calls termi-

TABLE II—PRIMARY TEST LOCATIONS

Mobile, Ala.	Omaha, Nebr.
Sacramento, Calif.	Concord, N. H.
Miami, Fla.	Rockaway, N. J.
Woodstock, Ill.	New York, N. Y.
Quincy, Mass.	Cleveland, Ohio
Trufant, Mich.	Sharon, Pa.

nated and which served as transmitting sites for most transmission tests. A substratification was imposed before selection took place. Three substrata were defined on the basis of airline distance. Connections from 0 to 180 airline miles in length were placed into one substratum. Those from 180 to 725 airline miles were placed into a second. All remaining connections were placed into the third. At least two secondary sites were selected in each of the three mileage strata for each primary site. Additional secondary sites were selected in an effort to approximate self-weighting in each substratum. With self-weighting within substrata, each data point equally represents the population for its substratum. A total of 32 secondary sites was selected in the short mileage stratum. In both the medium and long mileage strata, 33 secondary sites were selected.

The third-stage sample elements were repeated calls originating from a primary site and terminating in one of its associated secondary sites. Approximately six connections were established between each primary and each of its associated secondaries. Repetitions were desired to account for the effects of alternate routing of toll connections and to increase the amount of data gathered while at the test sites. Analog transmission tests were conducted on 188 connections belonging to the short mileage category, 227 medium length connections, and 209 long connections. The complete array of analog measurements was not obtained on all connections since 60 were prematurely disconnected. It is believed many of these disconnects were caused inadvertently by survey test personnel.

IV. TESTING PROCEDURES

4.1 *Scheduling*

Personnel from Bell Laboratories performed the tests at both ends of the connections. Separate field teams were scheduled for the tours associated with each primary site—three persons at the primary and two at each secondary. A total of 56 persons participated. Generally, two secondary teams were associated with each primary; in one case, three teams were required. All teams received training in the test procedures before going to the field. Figure 2 shows the primary and secondary locations. Schedules were planned to minimize travel distance. The testing schedule, as modified by experience at the first primary site, provided essentially two full days at the first site visited by a secondary team for them to become accustomed to and perform

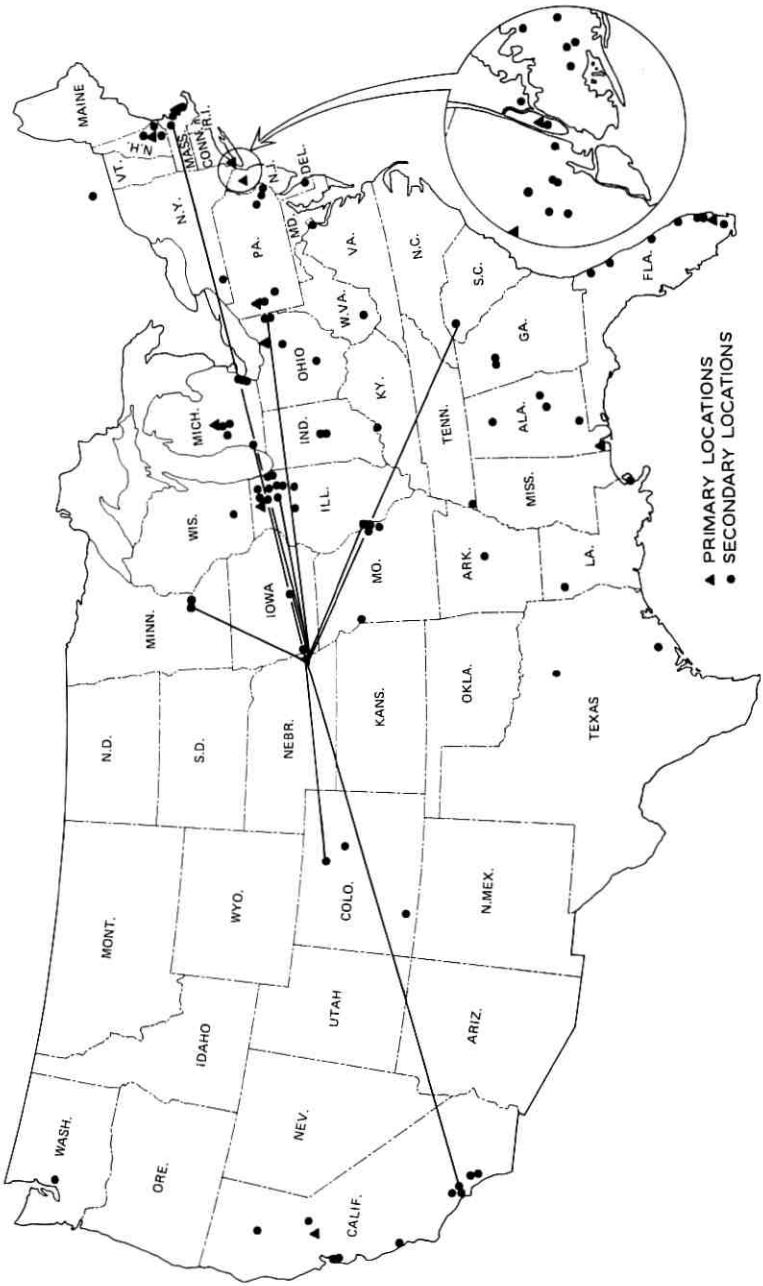

Fig. 2—Survey test locations. Lines connect Omaha and its secondaries.

the tests. Thereafter, only one day was scheduled for testing six connections.

4.2 *Placing Calls*

A testing sequence was begun in the morning by the primary team placing three test calls, one after another, from the primary to that day's secondary. As each call was answered, a few words of conversation were exchanged to assure two-way transmission to the correct number, the connection was held at both ends (push buttons on the consoles), and then the primary dialed the next test call. With three test connections established, a call was placed to serve as an "order wire" to coordinate the test activities and a call was placed to establish a data link to the Bell Laboratories Holmdel, N. J., location.

4.3 *Testing Procedures*

After the connections were established, testing was begun on all three and continued until the block of tests was completed, requiring about an hour. On one connection, a 2000-b/s data set was operated for 30 minutes, followed by a 1200-b/s data set for the next 30 minutes.[8] On a second connection, a 150-b/s data set was operated for 40 minutes, then a 3600- or 4800-b/s data set for 20 minutes.[9,8] If the secondary team was not equipped with a 3600- or 4800-b/s data set, the 150-b/s set was operated for an hour. On the third connection, the sequence of analog tests was performed. At the end of the first sequence of testing, the assignments of toll connections to the test equipments were rotated and the tests were repeated. At the end of the second hour of testing, the assignments were rotated again and testing continued until all tests had been made on each test connection. When all tests were completed, including any necessary check or verification tests, the calls were disconnected. In the afternoon, the entire sequence was repeated. When a call was inadvertently disconnected during testing, a new call was established. Testing usually continued from that point in the test sequence. An attempt normally was made to repeat the tests made on the original call but time did not always permit. Analog measurement results were read from meters and dials of the test sets. The values were recorded at the primary on a preprinted data form. At an appropriate time in the test sequence, the information was transferred to a data management system.

4.4 *Analog Data Management Procedures*

As measurements were made, results were entered into a data man-

agement system residing in a time-shared computer. Since test equipment characteristics contribute to the transmission characteristic values being measured, each data point was calibrated to subtract those contributions. It was then compared with the results calculated on the basis of previously collected data. If the data point greatly differed from previous data, information to that effect was transmitted to the test site. Field personnel verified if the measurement was correct by redoing the test since the connection was still established. Under no circumstances was a data point screened out simply because it differed greatly from other values. If the retest indicated the value was correct, then it was accepted.

Past surveys did not have immediate data processing available. Experience in this survey has clearly established the value of such a data management system providing feedback information to the test sites. Since data "laundering" was being carried out as the survey progressed, only a moderate amount remained to be done after field operations were completed. This produced two outstanding advantages. For the most part, the validity of the data was verified by people at the test site capable of investigating problems while connections were still established; secondly, analysis of data could begin immediately after field tests were completed.

4.5 *Data Analysis*

Analysis of the survey data was accomplished using computer programs based upon statistical formulas for multistage sample surveys.[12,13] Although an attempt was made to approximate self-weighting within each mileage category, it was convenient to select secondary test sites for individual primaries as the second-stage sampling frames became available. This restricted the degree to which self-weighting could be achieved. The absence of self-weighting means that some data points in a mileage category have more weight associated with them than others in translating sample measurements into population estimates. Because of this, appropriate weights were calculated and used in the analysis.

Recall that the sample design required selection of one primary unit in each primary stratum. This does not allow calculation of the variance due to the first stage of sampling when estimating a confidence interval. To solve this problem, the concept of collapsed strata was used.[14] Thus the data were analyzed as though the sample design called for six primary strata with two primary units in each. All weights were adjusted appropriately to reflect this change.

In addition to analog characterization of the voice network, an analysis to characterize analog transmission on that part of the network appropriate for data transmission was carried out. With the exception of impulse noise, only minor differences were seen when these results were compared to those for the entire voice network. Based on these findings, results for impulse noise will be presented as they relate to the entire voice network and as they relate to that part of the network serving data customers.

V. ANALOG TRANSMISSION RESULTS

Estimates of the population mean with accompanying 90-percent confidence interval and of the standard deviation are provided for most transmission characteristics. Results are presented for the population of all toll connections and for connections in three mileage categories defined on the basis of airline distance. Sampling weights reflecting the distribution of message telephone traffic were applied to the data to calculate all estimates. Generally, results for all toll calls resemble results for the short mileage category. Approximately 85 percent of all toll calls placed in the telephone network belong to the short category.[3]

When a cumulative distribution function (CDF) for a transmission characteristic indicates that the distribution has an elongated tail for large values of the characteristic, it is described as being positively skewed. If the tail of the distribution is elongated for small values of the characteristic, the distribution is described as being negatively skewed. Complete CDFs are presented to illustrate the degree of skewness for some characteristics. When a distribution of a characteristic deviates substantially from normal, the 10-, 50-, and 90-percent points are listed.

Generally, the variance of a transmission characteristic is largest in the short mileage category. Differences among the types of transmission facilities account for this large variance. A large variance along with a relatively small sample size results in a large variance for the estimator used to calculate the mean. Since the variance of that estimator is used to calculate the accompanying confidence interval, the resulting interval will be wide. As a result of this, the confidence intervals accompanying estimates for short connections are generally wider than those accompanying estimates for medium and long connections.

5.1 *Noise*

The subjective impairment due to noise in a transmission channel used for voice transmission is most directly related to the power and frequency spectrum of the noise. C-message weighted noise power is a good measure of the impairment.[10] Errors in data transmission may result from high-amplitude noise peaks; therefore, a count of the number of noise peaks exceeding a specified threshold is a better measure of the noise impairment for data transmission. This characteristic is called impulse noise.

5.1.1 *Message Circuit Noise*

Circuit noise was measured using a 3A Noise Measuring Set[10] with C-message and with 3-kHz flat weighting networks. The latter measurement includes low-frequency noise components. In addition, both measurements were recorded without and with a signal transmitted over the connection. The former indicates noise present during quiescent intervals on the telephone circuit. The latter measurements were made while a 2750-Hz tone at −12 dBm was transmitted. Since a connection may contain compandors, the tone was transmitted to provide energy to hold the compandors at a nominal gain. A band-reject filter was used to remove the tone at the receiving end of the connection before measurements were made. These measurements are an indication of the noise on a line as it would appear to a data modem. The measurements are referred to as C-message notched noise and 3-kHz flat notched noise. Results for these characteristics are listed in Table III.

C-message and 3-kHz flat noise without a tone applied to the telephone circuit were measured at both primary and secondary test offices. A comparison of C-message noise measured at the primary test offices with C-message noise measured at the secondary test offices does not indicate substantial differences. A comparison of the results for 3-kHz flat noise is not very meaningful because of the poor precision accompanying the results for measurements made at the primary offices. The precision is poor because the differences between primary test offices with respect to 3-kHz flat noise was substantial. Near-end noise contributions (60-cycle hum) accounted for these differences. Precision accompanying the results for measurements made at the secondary offices is better because there were eight times as many secondary offices. This gave a better cross-section of the near-end noise contributions.

TABLE III—RESULTS OF MESSAGE CIRCUIT NOISE TESTS ON TOLL CONNECTIONS*

Connection Length (airline miles)	C-Message Weighting		3-kHz Flat Weighting		C-Message Notched		3-kHz Flat Notched	
	Primary		Primary		Primary		Primary	
	Mean (dBrnC)	S.D.† (dB)	Mean (dBrn)	S.D. (dB)	Mean (dBrnC)	S.D. (dB)	Mean (dBrn)	S.D. (dB)
All‡	21.6 ± 3.6	9.1	42.7 ± 2.8	8.3	30.7 ± 2.9	11.4	44.8 ± 2.9	7.7
0–180	18.7 ± 3.7	8.3	42.2 ± 2.4	8.2	29.5 ± 3.6	12.6	44.5 ± 2.4	7.6
180–725	29.3 ± 0.6	3.1	43.6 ± 3.8	8.4	34.3 ± 1.4	5.2	45.1 ± 4.4	8.1
725–2900	32.7 ± 0.6	3.5	45.4 ± 5.7	8.7	34.9 ± 0.8	4.0	46.3 ± 5.6	8.1

Connection Length (airline miles)	C-Message Weighting		3-kHz Flat Weighting		1966 Connection Survey Results			
	Secondary		Secondary		C-Message Weighting		3-kHz Flat Weighting (DDD)	
	Mean (dBrnC)	S.D. (dB)	Mean (dBrn)	S.D. (dB)	Mean (dBrnC)	S.D. (dB)	Mean (dBrn)	S.D. (dB)
All	22.9 ± 3.5	8.5	43.1 ± 1.4	7.3	—	—	—	—
0–180	20.0 ± 3.7	7.6	43.1 ± 1.7	7.7	21.6 ± 0.8	6.4	42.5 ± 1.5	5.8
180–725	30.0 ± 0.5	3.7	43.3 ± 1.2	6.1	29.6 ± 0.7	4.2	43.6 ± 1.4	5.2
725–2900	33.8 ± 1.3	3.8	42.3 ± 1.9	6.2	32.5 ± 1.0	4.1	43.9 ± 1.1	4.2

* Sample weights reflecting the distribution of message telephone traffic were applied to the data to calculate all estimates in this paper.

† S.D. indicates standard deviation

‡ All indicates all connections (0–2900 airline miles)

C-message and 3-kHz flat noise have been well documented in past surveys, the most recent having been conducted in 1966.[3] A comparison of current C-message results with those of 1966, also shown in Table III, indicates substantially the same findings. In general, the mean C-message noise increases with distance while the standard deviation tends to decrease. Confidence intervals accompanying estimated means for both surveys overlap. The estimated standard deviation for short connections is greater than in 1966. The estimated standard deviations for medium and long connections are smaller than in 1966. Distributions for C-message noise are all close to normal.

Results for the 1966 survey contain 3-kHz flat noise for operator and DDD-handled calls. Since all calls in the 1969–70 survey were placed via DDD, a comparison was made with the corresponding results from 1966. The estimated means are similar for all mileage categories. Estimated standard deviations in all mileage categories are greater than in 1966. Short and long connections show approximately a 2.0-dB increase. Distributions for 3-kHz flat noise are positively skewed.

Since notched noise readings were measured only at the primary test sites, they are compared with C-message and 3-kHz flat results for the primaries. Both mean and standard deviation are larger for C-message notched noise than for C-message noise in each mileage category. The differences between the characteristics diminish with increasing distance. C-message notched noise is dependent upon the length of a connection; the means increase with distance. The standard deviation monotonically decreases with increasing distance. Distributions for C-message notched noise are close to normal in the medium and long categories. The distribution for short calls is negatively skewed.

Notched noise with 3-kHz flat weighting does not differ greatly from 3-kHz flat noise measured at primary test sites. There is a tendency for means to be slightly higher and for standard deviations to be slightly lower when a tone is present. Distributions for 3-kHz flat notched noise are positively skewed.

5.1.2 *Impulse Noise*

To measure impulse noise, a 2750-Hz signal at −12 dBm was transmitted. At the receiving end of the connection, a 6F Impulse Noise Counter was used to detect impulses of noise exceeding four different voltage levels. The levels were separated by 4-dB intervals. These levels were set so that the impulse noise counter thresholds were

5 and 1 dB below and 3 and 7 dB above the expected rms level of a received data signal. Connections were monitored for 15-minute intervals and the C-message notched weighting network was used to block the 2750-Hz tone.

Impulse noise count distributions are not normal. J. H. Fennick[15] has shown that the distribution of the logarithm of impulse noise counts is approximately normal for intertoll trunks. The logarithm of impulse noise counts is approximately normally distributed for connections as well. The mean, median, and standard deviation are listed in Table IV for the count distributions. The 10-, 50-, and 90-percent points are listed in Table V. These results characterize impulse noise on the entire voice network.

The number of counts decreases as the threshold of the impulse noise counter is raised. This is expected since the amplitude of the impulse must exceed the threshold of the counter to register. An equivalent way of phrasing the first sentence is to say that the number of impulse noise counts decreases as the signal-to-impulse-noise counter threshold gets smaller. Results in Table IV are presented for the four signal-to-impulse-noise counter thresholds used when monitoring a connection.

Impulse noise counts are dependent upon the length of a connection. The number of counts registered increases with airline distance. This is clearly illustrated in the first section of Table V where 10-, 50-, and 90-percent points are listed.

Earlier it was mentioned that results for impulse noise differed substantially when comparing the analog characterization of the voice network and the analog characterization of that part of the network providing *Data-Phone* service. The two sections of Table V permit this comparison. As discussed in Ref. 8, the sample for evaluating *Data-Phone* service excludes panel offices at either end of a connection. It also excludes originating step-by-step offices where the impulse noise level due to office equipment alone exceeded a specified limit. Reference 8 discusses this sample in detail.

5.2 *1000-Hz Loss*

A 1000-Hz 0-dBm signal was applied to the connection and the received signal power measured with a 25B Voiceband Gain and Delay Measuring Set. Loss results for measurements made at primary and secondary test sites are tabulated in Table VI. A comparison of the two sets of results does not indicate substantial differences. However, a comparison of the two measurements on a connection-by-connection

TABLE IV—IMPULSE NOISE COUNTS ON TOLL CONNECTIONS (15-MINUTE INTERVAL)

Signal-to-Impulse-Noise Counter Threshold	All			0–180 Miles			180–725 Miles			725–2900 Miles		
	Mean	Med.*	S.D.	Mean	Med.	S.D.	Mean	Med.	S.D.	Mean	Med.	S.D.
+5	39 ± 21	4	128	32 ± 15	3	105	48 ± 44	7	150	74 ± 48	15	219
+1	18 ± 11	2	68	13 ± 6	1	40	27 ± 30	2	90	44 ± 32	7	148
−3	11 ± 8	1	56	7 ± 5	0	23	24 ± 26	1	115	24 ± 20	2	87
−7	7 ± 6	0	34	5 ± 4	0	19	15 ± 18	0	72	10 ± 11	0	28

* Med. indicates median

TABLE V—IMPULSE NOISE COUNTS ON TOLL CONNECTIONS (15-MINUTE INTERVAL)
Percentage Points from Cumulative Distribution Curves

(Voice Network Characterization)

Signal-to-Impulse-Noise Counter Threshold	All			0–180 Miles			180–725 Miles			725–2900 Miles		
	10%	50%	90%	10%	50%	90%	10%	50%	90%	10%	50%	90%
+5	0	4	78	0	3	62	0	7	109	1	15	154
+1	0	2	36	0	1	29	0	2	76	0	7	95
−3	0	1	16	0	0	13	0	1	34	0	2	57
−7	0	0	7	0	0	5	0	0	19	0	0	22
	(*Data-Phone* Service Characterization)											
	10%	50%	90%	10%	50%	90%	10%	50%	90%	10%	50%	90%
+5	0	2	40	0	2	36	0	4	42	0	6	50
+1	0	1	14	0	1	12	0	1	14	0	2	28
−3	0	0	6	0	0	5	0	0	6	0	0	8
−7	0	0	3	0	0	3	0	0	3	0	0	5

TABLE VI—COMPARISON OF CONNECTION LOSSES AT 1000-HZ FROM 1966 AND 1969/70 SURVEYS

Connection Length (airline miles)	1969/70 Survey				1966 Survey	
	Primary		Secondary		(DDD)	
	Mean (dB)	S.D. (dB)	Mean (dB)	S.D. (dB)	Mean (dB)	S.D. (dB)
All	6.7 ± 0.6	2.1	6.6 ± 0.3	2.1	—	—
0–180	6.5 ± 0.7	2.0	6.4 ± 0.4	2.1	7.0 ± 0.4	2.3
180–725	7.3 ± 0.4	2.3	7.1 ± 0.6	2.1	8.5 ± 0.6	2.5
725–2900	7.7 ± 0.5	2.5	7.3 ± 0.3	2.0	8.9 ± 0.6	3.0

basis shows that a difference of 5 dB between loss measurements for the two directions of transmission is not uncommon. In one instance the difference was 20 dB.

Results from the 1966 survey are also included in Table VI.[3] Both surveys indicate that the means of the loss distributions increase with distance. However, the amount of increase with length is less than existed in 1966. Both mean loss and standard deviation are smaller in all categories when compared with the 1966 survey. On the basis of non-overlapping confidence intervals, the differences appear significant for medium and long connections. Distributions for loss are positively skewed.

5.3 *Signal to C-Notched Noise*

To obtain a measure of the effect of circuit noise upon data transmission, the ratio of received signal power to C-notched noise was calculated. Loss at 1000 Hz was used to determine the received power of a signal transmitted at −12 dBm. The distributional parameters are tabulated in Table VII.

The results from this survey clearly indicate that the ratio of signal to C-notched noise is dependent upon connection length. Both mean and standard deviation decrease with increasing distance. Note that larger ratios imply better transmission quality with respect to noise interference.

Distributions of signal to C-notched noise are negatively skewed for medium and long connections. The distribution for short connections is positively skewed. Since this characteristic is of particular interest for data transmission, the cumulative distribution functions are given in Fig. 3.

TABLE VII—RESULTS OF SIGNAL-TO-C-NOTCHED-NOISE RATIO FOR TOLL CONNECTIONS

Connection Length (airline miles)	Mean (dB)	S.D. (dB)
All	40.6 ± 3.0	11.8
0–180	42.1 ± 3.8	13.0
180–725	36.5 ± 1.3	5.3
725–2900	35.4 ± 0.9	3.8

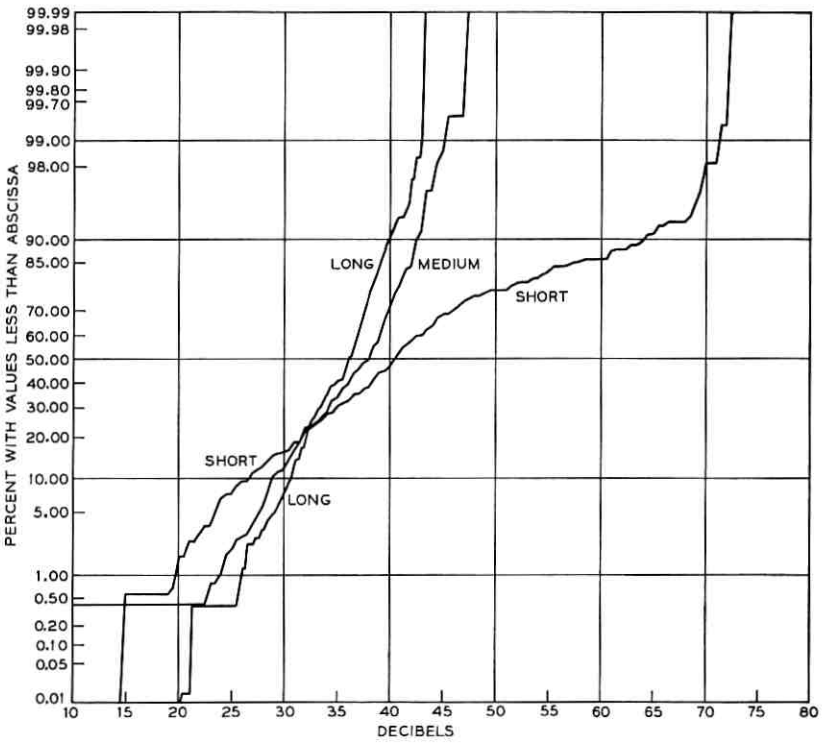

Fig. 3—Cumulative distribution curves: signal-to-notched noise with C-message weighting.

5.4 *Attenuation Distortion Relative to 1000 Hz*

Attenuation distortion is a measure of the change in loss caused by a corresponding change in the frequency of a transmitted signal.

The test was initialized by sending a 1700-Hz signal at 0 dBm and, at the receiving end of the connection, adjusting a preamplifier to obtain a high reading on a 25B Voiceband Gain and Delay Measuring Set. Once the preamplifier was set for a particular connection, the setting was not changed throughout the remainder of the test. The signal was then sent at each frequency listed in Table VIII and the received signal measured. When the power of the received signal was too low to be detected by the test equipment, the lowest detectable value was assigned. This occurred at the lower and upper edge frequencies of the voiceband (200, 3200, 3300, and 3400 Hz).

Loss is treated as a positive quantity for data analysis. Increasing positive quantities represent greater loss conditions. To obtain the attentuation distortion, the 1000-Hz loss of each connection was subtracted from the losses at all frequencies for that connection. Results for the lower and upper edge frequencies mentioned above are interpreted as indicating that the distortion is at least that great.

Attenuation distortion in all mileage categories is essentially the same between 800 and 2300 Hz. Short connections experience less distortion at both the lower and upper edges of the voiceband when compared to medium and long connections. Distortion on long connections is similar to that on short connections for the lower edge frequencies of the voiceband (200–600 Hz) and it is similar to the distortion on medium length connections at the upper edge frequencies of the voiceband (2450–3400 Hz). Attenuation distortion distributions are slightly to moderately skewed. In most cases the skewness is positive.

A graphical presentation of means listed in Table VIII is given in Fig. 4. The means for all connections combined are not plotted, since they are similar to the means for short connections. The figure provides a first-order approximation for attenuation distortion bandwidth. The 1959 survey noted an average 20-dB bandwidth of about 3000 Hz for both short (0–400 miles) and long (400–2900 miles) connections.[1] Calculating the differences in frequency between the low-end and high-end 20-dB points in Fig. 4 gives approximately 3100 Hz. Attenuation distortion curves generally are nearly linear from about 1000 Hz to 2800 Hz. The loss difference between 2750 Hz and 1000 Hz provides a measure of this slope. Accordingly, the average slopes for the curves are 3.5, 4.1, and 4.7 dB for short, medium, and long connections respectively. These results indicate a decrease in slope since 1959. When the data from the 1959 survey are adjusted to eliminate the contributions of loops, the amount of decrease is in the neighborhood of 2 to 3 dB.

TABLE VIII—ATTENUATION DISTORTION RELATIVE TO 1000-HZ ON TOLL CONNECTIONS

Frequency (Hz)	All		0–180 Miles		180–725 Miles		725–2900 Miles	
	Mean (dB)	S.D. (dB)	Mean (dB)	S.D. (dB)	Mean (dB)	S.D. (dB)	Mean (dB)	S.D. (dB)
200*	11.8 ± 1.9	5.1	11.4 ± 2.4	5.1	13.7 ± 1.5	4.5	12.4 ± 2.4	5.0
250	6.6 ± 0.9	3.0	6.4 ± 1.1	2.7	8.0 ± 1.3	3.7	6.8 ± 1.6	3.1
300	4.1 ± 0.6	2.1	4.0 ± 0.7	1.9	4.8 ± 0.9	2.8	4.0 ± 0.9	2.1
400	2.3 ± 0.3	1.6	2.2 ± 0.4	1.4	2.8 ± 0.6	2.2	2.0 ± 0.3	1.4
600	1.1 ± 0.1	1.1	0.9 ± 0.1	0.9	1.6 ± 0.4	1.9	1.2 ± 0.2	0.8
800	0.5 ± 0.1	0.5	0.4 ± 0.0	0.5	0.7 ± 0.2	0.5	0.5 ± 0.1	0.4
1200	−0.1 ± 0.1	0.3	−0.1 ± 0.1	0.3	−0.3 ± 0.1	0.4	−0.3 ± 0.0	0.4
1400	−0.1 ± 0.1	0.6	0.0 ± 0.1	0.6	−0.3 ± 0.1	0.6	−0.3 ± 0.1	0.5
1700	0.3 ± 0.1	0.9	0.3 ± 0.1	0.9	0.1 ± 0.2	0.8	0.2 ± 0.2	0.8
2000	0.8 ± 0.1	1.1	0.8 ± 0.1	1.1	0.8 ± 0.2	1.1	0.7 ± 0.3	1.0
2300	1.4 ± 0.2	1.4	1.4 ± 0.3	1.3	1.4 ± 0.3	1.4	1.7 ± 0.5	1.4
2450	1.9 ± 0.4	1.6	1.8 ± 0.4	1.5	2.0 ± 0.4	1.6	2.4 ± 0.6	1.7
2750	3.7 ± 0.8	2.5	3.5 ± 1.0	2.5	4.1 ± 0.5	2.2	4.7 ± 1.0	2.3
2850	4.7 ± 1.1	3.0	4.4 ± 1.2	3.0	5.4 ± 0.6	2.6	6.1 ± 1.1	2.7
3000	6.9 ± 1.5	4.1	6.4 ± 1.6	4.1	8.1 ± 1.0	3.6	9.2 ± 1.9	4.3
3100	9.5 ± 1.7	5.7	9.0 ± 1.9	5.9	10.6 ± 1.5	4.7	11.6 ± 2.7	5.2
3200*	13.4 ± 2.1	7.8	12.9 ± 2.5	8.0	14.7 ± 2.1	6.8	15.2 ± 3.4	6.6
3300*	18.2 ± 2.7	9.5	17.6 ± 3.2	10.0	20.0 ± 3.1	8.0	19.8 ± 3.7	7.6
3400*	22.1 ± 3.0	9.2	21.2 ± 3.6	9.8	24.4 ± 2.8	6.4	25.1 ± 1.7	6.1

* Distortion values at these frequencies are at least as great as shown.

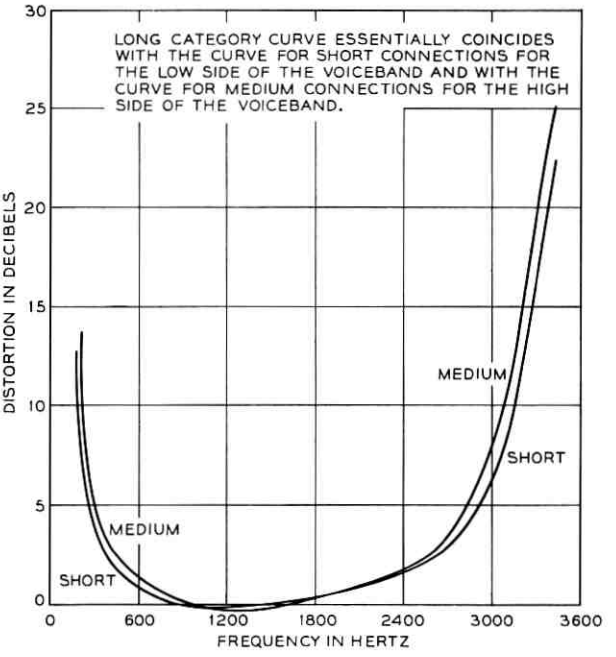

Fig. 4—Locus of means for attenuation distortion relative to 1000 Hz.

5.5 *Envelope Delay Distortion Relative to 1700 Hz*

In general, the change in phase of a signal introduced by a transmission channel depends upon the frequency of the signal. Envelope delay is the derivative of the phase characteristic with respect to frequency. Envelope delay distortion is the envelope delay minus the constant delay term.[16] Table IX presents results of envelope delay distortion relative to the delay at 1700 Hz for 19 frequencies throughout the voiceband.

Relative envelope delay distortion distributions are positively skewed. The degree of skewness varies considerably. Means and standard deviations for medium and long toll connections are very similar; generally the means are separated by less than 100 microseconds at frequencies between 800 and 2450 Hz and by less than 250 microseconds elsewhere in the voiceband. Furthermore, the means are slightly lower for long connections between the frequencies 200 and 1400 Hz. Between the frequencies 2000 and 3400 Hz, the results display slightly higher means for long connections. The standard deviation

TABLE IX—ENVELOPE DELAY DISTORTION RELATIVE TO 1700-HZ ON TOLL CONNECTIONS

Frequency (Hz)	All		0–180 Miles		180–725 Miles		725–2900 Miles	
	Mean (μsec.)	S.D. (μsec.)	Mean (μsec.)	S.D. (μsec.)	Mean (μsec.)	S.D. (μsec.)	Mean (μsec.)	S.D. (μsec.)
200*	5187 ± 566	2672	4580 ± 518	2461	7526 ± 404	1851	7505 ± 473	2422
250*	3934 ± 410	2010	3384 ± 326	1727	5866 ± 417	1595	5880 ± 314	1870
300	3290 ± 289	1660	2816 ± 209	1407	4884 ± 384	1375	4901 ± 297	1510
400	2091 ± 221	1220	1695 ± 128	930	3413 ± 341	1215	3163 ± 218	1144
600	843 ± 96	583	656 ± 43	430	1467 ± 183	628	1335 ± 127	592
800	392 ± 50	342	290 ± 20	263	737 ± 114	371	649 ± 88	350
1000	190 ± 28	206	133 ± 15	165	380 ± 73	227	335 ± 53	209
1200	80 ± 16	125	48 ± 10	103	187 ± 45	139	156 ± 32	128
1400	17 ± 5	74	3 ± 8	66	63 ± 16	83	56 ± 15	76
2000	51 ± 20	67	50 ± 18	62	36 ± 26	66	80 ± 51	95
2300	175 ± 47	136	152 ± 43	122	226 ± 54	133	273 ± 76	180
2450	284 ± 65	179	248 ± 64	159	363 ± 48	153	442 ± 89	230
2750	577 ± 120	339	485 ± 102	276	811 ± 99	273	934 ± 189	457
2850	729 ± 144	420	616 ± 120	338	1017 ± 137	348	1166 ± 263	573
3000	1041 ± 183	570	889 ± 164	456	1437 ± 144	468	1614 ± 303	816
3100	1335 ± 241	728	1128 ± 217	578	1903 ± 153	585	2071 ± 329	993
3200	1636 ± 330	956	1319 ± 279	697	2475 ± 191	750	2734 ± 414	1285
3300*	1919 ± 461	1227	1526 ± 363	917	3208 ± 343	1095	3333 ± 395	1356
3400*	2367 ± 693	1645	1935 ± 556	1277	4040 ± 553	1634	4248 ± 752	2018

* A significant percentage of connections were not measurable at these frequencies.

of the distribution of relative envelope delay distortion at each frequency for long connections is the same or moderately higher than for medium length connections.

A comparison of the results with the 1959 survey indicates less delay distortion on telephone circuits today.[1] Results for both medium and long categories compare favorably with the 1959 results for short toll connections (0–400 miles).

Except for the three lower edge frequencies, the results for short toll connections indicate that envelope delay distortion at a given frequency is about half that experienced on medium and long connections. Standard deviations for short connections are either lower or essentially the same with the exception of the three lower edge frequencies once again. Figure 5 graphically displays the means listed in Table IX. The

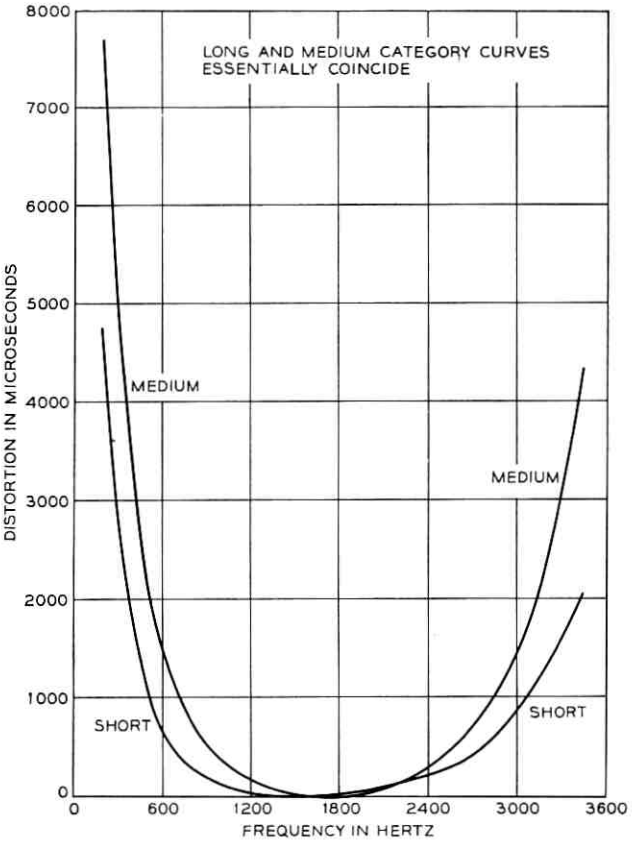

Fig. 5—Locus of means for envelope delay distortion relative to 1700 Hz.

locus of means for the population of all toll connections falls between the curves plotted for short and medium length connections. Figure 5 provides a first-order approximation for envelope delay distortion bandwidth.

At the lower and higher edge frequencies of the voice band, envelope delay distortion may not be measurable. This occurs when the circuit has a high loss at a given frequency. Since the envelope delay distortion cannot be predicted when this condition arises, the sample size diminishes at the outer edge frequencies. This reduction in sample size is as high as 27 percent at 250 and 3300 Hz. It is as high as 41 percent at 200 Hz and 54 percent at 3400 Hz.

5.6 *Peak-to-Average Ratio (P/AR)*

P/AR is a single parameter measure of the transmission quality of a connection.[11] A 27E P/AR generator was used to introduce a continuous pulse train into the telephone channel. The reading on a 27B P/AR Receiver measures the dispersion introduced by that channel. Since amplitude distortion, phase distortion, nonlinear distortion, and noise influence the dispersion that will be introduced, P/AR measurements are related to measures of each of these impairments. High values of P/AR represent favorable transmission conditions.

Results for P/AR appear in Table X. Although the mean does not show a monotonic trend with length of connection, it is dependent upon mileage. The standard deviation increases with connection length. All P/AR distributions are negatively skewed. To illustrate the low end tails of the distributions, the CDFs for short, medium, and long toll connections are given in Fig. 6.

5.7 *Absolute Frequency Offset*

The frequency of a signal may shift when transmitted over a carrier telephone channel. This will occur when modulating and demodulating

TABLE X—RESULTS FOR PEAK-TO-AVERAGE RATIO (P/AR) ON TOLL CONNECTIONS

Connection Length (airline miles)	Mean	S.D.
All	79.5 ± 3.0	9.9
0–180	81.7 ± 3.3	8.6
180–725	72.5 ± 3.3	10.5
725–2900	74.2 ± 2.0	11.0

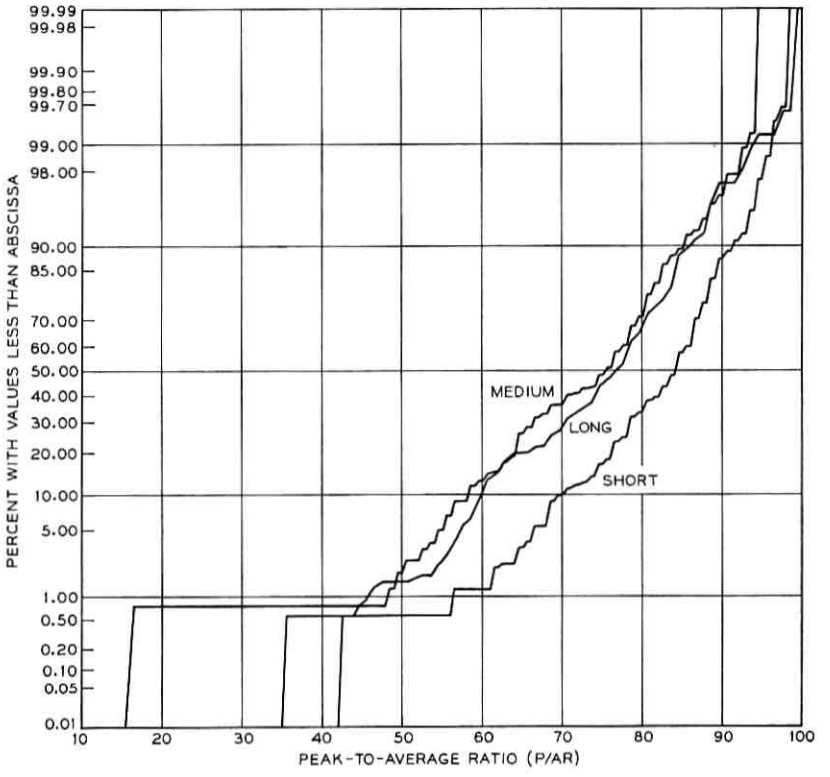

Fig. 6—Cumulative distribution curves: peak-to-average ratio (P/AR).

carrier supply frequencies are not identical. The change in frequency is called frequency offset. The offset is positive if the frequency increases and negative if it decreases. Absolute frequency offset is defined as the absolute value of the change in frequency.

A precise 1200-Hz signal was transmitted at −12 dBm. At the receiving end of the connection, a frequency counter with a 10-second averaging period was used to measure the frequency of the received signal. Results for absolute frequency offset are given in Table XI.

Distributions of absolute frequency offset are not normal. The value is 0 for 87, 59, and 43 percent of all connections in the short, medium, and long categories, respectively. Accordingly, 10-, 50-, and 90-percent points are listed in Table XI. The table indicates very little frequency offset was detected. However, an offset greater than 3 Hz was measured on two connections in the long mileage category.

TABLE XI—RESULTS FOR ABSOLUTE FREQUENCY OFFSET ON TOLL CONNECTIONS
(Percentage Points from Cumulative Distribution Curves)

Connection Length (airline miles)	Offset in Hz		
	10%	50%	90%
All	0	0	0.2
0–180	0	0	0.1
180–725	0	0	0.3
725–2900	0	0.1	1.1

5.8 *Level Tracking*

Level tracking is a measure of change in loss as a function of the power of a signal at the input to a connection. It provides an indication of the presence of compandored facilities, particularly any mismatch of signal-power-controlled compressor gains and expandor losses. Results are presented in Table XII in the form of deviations from the gain measured with −10-dBm input power. The results show that over the measured range there is a slight decrease in gain as the input test signal power is increased.

Distributions for gain deviations with signal power are skewed toward greater deviations. Thus, distributions for input powers greater than −10 dBm are negatively skewed, while distributions for input powers lower than −10 dBm are positively skewed. It is noted that the greatest deviations are concentrated in the medium length category. This reflects the fact that more compandors are likely to be encountered on medium length connections. This is indicated by the facility composition of intertoll trunks presented in Ref. 5. Medium-length connections often consist of a short intertoll trunk and a medium-length intertoll trunk in tandem or two short intertoll trunks in tandem. These arrangements increase the likelihood of encountering compandors.

5.9 *Nonlinear Distortion*

Estimates of nonlinear distortion were obtained using intermodulation and harmonic distortion measurements. For intermodulation distortion, two tones, 1250 Hz (tone A) and 700 Hz (tone B), were transmitted at −13 dBm each (−10 dBm total) and the power of each intermodulation product in Table XIII was measured. For harmonic distortion, a 525-Hz tone was transmitted at −12 dBm and the received

TABLE XII—DEVIATIONS FROM GAIN MEASURED WITH −10-DBM TRANSMITTED SIGNAL ON TOLL CONNECTIONS

Connection Length (airline miles)	0 dBm Input		−5 dBm Input		−15 dBm Input		−20 dBm Input	
	Mean (dB)	S.D. (dB)	Mean (dB)	S.D. (dB)	Mean (dB)	S.D. (dB)	Mean (dB)	S.D. (dB)
All	-0.5 ± 0.1	0.5	-0.3 ± 0.1	0.3	0.4 ± 0.1	0.3	0.7 ± 0.1	0.6
0–180	-0.5 ± 0.1	0.5	-0.3 ± 0.1	0.3	0.3 ± 0.1	0.3	0.7 ± 0.2	0.6
180–725	-0.7 ± 0.2	0.5	-0.4 ± 0.1	0.3	0.5 ± 0.1	0.4	0.9 ± 0.2	0.7
725–2900	-0.5 ± 0.1	0.4	-0.3 ± 0.1	0.3	0.4 ± 0.1	0.3	0.6 ± 0.1	0.4

TABLE XIII—RESULTS FOR THE RATIO OF THE TOTAL RECEIVED POWER OF A TWO-TONE SIGNAL TRANSMITTED AT −10DBM TO INDIVIDUAL INTERMODULATION PRODUCT POWERS ON TOLL CONNECTIONS

Product A = 1250 Hz B = 700 Hz		All		0–180 Miles		180–725 Miles		725–2900 Miles	
Type	Freq. (Hz)	Mean (dB)	S.D. (dB)	Mean (dB)	S.D. (dB)	Mean (dB)	S.D. (dB)	Mean (dB)	S.D. (dB)
A − B	550	42.8 ± 2.3	10.6	43.2 ± 3.2	11.4	40.8 ± 1.8	7.7	42.9 ± 0.7	7.0
2B	1400	50.1 ± 2.5	11.5	51.3 ± 3.2	12.7	46.1 ± 1.7	5.8	46.8 ± 1.0	5.2
A + B	1950	43.9 ± 3.0	12.0	44.9 ± 3.8	13.1	39.9 ± 2.4	7.3	42.7 ± 1.4	6.7
3B	2100	54.3 ± 1.2	7.4	54.7 ± 1.5	8.0	53.5 ± 1.5	5.0	52.7 ± 1.6	5.0
2A	2500	48.6 ± 2.2	11.2	49.3 ± 2.9	12.3	45.7 ± 2.5	6.5	48.0 ± 1.5	6.0
2B + A	2650	50.0 ± 2.2	12.3	51.1 ± 2.8	13.6	46.0 ± 2.2	6.6	46.8 ± 1.1	4.8
2A − B	1800	43.6 ± 2.4	10.9	45.0 ± 3.1	11.9	39.3 ± 2.4	6.3	40.1 ± 1.3	4.9
Equivalent A ± B		42.1 ± 2.2	10.6	42.8 ± 3.0	11.6	39.0 ± 2.1	5.9	41.3 ± 1.2	5.7

powers of the signal, the second harmonic (1050 Hz), and the third harmonic (1575 Hz) were measured. Results in Tables XIII and XIV give the powers of the products in dB below received signal.

Current work on characterizing nonlinearities has shown that the power average of the second-order products should be used to compute second-order distortion and the 2A-B product used directly to compute third-order distortion.[17] This measure of second-order distortion is labeled "equivalent A ± B" product in Table XIII and was computed for each connection by taking the ratio of total received signal power to the average power of the A + B product, the A − B product, and the 2A and 2B products each adjusted by 6 dB to make them equivalent to A ± B products.[16] Figures 7 and 8 give the CDFs for second- and third-order ratios.

Nonlinear distortion is time-variable on some channels. When an intermodulation or harmonic distortion product varied with time, the maximum value was recorded. This causes estimates of nonlinear distortion to indicate slightly poorer ratios for second-order products. Laboratory simulations have shown that the maximum value is the best indication of performance for third-order products and the average of the maximum and minimum values should be used for second-order products.

Distributions for intermodulation distortion ratios exhibit positive skewness for short connections while the data for both medium and long connections generally are close to normal. For all ratios the standard deviation decreases in longer mileage categories. This trend is not true for the means of the distributions. Generally the mean is lowest for medium length connections.

The ratio of fundamental to second harmonic of the 525-Hz tone has a distribution which is positively skewed for short connections.

TABLE XIV—RESULTS FOR THE RATIO OF RECEIVED 525-HZ FUNDAMENTAL TO THE SECOND AND THIRD HARMONICS ON TOLL CONNECTIONS

Connection Length (airline miles)	Second		Third	
	Mean (dB)	S.D. (dB)	Mean (dB)	S.D. (dB)
All	41.8 ± 2.5	11.6	45.7 ± 2.4	12.3
0–180	42.6 ± 3.3	12.4	47.3 ± 2.6	13.3
180–725	38.2 ± 1.9	7.8	39.7 ± 2.4	6.3
725–2900	41.6 ± 1.4	7.6	42.0 ± 1.6	5.3

The distributions are close to normal for medium and long connections. The ratio of fundamental to third harmonic has a distribution positively skewed for both short and medium connections. The distribution is close to normal for long connections. Both ratios are poorest in the medium category. Standard deviations decrease in the longer categories.

The skewness in the distributions of ratios noted above reflects the fact that the harmonic or intermodulation product was very weak on some connections. When either an intermodulation or harmonic product was below the noise measured in a slot around the frequency of the product, the noise value was recorded. This leads to slightly lower ratios.

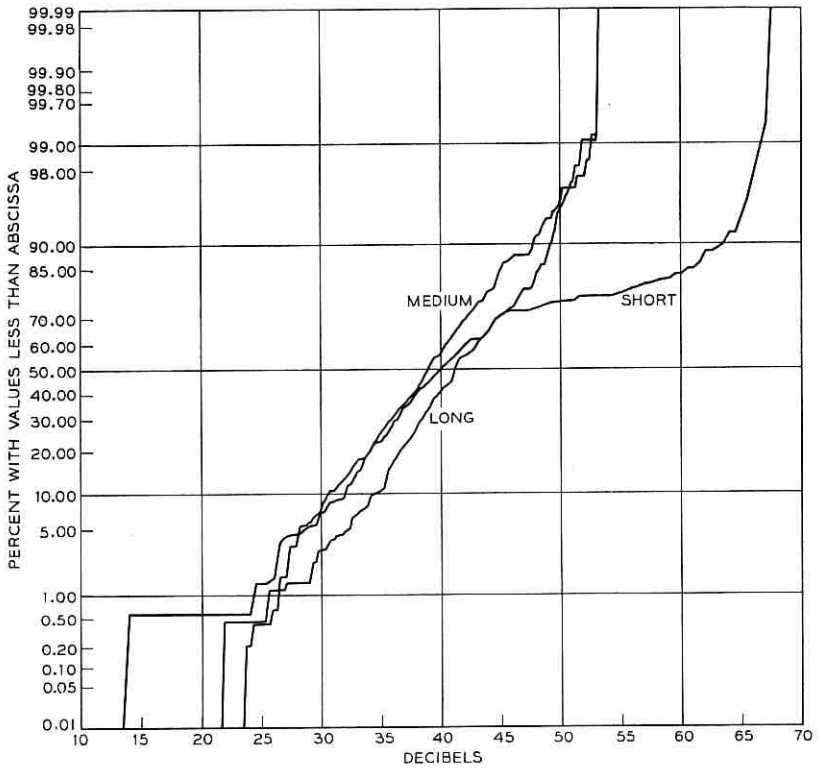

Fig. 7—Cumulative distribution curves: signal-to-second-order distortion product at −10 dBm transmit power.

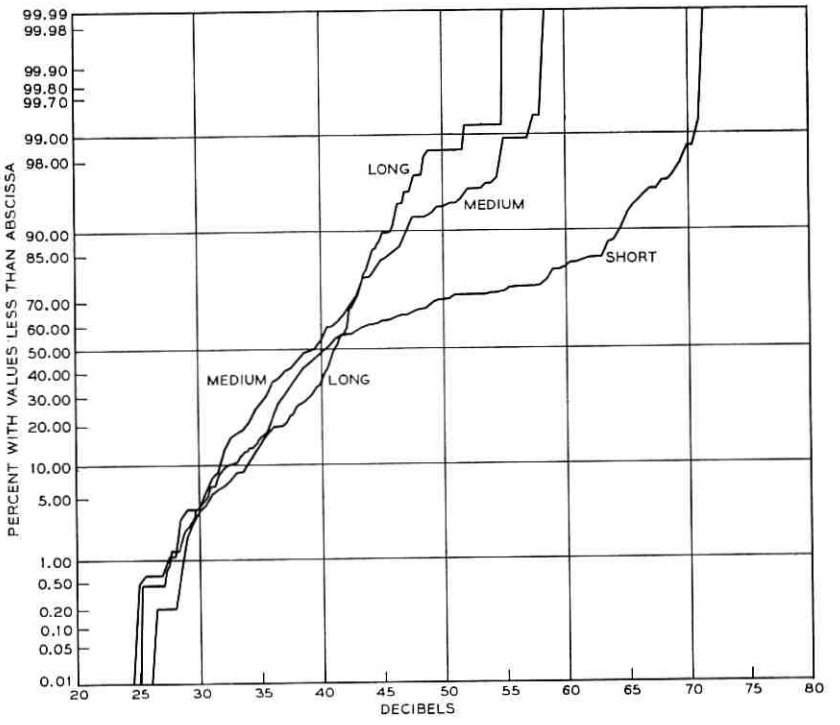

Fig. 8—Cumulative distribution curves: signal-to-third-order distortion product at −10 dBm transmit power.

5.10 *Peak-to-Peak Phase Jitter*

Phase jitter is defined as incidental frequency modulation or phase variations introduced into signals transmitted over telephone channels. To measure the components of jitter in several frequency bands, a 1700-Hz signal was transmitted at 0 dBm. At the receiving end, phase excursions of the 1700-Hz tone were detected. Peak-to-peak phase jitter in degrees was measured in six octave bands between 12 and 768 Hz and for the entire band of 12 to 768 Hz.

Distributions of phase jitter are not normal. In most instances, the distributions exhibit a high degree of truncation at 0 degrees. Accordingly, Table XV contains 10-, 50-, and 90-percent points for short, medium, and long connections in each frequency band measured. Results published for the 1966 survey described jitter components between 10 Hz and 120 Hz.[3] They are reproduced in Table XV. A

TABLE XV—RESULTS FOR PEAK-TO-PEAK PHASE JITTER ON TOLL CONNECTIONS
(Percentage Points from Cumulative Distribution Curves)

Frequency Band (Hz)	All			0–180 Miles			180–725 Miles			725–2900 Miles		
	degrees			degrees			degrees			degrees		
	10%	50%	90%	10%	50%	90%	10%	50%	90%	10%	50%	90%
12–768	0	3.0	7.0	0	2.0	6.0	2.0	4.0	8.0	2.0	5.0	9.0
12–24	0	0	2.0	0	0	1.0	0	1.0	3.0	0	1.0	3.0
24–48	0	0	1.0	0	0	1.0	0	1.0	2.0	0	1.0	2.0
48–96	0	0	2.0	0	0	1.0	0	1.0	4.0	1.0	2.0	5.0
96–192	0.3	0.3	1.3	0	0	0.3	0.3	0.3	2.3	0.3	0.3	2.3
192–384	0	0.5	1.5	0	0.5	1.5	0.5	0.5	1.5	0.5	0.5	1.5
384–768	0	0.6	1.6	0	0.6	1.6	0	0.6	1.6	0.6	0.6	1.6

(1966 Connection Survey Results)

Connection Length (airline miles)	Phase Jitter (degrees) (DDD)		
	10%	50%	90%
0–180	1	2	9
180–725	2	6	18
725–2900	3	12	21

comparison with the current results clearly indicates a dramatic improvement. There is much less jitter in the band 12 Hz to 768 Hz now, than in the much narrower band in 1966.

5.11 *Time to Receipt of Audible Ringing*

Time to receipt of audible ringing is defined as the interval of time which elapses between dialing the last digit of a telephone number and receiving the audible ringing signal. This was recorded for each test connection and the results are listed in Table XVI. Results for time to connect on DDD-handled calls are reproduced from the 1966 survey in Table XVII.

In the 1966 survey, calls were made to standard milliwatt supply terminations at the far-end offices.[3] Time to connect on DDD calls was recorded as the time which elapsed between dialing the last digit of the telephone number and receipt of the milliwatt signal. Since the milliwatt signal is transimtted about 100 milliseconds after application of the ringing signal, the measurement procedures of the surveys are comparable.

A note of caution must be given. Calls generally were placed at 8 a.m. and 12 noon in this survey and were held for approximately four hours. In 1966 they were placed at any time between the hours of 8 a.m. and 5 p.m.

The estimated mean and standard deviation for time to receipt of audible ringing are largest for medium-length connections in this survey. Distributions for time to receipt of audible ringing are close to normal in all mileage categories. A comparison with the 1966 survey shows that the confidence intervals overlap in all mileage categories.

VI. REMARKS

Comparisons have been made with past surveys. They indicate a

TABLE XVI—RESULTS FOR TIME TO AUDIBLE RINGING ON TOLL CONNECTIONS

Connection Length (airline miles)	Mean (seconds)	S.D. (seconds)
All	11.7 ± 1.8	4.3
0–180	10.8 ± 1.5	3.7
180–725	14.7 ± 3.2	5.0
725–2900	13.9 ± 2.6	4.5

TABLE XVII—RESULTS FOR TIME TO CONNECT ON DDD TOLL CONNECTIONS IN 1966

Connection Length (airline miles)	Mean (seconds)	S.D. (seconds)
0–180	11.1 ± 0.9	4.6
180–725	15.6 ± 1.0	5.0
725–2900	17.6 ± 2.1	6.6

trend towards improved transmission performance. Substantial improvement has been observed for phase jitter. Relative envelope delay distortion, attenuation distortion slope, and 1000-Hz loss results also indicate improvements.

In addition to the impairments previously measured to evaluate transmission performance, new measures have been made on a system-wide basis for toll connections. They include P/AR, frequency offset, level tracking, and nonlinear distortion. These should be of particular interest to those involved in data transmission.

Time-shared computer processing of data and the use of trained test teams at originating and terminating ends of connections are a powerful combination. They provide the advantages of control and flexibility. Since data "laundering" was concurrent with field operations, the data management system provided means for accurate and current reporting of survey results.

VII. ACKNOWLEDGMENTS

The efforts of many individuals contributed to the survey reported in this paper. We would like to single out Ingemar Näsell to acknowledge his work in designing the sample plan of the survey. Members of Bell Telephone Laboratories traveled throughout the United States and to Canada to collect the data. The authors wish to thank them for their conscientious contributions. Members of the AT&TCo headquarters staff coordinated the necessary interplay between Bell Telephone Laboratories and the Bell System Operating Companies. In particular, the authors thank Calvin White. Field tests could not be conducted so smoothly without the assistance received from central office foremen and craftsmen throughout the Bell System. The authors and all Bell Laboratories test team members express their appreciation and thanks to these men. In the area of data analysis the authors

wish to thank Robert Byorick, Charles Ellison, John Fennick, and Gale McNamara for their assistance and discussions. The authors wish to acknowledge the work of Miss Janet Russo and Mrs. Alice Silver in processing the sampling frames and of Terry Bequette in supervising the sample selection process. Finally, the contributions of Jack Doncourt and Thomas Hack in constructing the special analog test equipment are acknowledged.

REFERENCES

1. Alexander, A. A., Gryb, R. M., and Nast, D. W., "Capabilities of the Telephone Network for Data Transmission," B.S.T.J., *39*, No. 3 (May 1960), pp. 431–476.
2. Näsell, I., "The 1962 Survey of Noise and Loss on Toll Connections," B.S.T.J., *43*, No. 2 (March 1964), pp. 697–718.
3. Näsell, I., "Some Transmission Characteristics of Bell System Toll Connections," B.S.T.J., *47*, No. 6 (July-August 1968), pp. 1001–1018.
4. Fennick, J. H., and Näsell, I., "The 1963 Survey of Impulse Noise on Bell System Carrier Facilities," IEEE Trans. Commun. Technology, *COM-14*, No. 4 (August 1966), pp. 520–524.
5. Näsell, I., Ellison, C. R., Jr., and Holmstrom R., "The Transmission Performance of Bell System Intertoll Trunks," B.S.T.J., *47*, No. 8 (October 1968), pp. 1561–1613.
6. Kessler, J. E., "The Transmission Performance of Bell System Toll Connecting Trunks," unpublished work.
7. Gresh, P. A., "Physical and Transmission Characteristics of Customer Loop Plant," B.S.T.J., *48*, No. 10 (December 1969), pp. 3337–3386.
8. Balkovic, M. D., Klancer, H. W., Klare, S. W., and McGruther, W. G., "1969–70 Connection Survey: High-Speed Voiceband Data Transmission Performance on the Switched Telecommunications Network," B.S.T.J., this issue, pp. 1349–1384.
9. Fleming, H. C., and Hutchinson, R. M., Jr., "1969–70 Connection Survey: Low-Speed Data Transmission Performance on the Switched Telecommunications Network," B.S.T.J., this issue, pp. 1385–1405.
10. Cochran, W. T., and Lewinski, D. A., "A New Measuring Set for Message Circuit Noise," B.S.T.J., *39*, No. 4 (July 1960), pp. 911–931.
11. Fennick, J. H., "The P/AR Meter: Applications in Telecommunications Systems," IEEE Trans. Commun. Technology, *COM-18*, No. 1 (February 1970), pp. 68–73.
12. Hansen, M. H., Hurwitz, W. N., and Madow, W. G., *Sample Survey Methods Theory*, Vols. I and II, New York: John Wiley and Sons, 1953.
13. Cochran, W. G., *Sampling Techniques*, New York: John Wiley and Sons, 1963.
14. Kish, L., *Survey Sampling*, New York: John Wiley and Sons, 1965.
15. Fennick, J. H., "Amplitude Distributions of Telephone Channel Noise and a Model for Impulse Noise," B.S.T.J., *48*, No. 10 (December 1969), pp. 3243–3263.
16. Members of Technical Staff, Bell Telephone Laboratories, *Transmission Systems for Communications*, Bell Telephone Laboratories, Inc., 1970.
17. McNamara, G. P., unpublished work.

THE BELL SYSTEM TECHNICAL JOURNAL
Vol. 50, No. 4, April, 1971
Printed in U.S.A.

1969-70 Connection Survey:

High-Speed Voiceband Data Transmission Performance on the Switched Telecommunications Network

By M. D. BALKOVIC, H. W. KLANCER, S. W. KLARE, and W. G. McGRUTHER

(Manuscript received December 4, 1970)

In this article we present estimates of data transmission error performance at data rates of 1200, 2000, 3600 and 4800 b/s on the Bell System Switched Telecommunications Network. The source data was collected as part of the 1969–70 Connection Survey conducted by Bell Laboratories. Results are based on measurements made on approximately 600 toll connections, dialed from 12 receiving to 92 transmitting sites in the United States and Canada. Standard Bell System Data-Phone® *data sets were used to transmit and receive the digital signals.*

Distributions of errors per call are given on a bit, burst and block basis. Information is also presented on the distribution of intervals between errors, the structure of error bursts, and the number of errors in blocks of various sizes. Some discussion is given on error causes observed for operation at 2000 b/s.

Results of error rate measurements indicate that for operation at 1200 and 2000 b/s approximately 82 percent of the calls have error rates of 1 error in 10^5 bits or better, assuming an equal number of short-, medium-, and long-haul calls. This represents a substantial improvement of performance in comparison with results of previous surveys. For each of the four data rates tested, 1000-bit block error rates of less than one block error for every 10^2 data blocks transmitted are achieved on 80 percent of the calls. For operation at 2000 b/s, a major cause of errors is shown to be impulse noise.

I. INTRODUCTION

Data-Phone service was introduced on the switched network in 1959. Since that time, the number of data sets in service has grown by ap-

proximately 50 percent per year, resulting in the connection of over 100,000 data terminals by 1970. A wide variety of data system applications has evolved with the trend being toward higher speeds, automatic operation, improved performance, and lower costs.

Since 1959 the overall switched telecommunications network has also experienced substantial growth and change. During this period the annual growth rate of the number of miles of voiceband channels in the network has been approximately 19 percent. More than half of the facilities in service today have been placed in service since 1959. Accompanying this growth has been the introduction of newly designed transmission and switching equipment. In addition, the growth of data services has resulted in data transmission considerations being reflected to a greater extent in the overall design, operation, and maintenance of the switched network.

Since the network has undergone considerable change there is a need for current information on performance. Such information is of value in the design of data systems including the design of modems and error control procedures. It is also of use in establishing performance objectives and in identifying areas where service improvements may be realized.

A number of surveys conducted in the past by BTL have provided information on the data transmission characteristics of the switched network. The most widely known is the report by A. A. Alexander, R. M. Gryb, and D. W. Nast[1] which together with followup reports by E. O. Elliott[2] and R. Morris[3] discusses error performance at 600 and 1200 b/s. Results of other tests conducted at 2000 and 3600 b/s on the switched network also have been reported.[4,5] This report is intended to supplement and update that information.

The results presented in this paper report on data transmission error performance for operation at 1200, 2000, 3600, and 4800 b/s. The source data was collected as part of a large scale field measurement program conducted by Bell Laboratories on the Bell System Switched Telecommunications Network. The purpose of the survey was to obtain current information on the transmission characteristics of dialed toll connections. Emphasis was placed on a detailed characterization of each test call. In addition to high-speed data transmission measurements reported herein, measurements of analog channel parameters such as loss, frequency response, envelope delay, P/AR (peak to average ratio), impulse and message circuit (background) noise, nonlinear distortion, and phase jitter were included in the survey. Results of these measurements are presented in a companion paper by F. P. Duffy and T. W.

Thatcher, Jr.[6] Also included were error performance measurements of operation at 150 b/s. Results of these tests are presented by H. C. Fleming and R. M. Hutchinson.[7]

The next two sections of this paper discuss the sampling plan by which a set of connections was chosen, and the equipment implementation used to carry out the testing of those connections. This is followed by a discussion of the results which is divided into three major sections: per call statistics, fine grain statistics, and causes of errors. Per call statistics are presented in terms of cumulative distribution functions and allow a determination of the percentage of calls exceeding a particular performance level. Bit error rate, burst rate and block error rate information is presented in this manner. Fine grain statistics give information on how errors occur within a call. Examples are burst length, error free gap length, and the probability of a specific number of errors in a block of data. These statistics are generally combined over the set of test calls and are presented as cumulative distributions of the probability of an occurrence.

II. SAMPLING PLAN FOR HIGH-SPEED DATA MEASUREMENTS

A major objective of the 1969–70 Connection Survey was to obtain estimates of data transmission performance achieved by *Data-Phone* service. A straightforward implementation to meet this objective implies sampling data traffic and testing connections between customer locations. Because detailed *Data-Phone* traffic records are not maintained, geographical dispersion was instead achieved by a sampling procedure based on overall toll traffic. This results in an additional complication since some local switching equipment is not suitable for high-speed data service. This equipment was not used, consistent with the present practice of providing high-speed *Data-Phone* service. A further consideration involves the fact that customer dialed connections have three basic parts: the loop between the station and the local switching office, the connection between switching offices, and the far-end loop. Performance is determined by the overall end-to-end characteristics. This implies the necessity of sampling loops as well as the connections between offices. Loops were not included in the basic test connection for several reasons. A loop is dedicated to a particular station, therefore the variability observed between repeated calls dialed from one particular location to another is primarily due to the different connections obtained between the switching offices. Furthermore, loops used for high-speed data transmission are subject to spe-

cific transmission requirements[8] which minimize their effect on error performance. Thus, results presented in this paper include only the toll connection between local switching offices. Some discussion is given on results of tests conducted using simulated loops.

The basic elements on which measurements were made were dialed toll connections between Bell System local switching offices. All tests were made during the normal business day; no tests were made at night or on weekends. Connection to the office was at the same point that a customer loop would terminate.

A three-stage sampling plan, stratified into three mileage bands, was used to select the test connections. The basic sampling plan has been described by Duffy and Thatcher[6]; the procedures used are outlined below, with emphasis on the selection of sites for high-speed data transmission tests.

The first stage of sampling resulted in the selection of 12 local switching offices (primary sites). This was done by subdividing the United States and Canada into 12 areas of approximately equal total originating toll traffic. Primary site selection within each subdivision was random with probability of selecting an office proportional to its annual originating toll traffic. Associated with each primary office, far-end local offices (secondary sites) were selected at random based on a record of specific toll traffic originating from the primary site. Secondary sites were stratified into three mileage bands: 0–180, 180–725, and 725–2900 miles distant from the primary. Stratification took place before secondary selection to obtain approximately the same number of test calls in each mileage band. A total of 32 secondary sites was selected in the short mileage band and 33 sites were selected in both the medium and long mileage bands.

Consistent with the sampling plan, all test calls were dialed from the primary site to the secondary site. The test plan called for the characterization of six test calls between each primary-secondary pair.

As discussed earlier, a sample obtained as described above could contain local switching equipment that is not suitable for high-speed data transmission. For example, offices with panel equipment and certain equipment associated with step-by-step (SXS) offices can cause high levels of impulse noise. In providing *Data-Phone* service on the switched network, it is necessary at times to bypass such equipment. Thus, the following procedures were used to modify the sample.

When a primary office containing panel equipment was selected, the measurements were made from an alternate, remote exchange office. The office used was that from which a high-speed data customer would

be served if the panel office in fact caused unsatisfactory data transmission performance. One primary office with panel equipment was selected but it also contained crossbar equipment. Thus high-speed measurements were made on the crossbar machine. In the case of panel secondaries, rather than testing at an alternate office, the results were omitted. This was done because the small amount of additional precision which would have been obtained by testing an alternate did not warrant the effort required. Six secondary sites were so affected.

When a primary office containing SXS equipment was encountered, inclusion in the sample was based on satisfactorily meeting the following impulse noise pretest. The number of impulse noise counts in 15-minute periods was measured at a threshold of 69 dBrnC (1 dB below the average received data signal level for a long-haul call[6]). This was done for several test lines from the office throughout the business day. If over 50 percent of the tests exhibited more than 15 noise counts due to office equipment, the survey measurements were made from the remote exchange office. Two such offices were encountered and the alternate offices were used as test sites. It was determined that the impulse noise in the excluded offices was largely caused by switches used to select outgoing trunks. Because all survey test calls were dialed from primary site to secondary site, this source of noise was not a problem at the secondary sites. No secondary offices with SXS equipment were excluded.

The resulting sample used to describe high-speed data performance contained 12 primary offices: seven had crossbar equipment, three had SXS equipment, and two had both crossbar and SXS. There were 92 secondary offices in the sample: 56 had crossbar equipment, 35 had SXS equipment, and one was an ESS office.

III. TEST PROCEDURE AND DATA COLLECTION EQUIPMENT

The general test arrangement is shown in Fig. 1 with emphasis on the data transmission tests. As shown in the figure, test word generators and data set transmitters were located at the secondary site. The data signals were transmitted to the primary site where the data set receivers and associated test equipment were located. Some of the data sets were connected through simulated subscriber loops. Also, an analog-to-digital converter was used to sample the received line signal of one modem.

A digital computer at the primary site monitored the errors and

carrier detector activity of the data sets on a bit-by-bit basis. This information was compacted by the computer and transmitted over a 2000 b/s data link to Bell Laboratories at Holmdel, New Jersey, where it was stored on magnetic tape for later analysis. To protect the integrity of the test results, the data link employed error detection with block retransmission for error correction.

To provide a cross reference with the data stored on the tapes and to provide protection against breakdowns of the main data collection system, a backup system was used to collect error rate information. During periods when the main data collection system was inoperative, no bit-by-bit information was collected. However, the backup system continued to collect bit error rate information.

Table I lists the data sets and bit rates that will be discussed in this paper. Included in the table is information on the length of test calls, length of the test words used, and the number of test calls made at each speed. In the implementation of the survey, the Data Set 203 was tested at 3600 b/s at all primary sites with approximately half

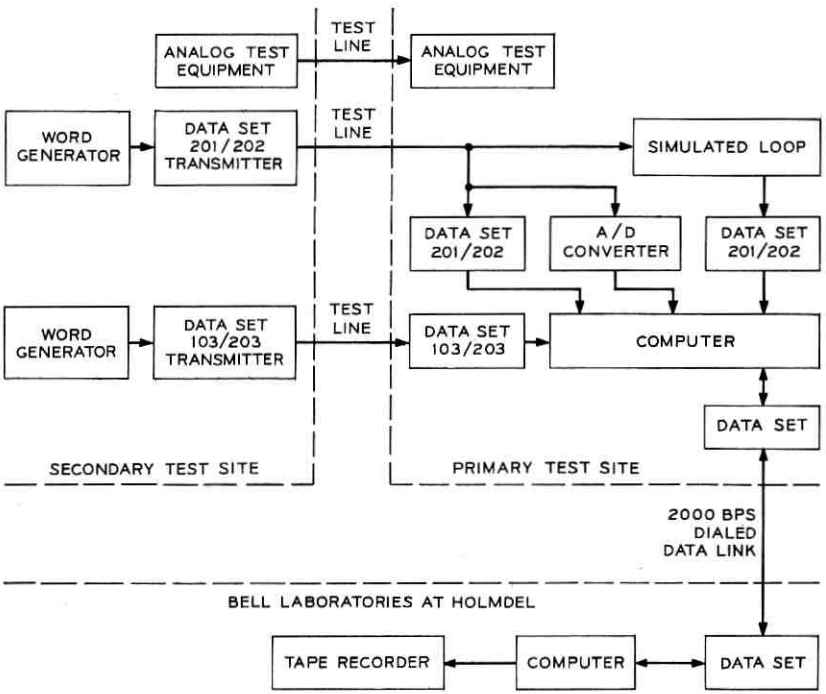

Fig. 1—General equipment arrangement for data set tests.

TABLE I—DATA SET TEST INFORMATION

Speed (b/s)	Data Set Code	Number of Test Calls	Number of Calls With Bit-by-Bit Data	Length of Data Run (min.)	Test Word (Bits)
1200	202	568	528	30	511
2000	201	567	544	30	511
3600	203	277	270	20	$2^{23} - 1$
4800	203	130	129	20	$2^{23} - 1$

of the secondary sites. It was tested at 4800 b/s from the other half of the secondary sites after the 4800 b/s option became available, approximately half way through the survey. Since this represents approximately 25 percent of the test calls, no information is given by mileage band or on fine grain statistics for operation at 4800 b/s.

3.1 *Test Procedure*

At the beginning of a test day, three test calls were dialed from the primary site to the secondary site. While analog transmission measurements were being made on one connection, voiceband data was transmitted on the other two. Data transmission on one connection was at 1200 and 2000 b/s, each for 30 minutes. On the other connection, tests were made at 150 b/s for 40 minutes and either 3600 or 4800 b/s for 20 minutes. After the completion of these tests, the roles of the test connections were exchanged and the procedure repeated until all tests had been made on all three connections. Upon completion of this sequence, all lines were disconnected and three new calls were dialed. Thus, on an average day, six connections were completely tested. There were occasions when some of the lines were disconnected prematurely; these disconnects were usually attributable to testing errors. Whenever possible, another call was dialed and as many tests as possible were made on the replacement.

As discussed earlier, measurements were made between local switching offices and did not include subscriber loops. To determine the effects on data set performance of the distortion introduced by the amplitude and phase characteristics of loops, the 1200 and 2000 b/s data sets were tested in two configurations. Two data set receivers of the same type were used concurrently; one was connected directly to the incoming line signal and the other was connected through an artificial cable section representing a pair of subscriber loops. Both receivers were simultaneously monitored by the data collection equip-

ment. Artificial cable sections representing various combinations of average and worst-case envelope delay and loss slope for pairs of subscriber loops[8,9] were interchanged from one test to the next. The 3600 and 4800 b/s modems were not tested in this configuration, since they contain adaptive equalizers which compensate for the effect of amplitude and phase distortion.

3.2 *Data Set Tests*

The data sets were operated according to standard Bell System practices. The transmitted line signal was −12 dBm at the serving central office. The 1200 and 2000 b/s receivers were operated using compromise equalizers; the 3600 and 4800 b/s modem used adaptive equalizers. The carrier detectors in all data sets caused the received data to be clamped to steady marking in the event of a carrier off indication. For the data sets with a reverse channel capability, the Data Sets 202 and 203, echo suppressors were disabled prior to data transmission.

A pseudorandom test word was used on the digital channel. After the modems were synchronized, the test word generators were synchronized and the data recording equipment was enabled. For all data sets, the data collection equipment recorded the bit error pattern and carrier fail indication on a bit-by-bit basis.

3.3 *1200 b/s (Data Set 202)*

The Data Set 202 employs frequency shift keying to transmit a signal on the telephone line. For the survey, a 511-bit pseudorandom word (CCITT Standard) was used as the data source at the secondary site. At the primary site, a locally generated version of the test word was compared with the received data signal, and the resulting error signal recorded.

This modem does not provide receiver timing. The timing signal used to operate the data collection equipment was recovered from the zero crossings of the received data bit stream. A stable clock recovery system was used to minimize the occurrences of synchronization loss between the received test word and its locally generated version. The clock used proved sufficiently stable to maintain synchronism during signal interruptions of up to ten seconds.

The Data Set 202 provides a low-speed reverse channel which was enabled during about half of the data runs. At the beginning of each 202 test, a tone was transmitted from receive site to transmit site to

disable echo suppressors in the connection and therefore allow simultaneous two-way transmission. On each call it was ascertained whether the reverse channel was operating properly. Failure to receive reverse channel energy was noted on only one test call.

3.4 *2000 b/s (Data Set 201)*

The Data Set 201 employs differentially encoded four-phase modulation. This modem was also tested with a 511-bit pseudorandom word as the data source.

The Data Set 201 provides recovered clock which was used to interpret the received data. Thus, all decisions on errors in the received data were based on this clock signal. However, a stable clock regenerator was used with the data collection equipment. This clock was capable of maintaining synchronism of the local word during clock interruptions of up to ten seconds.

To obtain information on the type of transients affecting the performance of the 2000 b/s modem, an analog to digital converter was used to sample the line signal entering the receiver. When bit errors occurred in the received data stream, the digital computer recorded the corresponding segment of the line signal. In this way, a record of error causing events was maintained. This analog to digital sampling technique was used at six of the 12 primary sites.

3.5 *3600 and 4800 b/s (Data Set 203)*

The Data Set 203 is a multilevel vestigial sideband AM data set which employs automatic adaptive equalization and coherent detection. For this modem, a specific startup procedure is necessary to achieve synchronization. This routine was performed at the beginning of each Data Set 203 test, and there were no test calls on which the modem would not achieve synchronism.

The received timing signal provided by the data set was used to interpret the received data. It can maintain synchronism for at least one second in the absence of line signal.

The Data Set 203 contains a scrambler to maintain the settings of the adaptive equalizer, to provide timing recovery information, and to keep the signal energy on the telephone line constant. This scrambler was used to produce the transmitted bit pattern. It consists of a 23-stage shift register which produces a pseudorandom word when the data input is steady spacing. At the receive end, a descrambler reverses the process. Because of the structure of the scram-

bler-descrambler, an event on the telephone line which causes a single bit error in the scrambled data results in the recording of three bit errors. The error pattern produced is

1 0 0 0 0 0 0 0 0 0 0 0 0 0 0 0 0 0 1 0 0 0 0 1

(the ones represent errors, the zeroes represent error-free bits and the left-most bit is the first bit delivered). This same error pattern is experienced in customer data during error occurrences. The effect of the scrambler will be noted several times in later sections of this paper.

The reverse channel of the Data Set 203 was used on all test calls to send a 511 bit pseudorandom word at 150 b/s concurrent with high-speed data transmission. No measure was made of reverse channel error performance. However, presence or absence of the reverse channel signal was noted. Improper operation occurred in two instances.

IV. BIT ERROR RATE RESULTS

Average bit error rate is the parameter most often used to describe the performance of a digital channel because it is easy to measure and is independent of any particular data system parameters, such as block size. Average bit error rate was determined for each call and is presented in Figs. 2, 3, and 4. These figures show cumulative distribution functions (CDFs) of the bit error rate per call for operation at 1200, 2000, and 3600 b/s in the short, medium, and long mileage strata. The CDFs include errors incurred during carrier off indications. As discussed earlier, the outputs of the data sets are clamped during carrier off indications; because of the randomness of the test words used, a 50 percent error condition is encountered.

In order to relate the sample obtained to the base population, the contribution of each test call to these CDFs is weighted by its probability of inclusion in the sample.[6] Figures 2, 3 and 4 therefore represent estimates of performance for the *Data-Phone* population. They differ only slightly from the sample distributions where each test call contributes equally. Table II presents estimates of the percent of error free calls at the three speeds for the three mileage bands. From Figs. 2, 3 and 4 and Table II, a trend toward poorer performance with increasing distance is evident. However, since for each data set the extremes of the bit error rate distributions in the three mileage categories overlap, the variation within a mileage category is considerably greater than the difference between the categories. The results also show that error rate performance at 1200 and 2000 b/s are comparable while error rates at 3600 b/s are somewhat larger.

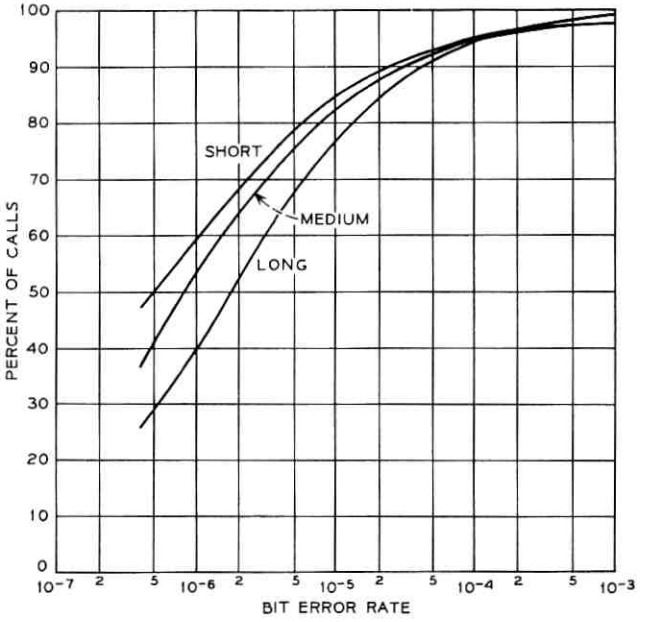

Fig. 2—Bit error rate distributions by mileage strata at 1200 b/s.

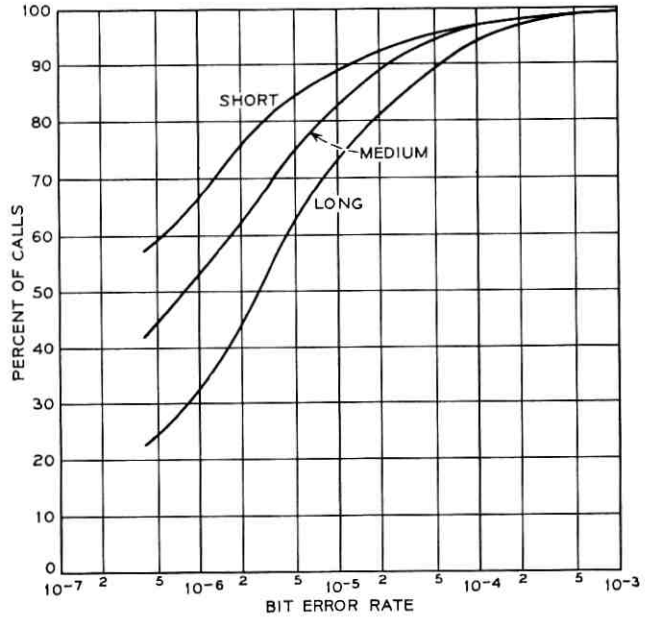

Fig. 3—Bit error rate distributions by mileage strata at 2000 b/s.

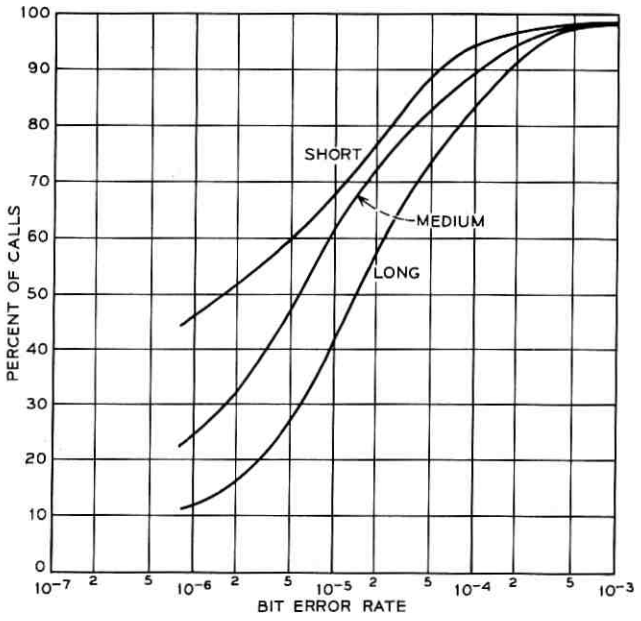

Fig. 4—Bit error rate distributions by mileage strata at 3600 b/s.

The means and 90 percent confidence intervals about the means for the error rate distributions are presented in Table III. Since the error rate distributions are skewed, the mean error rates are largely determined by the worst-case calls. For example, for all of the calls measured at 2000 b/s, 72 percent of the errors counted during the survey occurred on that 5 percent of the calls which had the poorest error rate. Similar results were obtained for the other data sets. For this reason the means fall above the 80th percentile and do not represent good measures of the locations of the distributions. The degradation of error rate performance with mileage seen in the relative positions of the CDFs is not shown by their means.

TABLE II—PERCENT OF ERROR FREE CALLS

Mileage Band	1200 b/s (30 min.)	2000 b/s (30 min.)	3600 b/s (20 min.)
Short	46	53	41
Medium	32	35	22
Long	24	18	10

TABLE III—ERROR RATE MEANS AND CONFIDENCE INTERVALS

		Arithmetic		Logarithmic	
Data Rate b/s	Mileage Band	Mean Error Rate	90% Confidence Interval About Mean	Antilog of Mean Log Error Rate	90% Confidence Factor
1200	Short	5.8×10^{-5}	$\pm 5.6 \times 10^{-5}$	8.5×10^{-7}	1.5
	Medium	7.7×10^{-5}	$\pm 8.0 \times 10^{-5}$	1.3×10^{-6}	2.0
	Long	6.4×10^{-5}	$\pm 5.2 \times 10^{-5}$	2.8×10^{-6}	1.7
2000	Short	2.4×10^{-5}	$\pm 2.0 \times 10^{-5}$	8.9×10^{-7}	1.6
	Medium	1.2×10^{-5}	$\pm 8.8 \times 10^{-6}$	1.4×10^{-6}	2.0
	Long	2.1×10^{-5}	$\pm 8.4 \times 10^{-6}$	3.0×10^{-6}	1.7
3600	Short	5.4×10^{-5}	$\pm 6.1 \times 10^{-5}$	2.3×10^{-6}	3.0
	Medium	8.1×10^{-5}	$\pm 6.5 \times 10^{-5}$	5.3×10^{-6}	2.0
	Long	7.3×10^{-5}	$\pm 1.9 \times 10^{-5}$	1.3×10^{-5}	1.5

Because the error rate distributions are approximately log normal, means and confidence intervals have also been calculated for the log of the error rate. For the special case when the call was error free, the minimum error rate was assigned, i.e., one error per call. The antilogs of the result of this calculation are given in Table III. The confidence interval is represented as a factor, which when used to multiply and divide the logarithmic mean shown in Table III will result in the upper and lower confidence limits respectively. These means are closer to the median and are consistently larger with distance.

V. BURST AND BLOCK ERROR RATE PERFORMANCE

Errors on telephone channels tend to occur in bursts. To characterize this property, measures of error performance other than error rate are needed. In these results an error burst is defined to be a collection of one or more bits beginning and ending with an error and separated from neighboring bursts by 50 or more error free bits. The intent of this definition is to associate errors caused by a single event and dissociate errors caused by separate events and thus obtain a measure of the frequency of error causing events on a particular test call. Burst rate, then, is the number of bursts in a call divided by the number of bits transmitted. Discussion is given later on the use of the parameter of 50 bits for this purpose.

Block error rate is a parameter of interest because data messages

are usually transmitted in a blocked format. Many data transmission systems reject blocks which contain bit errors and retransmit the entire block. Hence, the block error rate is often of greater practical significance than the bit error rate. A block in error is defined as a block containing one or more errors, or a carrier off indication, when a call is subdivided into contiguous blocks of a given size beginning with the first bit in a call. Block error rate is the probability of a block being received in error. The relationship between the bit and block error rates is accounted for by the burst nature of the channel.

Figures 5 through 8 present the CDFs of total burst and bit error rate and block error rate for block sizes of 100, 500, 1000, 5000 and 10000 bits for data rates of 1200, 2000, 3600 and 4800 b/s. These distributions were formed by averaging the distributions for short, medium, and long mileage strata assuming equal weight in each mileage category.

Averaging over the mileage bands is done here and in the remaining sections of this paper in order to obtain a more compact presentation. It is done when the effects of distance can be ascertained by reference

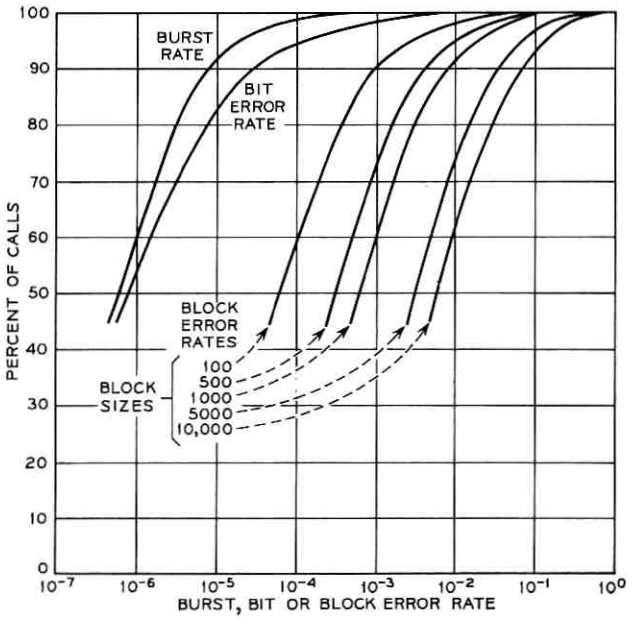

Fig. 5—Total burst, bit and block error rate distributions at 1200 b/s (Each mileage band weighted equally).

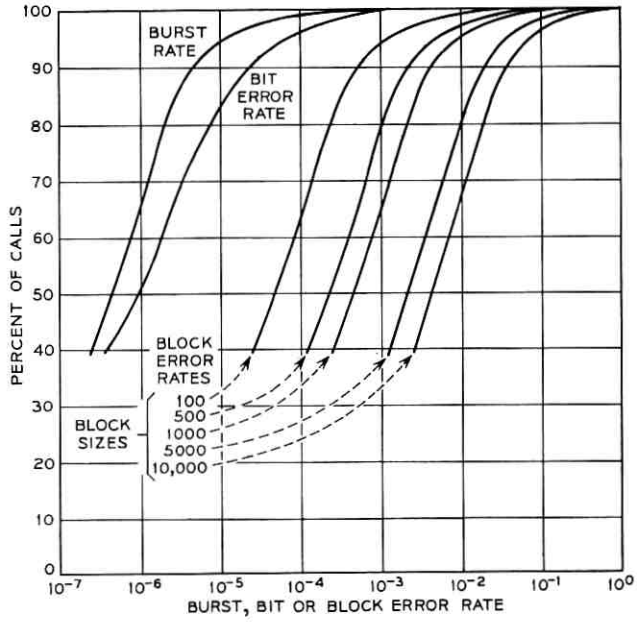

Fig. 6—Total burst, bit and block error rate distributions at 2000 b/s (Each mileage band weighted equally).

to an earlier result, or when the conclusions to be drawn are not strongly dependent on distance. For operation at 4800 b/s the results are presented in this fashion for a different reason. This data set was tested over a relatively small number of connections. Therefore, sufficient information was not available for an analysis by mileage band.

One method of combining the mileage band information would be according to the distribution of toll traffic on the Bell System Switched Network. The approximate percentages of toll traffic are 85, 11 and 4 percent in the short, medium, and long mileage strata respectively. If the distributions were combined in this way the characteristics of the short-haul calls would dominate, with the long-haul calls having little representation. In this paper, total performance is calculated by giving each mileage category equal weight and averaging the results for the three strata, making the result more meaningful for all mileages.

From Figs. 5 through 8, the burst nature of the channel can be seen in the separation between the distribution of burst and bit error rate.

It is noted that this separation generally increases with increasing error rate, indicating that calls with higher error rates tend to have more errors per burst. The effects of error bursts can also be observed by comparing the bit and block error rates. A measure of burstiness is the average number of errors per block in error. This may be estimated by multiplying the bit error rate by a given block size, then dividing by the block error rate. It has been calculated for 1000 bit blocks at the 80th percentile for all four data rates. At 1200 and 2000 b/s, the results are 2.6 and 3.5 errors per block in error respectively. For operation at 3600 and 4800 b/s, this number is approximately ten; the increase is largely due to the effect of the scrambler. As block size increases, the average number of errors per block in error increases slightly.

Another interesting observation that can be made from Figs. 5 through 8 is the relationship between the burst rate and block error rate distributions. It is noted that if the burst rate distribution is shifted to the right by the block size, it gives a good approximation to the block error rate distribution for that block size. This indicates

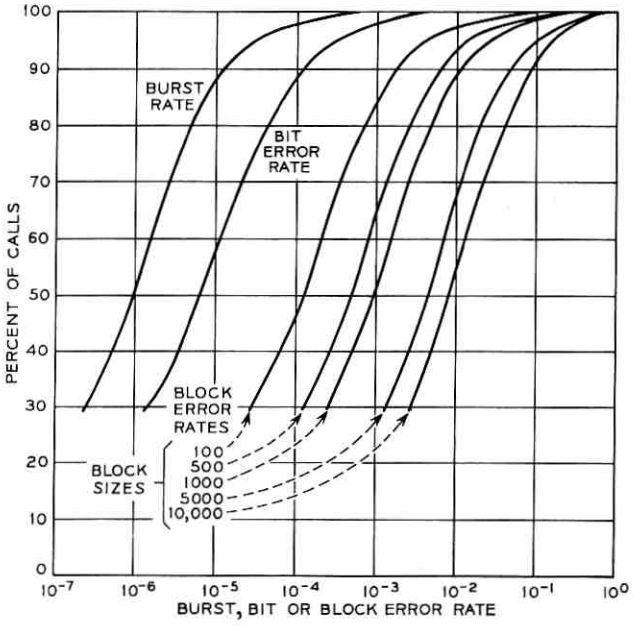

Fig. 7—Total burst, bit and block error rate distributions at 3600 b/s (Each mileage band weighted equally).

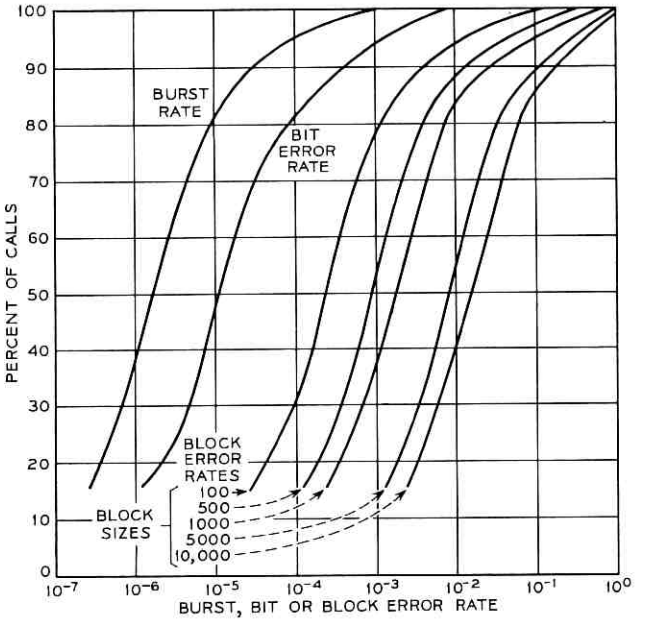

Fig. 8—Total burst, bit and block error rate distributions at 4800 b/s (Each mileage band weighted equally).

that the choice of 50 bits in the definition of a burst reasonably satisfies the intent of the definition.

On a mileage band basis the burst, bit and block error rate distributions maintain approximately the same relationships as for the total results given in this section. Therefore, a reasonable estimate may be obtained by mileage strata using Figs. 2, 3 and 4. To facilitate comparisons of bit and 1000-bit block error rate at the four speeds, Fig. 9 has been included.

VI. EFFECT OF CARRIER OFF INDICATIONS ON PERFORMANCE

Each of the data sets described in this paper is equipped with a carrier detector which indicates an ON condition during normal reception of data signals. An OFF indication is given in the absence of received signal energy. However, an OFF indication can also be caused by other severe line disturbances such as high amplitude impulse noise. Results for all three data sets indicate that the majority of carrier off indications were caused by disturbances other than loss of received line signal.

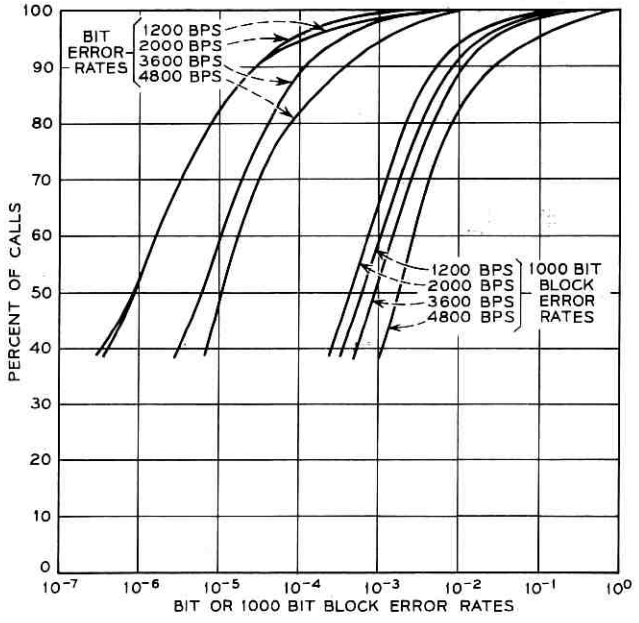

Fig. 9—Comparison of bit and 1000 bit block error rates. (Each mileage band weighted equally).

During a carrier off indication, the output of the data set is clamped to steady marking, thus forcing the error pattern to be an exact replica of the locally generated test word. All of the results presented earlier in the paper have included those errors. When they were removed and the bit and block error rate distributions recomputed, the curves were displaced upward by less than four percentage points.

Table IV gives the percentage of test calls which experienced carrier off indications. For the calls with one or more carrier off indications, the median call had three, two and one indications for the 1200,

TABLE IV—PERCENTAGE OF TEST CALLS WITH ONE OR MORE CARRIER FAILURE INDICATIONS

Mileage Band	1200 b/s	2000 b/s	3600 b/s
Short	7.0	9.1	14.3
Medium	7.9	14.8	7.2
Long	10.3	21.7	14.6

2000, and 3600 b/s data sets respectively. There were instances, however, where calls contained hundreds of carrier off indications.

The probability distributions of the duration of carrier off indications were computed for the three data sets. The results are contained in Fig. 10. Substantial differences can be seen between these distributions. These differences, as well as those shown between data sets in Table IV, are mainly due to differences in the design of the data sets.

VII. BURST PROPERTIES

This section discusses the characteristics of error bursts, based on the definition given earlier. The definition required an error free interval of 50 bits or more between bursts. Two measures of the size of error bursts have been calculated for the survey data. Burst weight is defined to be the number of errors in a burst and burst length is defined to be the number of bits in a burst. The probability distributions of these parameters are plotted in Figs. 11 and 12. The distributions have been computed by combining all of the test calls because burst characteristics did not appear to be closely related to mileage.

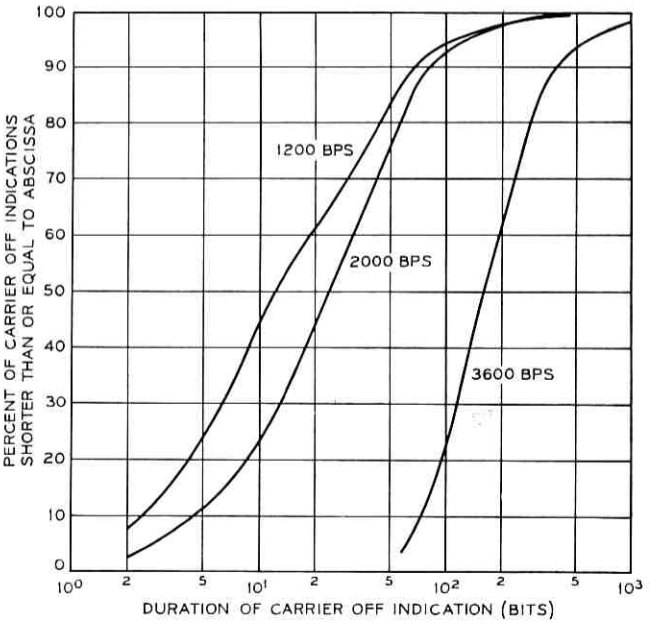

Fig. 10—Distribution of durations of carrier off indications.

The properties of bursts which occurred when the carrier indication was on are presented here. The characteristics of errors occurring during carrier off indications were discussed in the preceding section.

The difference in bit rates and signaling formats for the three data sets contribute to the differences which are evident in these curves. From Figs. 11 and 12, it can be seen that small bursts for the 2000 b/s data set tend to be slightly larger than small bursts for the 1200 b/s set. This may be due to the use of differential encoding. The effect is overcome when bursts of any appreciable size are encountered.

The scrambler used in the 3600 b/s data set causes burst structures considerably different from the lower speed sets. To estimate what the distribution of burst weight would be for the high-speed set with no scrambler, the scale of the abscissa should be divided by three. When this is done for the curve in Fig. 11, it is very similar to those of the other data sets. To remove the effect of the scrambler on burst length, a different procedure must be used. There is a residual effect in any burst of 23 bits while the descrambling shift register clears, thus an estimate of the unscrambled burst length distribution can

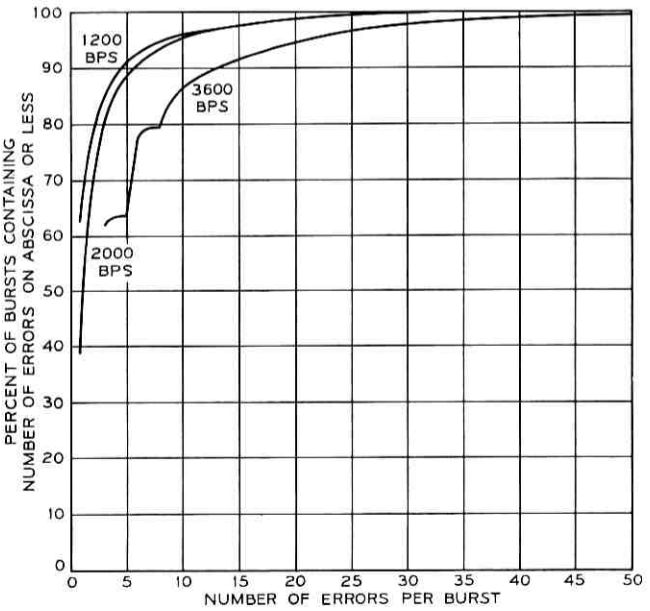

Fig. 11—Burst weight distributions.

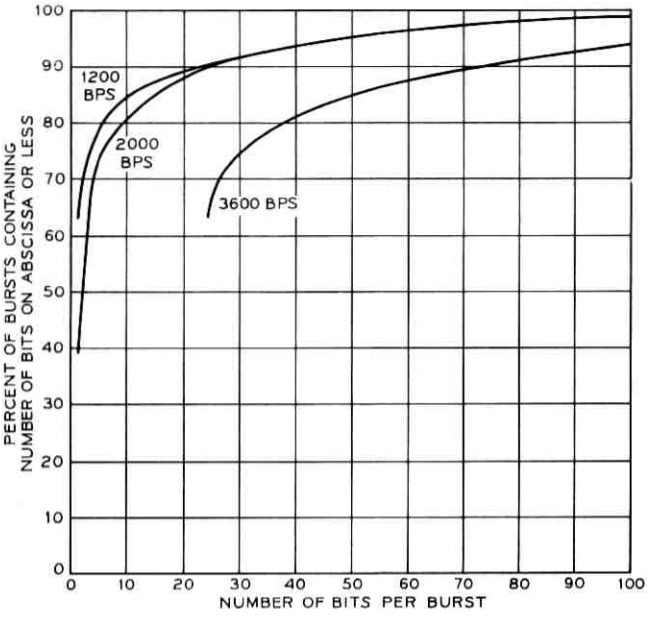

Fig. 12—Burst length distributions.

be obtained by shifting the curve 23 bits to the left. Once again the curve obtained is similar to those of the other data sets.

The burst weight distributions given in Fig. 11 may tend to obscure bursts with many errors because of the frequency of small bursts. Thus, for each test call, the number of errors in the largest burst has been calculated. Figure 13 presents the CDF of the percent of calls versus maximum burst weight per call for the three data rates. Note from this figure that 80 percent of the calls for the 1200 and 2000 b/s modems have maximum burst weights of less than three and six errors respectively. For 3600 b/s operation, the maximum weight is approximately 25 at this point. This increase is mainly attributable to the error tripling effect of the scrambler.

VIII. PROBABILITY OF M ERRORS IN A BLOCK OF N BITS

The number of errors per block is a measure which is useful for evaluation of error control procedures using block transmission. The probability distributions for m or more errors in a block of n bits $[P(\geqq m, n)]^2$ are presented in Figs. 14, 15, and 16 for data rates of 1200, 2000, and 3600 b/s.

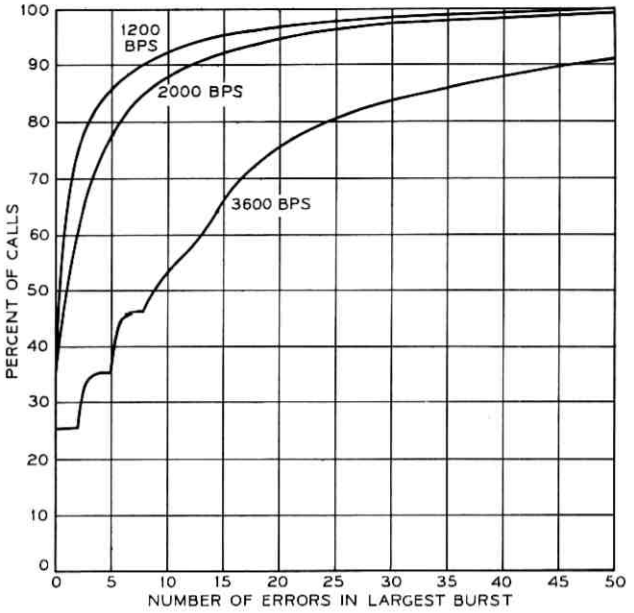

Fig. 13—Distributions of the maximum burst weight per call.

Since the results are not strongly related to distance, these curves were calculated by averaging over all of the calls. Blocks which contained carrier off indications were not included in these calculations.

These curves indicate the overall similarity of the three sets as measured by the block error probability [i.e., $P(\geqq 1, n)$]. The 2000 b/s data set has the lowest probability of a block error and the 3600 b/s set the highest; they differ by approximately a factor of two.

Because the 2000 b/s and 3600 b/s data sets tend to have relatively more multiple errors, the probabilities, $[P(\geqq m, n)]$, for the 1200 b/s set are smaller than for the other two sets, for m greater than one.

IX. GAP LENGTH DISTRIBUTIONS

The probability distributions of the number of good bits between errors (gap length distribution) provide additional insight into the error process. They are presented in Figs. 17, 18 and 19 for the 1200, 2000, and 3600 b/s data sets. All of the test calls have been used without regard to mileage band. Bits which coincided with a carrier off indication were removed. Since instances where carrier off indications

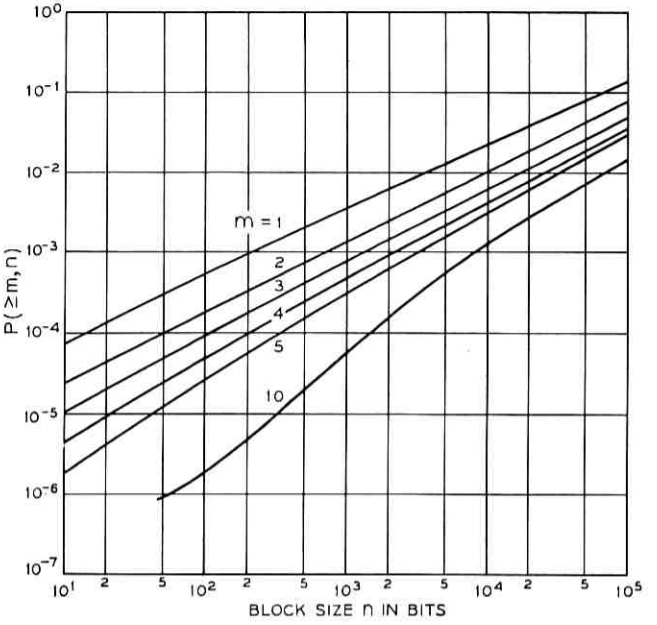

Fig. 14—Probability of m or more errors in a block of size n [$P(\geqq m, n)$] at 1200 b/s.

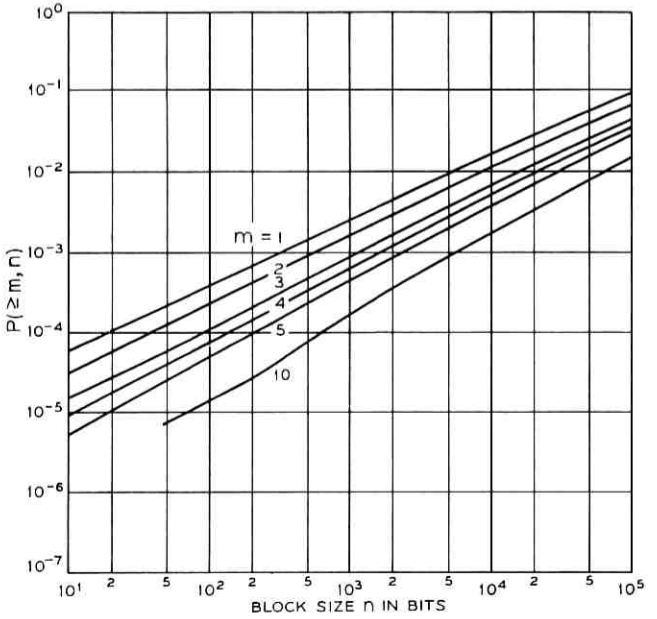

Fig. 15—Probability of m or more errors in a block of size n [$P(\geqq m, n)$] at 2000 b/s.

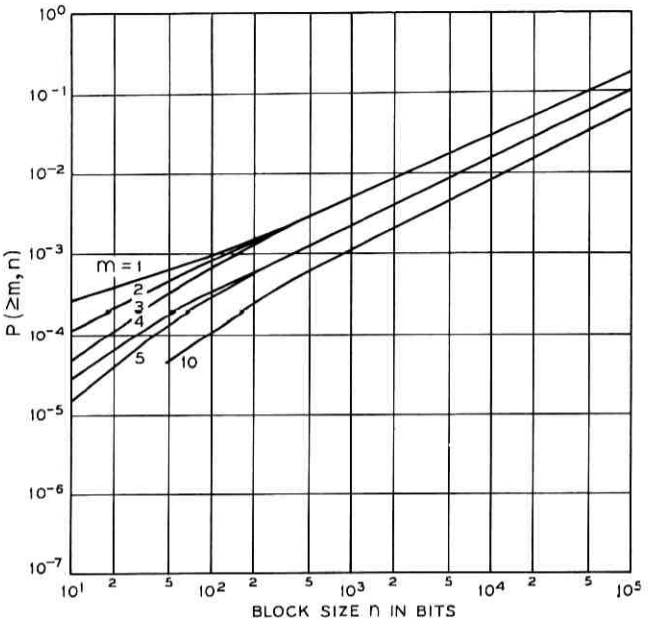

Fig. 16—Probability of m or more errors in a block of size n [$P(\geqq m, n)$] at 3600 b/s.

are not preceded by errors are rare, this culling should have an effect on the number of very short gaps but not on the number of long gaps.

Four curves are presented in each of these figures. The curves labeled Pooled Bit Error Gap Distribution were computed by pooling all of the test calls together and calculating the gap length distribution of the result. That is, for each data set, the pooled distribution contains all gaps from all calls. A call with a poor error rate contributes many more gaps than one with a good error rate. The pooled gap length distribution may be a reasonable estimate of the overall gap length distribution if it can be assumed that the error sequences of the individual test calls are segments of one call of long duration. If this assumption about the error process is not valid, then the pooled estimate may be unreasonable since in it, equal weight is assigned to each gap, causing calls with a large number of errors to contribute the major share of the information. In fact, for 2000 b/s operation one call accounted for approximately 11 percent of the errors made in the entire survey. One can be fairly certain that the pooled distribution will not be very different from the gap length distribution of that call.

In order to assign equal weight to each call in the sample, the gap

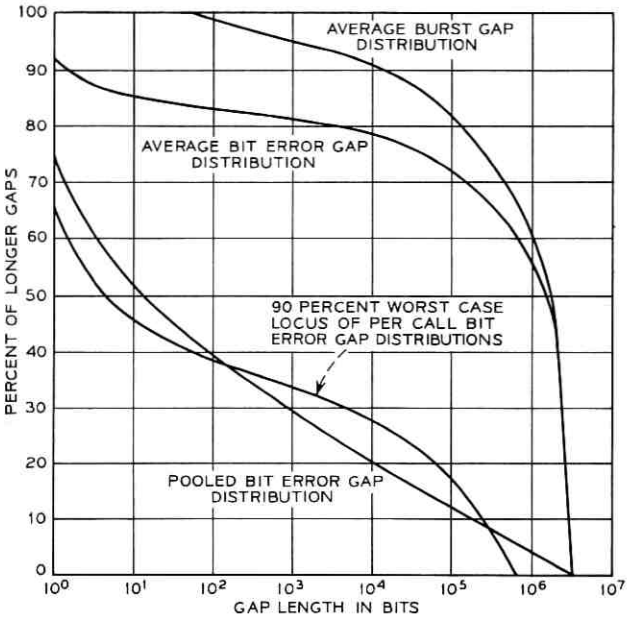

Fig. 17—Total gap length distributions at 1200 b/s.

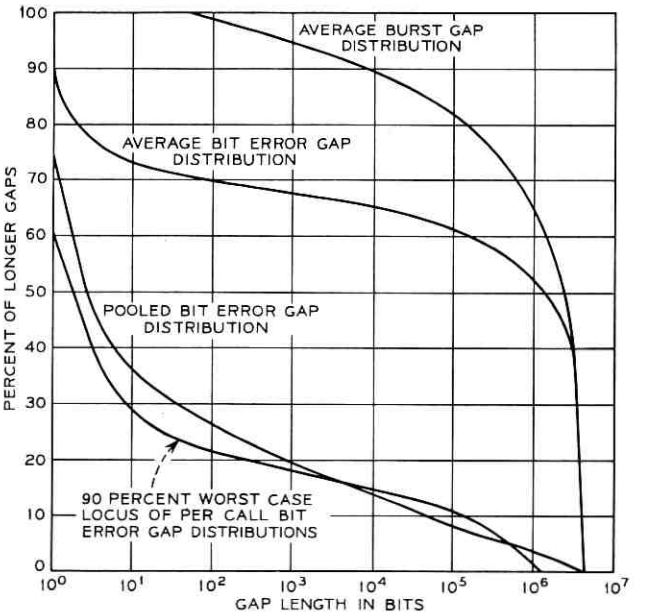

Fig. 18—Total gap length distributions at 2000 b/s.

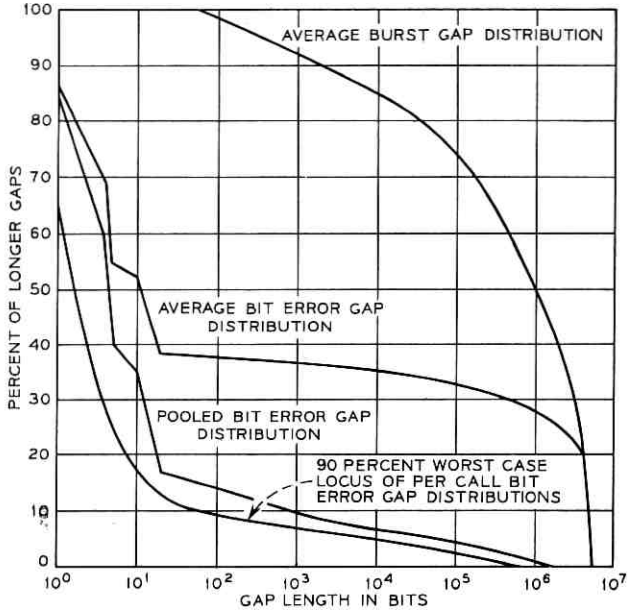

Fig. 19—Total gap length distributions at 3600 b/s.

length distribution was computed for each call and the results averaged to obtain an overall distribution. This is done by summing the per call ordinates for each gap length and dividing by the number of calls. Using this method, no one call can determine the shape of the distribution. The curves labeled Average Bit Error Gap Distribution in Figs. 17, 18 and 19 have been computed in this way.

The product limit[10] method of estimation has been used to calculate the gap length distributions. In this method the observed gaps are used to compute the conditional probability

$$P\{\text{Gap} \geqq g \mid \text{Gap} \geqq g-1\} = \frac{P\{\text{Gap} \geqq g\}}{P\{\text{Gap} \geqq g-1\}} \tag{1}$$

for a number of cell sizes ranging from 0 (consecutive errors) to the test call length in bits (error free call). Since

$$P\{\text{Gap} \geqq 0\} = 1,$$

the gap length distribution is computed as follows

$$P\{\text{Gap} \geqq g \mid \text{Gap} \geqq g-1\} \cdot P\{\text{Gap} \geqq g-1\} = P\{\text{Gap} \geqq g\}.$$

The advantage of using this method is that the gap which precedes the first error and that which follows the final error in the test call are used in equation (1) as long as they contain information, that is, up to their length. At this point they disappear from both the numerator and the denominator simultaneously.

The 90 percent worst-case distribution shown in Figs. 17, 18 and 19 is the locus of points such that for each gap length the ordinates of 90 percent of the calls lie above that point. Note that for all three data sets, the pooled distribution falls roughly at this 90 percent worst case locus. Since, for each data set, between 80 and 90 percent of the calls have error rates better than the average error rate, the effect of pooling on determining the gap length distribution estimate is approximately the same as its effect on the calculation of average error rate. For the 3600 b/s data set, the mean is approximately the 80 percent point and for this data set the pooled distribution is uniformly above the 90 percent worst-case locus.

A comparison of the gap length distribution of the different types of data sets is complicated by the fact that the sets use different transmission techniques and different speeds. The 2000 b/s modem is a differentially encoded four-phase set which transmits dibits. The 1200 b/s set is an FM set which transmits a single bit per signaling element. Hence, one might expect more short gaps for the higher speed modem. As shown by the gap length distributions, this in fact occurs. For the 3600 b/s data set, gaps of length 17 and 4 are common since those are the bit spacings on the descrambler shift register.

The relative flatness of all of the gap length distributions following the initial decline indicates a relative insensitivity to the critical length of 50 bits used in the burst definition. This flatness also gives insight into the fact that the spacings between the block error rate curves given in Figs. 5, 6 and 7 are approximately equal to the ratios of the block sizes. The same point can be observed in the linearity of the $P(\geqq m, n)$ curves given in Figs. 14, 15 and 16.

Since every gap of length 50 or longer separates bursts and only gaps of length 50 or longer do so, the distribution of bits between bursts for each call can be derived from the gap length distribution by simply renormalizing the curve for gaps of size 50 and greater. This has been done for the survey calls and the resulting curves averaged to arrive at the average burst gap distributions also shown in Figs. 17, 18 and 19. The pooled burst gap distribution can be obtained by renormalizing the pooled bit error gap distribution.

Figure 20 contains the average gap length distributions for the

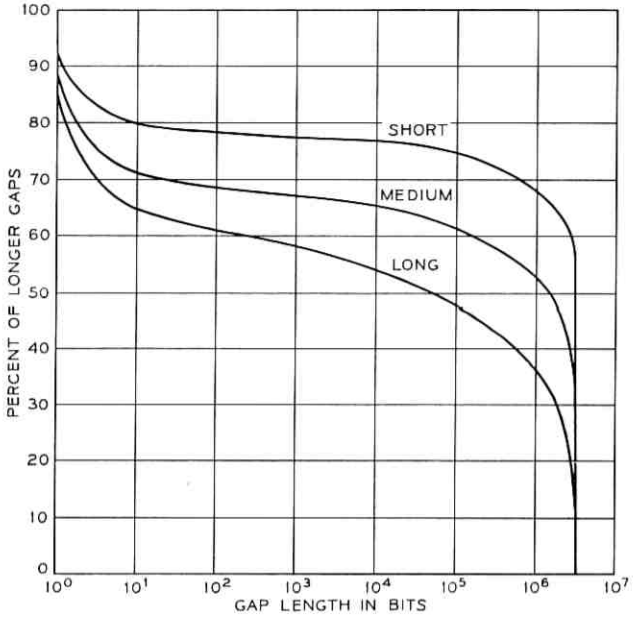

Fig. 20—Gap length distributions by mileage strata at 2000 b/s.

2000 b/s data set for the three mileage bands. As shown in this figure the additional transmission impairments encountered on long-haul calls manifest themselves throughout the range of the gap length distribution. The same relationship was observed for the other two sets, but in different degrees. The 1200 b/s set showed less sensitivity to distance and the 3600 b/s set showed greater sensitivity. Since 1200 b/s operation uses the channel least efficiently in terms of bit speed, it could be argued that it should have the greatest margin to error and should therefore be less sensitive to the additional impairments introduced when the transmission distance is increased.

For all three data sets, the gap length distribution of medium haul calls is very close to the overall average distribution.

X. Effect of Simulated Loops on the 1200 and 2000 b/s Data Sets

The 1200 and 2000 b/s data sets were also tested using simulated loop pairs to obtain information on the effect of amplitude and phase distortions introduced by the loop plant. The results indicate that the additional impairment added with the simulated loops had little influence on the performance of the data sets. For the distributions of

burst, bit and block error rates, performance with the loop was slightly better than without. For the 1200 b/s data set, performance with the loops resulted in a general upward shift of the distributions of less than four percent. At 2000 b/s this shift was approximately two percent. From this result it appears that the compromise equalizers of both data sets more nearly equalize the channel with loops. The major change in the analog channel characteristic caused by the addition of the loops is an increase in the loss frequency slope. The result obtained above may indicate that the 1200 b/s data set is more sensitive to this impairment than the 2000 b/s data set.

XI. Effects of Excluding SXS Switching Offices from the Sample

As discussed earlier two SXS offices which were initially selected, were not included in the sample used to estimate high-speed data transmission performance. These offices exhibited excessive amounts of high-level impulse noise which was mainly attributed to equipment used to select outgoing trunks. Based on the impulse noise pretest, three other offices having similar equipment were not excluded from the sample. To determine the effect of these three offices on the overall results, a subclass analysis was performed excluding calls which encountered this equipment. Figure 21 shows the bit error rate and 1000-bit block error rate at 2000 b/s for the total distributions of the overall sample and the sample excluding calls through this equipment. In performing this analysis, 21 percent of the test calls were excluded. From Fig. 21 it can be observed that the error rate distribution with this exclusion shows an improvement of approximately a factor of two. The block error rates differ by a smaller factor. At 1200 and 3600 b/s, the relationship between the distributions is similar.

Another analysis was performed excluding all calls which encountered SXS equipment at the primary or secondary sites. This resulted in an exclusion of 58 percent of the test calls. The resulting distributions show no additional improvement over those obtained above.

XII. Analysis of Error Causing Transients at 2000 b/s

The process which results in bit errors involves a combination of static impairments and transient phenomena acting on the data set line signal. In the absence of other factors, a data set can generally withstand fairly large amounts of impairments such as loss slope or delay distortion without producing errors. Thus, errors can be viewed as caused by transients such as impulse noise and phase changes, where

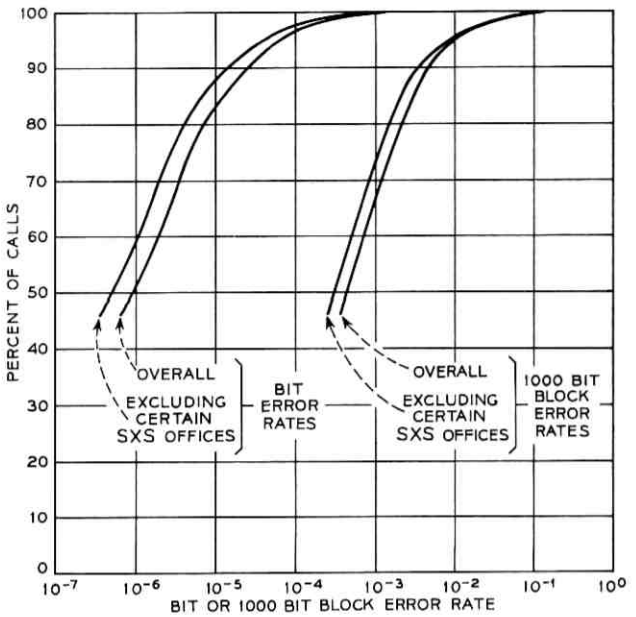

Fig. 21—The effect of excluding certain SXS offices on bit and block error rate at 2000 b/s.

the static impairments determine the sensitivity to these transients. Samples of the 2000 b/s line signal were recorded at six of the twelve receive sites to obtain information on the types of transient disturbances causing errors for this data set.

An analog to digital converter was used to obtain samples of the line signal entering the Data Set 201 receiver. When the received bit stream contained an error, a 50 ms sample of the line signal containing the error causing disturbance was stored for later analysis. No further samples were taken for approximately ten seconds. After this interval, another segment of line signal was stored for comparison with the first. The error causing transient had usually ended before the second segment was recorded.

This information has been analyzed, and major error causing disturbances have been separated into four categories: Short Transients, Additive Signals, Amplitude Changes and Phase Changes.

Short transients are defined arbitrarily as any disturbances of the line signal lasting for 4 ms or less. Transients observed affected both the amplitude and phase of the signal. The most common type of

short transient observed was additive impulse noise. However, transients which appeared to affect only the phase of the line signal were also common, especially in the long mileage category. Examples of an additive impulse and a phase transient are given in Figs. 22a and b. In Fig. 22a, the top trace is the line signal segment which contains the error causing transient; next is the reference version of the same line signal segment. The third trace is the difference between the upper two traces. The bottom trace is the bit pattern with the error bits indicated. This pattern is displaced to the right by approximately 2 ms from the line signal disturbance due to propagation delay through the data set receiver. Figure 22b has the same format, but the top two traces are superimposed. This disturbance caused one error which is not indicated on the figure, since it occurred beyond the last bit shown.

A second category of observed disturbances, additive signals, involved the addition of an extraneous waveform to the data signal. By the definition employed here, these additives lasted for more than 4 ms. Some causes of these disturbances were speech signals or tones crosstalking into the test line, or increases in noise level.

Data signal amplitude changes were observed where the resulting level lasted for more than 4 ms. Included in this category were occurrences of loss of line signal, generally referred to as dropouts. An example of an observed dropout is given in Fig. 22c.

Phase changes were also observed; the resulting phase differed from the original phase for more than 4 ms. Typically the phase change occurred in less than 1 ms. An example is shown in Fig. 22d. Other phase changes took place more gradually as the phase appeared to rotate slowly.

Categorizing the line signal samples allows some determination of the relative frequency of occurrence of these disturbances and their effects on error performance. Table V lists the percent of observed bit errors which were caused by the various categories of transient phenomena. It also lists the percent of observed line signal disturbances of each type, and the average number of errors per disturbance for each category. So that the results would not be dominated by a few calls with relatively poor performance, this table only includes calls with error rates better than 10^{-4}. Causes of errors for calls with error rates poorer than 10^{-4} are discussed in the next section.

At this point, it should be emphasized that these results are based on the observation of line signal disturbances resulting in errors incurred using a Data Set 201. Although the categorization is done on

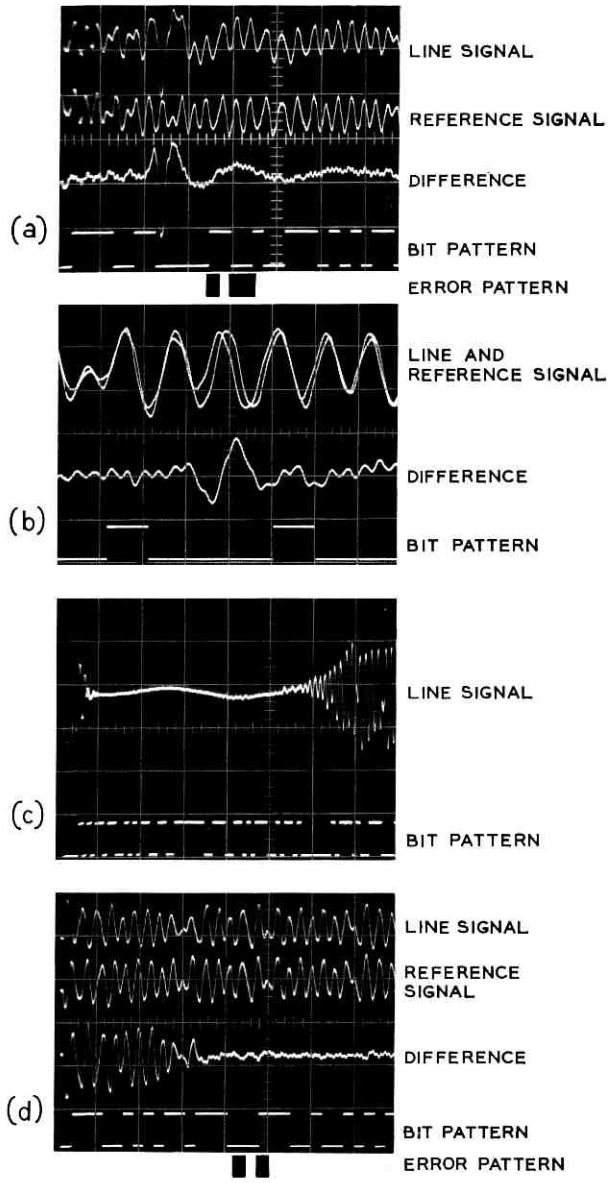

Fig. 22—Examples of observed transient disturbances. (a) Additive impulse (2 ms/div). (b) Phase transient (0.5 ms/div). (c) Dropout (5 ms/div). (d) Phase change (2 ms/div).

TABLE V—OBSERVED CAUSES OF ERRORS FOR OPERATION AT 2000 b/s

Type of Disturbance	Percent of Errors	Percent of Line Signal Disturbances	Average Number of Errors Per Disturbance
Short Transients	63	79	3
Additive Signals	25	6	17
Amplitude Changes	5	4	8
Phase Changes	7	11	2

the basis of transient disturbances, static impairments have a role in determining these percentages. Also, the results are based on a portion of all errors experienced during the survey. Thus, the results are useful to indicate trends, but caution must be used in extending these results to other modem types or to the performance of Bell System data services in general.

Additional information is obtained by analyzing the line signal samples on a mileage band basis. Disturbances such as phase changes and phase transients accounted for approximately three percent of the bit errors observed in the short mileage band, but accounted for approximately 26 percent of the observed errors in the long mileage band. On the other hand, impulse noise is a significant cause of errors in all mileage strata. Short transients identified as additive impulses accounted for 45 percent of all the bit errors observed.

Results presented earlier in this paper have given information on the occurrences of carrier off indications on the data sets tested. Carrier off indications are usually thought of as being the result of line signal interruptions or dropouts. However, analysis of the line signal samples for the Data Set 201 indicates that 25 percent of the observed carrier off indications were caused by dropouts. The remaining 75 percent were caused by severe line signal disturbances such as high-level additive impulse noise.

12.1 *Analysis of 2000 b/s Calls With Error Performance Poorer Than 10^{-4}*

Although only 3.5 percent of the connections (20 calls) on which the 2000 b/s modem was tested had error rates poorer than 10^{-4}, 66 percent of all errors made by the Data Set 201 occurred on these calls. These connections were well distributed throughout the survey with no more than two such calls between any primary-secondary pair, and no primary site with more than three.

It was determined that the principal source of errors in more than half of these calls was additive impulse noise and other additive signals. Line signal dropouts and the various phase related phenomena mentioned earlier also caused several calls to have error rates poorer than 10^{-4}.

XIII. COMPARISONS WITH PREVIOUS SURVEYS

The results presented in this paper show a considerable improvement in error performance compared with the results of the 1959 Alexander, Gryb, Nast Survey.[1] For example, results of the present survey show that for operation at 1200 b/s 82 percent of the calls have error rates of 10^{-5} or better, for equal weighting in the three mileage bands. The AGN Survey reported 63 percent of their test calls achieving this performance level for operation at the same data rate. It should be pointed out, however, that a number of differences in the sampling plans and testing procedures exist between the two surveys precluding a detailed comparison of results. For example, the present survey used a sampling plan based on toll traffic which gave a wide distribution of test site locations, whereas the AGN Survey concentrated more on backbone routes. Also all test calls in the present survey were dialed. In the earlier survey a substantial number of calls were operator handled. Mileage categories were defined differently for the two surveys. Loops were not used in the present survey but were used by AGN. Also, the transmit level was −12 dBm at the serving central office for the present survey. It was −6 dBm at the same point for the AGN Survey.

Improvements in error performance of approximately the same size as those noted at 1200 b/s can be shown by comparing the results presented in this paper for 2000 b/s operation with results from the 1962 Townsend-Watts[2] field measurement program. Again, differences in sampling plan and test procedures do not allow precise comparisons.

For operation at 3600 b/s, bit error rate results presented in this paper are very similar to those obtained from the 1965 Farrow-Holzman[3] field measurements, even though the data set used in the 1969-70 Connection Survey employed a data scrambler, and the data set used in the earlier survey did not.

XIV. SUMMARY AND CONCLUSIONS

This paper has reported estimates of data transmission error performance for operation at 1200, 2000, 3600 and 4800 b/s based on

measurements made as part of the 1969-70 Connection Survey. Toll traffic was used as the basis for the sampling plan which resulted in the selection of approximately 600 dialed toll connections between geographically dispersed Bell System local switching offices.

A substantial improvement in performance has been noted in comparison with previous surveys.

Performance estimates have been based on the following measures: bit error rate, burst rate, block error probabilities and distribution of time between errors. Information has also been given on the structure of error bursts and the duration of data set carrier off indications.

A general tendency for performance to degrade with transmission distance has been noted. The magnitude of the degradation is not the same for all measures of performance.

In comparing the performance of the three data sets it must be remembered that they employ different transmission formats, modulation techniques, and widely differing bit rates. Because of transmission techniques used in the Data Set 203 it tends to have more errors per burst than either of the other sets. For this reason bit error performance at 3600 and 4800 b/s does not compare as well to bit error performance at 1200 and 2000 b/s as does block error performance at the higher speeds to block error performance at the lower speeds.

Line signal samples containing transient disturbances which resulted in bit errors for the 2000 b/s data set were recorded. The results indicate that impulse noise accounted for a large percentage of the observed errors. A strong relationship between transmission distance and the percentage of phase related disturbances was observed.

XV. ACKNOWLEDGMENTS

The authors would like to express their appreciation to the many people at Bell Laboratories, AT&TCo, and the Bell Telephone operating companies who have contributed to this survey. In particular we would like to acknowledge the contributions of Howard C. Johnson in the design of the data collection system, Jack Karp in the implementation and maintenance of the test equipment, and the contributions made by Kay Malleus in the management and analysis of the survey data.

REFERENCES

1. Alexander, A. A., Gryb, R. M., and Nast, D. W., "Capabilities of the Telephone Network for Data Transmission," B.S.T.J., *39*, No. 3 (May 1960), pp. 431–476.
2. Elliott, E. O., "A Model of the Switched Telephone Network for Data Communications," B.S.T.J., *44*, No. 1 (January 1965), pp. 89–109.

3. Morris, R., "Further Analysis of Errors Reported in Capabilities of the Telephone Network for Data Transmission," B.S.T.J., *41,* No. 4 (July 1962), pp. 1399–1414.
4. Townsend, R. L., and Watts, R. N., "Effectiveness of Error Control in Data Communications Over the Switched Telephone Network," B.S.T.J., *43,* No. 6 (November 1964), pp. 2611–2638.
5. Farrow, C. W., and Holzman, L. N., "Nationwide Field Trial Performance of a Multilevel Vestigial Sideband Data Terminal for Switched Network Voice Channels," Conference Record, 1968 IEEE Conf. Commun., June 12–14, Philadelphia, Pennsylvania, p. 782.
6. Duffy, F. P., and Thatcher, T. W., Jr., "1969–70 Connection Survey: Analog Transmission Performance on the Switched Telecommunications Network," B.S.T.J., this issue, pp. 1311–1347.
7. Fleming, H. C., and Hutchinson, R. M., Jr., "1969–70 Connection Survey: Low-Speed Data Transmission Performance on the Switched Telecommunications Network," B.S.T.J., this issue, pp. 1385–1405.
8. Data Communications Using the Switched Telecommunications Network, Bell System Data Communications Technical Reference, AT&TCo., August 1970.
9. Gresh, P. A., "Physical and Transmission Characteristics of Customer Loop Plant," B.S.T.J., *48,* No. 10 (December 1969), pp. 3337–3385.
10. Kaplan, E. L., and Meier, P., "Nonparametric Estimation from Incomplete Observations," J. Amer. Stat. Assn., *53,* June 1958, pp. 457–481.

THE BELL SYSTEM TECHNICAL JOURNAL
Vol. 50, No. 4, April, 1971
Printed in U.S.A.

1969-70 Connection Survey:

Low-Speed Data Transmission Performance on the Switched Telecommunications Network

By H. C. FLEMING and R. M. HUTCHINSON, JR.

(Manuscript received December 4, 1970)

Error statistics of low-speed, start-stop data transmission over the Bell System switched telecommunications network are reported in this article. During the 1969–70 Toll Connection Survey, measurements were made on 534 connections with over 21 million characters transmitted, to give an overall average character error rate of 1.46×10^{-4}. Over 90 percent of the low-speed test calls contained about 36,000 or 54,000 characters. A character error rate of 10^{-4} or less is indicated for 77.6 percent of all calls, while 95.0 percent of calls have a lost character rate of 10^{-4} or less. Error-free performance is shown for 48.3 percent of all calls, and 89.3 percent have no lost characters. Statistics of bursts, error-free intervals, block errors, and carrier failure durations are also presented.

I. INTRODUCTION

1.1 *Reasons for Measuring Low-Speed Data Performance*

Measurements of the accuracy of low-speed data transmission over the Bell System switched network have been included in the 1969–70 Toll Connection Survey; the results are presented in this article. There is widespread use of teletypewriters, computer ports, and other terminal devices that communicate by means of data organized in characters comprised of several bits, using start-stop transmission, at rates up to 300 bits per second (b/s). About 80,000 terminals of this type were being used for *Data-Phone*® service at the end of 1970.

This article presents the quantity and distribution of the character errors and lost characters observed during the low-speed data tests. These results are expected to meet a need for characterization of the switched telecommunications network for start-stop transmission of

low-speed data. Further analysis of the data is planned to pinpoint causes of errors for which remedial measures would be profitable, to suggest possible improvements in design of transmission equipment, and to indicate possible usefulness of error control systems.

The measurements were planned with the objective of characterizing low-speed data transmission performance as viewed by users. The error statistics are reported for channels extending from a transmitting data set, into which an error-free data signal is sent, to the point at the receiving end at which the characters are used or displayed.

1.2 *Design of Survey*

Detailed planning of the survey is described in a companion article by F. P. Duffy and T. W. Thatcher[1]; a very brief summary is presented here. A random selection of end points for approximately 600 toll calls was made by means of a three-stage sampling plan. The first stage consisted of division of the 48 contiguous United States and the provinces of Ontario and Quebec in Canada into 12 geographical areas that originated roughly equal numbers of completed toll calls. A "primary" end office was randomly chosen from each area with probability proportional to the originated toll traffic from that office. In the second stage, two to six calls which determined "secondary" or far-end test offices were selected randomly in each of three mileage bands (0–180, 180–725, and 725–2900 miles) relative to each primary office location. The calls were selected from traffic printouts from each primary office; thus the chosen secondary offices had probability of selection proportional to traffic originated from the primary office destined to the secondary office. The third stage consisted of six or more test calls dialed from each primary office to each of its associated secondary offices. Numerous analog transmission parameters and error performance for four Bell System data sets were measured on most connections.[1] Results for the Data Sets 201(2000 b/s), 202(1200 b/s), and 203(3600 and 4800 b/s) are reported by M. D. Balkovic, H. W. Klancer, S. W. Klare, and W. G. McGruther.[2] This article gives results for Data Set 103 at 150 b/s.

1.3 *Start-Stop Transmission*

The data transmitted at low speed were organized into successive 10-bit characters, and were sent in a start-stop mode. In this type of transmission the character consists of an initial "start" bit (binary 0, or space), followed by seven information bits used to encode 128 different characters—alphabetic, numeric, punctuation, and control

(American Standard Code for Information Interchange, ASCII), followed by a parity check bit (selected to give an even number of ones for the information bits and parity bit), and terminated by a "stop" interval of indefinite duration, one bit minimum (binary 1, or mark). Many terminal devices are designed to generate and respond to characters thus constituted.

Character error statistics, rather than bit error statistics, are the parameters of interest in this type of transmission because the message consists of a display (in teletypewriters) or use (in computers) of characters in most applications. Start-stop transmission is susceptible to sequences of character errors caused by a single bit error. This occurs because of the mechanism used to distinguish the start of a new character: the transition from a stop interval (mark) to a start bit (space). A disturbance that produces a space during a prolonged stop pulse, or changes a start bit (space) to a mark thus prolonging the stop pulse, will cause the receiving terminal to detect the start of the next character at the wrong point in the bit sequence and to record a character error. This condition—loss of character synchronization—persists until the correct stop-start transition is detected in a subsequent character. Some receiving circuits, for example regenerators, have built-in algorithms that minimize the resynchronizing interval. In other cases, the correct position is reached accidentally as a result of the pseudo-random bit pattern of the usual message. In short, loss of character synchronization may result from a single bit error and cause propagation of many character errors—an effect which is not present in synchronous transmission.

II. IMPLEMENTATION

2.1 *Test Arrangement*

Figure 1 shows the test arrangement used to measure the low-speed data transmission performance. The data were always transmitted from the secondary site because considerably less equipment was required at the transmitting end than at the receiving end with this arrangement, and tests were conducted for two weeks or more at a primary location compared to one or two days at a secondary site.

2.1.1 *Transmitting End*

A test sentence generator (WECo 911B) generated a repeated 72-character test sentence (FOX sentence) using ASCII 10-bit characters at 15 characters per second, or 150 b/s. The 72-character

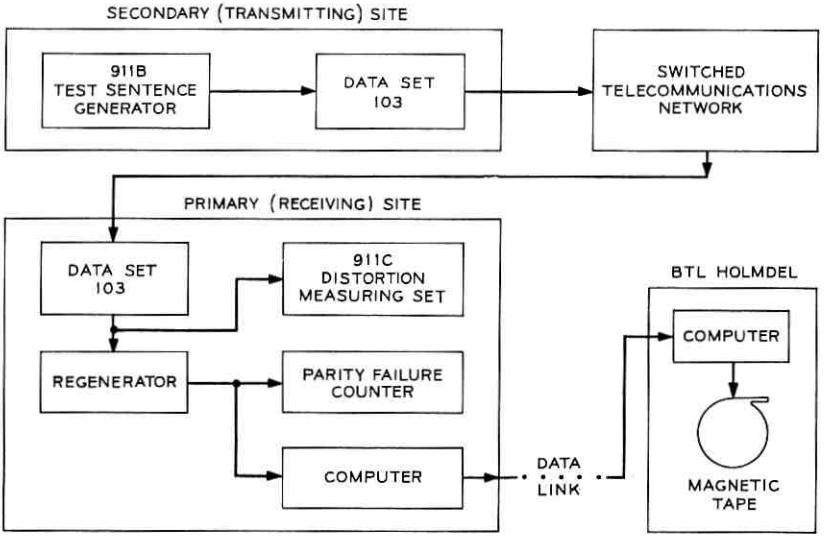

Fig. 1—150 b/s data transmission test of the 1969–70 Toll Connection Survey.

sentence produces the following line of printing on a teletypewriter followed by a delete character, two carriage returns, and a line feed: THE QUICK BROWN FOX JUMPED OVER A LAZY DOG'S BACK 1234567890 TESTING. A Bell System 103 type data set was chosen for the low-speed data transmission tests. This set is typical of the 100 series sets which are used to transmit low-speed serial data in all *Data-Phone* applications. It uses frequency shift keying (fsk) between 1070 (space) and 1270 (mark) Hz (low band) in one direction of transmission and 2025 (space) and 2225 (mark) Hz (high band) in the other direction, at rates up to 300 b/s. The 103 data set at the transmitting site modulated the test sentence to a binary fsk signal at either the low-band (F_1) or high-band (F_2) frequencies; these were alternated on successive calls.

The output signal power delivered to the connection was between −12 dBm and −13 dBm; both F_1 and F_2 were transmitted at the same power. These are the values normally produced at the central office. In a standard installation, there is a subscriber loop from the customer's premises to the main frame in the central office. In the survey, the test setup was connected to the main frame, thus including a loop of essentially zero loss. It was considered unnecessary to add real loops to customer locations because loops should not degrade the

error performance of a connection significantly. Moreover, real loops are nonrandom in nature; that is, a subscriber station uses the same loop for all calls.

2.1.2 *Receiving End*

The data set at the receiving site demodulated the binary fsk received signal to baseband mark or space voltage. The data set contains a frequency modulation discriminator which continuously makes the binary decision as to whether marking or spacing frequency is being received. There is no timing or sampling associated with this decision.

The data signal at the output of the receiving data set differs from the signal at the input to the transmitting data set because of imperfections in the transmission characteristics of the connection. One difference is displacement in time of the mark to space transitions—telegraph distortion. This was measured by the distortion measuring set (WECo 911C) in Fig. 1. Receiving terminal devices differ in their error performance susceptibility to telegraph distortion. The test arrangement included a regenerator at the output of the receiving data set which reduces the telegraph distortion to a negligible amount. Thus, the test results apply to any terminal arrangement that uses this regenerator, and are independent of the following receiving circuits. With this arrangement, the receiving terminal—regenerator plus detecting circuits—resembles many terminals in use. The specific regenerator employed is one used optionally with the Model 37 Teletypewriter.[3]

The computer at the primary site interpreted the regenerator output in terms of ASCII characters in the same manner that a teletypewriter would in most instances. The computer detected and recorded characters received in error and carrier failure indications, which occur when the received line signal level drops to a very low value (approximately −50 dBm or lower).

The parity failure counter incremented whenever a received character failed parity. Since a large fraction (about 80 percent) of characters received in error will also fail parity, the parity count provided the testers with an immediate indication of the occurrence of character errors.

2.2 *Data Collection*

Information identifying each low-speed data test run and giving measurements of parity failure counts and distortion was recorded

on log sheets at the primary location. It was also entered into the primary site computer by teletypewriter, and then transmitted over a data link to a computer at Bell Telephone Laboratories in Holmdel, New Jersey, where it was stored on magnetic tape. The data link was a switched network connection with transmission accuracy enhanced by error detection and block retransmission.

The computer at the primary site was programmed to recognize characters from the low-speed data regenerator and compare them with the expected characters, making use of a FOX sentence which was stored in its memory. Any discrepancy in the character's bits was considered to be a character error; the computer recorded the identity (bit pattern) of the received erroneous character and the number of characters received since the last previously recorded event.

As described earlier, character synchronization may be lost as the result of an error in a start or stop bit, usually causing several successive character errors. Character synchronization might be recovered on the wrong character—a condition described as loss of sentence synchronization. To prevent the computer from recording character errors interminably, when five character errors were detected in succession the computer was declared to be out of sentence synchronism (OSS) and a resynchronizing procedure was begun. During an OSS period, a complete record of the bits in all received characters was taken.

The recorded information described above and a record of the time of occurrence and duration of all carrier failures were transmitted over the data link to the Holmdel computer. This information was recorded on magnetic tape, along with the other low-speed test information mentioned above and other similar information about the high-speed data tests.[2]

2.3 *Data Processing*

The low-speed test results were separated from the other information on the magnetic tape and edited. The result was a complete record of (*i*) the bit pattern and time of occurrence of all characters, except those removed by the editing, reported by the primary site computer (isolated character errors and characters reported during OSS periods) and (*ii*) the time of beginning and end of carrier failure indications and OSS conditions.

Every transmitted character was classified as to whether it was received correctly, received in error, or not received (lost)—a conse-

quence of a carrier failure. The first character in a carrier failure was defined to be a character error, since this character is very likely to be received in error because of loss of signal during the transmission of the character. A teletypewriter would very probably print an error for this character. (This definition was necessary because the primary site computer did not check this character for bit errors.)

OSS intervals were analyzed as follows. The received characters reported by the computer were compared with the FOX sentence characters. When the received character was in the FOX sentence, checks of subsequent characters determined whether sentence sync had been recovered. This generally occurred before the computer completed its resynchronizing procedure, which was based on detection of a specific FOX sentence character. Characters transmitted during that part of an OSS interval preceding recovery of sentence sync were character errors. Status of characters following recovery of sync was based on comparison with the corresponding FOX sentence characters.

Finally, cards were punched for each call containing information identifying the call and summarizing the character statistics. In addition, the entire call was recorded on cards in a format which described the exact sequence of characters received correctly, in error, or lost. This information was condensed by recording the length (in characters) of intervals of received characters for each category.

This set of cards comprised the input data from which all error statistics reported in the remainder of this article were computed.

III. DISTRIBUTIONS OF CHARACTER ERROR AND LOST CHARACTER RATES* OF CALLS

3.1 *Calls Included in Analysis*

The set of calls for which data transmission error statistics are reported in this article is the same as that for which error statistics are reported for the high-speed voiceband data sets,[2] except for connections on which both low-speed and high-speed data measurements could not be completed. For reasons given in companion articles,[1,2] the set differs somewhat from the set selected by the sampling plan described earlier. The essential difference is that two primary offices in the original sample were replaced by nearby offices, from which high-

* Character error rate of a call = character errors/characters transmitted in that call.

speed voiceband data users in that area would normally be served. In addition, all calls that were switched by panel type central office equipment at either end of the connection were excluded; panel offices do not normally serve data customers. Only one primary office contained panel equipment, but it also contained crossbar equipment and calls originated through the latter equipment were included.

3.2 *Magnitude of Low-Speed Data Survey*

Table I summarizes the quantities of calls and primary and secondary locations.

The duration of a low-speed data test was nominally 40 minutes except when the 3600–4800 b/s data set was not tested (for about half the calls in the first half of the survey). In this case, the duration was about an hour. Equipment problems and dropped connections sometimes resulted in shorter runs—13 calls shorter than 23 minutes, with a minimum of 1.1 minutes. In 15 cases, extra available time was used for tests longer than 65 minutes, with a maximum of 145 minutes.

Table II summarizes some of the total survey statistics. Character errors are characters in which at least one bit is received in error, with the result that an erroneous character may be printed or an undesired action may take place (for example, carriage return) on the receiving teletypewriter. Lost characters are those for which no bits are received, usually because of a loss of the received signal, resulting in characters missing from the teletypewriter printout. Statistics are presented separately for these two types of impairments because they differ in the extent to which they damage the communication. Character errors may result in acceptance of incorrect information (an order for one carload might be received as an order for nine carloads), whereas lost characters represent missing information, perhaps requiring retransmission of the message.

TABLE I—CALL AND LOCATION STATISTICS

	Total	Mileage Band		
		Short	Medium	Long
Calls	534	171	186	177
Primary Locations	12			
Secondary Locations	91	29	32	30
Secondaries Per Primary	5 to 11			
Calls Per Primary	22 to 62	5 to 33	6 to 29	8 to 23

TABLE II—TOTAL SURVEY CHARACTER ERROR AND LOST CHARACTER STATISTICS

	All Calls	Mileage Band		
		Short	Medium	Long
Calls	534	171	186	177
Characters Transmitted	21.31×10^6	7.00×10^6	7.48×10^6	6.83×10^6
Character Errors	3,110	751	1,053	1,306
Lost Characters	14,511	9,581	1,476	3,454
Character Error Rate	1.46×10^{-4}	1.07×10^{-4}	1.42×10^{-4}	1.90×10^{-4}
Lost Character Rate	6.81×10^{-4}	13.7×10^{-4}	1.98×10^{-4}	5.03×10^{-4}

3.3 *Overall Average Rates*

Overall average error rates are also listed in Table II. These are useful as single number parameters that characterize the survey. Distributions of per call statistics are more significant; these are presented later in this article. The average character error rate—total character errors observed during the survey divided by total characters transmitted—is 1.46×10^{-4}, which corresponds to one error for every 1.7 pages of average single-spaced typed text. As Fig. 2, curve (A), shows, the average character error rate was not dominated by a few bad calls; it drops by a factor of only 1.6 (to 9.1×10^{-5}) when the eight worst calls are omitted.

The average lost character rate is 6.81×10^{-4}, corresponding to about 2.7 lost characters per page of text. This average is definitely dominated by a few bad calls; omission of the eight worst calls, which contain 93.3 percent of the total lost characters, improves the average by a factor of 14.5 to 1, to 4.7×10^{-5} [Fig. 2, curve (B)].

The average character error rate becomes progressively poorer as the mileage band gets longer, although the span of the increase is not large, only a factor of 1.8. Lost character rate is poorest in the shortest mileage band; however, omission of two calls—the worst and third worst for all calls—improves the rate in the short band to 1.55×10^{-4}, which is better than the medium and long bands.

3.4 *Weighting of Data for Calls*

Error statistics of calls include application of weighting factors to each call, based on the details of the sampling procedure by which the set of calls was selected. One contribution to the weighting arises

from unequal toll traffic originated within the 12 areas into which the United States and Canada were divided. A second and much larger component of the weighting factor which is applied to the set of all calls results from large differences in the total toll traffic from a primary to offices in each mileage band. A third component is the actual number of calls for which low-speed data error statistics were collected between specific primary and secondary locations. In this article, weighting was applied only to the error statistics of calls presented in Section 3.5 and not to the remaining parameters, which are related to the time sequence of occurrence of errors.

3.5 *Cumulative Distributions*

Figures 3a, b, c, and d show weighted cumulative distributions for character error rate and lost character rate of calls. The unweighted distributions for all calls are shown for comparison.

The curves in Figs. 3a, b, c, and d have been left unsmoothed to reflect the actual results observed. Large discontinuities sometimes occur when the number of character errors or lost characters changes from 0 to 1, 1 to 2, etc.

The weighted results of average character error rates (Figs. 3a and b) for all calls are closer to the results for the short mileage band than

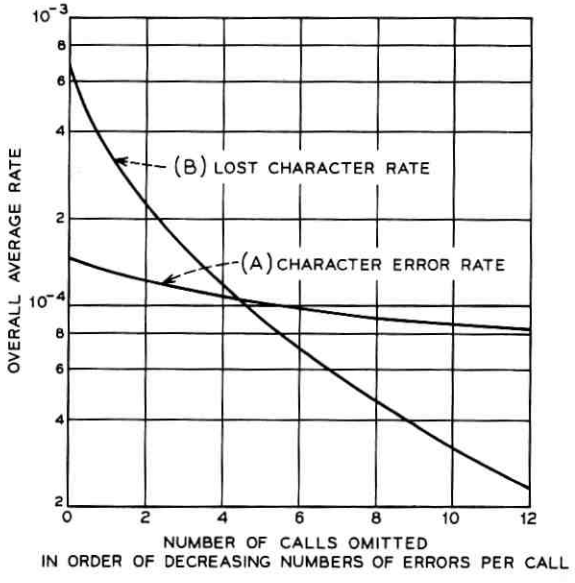

Fig. 2—Sensitivity of overall average rates to omission of worst calls.

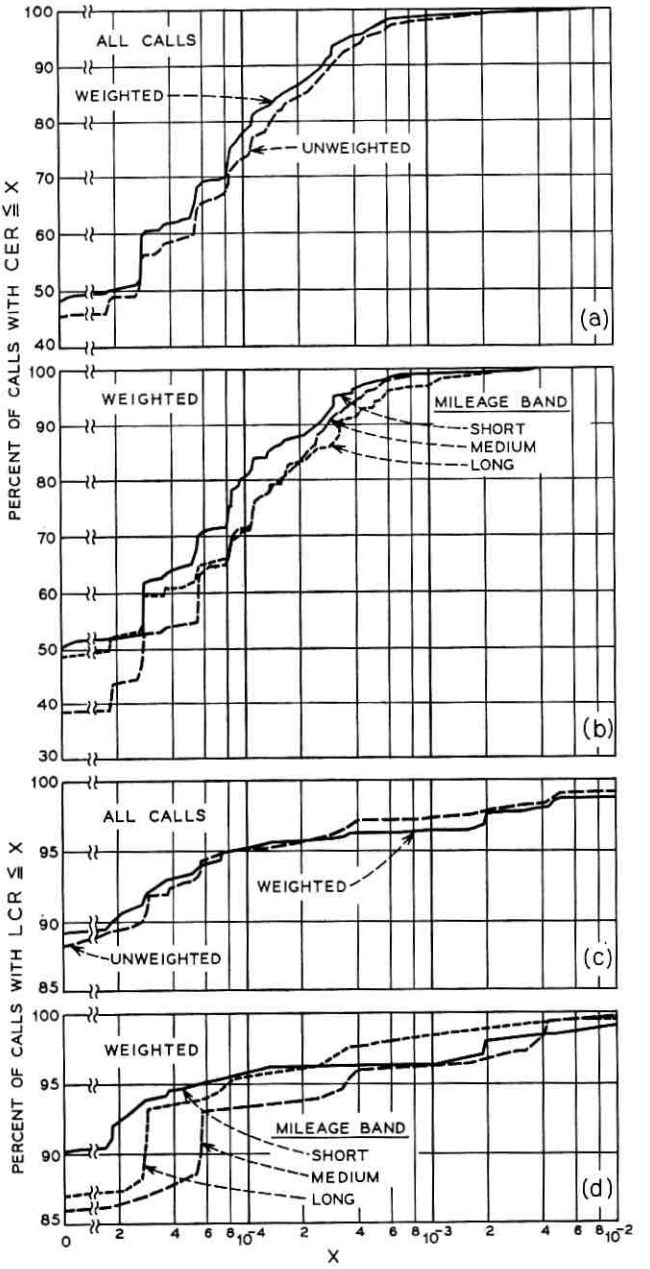

Fig. 3a—Cumulative distribution of average character error rate $(CER)_a$ of call.
Fig. 3b—Weighted cumulative distribution of average character error rate $(CER)_a$ of call.
Fig. 3c—Cumulative distribution of average lost character rate $(LCR)_a$ of call.
Fig. 3d—Weighted cumulative distribution of average lost character rate $(LCR)_a$ of call.

the unweighted data because this band has more toll traffic (85 percent of the total) and therefore a larger weighting factor than the other bands. However, application of weighting does not change the results markedly. At error rates above 10^{-4}, the results tend to get poorer as the mileage increases but not to a large degree.

Lost characters (Figs. 3c and d) were observed on relatively few calls; close to 90 percent of all calls have no lost characters. Their occurrence appears to be unrelated to mileage band. All distributions have long tails to the right because of the occurrence of a few long bursts of lost characters with rates per call greater than 10^{-2}.

Some of the results shown by the distributions are listed in Table III.

The weighted statistics show almost 50 percent of calls to be error free and almost 90 percent free of lost characters. About 78 percent of the calls have error rates equal to or less than 10^{-4}, and 95 percent of the calls have lost character rates equal to or less than 10^{-4}. About 81 percent have error rates better than the average for all calls; the corresponding number for lost characters is 96 percent.

Table III includes 90 percent confidence intervals for most of the parameters ($\hat{p} \pm \Delta$), meaning that there is 90 percent confidence that the true value of the parameter (p) for the entire population of switched network toll calls from which the survey sample was selected lies within the stated interval.*

The confidence interval for the average of lost character rate of calls (LCR) is very wide. This is because of the very large variance of LCR, the values of LCR ranging from 0 (89 percent of the calls) to 0.13. Ten calls had values of LCR greater than 0.01; the large departure from the average of 9.5×10^{-4} contributes to the large variance and wide confidence interval. The poor confidence indicated for this parameter is consistent with the sensitivity of the overall average LCR for all calls to the omission of a few bad calls, as noted in Section 3.3. It is concluded that average LCR for this survey is not a very significant parameter.

All other confidence intervals in Table III are reasonably narrow.

IV. BURST PROPERTIES

The distribution in time of character errors is far from uniform, nor is it Poisson (equal probability, overall average character error

* Stating this more precisely, if another survey were conducted, there would be 0.9 probability that the confidence interval for that survey, $\bar{p} \pm \Delta$, would contain p. Intervals were computed as described in Ref. 1. The formulas are derived for a normal distribution; the confidence intervals herein reported are only approximate because of departures of the distribution from normal.

TABLE III—ERROR STATISTICS OF CALLS

(A) Average Character Error Rate (CER) of Calls

	Weighted	Unweighted	Mileage Band (Weighted)		
			Short	Medium	Long
Average CER*	$1.12 \pm 0.31 \times 10^{-4}$	1.46×10^{-4}	$1.03 \pm 0.39 \times 10^{-4}$	$1.22 \pm 0.62 \times 10^{-4}$	$1.56 \pm 0.56 \times 10^{-4}$
Percent of Calls with CER = 0	48.3 ± 8.5	45.8	50.5 ± 10.8	38.5 ± 7.5	48.9 ± 11.4
Percent of Calls with CER $\leqq 10^{-4}$	77.6 ± 5.8	73.4	80.1 ± 5.6	71.2 ± 8.5	70.8 ± 13.3
Percent of Calls with CER $\leqq$ Average	81.0	80.5	80.8	77.0	80.7

(B) Average Lost Character Rate (LCR) of Calls

Average LCR	$9.53 \pm 12.6 \times 10^{-4}$	6.8×10^{-4}	$1.16 \pm 1.78 \times 10^{-3}$	$2.82 \pm 2.53 \times 10^{-4}$	$4.91 \pm 7.56 \times 10^{-4}$
Percent of Calls with LCR = 0	89.3 ± 7.1	88.3	90.3 ± 8.0	86.0 ± 10.0	87.0 ± 6.6
Percent of Calls with LCR $\leqq 10^{-4}$	95.0 ± 3.5	95.1	95.4 ± 4.4	93.0 ± 4.5	95.4 ± 2.1
Percent of Calls with LCR $\leqq$ Average	96.4	97.2	96.0	94.2	97.8

* Note that $\pm$ values represent 90 percent confidence intervals.

rate, that any single character is received in error, regardless of the previous history). Instead, there is considerable bunching of character errors; once an error occurs, the probability of another error in any of the next several characters is much higher than the overall average character error rate.

These burst properties are shown in Figs. 4a and b. Burst density is here defined as the character error rate in an interval of L characters following a character error. No new interval is observed until the previous one is completed. Each interval (rather than each call) is weighted equally in computing the average burst density. This analysis of burst properties differs from that used in the analysis of high-speed voiceband error statistics.[2] Figure 4a is a plot of average burst density for all intervals on all calls in the survey, versus L. The probability that the character following an error is also received in error is about 0.45 for all calls, compared to 0.000146—the overall average character error rate. Complete subsiding of burst properties for interval lengths greater than a specific value of L would result in a plot approximately as shown (for $L = 10$), starting with a slope of unity (on a log-log plot). The actual plot for all calls settles into a straight line with slope less than unity beyond $L \cong 10$, indicating that there is little correlation of errors beyond this value, although there is no clear-cut maximum value of L at which burst properties subside completely.

Plots of average burst density for the three mileage bands separately are almost indistinguishable from that for all calls, indicating that burst properties are independent of distance.

The standard deviation of the distribution of burst densities is plotted versus L in Fig. 4b. The value for all calls decreases monotonically as L increases. The standard deviation is greater than the average (Fig. 4a) for all values of L; clearly, the distribution departs considerably from normal. Again, the plots for the separate mileage bands differ little from that for all calls.

V. ERROR-FREE INTERVALS

An error-free interval (EFI) occurs when one or more characters are received correctly between character errors. Its length (L) is the number of correctly received characters between the two character errors. Statistics of the duration of EFIs are of interest to users whose applications include error control.

5.1 *Interpretation of EFI at Start and End of Call*

The lengths of the EFIs preceding the first and following the last

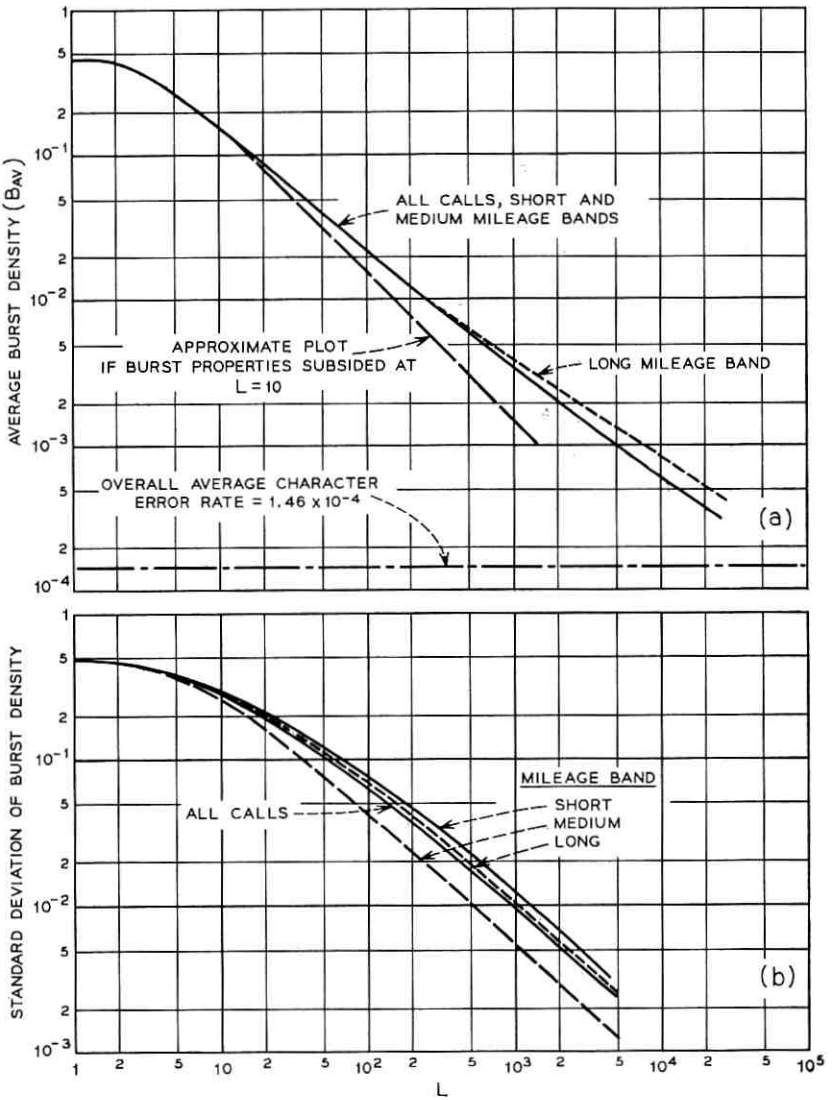

Fig. 4a—Average burst density versus L. Burst density (B) = character error rate in interval of length L (characters) following a character error.
Fig. 4b—Standard deviation of burst density versus L.

character errors in a call are unknown. These intervals are called end intervals (EIs). Since most calls have few if any errors, there are nearly as many EIs as complete error-free intervals.

An EI is part of an error-free interval which is at least as long as the EI. This information was used in estimating the probability, $P(\ell)$, that the length of an error-free interval is at least ℓ characters long, using the iterative procedure* of equation (1),

$$P(\ell) = \text{Prob}\,\{L \geqq \ell \mid L \geqq \ell - a\}P(\ell - a). \tag{1}$$

The procedure started with $P(0) = 1$. Each step required only the estimate of Prob $\{L \geqq \ell \mid L \geqq \ell - a\}$. This estimate equals the fraction of error-free intervals or EIs at least $\ell - a$ characters long which were also at least ℓ characters long. EIs shorter than ℓ were not used for this estimate.

5.2 *Cumulative Distribution of EFI Length*

This distribution is plotted in Fig. 5a. A Poisson distribution is shown for comparison. The difference between the survey and the Poisson curve shows the tendency of character errors to occur in bursts. For example, the survey data for all calls show that both short and long EFIs are more probable than for a Poisson distribution. For example, 19.5 percent of the survey EFIs are shorter than 100 characters compared to 1.45 percent for Poisson, and 48.6 percent of the survey EFIs are equal to or larger than 10,000 characters compared to 23.2 percent for Poisson. The latter comparison indicates that more error-free messages of long duration will result from the survey distribution than from Poisson. Equally spaced errors at the average error rate would result in all intervals having lengths of 6850 characters (Fig. 5a).

5.3 *Lost-Character-Free Intervals*

A lost-character-free interval (LFI) is the interval between lost characters; it is the corresponding parameter to EFI for lost characters. Its length is the number of received characters between the two lost characters.

The procedure described in Section 5.1 was followed for nonterminating lost character intervals. The cumulative distribution of LFI lengths is plotted in Fig. 5b. The plot shows that most LFIs tend to be much longer than EFIs (Fig. 5a); 95 percent exceed 10,000 characters for all calls. This seems inconsistent with the higher overall average lost character rate, almost five times the character error rate

* This is the same as the product limit method used in Ref. 2.

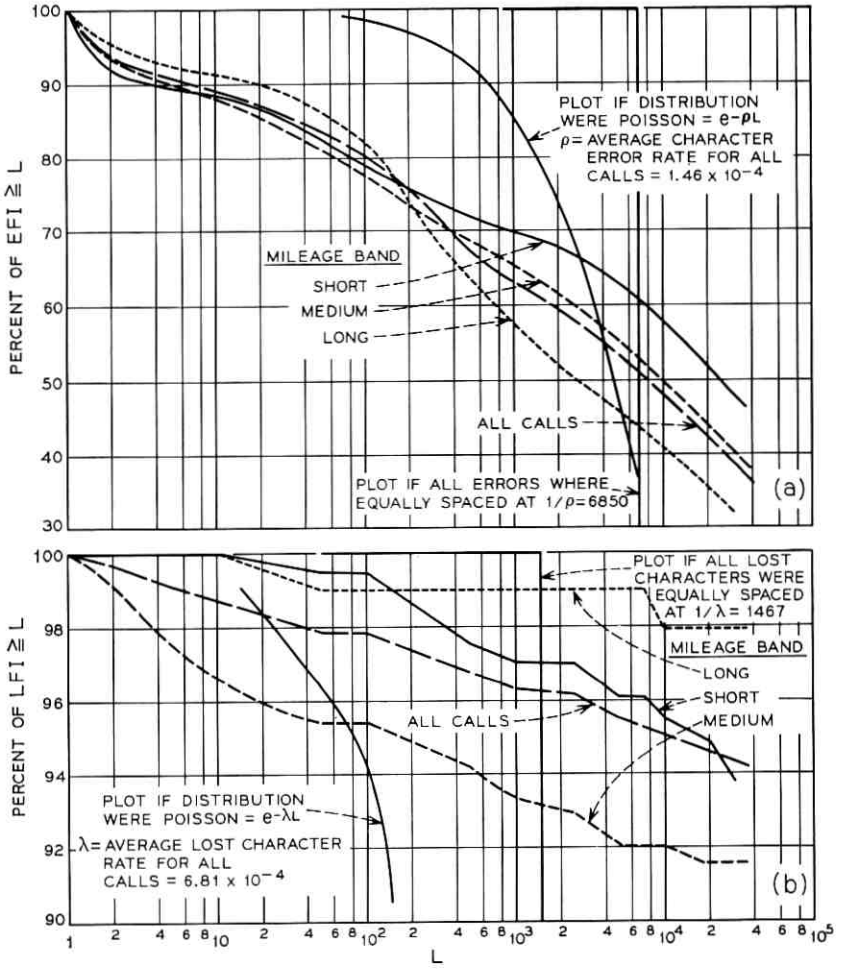

Fig. 5a—Cumulative distribution of character error-free interval (EFI) lengths (L characters).
Fig. 5b—Cumulative distribution of lost-character-free interval (LFI) lengths (L characters).

(Table II), but is explained by the occurrence of lost characters in long, continuous bursts.

VI. BLOCK ERROR STATISTICS

Error statistics in terms of blocks of many characters are useful in describing to a customer the accuracy that he might expect in transmission of messages of fixed length that he normally sends. For ex-

ample, the customer may be interested in what percent of his messages will be error free, or have no more than one error, etc. In addition, block error statistics are useful in evaluating performance of error control systems.[4,5]

Figures 6a and 6b give block error statistics for the survey data. These are obtained by dividing each call into consecutive blocks of equal duration (L characters). To obtain statistics independent of an arbitrary starting point, the division is made for 10 different starting points (phases) of the first block: 0, 1, 2, etc., tenths of a block from the beginning of the call. The statistics are then averaged for all 10 phases. Figure 6a shows average block error rate plotted against block length for various minimum numbers of character errors per block. Plots for uniform distribution and Poisson distribution of character errors are included for blocks with one or more errors.

Figure 6b shows cumulative distributions of block errors: probability of a block having more than E character errors versus E, for various block lengths.

The distribution for Poisson distributed errors is shown for blocks of 1000 characters. The bunching of errors in the survey data is shown by the comparison of the appropriate curves. The Poisson distribution has less probability of error-free blocks (0.864 versus 0.964) and greater probability of less than several errors (0.9999 versus 0.9928 for five errors); that is, the Poisson curve is much steeper than the survey curve.

VII. CARRIER FAILURES

Figure 7 shows a cumulative distribution of durations of carrier failures. These curves resemble the distributions of lost character rates per call (Figs. 3c and d). A large percentage of carrier failures have durations of one character or less (90.4 percent for all calls). Nevertheless, several long duration carrier failures (0.4 percent longer than 1000 characters) contain the bulk of the lost characters. The crisscrossing plots for the three mileage bands indicate the random occurrence of carrier failures and the lack of dependence on length of connection.

VIII. CONCLUSIONS

Several parameters describing error performance of low-speed, start-stop, data transmission over the Bell System switched telecommunications network have been presented. These include distributions

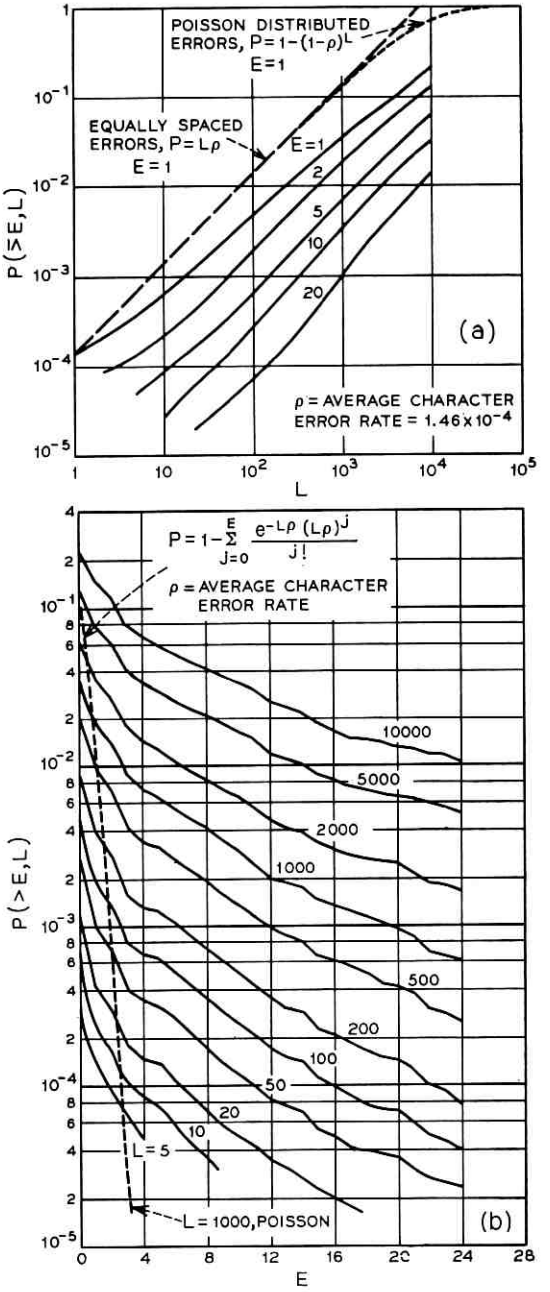

Fig. 6a—Probability of at least E character errors in block of length L (characters). $P(\geqq E, L)$ versus L.

Fig. 6b—Probability of more than E character errors in block of length L (characters). $P(>E, L)$ versus E.

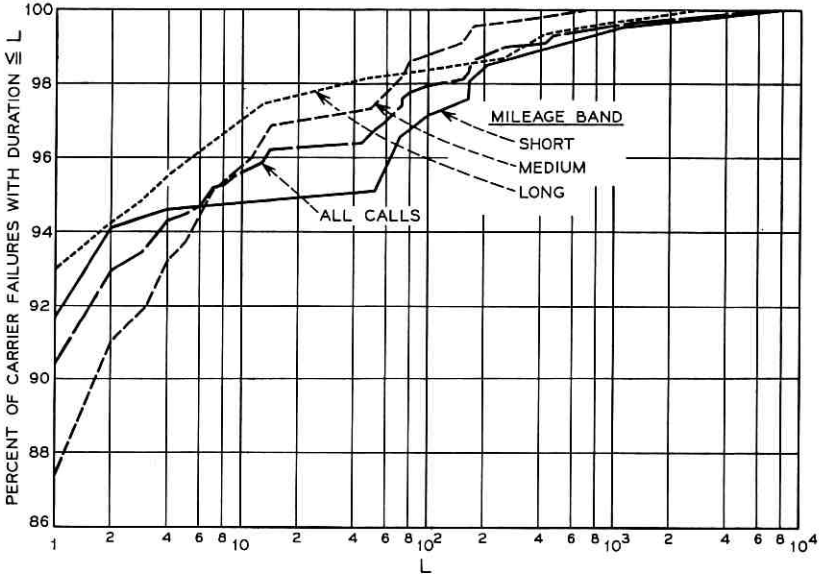

Fig. 7—Cumulative distribution of duration of carrier failures.

of averages per call of character error and lost character rates, and other parameters that relate to distributions in time of erroneous and missing characters. The intent has been to characterize accuracy of transmission from the sending data set input to the receiving device display by a teletypewriter or storage in a computer.

There have been no previous low-speed data surveys with which to compare the results of this one. Some comparisons with the results of the voiceband data measurements[2] are possible. The distribution of durations of carrier failures during low-speed data tests (Fig. 7) tails off to considerably longer periods than for the voiceband data tests (Ref. 2, Fig. 10). During low-speed tests, two percent of all calls had carrier failures longer than 7.5 seconds. The corresponding period for the voiceband tests was less than 0.3 second. The relatively long carrier failures and the resulting high lost character rate in the low-speed tests are believed to be fortuitous.

A comparison of error performance requires estimating the bit error rate at low speed, since this has not been computed. A rough approximation of the bit error rate is one-tenth of the character error rate since a character contains 10 bits. Isolated character errors have one bit or more in error, but this factor is compensated by the occurrence

of many character errors in OSS periods with no bit errors. Thus the low-speed result of 78 percent of calls with a character error rate of 10^{-4} or less may be compared with about 88 percent, for the 2000-b/s data set, and 84 percent, for the 1200-b/s data set, with a bit error rate of 10^{-5} or less (including bit errors during carrier failures), both greater than the percent for low speed. However, the overall average error rates for the voiceband data are about 1.9×10^{-5} (2000 b/s) and 6.6×10^{-5} (1200 b/s), greater than the low-speed value (approximately 1.46×10^{-5}). This apparent contradiction results from long tails on the voiceband distributions—a few calls with high error rates.

The results of the low-speed survey give much needed information on the error performance that may be expected on switched network calls. It is expected that further analysis of the statistics will give insight to the causes of errors which will suggest approaches to improve error performance.

IX. ACKNOWLEDGMENTS

Miss A. C. Weingartner and F. Brophy prepared the computer programs used to compact the data and determine the error statistics; the former also gave important assistance in the preparation of this article. Programs to separate the low-speed test results from the other records on the Holmdel computer magnetic tape were written by Mrs. K. D. Malleus. Editing of the preliminary records and other clerical tasks were performed by members of the Holmdel clerical pool, in particular, Mrs. S. D. Claus. Implementation and maintenance of test circuits was performed mostly by H. Hagen, who also devoted considerable time to the collection of data, as did many others.

REFERENCES

1. Duffy, F. P., and Thatcher, T. W., Jr., "1969–70 Connection Survey: Analog Transmission Performance on the Switched Telecommunications Network," B.S.T.J., this issue, pp. 1311–1347.
2. Balkovic, M. D., Klancer, H. W., Klare, S. W., and McGruther, W. G., "1969–70 Connection Survey: High-Speed Voiceband Data Transmission Performance on the Switched Telecommunications Network," B.S.T.J., this issue, pp. 1349–1384.
3. Model 37 Regenerator—Circuit Description 8383 WD, Issue 3, Teletype Corporation, Skokie, Illinois.
4. Elliott, E. O., "A Model of the Switched Telephone Network for Data Communications," B.S.T.J., *44*, No. 1 (January 1965), pp. 85–109.
5. Elliott, E. O., "Estimates of Error Rates for Codes on Burst-Noise Channels," B.S.T.J., *42*, No. 5 (September 1963), pp. 1977–1998.

THE BELL SYSTEM TECHNICAL JOURNAL
Vol. 50, No. 4, April, 1971
Printed in U.S.A.

Maximum Power Transmission Between Two Reflector Antennas in the Fresnel Zone

By T. S. CHU

(Manuscript received August 11, 1970)

Power transfer between two ellipsoidal reflector antennas with common focal points and dual-mode feeds has been investigated. Assuming a circularly symmetric feed pattern, the H-plane pattern of an open-end circular waveguide excited by the TE_{11} mode, the maximum transmission coefficient between reflector apertures is found to be within 0.5 percent of the value computed for transmission between two circular apertures with optimum illumination described by the generalized prolate spheroidal function. Transmission loss between two reflector antennas versus illumination taper is computed for various values of the parameter $[p = (ka_1a_2)/R]$. The minimum transmission loss is obtained as a compromise between feed spill-over and aperture transmission efficiency.

In view of the inconvenience of building different ellipsoidal reflectors for different antenna spacings in order to achieve maximum power transfer, we examine the feasibility of using a defocused ellipsoid to simulate ellipsoids of different focal lengths. The deviation of the aperture phase distribution of a defocused ellipsoid from a required spherical phase front is approximately given by an explicit expression. A simple upper bound of the transmission loss due to small phase deviation is obtained for a given maximum phase deviation.

I. INTRODUCTION

Millimeter waves have never been used in long-haul radio transmission systems because of rain attenuation. However, wideband transmission over short span (say less than 1 km) can be accomplished by millimeter wave systems, for example, the *Picturephone*® distribution in large cities proposed by R. Kompfner. The very high transmission

efficiency may leave a large margin for rain attenuation to insure high reliability. Here the transmitting and receiving antennas may be within the Fresnel zones of each other.

Maximum power transfer between two apertures in the Fresnel region takes place when the field distribution appears as the lowest order mode of a confocal open resonator.[1, 2] Two ellipsoidal reflectors with common focal points may provide the required aperture phase distribution which is a spherical wave front with the center of curvature located at the center of the other aperture. The optimum amplitude distribution is a prolate spheroidal function for a rectangular aperture or a generalized prolate spheroidal function for a circular aperture. S. Takeshita[3] has shown that truncated gaussian illumination, which is asymptotically identical to the generalized prolate spheroidal function, may give a transmission efficiency between two circular apertures almost as good as that using generalized prolate spheroidal illumination. However, the truncated gaussian distribution only looks simpler in terms of mathematical manipulation while its practical realization appears not any easier than that of prolate speroidal functions. Furthermore, if a lens or reflector is used to produce the spherical phase front, the feed spill-over must be taken into account. The maximum power transfer between the feeds of two reflector antennas will be obtained as a compromise between feed spill-over loss and aperture transmission efficiency. This procedure is similar to optimizing the gain of a paraboloidal antenna. The aperture blocking effect can be made very small by using the periscope type structure[4] which virtually eliminates the feed supports. This paper will present the calculated results of Fresnel zone transmission between two ellipsoidal reflector antennas with dual-mode feeds. In view of the inconvenience of building different ellipsoidal reflectors for different antenna spacings, we will also examine the feasibility of using a defocused ellipsoid to simulate ellipsoids of different focal lengths.

II. MAXIMUM POWER TRANSFER

Neglecting the interaction between the antennas and assuming that the tangential components of the electric and magnetic fields are related by the free space impedance at each point of the two apertures A_1 and A_2, the ratio of the received to transmitted power between two apertures* at any separation can be shown[5] to be

* Not to be confused with transmission between two antennas which includes spill-over of the feeds.

$$\frac{P_R}{P_T} = \frac{\left| \int_{A_1} \int_{A_2} E_1^t \frac{\exp(-jkL)}{L} E_2^t \, ds_1 \, ds_2 \right|^2}{\lambda^2 \left\{ \int_{A_1} |E_1^t|^2 \, ds_1 \right\} \left\{ \int_{A_2} |E_2^t|^2 \, ds_2 \right\}} \tag{1}$$

where E_1^t and E_2^t are tangential components of the aperture field distributions when A_1 and A_2 are transmitting respectively. Using the small angle Fresnel approximation, the distance L may be approximated by

$$\begin{aligned} L &= [R^2 + (x - \xi)^2 + (y - \eta)^2]^{\frac{1}{2}}, \\ &\approx R + \frac{(x - \xi)^2 + (y - \eta)^2}{2R}, \end{aligned} \tag{2}$$

where the coordinate system is illustrated in Fig. 1. Then the near field power transmission formula becomes

$$T = \frac{P_R}{P_T} = \frac{\left| \int_{A_1} \int_{A_2} E_1 \exp\left[j \frac{k(x\xi + y\eta)}{R} \right] E_2 \, ds_1 \, ds_2 \right|^2}{R^2 \lambda^2 \left\{ \int_{A_1} |E_1|^2 \, ds_1 \right\} \left\{ \int_{A_2} |E_2|^2 \, ds_2 \right\}} \tag{3}$$

where

$$E_1 = E_1^t \exp\left[-j \frac{k(x^2 + y^2)}{2R} \right], \tag{4a}$$

$$E_2 = E_2^t \exp\left[-j \frac{k(\xi^2 + \eta^2)}{2R} \right]. \tag{4b}$$

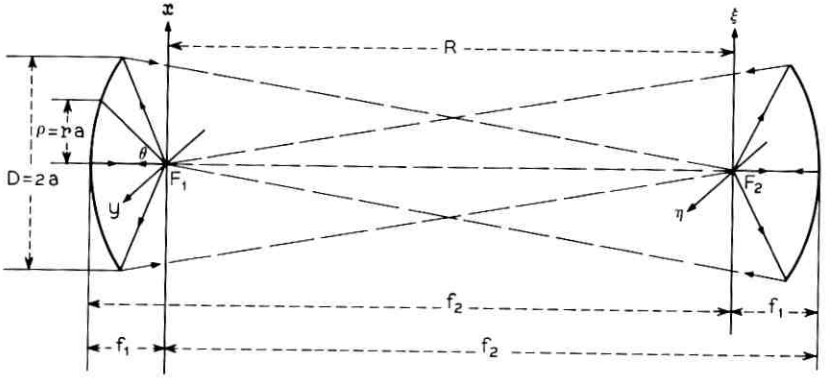

Fig. 1—Two ellipsoidal reflectors with common focal points.

If the aperture distributions are circularly symmetric, equation (3) can be reduced to

$$\frac{T}{p} = \frac{\left| \int_0^1 \int_0^1 E_1(r)\sqrt{r}\, E_2(r')\sqrt{r'}\, J_0(prr')\sqrt{prr'}\, dr\, dr' \right|^2}{\left\{ \int_0^1 |\, E_1(r)\sqrt{r}\,|^2\, dr \right\} \left\{ \int_0^1 |\, E_2(r')\sqrt{r'}\,|^2\, dr' \right\}} \tag{5}$$

where $p = (ka_1a_2)/R$ for two circular apertures of radii a_1 and a_2. One notes that the transmitting and receiving apertures may have different radii, while the optimum illumination function is identical for the two apertures. When both E_1 and E_2 are real, the Schwartz principle gives the following condition for the maximization of equation (5)

$$\sqrt{\frac{T}{p}}\, E(r)\sqrt{r} = \int_0^1 E(r')\sqrt{r'}\, J_0(prr')\sqrt{prr'}\, dr'. \tag{6}$$

The subscript of E has been dropped because equation (6) is satisfied by both E_1 and E_2. The above integral equation has been thoroughly investigated by D. Slepian[6] and $\phi(r) = E(r)\sqrt{r}$ is designated as a generalized prolate spheroidal function. The optimum transmission coefficient T taken from Slepian's work is given in Table I for reference.

Now a simple way of approximately realizing the optimum aperture distribution appears to be the illumination of an ellipsoidal reflector by a dual-mode feel. In the vicinity of the reflector, the reflected field will follow the geometrical optics rays which are pointed toward the remote focal point as shown in Fig. 1, and thus the required spherical phase front will be created in the aperture. An experiment on dual-mode apertures[7], one to two wavelengths in diameter, showed the measured patterns to be circularly symmetric and essentially in agreement with the H-plane pattern of an open-end circular waveguide excited by TE_{11} mode, i.e.,

$$F(\theta) = \left[\sqrt{1 - \left(\frac{1.841}{u}\right)^2} + \cos\theta \right] \frac{J_1'(u \sin\theta)}{1 - \left(\frac{u \sin\theta}{1.841}\right)^2} \tag{7}$$

where u is the circumference of the waveguide in wavelengths. Since the ellipsoidal reflector is very closely a defocused paraboloid, as will be shown in the next section, the space attenuation factor needed for the variable distance from the feed to the reflector surface is essentially the same as that of a paraboloid. Then the aperture distribution is related to the feed pattern by

$$E(r) = F(\theta) \cos^2 \frac{\theta}{2} \tag{8}$$

where $ar/2f = \tan \theta/2$ and f is the focal length of the reflector. The combination of equations (7) and (8) can be used to determine the value of u for any corresponding illumination taper as plotted in Fig. 2. Substituting equation (8) into equation (5), numerical integration will give the transmission coefficient between two ellipsoidal reflector apertures excited by dual-mode feeds. The computed data have been plotted in Fig. 3 for $f/D = 0.5$ and various values of the parameter p. The maximum efficiency using dual-mode feed and excluding spill-over has been tabulated in Table I for comparison with the optimum efficiency using amplitude illumination of generalized prolate spheroidal functions.

The agreement between the second and third columns in Table I is indeed excellent. The insensitivity of the transmission coefficient to small differences in illumination is not surprising in view of the stationary property of equation (5). Table I does not show the maximum efficiency with dual-mode feed for $p = 2$ and 10, because the mathematical model in equation (7) for the dual-mode pattern has not been experimentally verified for the circumference of the waveguide outside the range $3 \leqq u \leqq 6$. However, this model covers the most interesting range and demonstrates that efforts to synthesize a truncated gaussian distribution are unwarranted. As far as maximum power transfer between two apertures is concerned, any aperture distribution which resembles the generalized prolate spheroidal function may achieve practically the optimum transmission efficiency. As an example of tolerable discrepancy, the dual-mode feed illumination function of a taper strength which maximizes the transmission coefficient for $p = 5$ is compared with the corresponding generalized prolate spheroidal function

TABLE I—POWER TRANSFER EFFICIENCY OF TWO CIRCULAR APERTURES

$p = ka_1a_2/R$	Optimum Illumination Efficiency	Dual Mode Illumination Maximum Efficiency
2.0	0.630	
3.0	0.887	0.886
4.0	0.975	0.972
5.0	0.995	0.992
10.0	1.000	

in Fig. 4. One notes that the over-all similarity is sufficient to achieve transmission coefficients differing by only 0.3 percent while the edge illuminations differ by more than 3 dB.

Next we turn our attention to the spill-over loss of a feed. If the reflector is illuminated by a circularly symmetric feed pattern $F(\theta)$, then the fraction of the energy intercepted by the reflector will be

$$\alpha = \int_0^{\theta_0} [F(\theta)]^2 \sin \theta \, d\theta \Big/ \int_0^{\pi/2} [F(\theta)]^2 \sin \theta \, d\theta \tag{9}$$

where θ_0 is the half angle subtended by the reflector at the focus and the back lobes have been neglected. Substituting equation (7) into equation (9), we compute the total spill-over loss in decibels from $2[10 \log_{10} (1/\alpha)]$ as shown in Fig. 3. The presence of two feeds in the system accounts for the factor two. It is seen that the spill-over loss is as important as the power transfer loss between two reflector apertures in determining the total transmission loss between two reflector antennas. The minimum total transmission loss between feeds will always be greater than the power transfer loss between the reflector apertures, and always occurs at an illumination taper stronger than that for the maximum transmission between two apertures. Any slight decrease in transmission loss due to deviation of the aperture distribution from the generalized prolate spheroidal function will certainly be swamped by the feed spill-over loss. Figure 3 indicates that the illumination taper corresponding to the maximum power transfer decreases as the parameter p decreases. As the distance between two reflectors increases toward the far zone condition $p = 0$, the optimum illumination taper

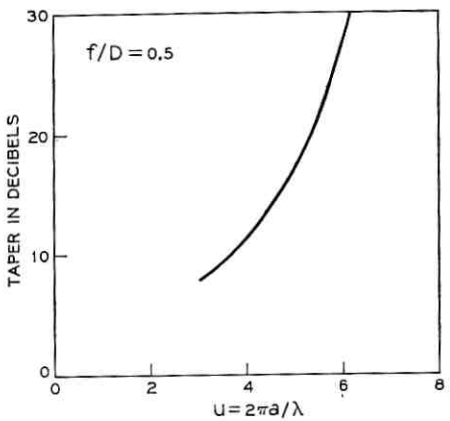

Fig. 2—Relation between feed pattern parameter and taper.

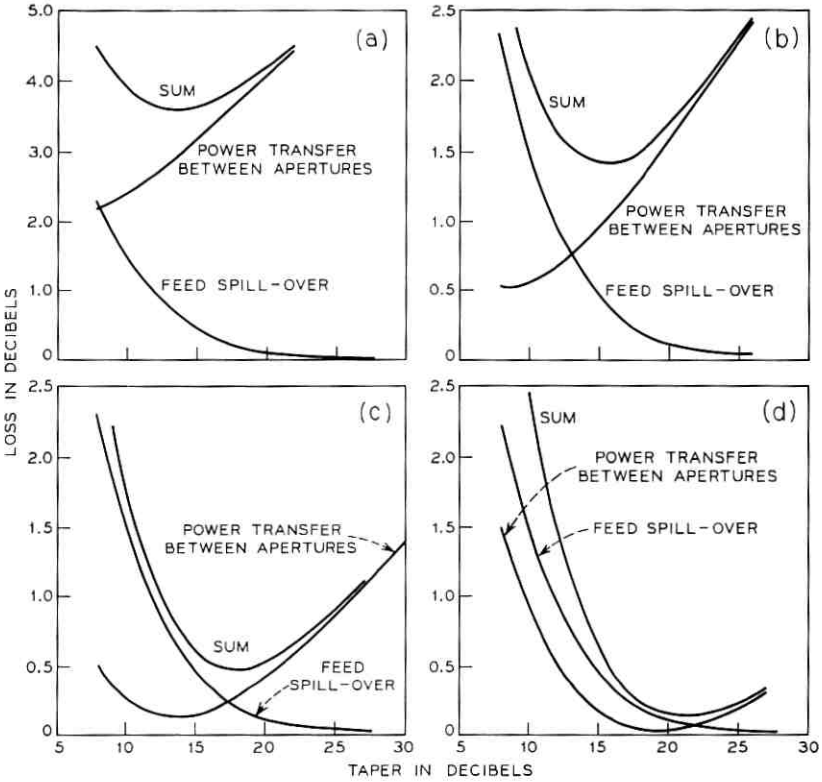

Fig. 3—Power transfer between ellipsoidal reflector antennas with dual mode feeds. (a) $ka_1a_2/R = 2$, (b) $ka_1a_2/R = 3$, (c) $ka_1a_2/R = 4$, (d) $ka_1a_2/R = 5$.

will approach 12 dB which maximizes the Fraunhofer gain of a paraboloidal antenna.[8] One notes that 12-dB aperture taper corresponds to 10-dB feed pattern taper, allowing a 2-dB space attenuation factor, for 0.5 f/D ratio. When f/D decreases to smaller values, the spill-over loss curve will be shifted to the right because of increasing space attenuation factor. Then the minimum of the sum will be also moved to the right and upward. Large f/D ratio which requires narrow feed pattern may cause significant loss due to aperture blocking which has been neglected in the above calculations.

III. OPTIMUM DEFOCUSING OF AN ELLIPSOID

In the preceding section we have shown that ellipsoidal reflectors are needed for maximum power transfer between two reflector antennas in the Fresnel region. The required focal lengths of the ellipsoidal re-

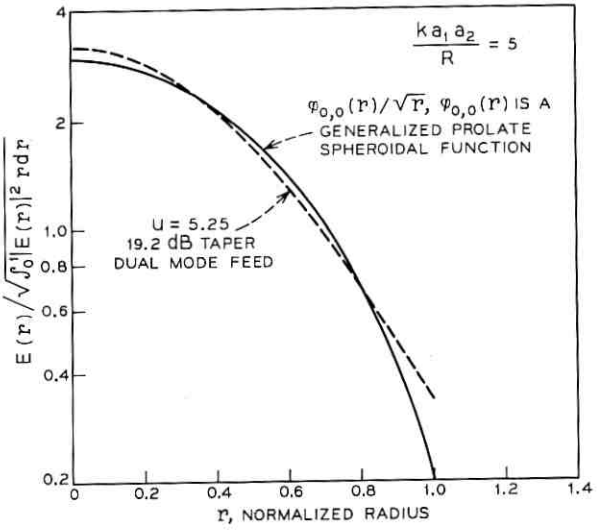

Fig. 4—Comparison between optimum aperture distributions.

flectors are determined by the distance between the reflectors and the desired f/D ratio. It is obviously inconvenient to build different ellipsoidal reflectors for different antenna spacings; however, approximating ellipsoids of different focal lengths by a defocused ellipsoid can be an attractive possibility in some practical situations. The necessary displacement of the feed along the axis will be first determined. Then we will calculate the approximate phase deviation between the wave front reflected from a defocused ellipsoid and the spherical wave front in the aperture of a required ellipsoidal reflector. An upper bound of the transmission loss will be obtained for a given maximum phase deviation.

The equation of an ellipsoid can be written as

$$Z = \frac{f + R}{2}\left[1 - \sqrt{1 - \frac{\rho^2}{fR}}\right] \tag{10}$$

where f and R* are the two focal lengths. Now let us consider another ellipsoid with corresponding focal lengths f' and R'

$$Z = \frac{f' + R'}{2}\left[1 - \sqrt{1 - \frac{\rho^2}{f'R'}}\right]. \tag{11}$$

* R may be taken as any distance between $f_2 - f_1$ and f_2, where f_1 and f_2 are the two focal lengths of the ellipsoid. This slight ambiguity results from the aperture approximation for reflector antenna, and is unimportant provided that f_2 is orders of magnitude greater than f_1.

These two ellipsoids coincide at the tip $\rho = 0$. We will impose the condition that the two ellipsoids also coincide at the edge $\rho = a$ as shown in Fig. 5. Taking the first three terms of the binomial expansion of the square root in equations (10) and (11), we obtain an expression for the required defocus distance:

$$\epsilon = f' - f = \frac{f^2(R - R')}{RR'}\left[1 + \left(\frac{a}{2f}\right)^2\right] \tag{12}$$

in which the approximations $f \ll R$ and $f' \ll R'$ have been used. Substituting equation (12) into equations (10) and (11), the approximate deviation between the two ellipsoids becomes

$$\Delta Z = \frac{1}{4}\left(\frac{a}{2f}\right)^2 r^2(1 - r^2)\frac{a^2(R - R')}{RR'} \tag{13}$$

where $r = \rho/a$ is the normalized radius. Multiplying equation (13) by the factor $(1 + \cos\theta)$ yields the phase deviation between the two wave fronts reflected from the two ellipsoids as shown in Fig. 5. Since these ellipsoids differ little from paraboloids, the relation $\tan\theta/2 = ar/2f$ is approximately valid. Then one arrives at the following expression

$$\frac{\delta}{\lambda} = \left[\tfrac{1}{2}r^2(1 - r^2)\frac{\left(\frac{a}{2f}\right)^2}{1 + \left(\frac{a}{2f}\right)^2 r^2}\right]\frac{a^2}{\lambda R'}\frac{R - R'}{R}. \tag{14}$$

The last factor in equation (14) is always less than unity when $R > R'$. This factor approaches unity when $R \to \infty$, i.e., approximating an ellipsoid by a defocused paraboloid. The quantity inside the bracket of equation (14) is the phase deviation[9] of a wave front produced by a

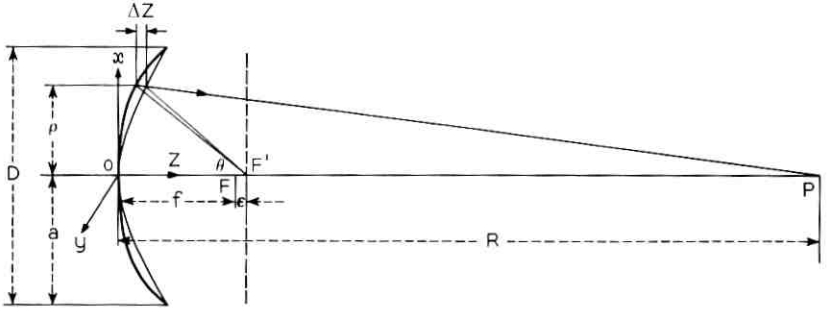

Fig. 5—Geometry of defocused ellipsoid.

defocused paraboloid from a desired spherical wave front for a Fresnel number $(a^2/\lambda R)$ of unity, and has been plotted in Fig. 6 for various values of f/D ratio. The maximum phase deviation is found to be located at

$$\rho^2 = 4f^2\left[\sqrt{1 + \left(\frac{a}{2f}\right)^2} - 1\right]. \tag{15}$$

When $(a/2f)^2 \ll 1$, the above equation can be reduced to

$$\rho^2 = \frac{a^2}{2}\left[1 - \frac{1}{4}\left(\frac{a}{2f}\right)^2\right]. \tag{16}$$

If the variation of antenna spacing covers a range from R_1 to R_2, the optimum ellipsoid for minimizing the phase deviation of equation (14) can be found by equating

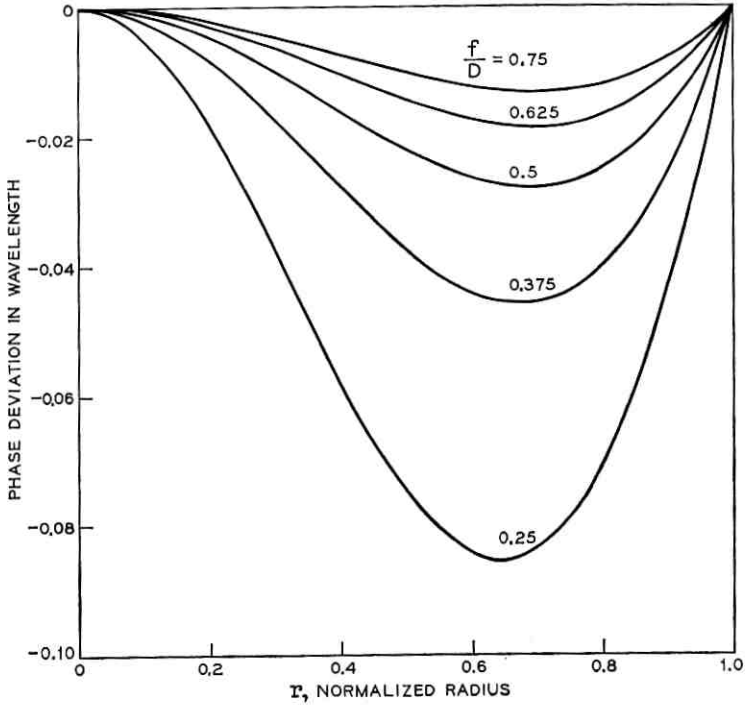

Fig. 6—Aperture phase deviation between a defocused paraboloid and an ellipsoid for unity Fresnel number.

$$\frac{R_2 - R'}{R_2R'} = \frac{R' - R_1}{R_1R'}. \tag{17}$$

Solving the above equation, we have

$$R' = \frac{2R_2R_2}{R_1 + R_2}. \tag{18}$$

Substituting equation (18) into equation (14), the maximum phase deviation becomes

$$\frac{\delta}{\lambda} = \left[\tfrac{1}{2}r^2(1 - r^2) \frac{\left(\frac{a}{2f}\right)^2}{1 + \left(\frac{a}{2f}\right)^2 r^2} \right] \frac{a^2}{\lambda R_1} \frac{R_2 - R_1}{2R_2}. \tag{19}$$

One notes that the above total phase deviation is twice the maximum absolute magnitude of the phase error for the defocused ellipsoid. In the Appendix an upper bound of the transmission loss due to small phase error has been approximately determined as $(m_1 + m_2)^2$ for optimum aperture distributions where m_1 and m_2 are the maximum absolute magnitudes of phase error of the two apertures respectively. As a numerical example, if the antenna spacing varies by a factor of 3, equation (19) and Fig. 6 will give $m_1 = m_2 = (\frac{1}{2}(\delta/\lambda)) \cdot 2\pi = 0.03$ for a Fresnel number of unity and an f/D ratio of 0.5. Then the fractional transmission loss due to phase error will be less than 0.4 percent.

IV. DISCUSSION

The above calculations have demonstrated the potential of optimum Fresnel zone transmission between two antennas with ellipsoidal reflectors illuminated by dual-mode feeds. In spite of the discrepancy between the illumination function of a dual-mode feed and the optimum illumination of a generalized prolate spheroidal function, the maximum power transmission between reflector apertures is practically the same for the two cases. However, the feed spill-over loss is as important as the transmission loss between reflector apertures in determining the total transmission loss between reflector antennas. More sophisticated feed design, such as the synthesis of more than two modes, may reduce the spill-over loss. Here the resulting increase in aperture blocking of the reflector is undesirable. The use of a lens in place of a reflector would avoid aperture blocking but would give rise to interface matching problems. Furthermore, the proper organiza-

tion of many modes implies narrow bandwidth and stringent tolerances.

From a geometrical optics point of view, one is tempted to have the ellipsoidal reflectors focused at the midpoint between them. This scheme corresponds to a concentric resonator. The aperture distribution created by the two reflectors which are portions of the same ellipsoid, as shown in Fig. 1, is equivalent to a confocal resonator. The diffraction loss of a concentric resonator is much greater than than of a confocal resonator. The gaussian beam theory[10] predicts a beam waist, i.e., an effective focal region, in the middle of the confocal resonator. These observations indicate the failure of geometrical optics, although the reflectors are in the Fresnel zones of each other. Converting the reflected field into the aperture distribution employs geometrical optics ray tracing only in the immediate vicinity of the reflector. The validity of this procedure should be as good as that of calculating the diffraction pattern from the aperture distribution of a paraboloidal antenna.

The feasibility of using a defocused ellipsoid to simulate ellipsoids of different focal lengths has been investigated. The optimum defocusing of an ellipsoidal reflector for obtaining another spherical wavefront is similar to that of defocusing a spherical reflector for obtaining an approximate plane wave front. The explicit expression for phase deviation shows its simple dependence on the f/D ratio, the Fresnel number, and the variation of antenna spacing. Since a defocused paraboloid is a special case of a defocused ellipsoid, the criteria obtained here will also be useful for measuring the Fraunhofer radiation pattern of a paraboloidal antenna in the Fresnel region. In particular, it clarifies the inconsistency among various schemes for this latter problem, proposed by D. K. Cheng.[9,11]

V. ACKNOWLEDGMENT

The author wishes to thank A. B. Crawford for suggesting this problem and for helpful discussions.

APPENDIX

An upper bound of the transmission loss due to small phase error will be given below for nearly optimum aperture distributions. The phase error may be either deterministic or random. A small phase error simply introduces an additional factor $\exp(j\Delta\phi)$ into the

numerator of equation (5), where $\Delta\phi = \Delta(r) + \Delta(r')$. For small values of $\Delta\phi$,

$$\exp(j\Delta\phi) \approx 1 - \tfrac{1}{2}(\Delta\phi)^2 + j\Delta\phi. \tag{20}$$

Then the modified equation (5) becomes

$$\frac{T}{p} = \left| \int_0^1 \int_0^1 M_1(r)M_2(r')J_0(prr')\sqrt{prr'}\left[1 - \frac{(\Delta\phi)^2}{2}\right] dr\, dr' \right|^2 + \left| \int_0^1 \int_0^1 M_1(r)M_2(r')J_0(prr')\sqrt{prr'}\,\Delta\phi\, dr\, dr' \right|^2 \tag{21}$$

where

$$M_i(r) = \frac{E_i(r)\sqrt{r}}{\int_0^1 |E_i(r)\sqrt{r}|^2\, dr}, \qquad i = 1, 2. \tag{22}$$

If E_1 and E_2 are optimum aperture distributions, then for any perturbation factors $A(r)$ and $B(r')$ with maximum magnitudes m_A and m_B, the following inequality holds,

$$\left| \int_0^1 \int_0^1 A(r)M_1(r)B(r')M_2(r')J_0(prr')\sqrt{prr'}\, dr\, dr' \right|^2 \leqq m_A^2 m_B^2 \left| \int_0^1 \int_0^1 M_1(r)M_2(r')J_0(prr')\sqrt{prr'}\, dr\, dr' \right|^2, \tag{23}$$

where A and B can be either of the following combinations

$$\begin{cases} A = \Delta(r) \\ B = \Delta(r') \end{cases}, \quad \begin{cases} A = [\Delta(r)]^2 \\ B = 1 \end{cases}, \quad \begin{cases} A = 1 \\ B = [\Delta(r')]^2 \end{cases}. \tag{24}$$

It follows that

$$T \geqq T_{\text{opt}} \left[1 - \frac{(m_1 + m_2)^2}{2}\right]^2, \tag{25}$$

where $m_1 = |\Delta(r)|_{\max}$ and $m_2 = |\Delta(r')|_{\max}$. The maximum fractional transmission loss due to small phase error is

$$1 - \frac{T}{T_{\text{opt}}} \leqq (m_1 + m_2)^2 \left[1 - \frac{(m_1 + m_2)^2}{4}\right]. \tag{26}$$

The above upper bound of the effect of phase error on the Fresnel zone transmission loss represents a conservative estimate.

REFERENCES

1. Borgiotti, G. V., "Maximum Power Transfer Between Two Planar Apertures in the Fresnel Zone," IEEE Trans., *AP-14,* No. 2 (March 1966), pp. 158–163.
2. Heurtley, J. C., "Maximum Power Transfer Between Finite Antennas," IEEE Trans., *AP-15,* No. 2 (March 1967), pp. 298–300.
3. Takeshita, S., "Power Transfer Efficiency Between Focused Circular Antennas with Gaussian Illumination in Fresnel Region," IEEE Trans., *AP-16,* No. 3 (May 1968), pp. 305–309.
4. Crawford, A. B., and Turrin, R. H., "A Packaged Antenna for Short-Hop Microwave Radio Systems," B.S.T.J., *48,* No. 6 (July–August 1969), pp. 1605–1622.
5. Hu, M. K., "Near-Zone Power Transmission Formulas," IRE Nat. Conv. Record, *6,* pt. 8, 1958, pp. 128–135.
6. Slepian, D., "Prolate Spheroidal Wave Functions, Fourier Analysis and Uncertainty-IV; Extensions to Many Dimensions; Generalized Prolate Spheroidal Functions," B.S.T.J., *43,* No. 6 (November 1964), pp. 3009–3057.
7. Turrin, R. H., "Dual Mode Small Aperture Antennas," IEEE Trans., *AP-15,* No. 2 (March 1967), pp. 307–308.
8. Kelleher, K. S., "High-Gain Reflector-Type Antennas," *Antenna Engineering Handbook,* H. Jasik, editor, New York: McGraw-Hill, 1961, Chapter 12.
9. Chu, T. S., "A Note on Simulating Fraunhofer Radiation Patterns in the Fresnel Region," to be published in IEEE Trans., *AP-19* No. 5 (September 1971).
10. Kogelnik, H., and Li, T., "Laser Beams and Resonators," Proc. IEEE, *54,* No. 10 (October 1966), pp. 1312–1329.
11. Cheng, D. K., "On the Simulation of Fraunhofer Radiation Patterns in the Fresnel Region," IEEE Trans., *AP-5,* No. 4 (October 1957), pp. 389–402.

THE BELL SYSTEM TECHNICAL JOURNAL
Vol. 50, No. 4, April, 1971
Printed in U.S.A.

A Digital Approach to Adaptive Delta Modulation

By DAVID J. GOODMAN

(Manuscript received November 12, 1970)

A fixed-step-size delta modulator followed by digital circuits for generating an adaptive delta modulation signal provides an attractive compromise between code efficiency and cost. In order to control the total quantizing noise, the fixed-step-size delta modulation sampling rate is higher than the adaptive delta modulation output rate. Computer simulations, based on the adaptive delta modulation technique described by N. S. Jayant, indicate that the sampling rate required for negligible degradation relative to a conventional adaptive delta modulator is well within the current state of the art. Our approach lends itself to any scheme of step-size variation and may use any means of single-integration, fixed-step-size delta modulation.

I. INTRODUCTION

Since the invention of delta modulation, considerable effort has been devoted to devising means of improving code efficiency without sacrificing the inherent simplicity of the analog-to-digital converter. The key to success in this respect is the retention of a single binary decision for each sample of the analog input. Early work concentrated on sophisticated linear signal processing to be introduced either at the input to the delta modulator, as a predictor in the feedback loop, or as an error filter in the forward loop.[1-3] In recent years, the use of a time-varying step size in the feedback loop has been emphasized.[4-8] Although the step-size variation, in a sense, transforms the delta modulator from a binary to a multilevel device, implementation is likely to be more economical than that of a conventional multilevel quantizer. The variable-step-size, sometimes called "adaptive" or "companding," mechanism provides considerable improvement in efficiency and it is possible that for speech encoding, this form of

delta modulation will result in better performance characteristics in the 20–40 kilobit/second range than conventional PCM.

II. THE DIGITAL DELTA MODULATOR

The purpose of this paper is to present a new approach to the implementation of adaptive delta modulators. The approach is motivated by current trends in electronic device technology that suggest that digital hardware implementations based on standardized building blocks will offer advantages of economy and flexibility relative to analog techniques. This hypothesis combined with the observation that *transmission rate rather than analog-to-digital conversion rate* influences the overall cost of a digital communication system suggests the use of the very simple single-integration delta modulator for analog-to-digital conversion and digital hardware for converting the single-integration, fixed-step-size representation to the desired efficient format. By separating analog-to-digital conversion from source encoding, we obtain a compromise between the goals of economy of implementation and efficiency of representation. This compromise, based on the addition of only digital devices to the simple delta modulator, promises, in many situations, to be more economical than the conventional approach of performing analog-to-digital conversion and source encoding in one step. This point of view has led to a new type of PCM encoder that combines a delta modulator with a nonrecursive digital filter.[9]

The digital circuits required to convert a simple delta modulation signal to a variable-step-size format comprise a "digital delta modulator" operating on the integrated output of the first delta modulator. In addition to a sequential circuit that determines the appropriate step size at each instant, the digital delta modulator contains only binary counting and addition circuits and one simple decision element. Figure 1 is an operational block diagram of the entire encoder.

III. PERFORMANCE CHARACTERISTICS

Computer simulations have verified the feasibility of the combination of a fixed-step-size delta modulator and a digital delta modulator. N. S. Jayant's scheme of adaptive delta modulation[6] was simulated by means of software provided by Jayant and Mrs. K. Shipley. For a given output rate, the operation of the digital delta modulator in Fig. 1 is determined completely by the step-size logic. At each instant, the step size depends on the previous step size and the cur-

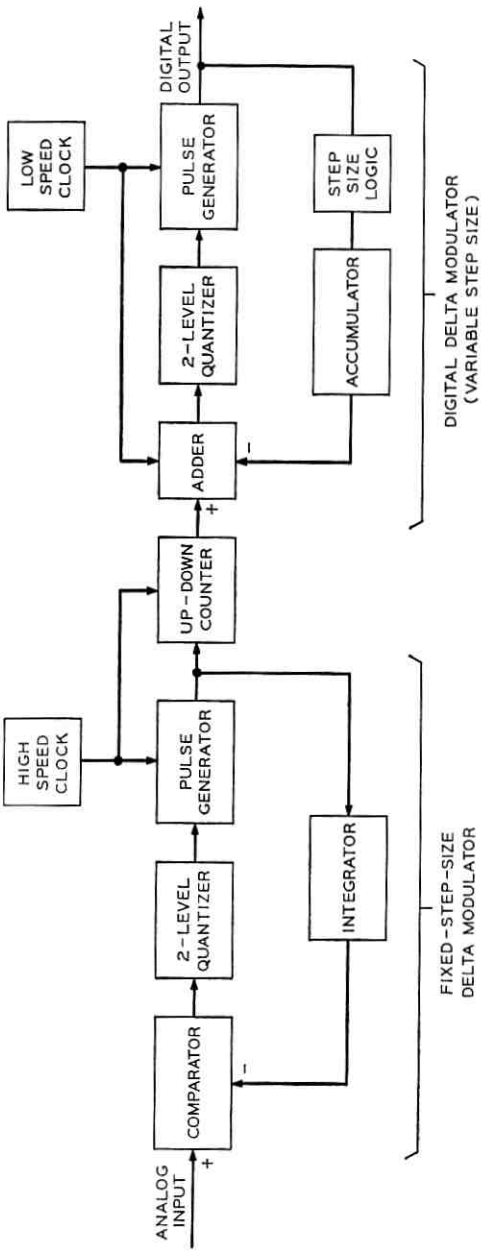

Fig. 1—Functional block diagram.

rent and previous binary outputs. If the binary outputs are identical, the current step size is 1.5 times the previous step size; if they differ, it is 0.66 times the previous step size. In addition to the output rate of the digital delta modulator, the design parameters in Fig. 1 are the step size and sampling rate of the fixed-step-size delta modulator. In our simulations, the product of step size and sampling rate, and thus the maximum slope of the delta modulator, was held constant. This constant was chosen on the basis of previous simulations by Jayant of fixed-step-size delta modulators operating on the speech tapes used in our simulations.

Our results are shown in Fig. 2 as curves of output signal-to-noise ratio (S/N) plotted against the sampling rate of the fixed-step-size delta modulator for two different output rates. It is not surprising that for low sampling rates of the first delta modulator, it is the error performance of this device that largely determines the overall S/N. As the sampling rate increases, the integrated output of the fixed-step-size delta modulator becomes arbitrarily close to the analog input and the asymptotic S/N is identical to that of an adaptive delta modulator operating directly on the analog input. (A separate simulation has verified this statement.) The simulation results are quite encouraging

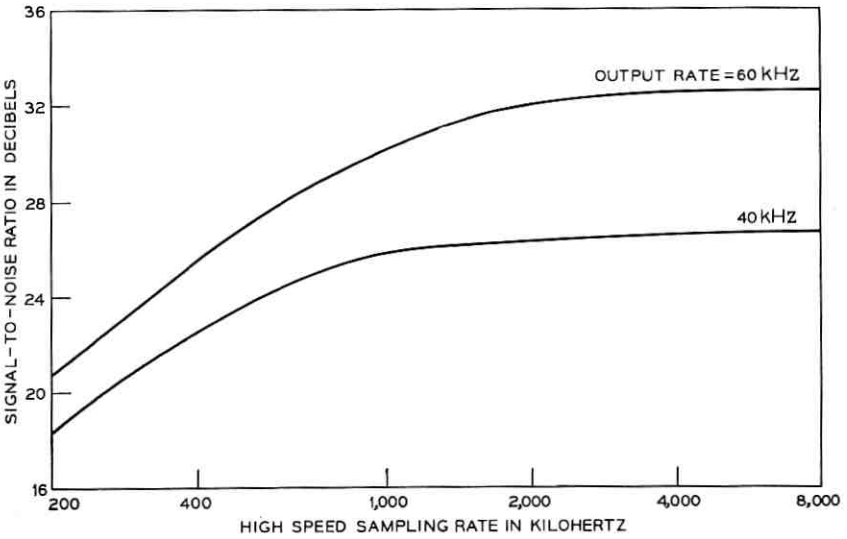

Fig. 2—Performance characteristics.

because they show that for the output rates considered, which are in the range of practical interest, the high-speed sampling rate required for negligible performance degradation relative to a conventional implementation is well within the state of the art.

By contrast with this empirical means of determining the rate and step size of the high-speed delta modulator, one may take the following conservative approach: (*i*) Set the step size at the minimum step size of the adaptive delta modulator, thus assuring that the quantizing resolution is not compromised and (*ii*) let the high-speed clock rate be the final output rate times the ratio of maximum to minimum step size so that the maximum slope is not reduced. A typical ratio of maximum to minimum step size is 128:1 so that with an output rate of 64 kb/s, the fixed-step-size delta modulator is required to operate at 8,192 kHz according to this conservative criterion.

IV. PRACTICAL IMPLEMENTATION

Figure 1 is a functional block diagram which indicates the required signal processing operations. In a hardware implementation, considerable simplification is possible. The up-down counter and the adder and accumulator of the digital delta modulator may be combined in a single accumulator as shown in Fig. 3. This accumulator is modified by $+1$ or -1 for each sample of the fixed-step-size delta modulator and it changes by the magnitude of the step size at each output sampling instant.

The two-level quantizer determines the polarity of each output pulse according to the state of a single bit of the accumulator. The step-size logic provides a digital representation of the current step size. Various means of providing this indication are possible, each appropriate to a different scheme of step-size variation. One method involves choosing the step size from a "dictionary" according to the output state of the adaptation logic. This technique lends itself to implementation by means of a "table-look-up" from a set of read-only memory registers, each containing one of the possible step sizes. Another technique is to specify the current step size as an arithmetic function of the previous step size—for example a multiple of or incremental change from the previous step size. For this type of adaption, the digital delta modulator could conveniently contain a step-size register which is arithmetically modified according to the output of the adaptation logic.

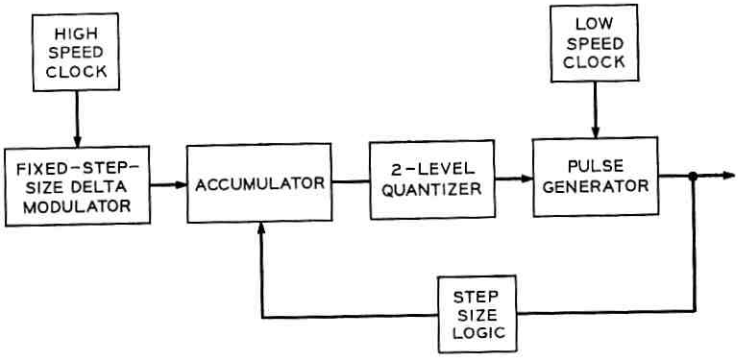

Fig. 3—Simplified implementation.

V. CONCLUSION

The technique described in this paper combines the simplicity of analog-to-digital conversion provided by fixed-step-size delta modulation with the code efficiency of variable-step-size delta modulation. Only a single step size need be precisely controlled with analog hardware; the step-size variation is controlled digitally, and is therefore exact. The technique lends itself to any scheme of step-size variation and any means of fixed-step-size, single-integration delta modulation.

REFERENCES

1. de Jager, F., "Delta Modulation, A Method of PCM Transmission Using 1-Unit Code," Philips Res. Rep., *7*, No. 6 (December 1952), pp. 442–466.
2. Kimme, E. G., and Kuo, F. F., "Synthesis of Optimal Filters for a Feedback Quantization System," IEEE Trans. Circuit Theory, *CT-10*, No. 3 (September 1963), pp. 405–413.
3. Brainard, R. C., and Candy, J. C., "Direct Feedback Coders: Design and Performance with Television Signals," Proc. IEEE, *57*, No. 5 (May 1969), pp. 776–786.
4. Winkler, M. R., "High Information Delta Modulation," IEEE Int. Conv. Record, *11*, Part 8 (March 1963), pp. 260–265.
5. Bosworth, R. H., and Candy, J. C., "A Companded One-Bit Coder for Television Transmission," B.S.T.J., *48*, No. 5 (May–June 1969), pp. 1459–1479.
6. Jayant, N. S., "Adaptive Delta Modulation with a One-Bit Memory," B.S.T.J., *49*, No. 3 (March 1970), pp. 321–342.
7. Schindler, H. R., "Delta Modulation," IEEE Spectrum, *7*, No. 10 (October 1970), pp. 69–78.
8. Greefkes, J. A., "A Digitally Companded Delta Modem for Speech Transmission," IEEE Int. Conf. Commun. Record, 1970, pp. 7.33–7.48.
9. Goodman, D. J., "The Application of Delta Modulation to Analog-to-PCM Encoding," B.S.T.J., *48*, No. 2 (February 1969), pp. 321–343.

THE BELL SYSTEM TECHNICAL JOURNAL
Vol. 50, No. 4, April, 1971
Printed in U.S.A.

Statistical Techniques for Talker Identification

By P. D. BRICKER, R. GNANADESIKAN, M. V. MATHEWS, MISS S. PRUZANSKY, P. A. TUKEY, K. W. WACHTER and J. L. WARNER

(Manuscript received November 16, 1970)

This paper provides an overview of work on statistical formulations and analyses associated with the problem of identifying persons on the basis of spectral energy representations of acoustical utterances. The investigation has been largely empirical and the paper focuses on the statistical techniques and strategies that have been developed in the context of analyzing two sizeable bodies of data. The problems and procedures to be discussed include: (i) data condensation and representation; (ii) efficient and practical criteria for classification and discrimination; and (iii) strategies for automatic identification of talkers in relatively large populations.

I. INTRODUCTION

Many of us can perhaps recall the experience of identifying a caller on the telephone from a relatively short utterance such as the word "Hello." This might indicate that even short utterances contain sufficient information for identification, and it is an intriguing and interesting problem to inquire whether automatic, objective, accurate and economic methods can be developed for talker recognition. The authors of at least ten papers in the last eight years have reported experiments with (simulated) automatic talker recognizers. Using a variety of approaches to different aspects of the problem, these experimenters have met with strikingly similar success—90 percent (or more) correct recognition.

Previous studies may be classified into two groups according to whether the problem addressed was *verification* (is the speaker who he claims to be?) or *identification* (assignment of an unknown utterance to one person in a given group of speakers). While two studies of the first kind involved 34 voices or less,[1,2] the third[3] and most extensive

(118 voices) was most successful, achieving an average of 99 percent correct verifications. Four studies of the second type used quite different bases for identification in small (10–30 voices) populations, varying from spectral analyses of nasal sounds[4] or whole words[5,6] to measurements of phonological features.[7] Whereas all the above studies required the speaker to utter a prescribed text, three others have achieved from 90 to 100 percent correct identification with no constraints on what the speaker says, provided that a sufficient quantity of speech from each talker is available. Again, the procedures employed in these last three studies have differed widely: spectral analyses of whole speech[8] or of vowels only,[9] and intervals between extremal points in various frequency bands[10] were used with three different recognition schemes.

These results with small populations suggest that the speech signal contains so much information about the talker that one can be distinguished from among 30 or so by a variety of procedures, and that we cannot learn from these studies the relative merits of various ways of representing the signal and reaching a decision. The only one of these studies that used a hundred or more voices[3] required only that each unknown be assigned to one of two classes (genuine or impostor); there have been no studies of identification in large populations. This paper describes the evolution of work addressed to both the small- and large-population identification problems by a group of people, including the present authors, over the last few years. Aside from the present authors, others who have participated in different facets of this work are: Mrs. M. H. Becker, Mrs. L. P. Hughes, T. L. DeChaine, R. S. Pinkham and M. B. Wilk.

The work to be described here evolved empirically and experimentally in the context of analyzing two bodies of data. With no general theory being available to aid in designing a process for talker identification, this work relied heavily on the analysis of data not only to generate ideas and techniques of possible relevance but also to assess the performance of any scheme. Thus, the pragmatic criterion of observed proportions of correct recognition in the two bodies of data was utilized as the touchstone rather than any general theoretical optimality properties. The data analytic orientation in this problem proves to be practical and productive, and most of the successful ideas and methods are fairly obvious—especially after the fact!

The presentation of the data analysis and decision processes may be viewed in four parts: (*i*) *The data*—the two bodies of data studied will be described, the basic digital format of an acoustical utterance will

be described and displayed, and finally, some features of the data will be discussed. (*ii*) *Data condensation*—several primitive procedures will be mentioned for deriving manageably low-dimensional representations from the original data. (*iii*) *Definition of a space and metrics*—the unknown, and the various candidates for assigning it to, may be represented in the space of the summary data, and several metrics may be specified for measuring the distance between the unknown and the candidates for identification. (*iv*) *Classification schemes and strategies for identification*—i.e., procedures for assigning an unknown in a relatively small population of contending speakers, as well as statistical strategies for allocation in relatively large populations of speakers.

II. THE DATA

The two bodies of data involved in our study both deal with repeated utterances of single words. The first set of data (cf. S. Pruzansky[5] for a detailed description) is from ten talkers each of whom yielded several repetitions of ten words commonly used in telephone conversations. The actual utterances were excerpted from sentences in which the words were embedded and the talkers, in fact, read the sentences. For most talker-word combinations there were seven replications with only a few missing. (693 utterances were available instead of $700 = 10 \times 10 \times 7$.)

The second body of data, which was collected subsequent to promising results obtained with the first set of data, deals with a population of 172 speakers each of whom repeated each of five digit names (*one, two, three, four* and *nine*) five times. The words were uttered in isolation rather than being embedded in sentences. The second body of data involved many more speakers, fewer words and fewer replications relative to the first set of data.

Whereas the first set of recordings was made under carefully controlled conditions (see Ref. 5), the second set was made in an unattended booth in a busy concourse. Although a high-quality microphone was used, it was housed in a telephone handset, held a short (but variable) distance from the lips. Automatic equipment controlled a display in the booth which cued the talkers as to which digit name to say and when. In both cases, all utterances by a given talker were recorded in one session.

In the present report, the displays and examples are drawn from analyses of both bodies of data and the presentation will switch back and forth between the two sets of analyses.

The most raw form of the data is just the audio recordings. However, for purposes of analysis, the audio recordings were fed into an analog filter bank and the filter outputs were sampled at fixed, frequent intervals of time (10-millisecond intervals in the first body of data and 6-millisecond intervals in the second set). In the first set of data, the outputs from 17 frequency channels covering a range of 100 to 7000 Hz were retained; the first 16 channels were approximately equally spaced along a Koenig scale from 200 to 4000 Hz, while the 17th covered the range 4000 to 7000 Hz. In the second set of data, the outputs from 20 frequency channels spanning the range 20 to 2900 Hz were retained; the upper and lower cutoff frequencies of each of the 20 filters are shown on the abscissa of Fig. 5. Each audio utterance input thus yielded a certain number (17 in the first set of data and 20 in the second) of separate time series as outputs, with each series representing the energy in a specific frequency band as it varies across time. Together the series represent the short-time spectrum of the utterance.

Thus, the basic digital form of the data for an utterance consists of a matrix of spectral energies classified according to frequency bands in each of a sequence of time intervals. (see Pruzansky & Mathews[6] for a description of energy-frequency-time quantization.) Table I is an example of a data matrix from the second set of data. One can obtain pictorial representations of such a matrix. The classic representation is the sound spectrogram, which is unfortunately not in a form easily read by computers. Figure 1 shows a contour plot of log energy as a function of time and frequency; it was obtained as a computer printout from a data matrix. Although derived in a straightforward way from computer-readable data, this plot conveys some of the visual aspects of the sound spectrogram.

Some comments on certain aspects of the data are in order: (*i*) The total volume of data is large. (*ii*) The basic digital representation of

TABLE I—DATA MATRIX FOR AN UTTERANCE

	Time in milliseconds						
Frequency in Hz.	006	012	018	024	030	036	...
0–100	14	11	7	19	35	62	...
50–150	16	17	11	20	44	74	...
100–200	14	8	16	17	25	56	...
.	.	.	.	.	.	.	
.	.	.	.	.	.	.	
.	.	.	.	.	.	.	

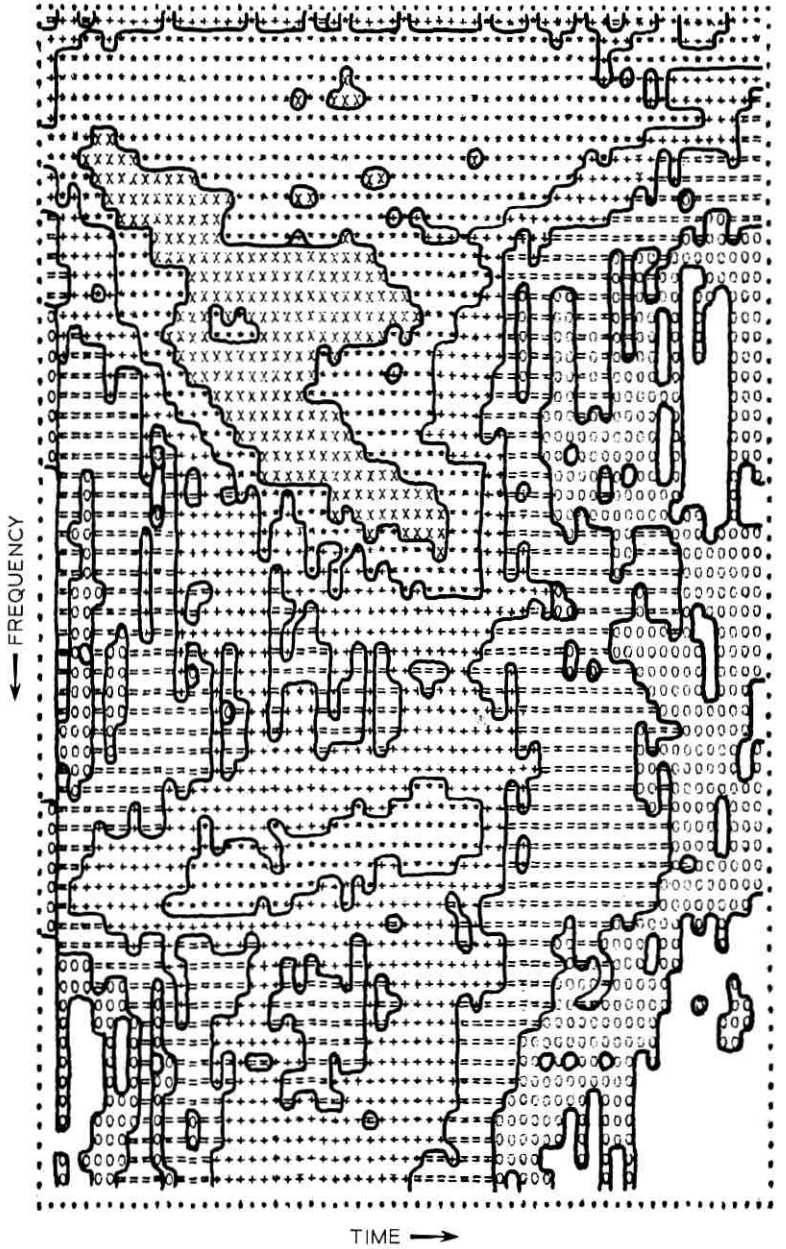

Fig. 1—Contour plot of log energy surface.

the data for an utterance is intractably high in dimensionality for performing statistical analyses. [For the first set of data the matrices were 17×50 (approx.), or 850-dimensional, per utterance; for the second they were 20×275 (approx.), or 5500-dimensional, per utterance!] (*iii*) The general level of the energies may shift from utterance to utterance of even the same speaker due to artefactual reasons. (Loudness may vary for example because of varying proximity to the microphone.) (*iv*) There is no natural time origin for the data and its specification is arbitrary in that what is labelled as time slot 1 does not depend on the actual commencement of the utterance; this implies a lack of alignment of the data for different utterances of a given word even by the same speaker.

The conjunction of the above four issues conveys certain implications for the subsequent analyses. First, it is essential, even for exploratory investigations, to pay attention to practicality and efficiency in computer procedures. Second, it is crucial to find effective lower-dimensional representations of the data using methods of summarization that will be of general utility both for different persons and for different words. Finally, adjustment must be provided for artefactual effects, such as energy-level variation and arbitrariness of the time origin. Such adjustments may be accomplished either by treating the data prior to analysis or by adopting analytical procedures which make provisions for the artefactual effects. Thus, for example, energy-level variation can be handled either by normalizing the energies so that their sum is unity for each utterance or by using classification procedures which allow for level changes amongst the replicated utterances of a speaker (cf. R. Gnanadesikan & M. B. Wilk[11]). Similarly, the arbitrariness of time origin may be handled either by pre-aligning the utterances by some criterion, such as the one used by Pruzansky[5] with the first body of data, or by using origin-invariant time information in later analyses.

III. DATA CONDENSATION

The high dimensionality of the basic quantitative representation of an utterance (viz., the matrix of spectral energies) is not only computationally untenable and conceptually difficult but also perhaps unnecessary. One would expect that the high physical and statistical correlations among the energies should imply redundancy. The limited number of replications available would, moreover, impose a mathematical constraint on usable dimensionality. For all these reasons, sum-

marization is necessary. The choices for summary statistics are legion and the consequences important. Various schemes for condensing the information in terms of manageably low-dimensional statistics were studied.

Table II shows a list of some of the types of information summaries that were investigated.

For instance, summarizing via the time margin means that one considers the energies (normalized) collapsed on to the time scale alone without any frequency breakdown. Similarly, frequency margin means that the energies (normalized) are summed over all the time intervals, thus eliminating the information about time variation of the spectrum. Looking at frequency slices implies the consideration of the energy distributions in each of the frequency channels. Within each of these ways of looking at the data, several alternate methods were investigated for summarizing the information. For instance, in studying the time margin both the energies themselves as well as characterizations of their distribution across time in terms of certain low-order moments (mean, standard deviation, etc.) were investigated. The distribution of energy within a frequency slice, however, was typified either by the deviations of its two tertiles (i.e., time values which divide the energy distribution into three equal parts) from the marginal time median or by the inter-tertile distance. These two time-dependent characterizations are origin invariant. (See Becker, et al.,[12] for more details concerning the reduction and analyses of first set of data.)

One of the important summaries, from the standpoint of performance in identification procedures, turns out to be the frequency margin normalized energies. This led to a 17-dimensional representation with the first body of data and a 20-dimensional representation in the

TABLE II—SUMMARIZATIONS OF DATA

(*i*) TIME MARGIN
- (*a*) Moments
- (*b*) Energies (normalized)

(*ii*) FREQUENCY SLICES
- (*a*) Tertile deviations from marginal median
- (*b*) Inter-tertile ranges

(*iii*) FREQUENCY MARGIN
- (*a*) Power spectral estimates derived from energies
- (*b*) Energies (normalized)

(*iv*) TIME × FREQUENCY
- (*a*) Moments
- (*b*) Variously grouped normalized energies

(*v*) VARIOUS COMBINATIONS OF INPUTS

second set. To illustrate how this summary representation may look, Figs. 2a and b each show the normalized energies in the frequency margin for all the utterances of a word by a specific talker. Figure 2a is for one speaker and Fig. 2b is for another. Qualitative and quantitative differences between the two speakers are evident as viewed against the relative cohesiveness of the different utterances within a speaker.

IV. SPATIAL REPRESENTATION AND CHOICE OF METRICS

Each scheme for summarizing the basic data leads to a set of input statistics whose values for each utterance yield a vector corresponding to that utterance. The analysis involved designating certain of the utterances from each speaker as unknown and treating the remaining utterances as the reference set of known utterances to be used for purposes of statistical estimation, etc., of the features of the reference population.

Thus, as shown in Table III, corresponding to the uth reference utterance (i.e., the talker is known) of a specific word by the ith talker, one would have a p-dimensional row vector of input statistics,

$$\mathbf{Y}'_{iu} = (y_{i1u}, y_{i2u}, \cdots, y_{ipu}); \quad i = 1, 2, \cdots, k, \quad u = 1, 2, \cdots, n_i,$$

where the jth element of the vector, y_{iju}, is the value of the jth input statistic for the uth utterance of the ith talker. There are k talkers in all and n_i known utterances from the ith talker. The n_i known utterances of the ith talker may then be used, as shown in Table III, to obtain the p-dimensional centroid, $\bar{\mathbf{Y}}'_i$, and the $p \times p$ covariance matrix, $\mathbf{S}_i$, for the ith talker.

Corresponding to an unknown utterance (i.e., the talker is unknown and is to be identified), which is known only to be an utterance of some one of the talkers in the study, one would similarly have a p-dimensional representation, shown in Table III as

$$\mathbf{Z}' = (z_1, z_2, \cdots, z_p).$$

Also shown in Table III are the overall centroid $\bar{\mathbf{Y}}'$ and two matrices $\mathbf{B}$ and $\mathbf{W}$. $\mathbf{B}$ is a measure of the dispersion of the speaker centroids in p-space and is called the between-talkers covariance matrix. $\mathbf{W}$ is a pooled measure of dispersion of the replicate known utterances around the talker centroids and is called the within-talkers covariance matrix.

If a metric or distance measure were defined in the p-dimensional space of the input statistics, then one could calculate the distance of the unknown, viz. $\mathbf{Z}'$, from each of the centroids, viz. $\bar{\mathbf{Y}}'_i$'s, of the

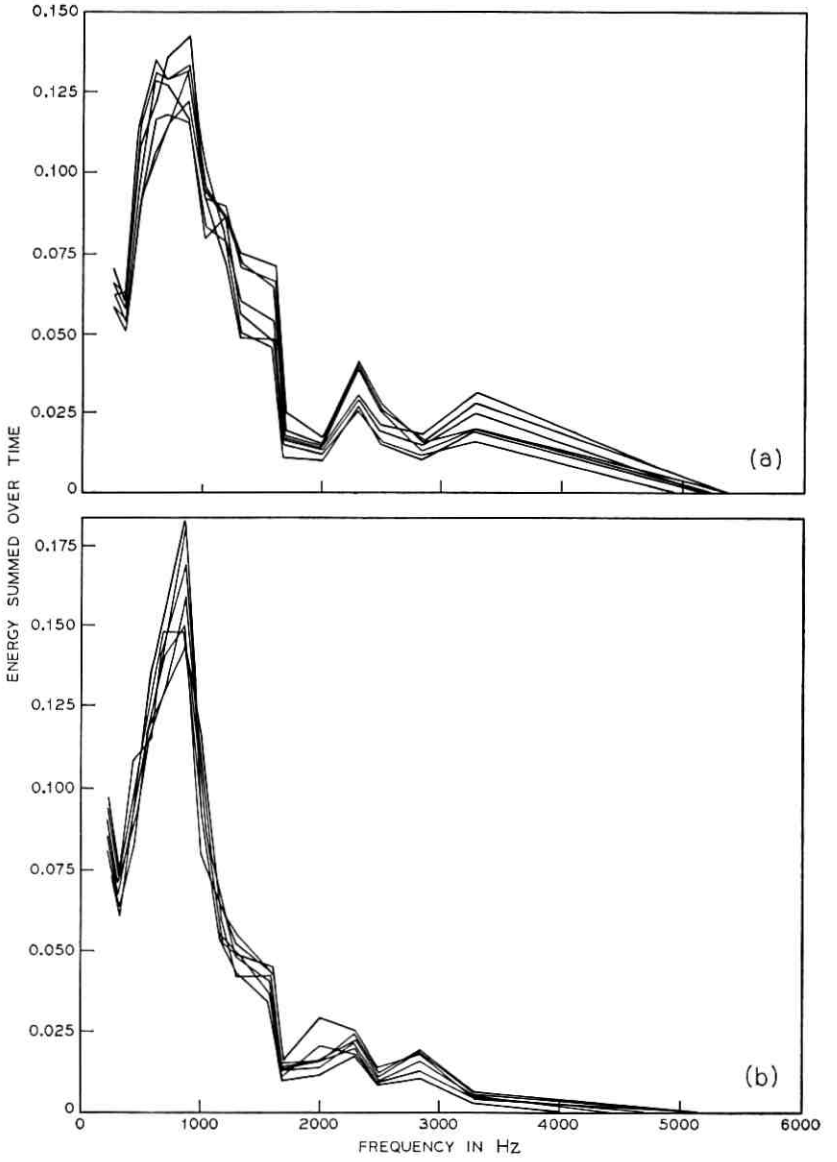

Fig. 2a—Frequency margin energy versus frequency (normalized data).
Fig. 2b—Frequency margin energy versus frequency (normalized data).

different talkers, and then use these distances to assign the unknown to one of the talkers.

All the measures of squared distance used in our work were positive semidefinite quadratic forms, a class whose typical member may be algebraically defined as shown in item (0) of Table IV. This class includes not only the familiar unweighted Euclidean squared distance ($\mathbf{M} = \mathbf{I}$) and the weighted Euclidean squared distance, which makes allowances for unequal variances of the different variables, but also measures of squared distance which allow for correlations among the variables. Figure 3, dealing with the case of two variables, shows an appropriate manner of measuring squared distance when the correlation is positive. According to such an elliptical measure of squared distance, points like A_1 and B_1 which lie on the same ellipse are considered to be the same distance away from the center C of the ellipse, whereas points like A_1, A_2 and A_3 which lie on the different ellipses numbered 1, 2 and 3 are considered to be at increasing distances away from C. The way to reflect this choice formally in the definition of squared distance is to use for $\mathbf{M}$ the inverse of an estimate of the covariance matrix of the variables.

Table IV also shows three specializations of the matrix $\mathbf{M}$ that lead to three squared distance measures D_1, D_2 and D_3 shown, respectively, as equations (1), (2) and (3).

The choice of $\mathbf{M}$ that leads to D_1 uses each talker's individual covariance matrix in measuring the distance of the unknown to that talker's

TABLE III—NOTATION AND ESTIMATES FOR REFERENCE SETS

(1) $\mathbf{Y}'_{iu} = (y_{i1u}, y_{i2u}, \cdots, y_{ipu}); \quad i = 1, \cdots, k, u = 1, 2, \cdots, n_i.$

(2) $\bar{\mathbf{Y}}'_i = \frac{1}{n_i} \sum_{u=1}^{n_i} \mathbf{Y}'_{iu}; \qquad \mathbf{S}_i = \frac{1}{(n_i - 1)} \sum_{u=1}^{n_i} \{(\mathbf{Y}_{iu} - \bar{\mathbf{Y}}_i)(\mathbf{Y}_{iu} - \bar{\mathbf{Y}}_i)'\}; \quad i = 1, \cdots, k.$

(3) $\mathbf{Z}' = (z_1, z_2, \cdots, z_p).$

(4) $\bar{\mathbf{Y}}' = \frac{1}{n} \sum_{i=1}^{k} n_i \bar{\mathbf{Y}}'_i$, where $n = \sum_{i=1}^{k} n_i$,

$$\mathbf{B} = \frac{1}{(k-1)} \sum_{i=1}^{k} n_i \{(\bar{\mathbf{Y}}_i - \bar{\mathbf{Y}})(\bar{\mathbf{Y}}_i - \bar{\mathbf{Y}})'\},$$

$$\mathbf{W} = \frac{1}{(n-k)} \sum_{i=1}^{k} (n_i - 1)\mathbf{S}_i.$$

TABLE IV—METRICS

(0) $D(i) = (\mathbf{Z} - \bar{\mathbf{Y}}_i)'\mathbf{M}(\mathbf{Z} - \bar{\mathbf{Y}}_i); \quad i = 1, 2, \ldots, k.$
$\mathbf{M}$ is p.s.d. so that $D(i) \geqq 0$.

(1) $\mathbf{M} = \mathbf{S}_i^{-1}; \quad D_1(i) = (\mathbf{Z} - \bar{\mathbf{Y}}_i)'\mathbf{S}_i^{-1}(\mathbf{Z} - \bar{\mathbf{Y}}_i); \quad i = 1, 2, \ldots, k.$

(2) $\mathbf{M} = \mathbf{A}_r\mathbf{A}_r'$, where $\mathbf{A}_r$ is $(p \times r)$ with r eigenvectors of $\mathbf{W}^{-1}\mathbf{B}$ for columns $(r = 1, 2, \ldots, t)$;
$D_2(i) = (\mathbf{Z} - \bar{\mathbf{Y}}_i)'\mathbf{A}_r\mathbf{A}_r'(\mathbf{Z} - \bar{\mathbf{Y}}_i); \quad i = 1, 2, \ldots, k.$

(3) $\mathbf{M} = \mathbf{W}^{-1}; \quad D_3(i) = (\mathbf{Z} - \bar{\mathbf{Y}}_i)'\mathbf{W}^{-1}(\mathbf{Z} - \bar{\mathbf{Y}}_i); \quad i = 1, 2, \ldots, k.$

centroid. This choice of $\mathbf{M}$ implies that the covariance matrix for each talker be nonsingular. This in general requires that the number of known utterances for every talker is at least one more than the number of input statistics. If p were large, therefore, in order to use D_1 one would require a large number of known utterances (replications) for each talker.

Also, this choice for $\mathbf{M}$ means that $\mathbf{M}$ changes from talker to talker with a consequent increase in computational time and effort. The hope is that there will be a pay-off in terms of efficiency to be gained from using a distance measure that is sensitive not only to the location (centroid) features of a talker but also to his individual covariance pattern. The use of this distance measure is thus particularly appropriate when different speakers do not have the same covariance matrix for their replicate utterances.

A second choice for $\mathbf{M}$, leading to D_2 in equation (2) of Table IV, is provided by the so-called discriminant analysis approach of multivariate statistical analysis. Here $\mathbf{M}$ is the product of a matrix by its transpose and the columns of the matrix are eigenvectors obtained from a discriminant analysis. The discriminant analysis attempts to reduce the number of dimensions in the space in which distances are measured by selecting a subspace which in a sense contains the most important information for discrimination purposes.

Broadly speaking, statistical discriminant analysis is concerned, in part, with finding a representation of the data from several prespecifiable groups (talkers) in terms of coordinates which separate the group centroids maximally relative to the variation within groups. Specifically, as shown in Table V, if $y_1, \cdots, y_p$ denote the variables in the initial p-dimensional representation of an utterance, then at the first stage one considers a linear combination, x, of the original coordinates. A one-way analysis of variance for this derived variable would lead to the F-ratio shown, where $\mathbf{B}$ and $\mathbf{W}$ were defined earlier. One can now

specify maximization of this F as a criterion for choosing the coefficients $(a_1, \cdots, a_p)$ in the linear combination. The required solution is to choose, for $\mathbf{a}$, the eigenvector corresponding to the largest eigenvalue of $\mathbf{W}^{-1}\mathbf{B}$. Having chosen one linear combination, a second different from the first may be sought so that its F-ratio will be maximized and so on. This method of seeking a linear transformation involves the eigenanalysis of $\mathbf{W}^{-1}\mathbf{B}$. There will be t positive eigenvalues, $c_1, c_2, \cdots, c_t$, in general, where t is the smaller of p and $(k-1)$. This is a consequence of the fact that if k (the number of talkers) is less than p (the dimensionality of the input data), then the k talker centroids are contained in a $(k-1)$-dimensional hyperplane. At any rate, one can use each eigenvector that corresponds with one of the nonzero eigenvalues to obtain the new coordinates $x_1, x_2, \cdots$. The space of x's may be called the *discriminant space* and the coordinates, $x_1, x_2, \cdots$ called *discriminant coordinates*, or CRIMCOORDS.

A geometrical interpretation of the discriminant analysis for the case of two variables is shown in Fig. 4. Centroids of the known talkers are shown in Fig. 4a surrounded by an ellipse indicating the distance measure appropriate to $\mathbf{W}$, the pooled within-talkers covariance matrix. The discriminant measure of distance is equivalent to: (*i*) transforming the space of Fig. 4a to one in which the ellipses have become circles by suitably compressing or expanding and reorienting the various coordinates—this space, with axes y_1^* and y_2^*, is shown in Fig. 4b; (*ii*) rotating the coordinates y_1^* and y_2^* in Fig. 4b so that the speaker centroids have maximum mean square separation in the direction of the first coordinate (x_1), next smaller separation in the direction of the

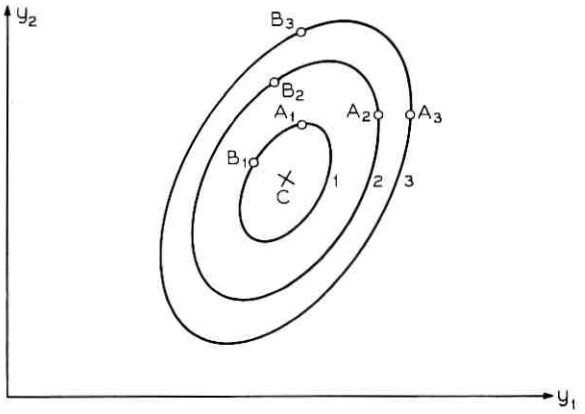

Fig. 3—Elliptical measure of squared distance.

TABLE V—STATISTICAL DISCRIMINANT ANALYSIS

(1) $\mathbf{y}' = (y_1, y_2, \ldots, y_p)$.

(2) $x = a_1y_1 + a_2y_2 + \ldots + a_py_p = \mathbf{a}'\mathbf{y}$.

One-way Analysis of Variance

	D.F.	M.S.
Between Talkers	$k - 1$	$\mathbf{a}'\mathbf{B}\mathbf{a}$,
Within Talkers	$n - k$	$\mathbf{a}'\mathbf{W}\mathbf{a}$,

$F_{\mathbf{a}} = \mathbf{a}'\mathbf{B}\mathbf{a}/\mathbf{a}'\mathbf{W}\mathbf{a}$.

(3) Choose $\mathbf{a}$ so as to maximize $F_{\mathbf{a}}$,
Solution: $\mathbf{a} = \mathbf{a}_1$ the eigenvector of $\mathbf{W}^{-1}\mathbf{B}$ corresponding to its largest eigenvalue.

(4) $c_1 \geqq c_2 \geqq \ldots \geqq c_t > 0, \quad t = \min(p, k - 1)$.
$\updownarrow \quad \updownarrow \qquad \updownarrow$
$\mathbf{a}_1 \quad \mathbf{a}_2 \quad \ldots \quad \mathbf{a}_t$

(5) $x_1 = \mathbf{a}_1'\mathbf{y}, \quad x_2 = \mathbf{a}_2'\mathbf{y}, \quad \ldots$.

second coordinate (x_2), etc; and (*iii*) measuring simple Euclidean distances in the space thus derived. (Note: With more than two variables, one may decide to use only the subspace formed from the first r coordinates of the discriminant space.) Discriminant analysis makes more intuitive sense if the individual talkers all have similar covariance matrices for their repeated utterances (so that each is similar to the pooled covariance matrix) than if they have widely differing covariance matrices.

The measure of squared distance, D_2, is just that Euclidean squared distance measure in the space of the first $r(\leqq t)$ CRIMCOORDS. While $\mathbf{M}$, chosen thus, does not change across talkers, yet it does depend on r, the number of eigenvectors to be used in the discriminant analysis approach. This use of an increasing number of the eigenvectors implies diminishing returns and may not necessarily improve the identification. By trial and error, a satisfactory value of r when the frequency margin energies were used as the initial variables was found to be 5 in the first body of data and 10 in the second set.

A third choice for $\mathbf{M}$, leading to the squared distance measure D_3 of equation (3) in Table IV is obtained by taking $\mathbf{M}$ equal to the inverse of the pooled within-talkers covariance matrix $\mathbf{W}$, defined earlier. This choice of $\mathbf{M}$, which requires $\mathbf{W}$ to be nonsingular, is in general possible whenever the number of input statistics, p, does not exceed the total number of known utterances of all talkers minus the number of talkers. This constraint on p (or, equivalently, on the number of known utterances) is far less restricting than the constraint on p imposed by the choice of $\mathbf{M}$ that leads to D_1.

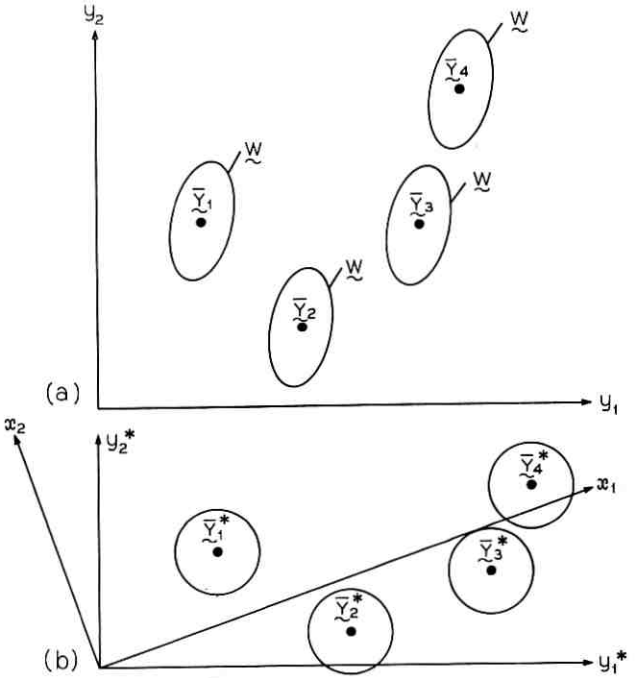

Fig. 4—Sketch to indicate geometrical interpretation of discriminant analysis.

There are certain relationships and equivalences amongst these three measures of squared distance. D_1 and D_3 are similar ellipsoidal measures (in the sense of Fig. 3) of squared distance and are identical if the talkers all have the same covariance matrix for their repeated utterances. Using $r = t$, the "maximum" number of eigenvectors from the eigenanalysis of $\mathbf{W}^{-1}\mathbf{B}$ would make D_2 entirely equivalent to D_3. Furthermore, D_3 is entirely equivalent to a discriminant analysis approach with a pairwise comparison of the distances of the unknown utterance from the centroids of the talkers considered in all possible pairs.

Other metrics, which were approximations to D_1, D_2 and D_3 in varying degrees of appropriateness and simplicity, were also investigated, but the results to be presented here are confined to these three measures.

V. IDENTIFICATION SCHEMES

5.1 *Classification Procedures for Small Populations of Talkers*

The distance measures are used for assigning an unknown utterance

to one of the speakers. For relatively small populations of speakers, one can compute the distance of an unknown from each of the speaker centroids, using any measure of distance, and then assign the unknown to the speaker whose centroid is closest. The empirical criterion used for evaluating the operating characteristics of any combination of input data and distance measure was the percent of unknowns that were correctly identified.

Table VI, based on the findings of the analysis of the first body of data, shows a summary table of percent correctly identified, for some of the different data summaries, when used with the three squared

TABLE VI—SUMMARY OF AVERAGE PERCENT CORRECT FOR VARIOUS TALKER IDENTIFICATION TECHNIQUES USED WITH FIRST BODY OF DATA

Input Statistics	Distances		
	D_1	D_2	D_3
Time Margin			
Moments	34†	55	62*
Energies	—	30	34
Frequency Slices			
Deviation of Tertiles from Median (TER)	—	82	—
Inter-Tertile Range (ITR)	—	67	—
Frequency Margin			
Power Spectral Estimates	—	73	—
Energies	—	91	97*
Time × Frequency Groupings			
μ_f, σ_f^2, σ_t^2, σ_{ft}, N_{50}	30†	—	—
2 × 17	—	86	100†
2 × 7	—	83	90†
2 × 3	—	57	70†
3 × 2	—	47	50†
16 × 2	—	40	40†
Combinations of Inputs			
Frequency Energies + Time Moments	—	91	97*
Frequency Energies + Time Energies	—	83	90
Frequency Energies + ITR	—	88	—
Frequency Energies + TER EIG	—	—	93
Frequency Energies + ITR EIG	—	—	94
Combinations of Eigenvector Transforms (EIG)			
Frequency Energies EIG + TER EIG	—	87	—
Frequency Energies EIG + ITR EIG	—	94	93
Combinations of Words	—	98	—

* All utterances of each word used as unknowns.
† Only used word 1.

distance measures D_1, D_2 and D_3. The dimensionality of several of the inputs was too high, relative to the number of replicated utterances available per talker, so that D_1 could not be used with these inputs. Dashes in the table denote such cases and others, wherein the particular combinations of input and distance measure were not studied.

As far as the distance measures are concerned, D_3 appears to perform best. However, D_2 because of the reduced dimensionality associated with it, and D_1 because of its sensitivity to variations in the dispersion characteristics of the talkers, may be more appropriate and efficient for some uses and should not necessarily be discarded.

The general conclusion to be drawn from the various attempts to summarize the original data in terms of input statistics appears to be that, by and large, frequency information is more important than time information. This is evident from the low percentages of correct identification (30 percent and 34 percent) for the time margin energies, at one extreme, and the high ones of 91 percent and 97 percent for the frequency margin energies, at the other extreme. The results for the various time-by-frequency groupings also suggest the same conclusion. As the time structure increases, the percent correctly identified decreases (cf. also Pruzansky & Mathews[6]). Certain schemes for using the time information as an adjunct to frequency information, however, do seem promising. Thus, using D_2, one achieves 91 percent correct identification on the basis of frequency margin energies alone, whereas an increase to 94 percent is possible by augmenting the frequency margin information with certain kinds of time information from the frequency slices.

A general indication of the results shown is that significant improvement may be achieved by using appropriate statistical methods for the choice of both the input statistics and the distance measures. Thus, for example, using the normalized energies in the frequency margin as a summary of the data, one could go from 91 percent correct identification to 97 percent by using D_3 instead of D_2, thus achieving a reduction in error rate by a factor of 3.

5.2 *Strategies for Large Populations*

Encouraged by the results of the first analysis, we undertook the collection of the second body of data. In order to simulate more practical situations, the recording conditions were not as strictly controlled this time and we also decided to increase the number of speakers and to prune the number of replications per speaker. The increase in the size of the speaker population introduces an immediate challenge for

the analysis. Even with the aid of modern high-speed computers, the effort required for comparing the distances of the unknown from every talker centroid would become prohibitive with a very large number of talkers. For this case of a large number of talkers, which is of great practical interest, one has to develop a method for limiting the number of contenders for assignment of an unknown.

The approach to be described next in broad outline is simple and seems to be effective for accomplishing the task with the 172 speakers involved in the second body of data. For the present discussion, only the normalized frequency margins (viz., the 20-dimensional input) will be used as the representation of any utterance.

The basic idea is to use the first few CRIMCOORDS for restricting the set of speakers with whom an unknown is to be compared. Before describing the essential nature of the approach, it is perhaps in order to comment on some properties of CRIMCOORDS as related to the present problem.

Firstly, there is the question of interpretability. Figure 5 shows a pictorial representation of the five eigenvectors of $\mathbf{W}^{-1}\mathbf{B}$ that correspond to the first five CRIMCOORDS. The lengths of the bars correspond to the magnitudes of the elements of a specific eigenvector and the orientations correspond to their signs. The first CRIMCOORD, which seems to be largely a difference between the energies in the two lowest frequency bands, appears to be reflecting a difference between male and female glottal fundamental frequencies for the early vowel part of the word *one*, which was the word that gave rise to the set of eigenvectors in Fig. 5. The first CRIMCOORD does indeed efficiently separate male and female speakers in the study. Unfortunately, the second and later CRIMCOORDS do not seem to have as easy an interpretation, perhaps due to the mathematical constraints imposed on the eigenvectors at the later stages.

The linear transformation to CRIMCOORDS is dependent on only the reference set of known utterances. It is perhaps interesting to inquire about the validity of the pooling of the separate within-talker dispersion matrices to obtain the pooled estimate $\mathbf{W}$ of variation among the replicate utterances. The pooling also underlies the justification for using unweighted Euclidean squared distance (viz., D_2) in the CRIMCOORDS space. An internal comparisons statistical technique was developed (cf. R. Gnanadesikan and E. T. Lee[13]) for assessing the comparability of the individual talker covariance matrices in terms of certain measures of their sizes. This method of assessment, when used with the frequency margin energies, suggested

that it is not unreasonable to pool the speaker dispersions to obtain **W**.

A third issue concerning CRIMCOORDS is their stability as they depend on the words and on the speakers. Based on an empirical investigation using the second body of data, they do seem to be word dependent but fairly stable with respect to the speakers, in that they do not seem to change substantially once they are based on the known utterances from about 80 speakers.

Returning now to the question of using the first few CRIMCOORDS for limiting the contenders for an unknown, one can look at a representation of the knowns in the space of say the first two CRIMCOORDS. As shown in Fig. 6, with only the ten speakers in the first study, some talkers are clearly separated (e.g., talkers 2, 4, 7 and 10) while others are clustered (e.g., talker 8 and 9) even in this two-

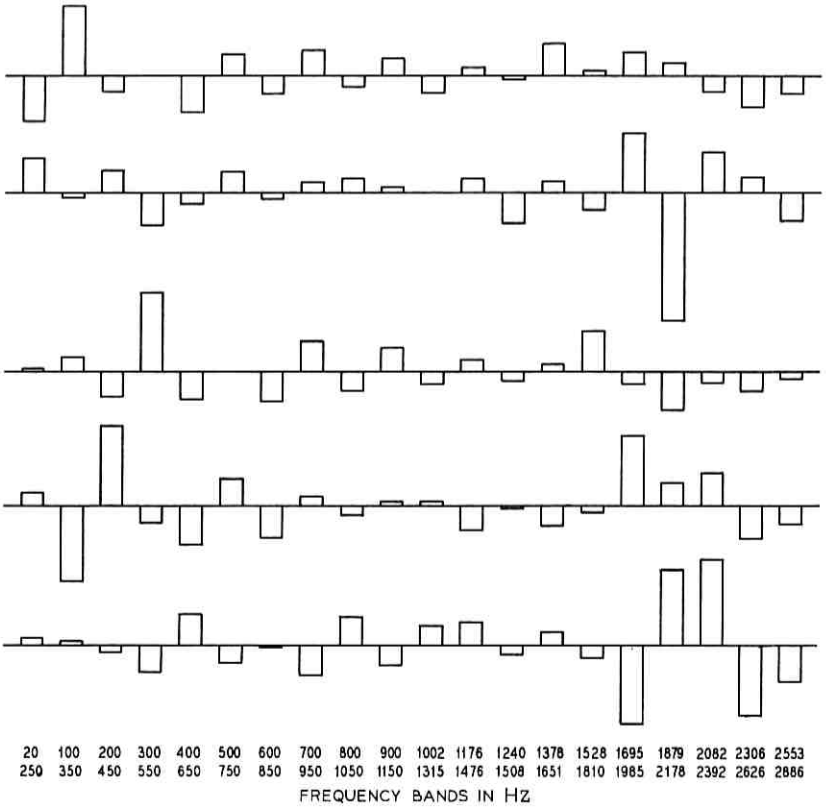

Fig. 5—First five eigenvectors of $\mathbf{W}^{-1}\mathbf{B}$.

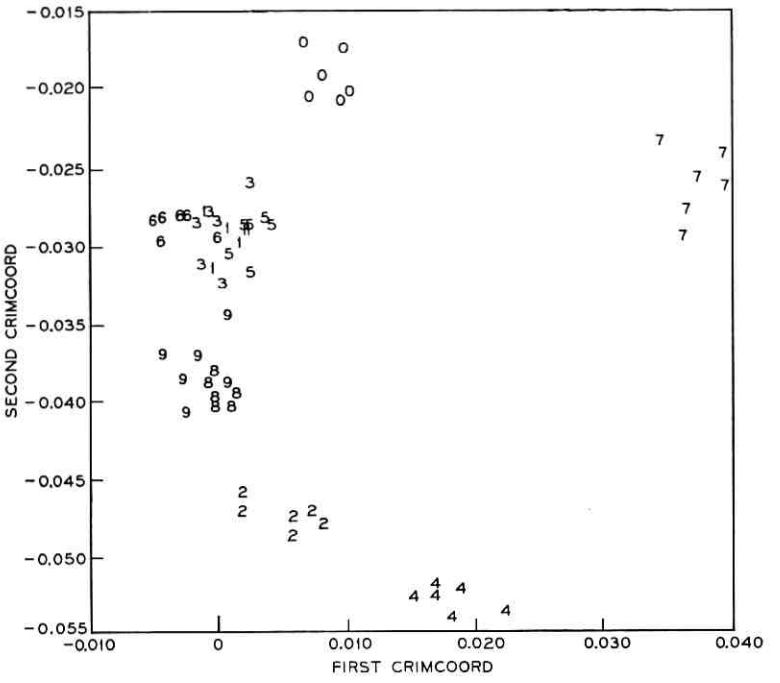

Fig. 6—Representation of utterances of ten speakers in space of first two CRIMCOORDS.

dimensional representation. However, with the 172 centroids of the talkers in the second set of data, one gets the configuration in Fig. 7a. There appear to be no obvious clusters here in the space of the first two CRIMCOORDS.

In this case, one approach is to divide the two-dimensional CRIMCOORDS space arbitrarily up into boxes as a first step. Figure 7b shows a division of the space into forty boxes which was accomplished by arbitrarily specifying nine quantiles (or percentage points) of the distribution of centroids along the first CRIMCOORD and three quantiles of the distribution along the second CRIMCOORD. Next, one determines in which of these boxes an unknown under consideration for assignment falls (cf. Fig. 7c) and then one can compare the unknown with all the speakers who fall in the same or a few nearby boxes (cf. Fig. 7d), discarding the speakers who are far removed. In the particular example used for Figs. 7a-d, while the 0 denotes the unknown, the x (cf. Fig. 7d) corresponds to the centroid

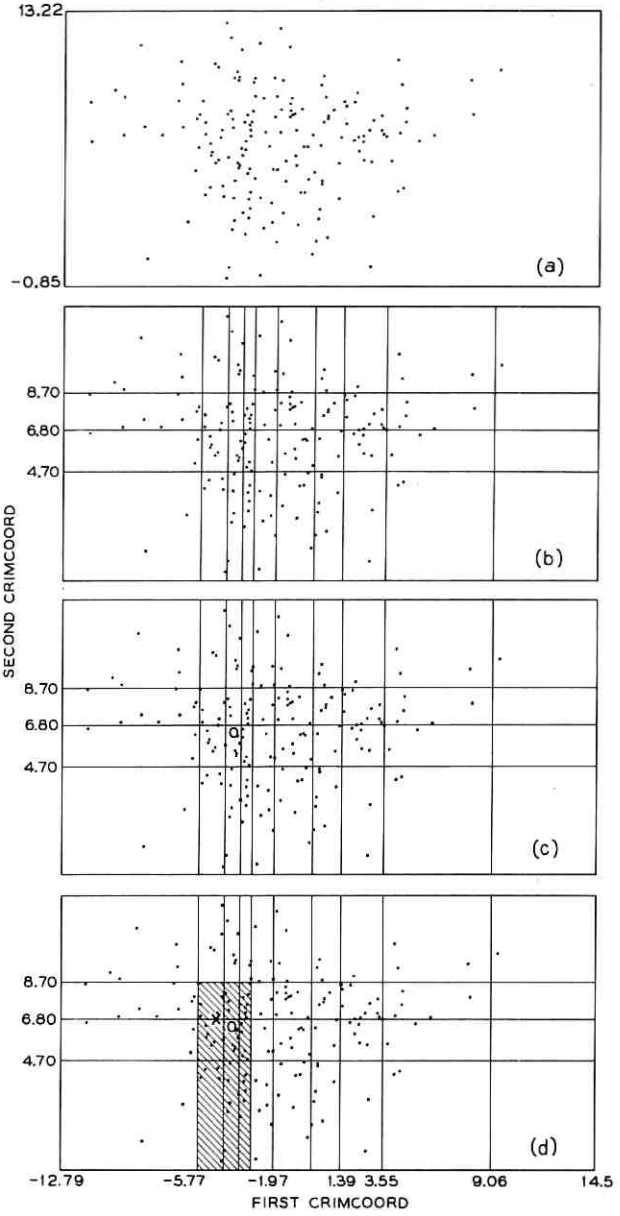

Fig. 7a—Centroids of 172 talkers in CRIMCOORDS space.
Fig. 7b—Division of CRIMCOORDS space into boxes.
Fig. 7c—Positioning of unknown (0).
Fig. 7d—Boxes searched initially (unknown, 0; corresponding talker centroid, X).

of the speaker from whom the unknown arose. While the x is not in the same box as the 0, it is in a neighboring box which is included for identification purposes.

The comparison of the unknown with the speakers in the neighboring boxes is made by calculating distances not just in the space of the first two CRIMCOORDS but by including additional CRIMCOORDS (e.g., using five or ten CRIMCOORDS in all). Based on the magnitude of the distance to the closest speaker and on the ratio of the second smallest distance to the smallest, a decision is made whether identifying the unknown with the closest speaker is safe or suspect. Statistical benchmarks for comparing observed values of quantities, such as the smallest distance or the ratio of the second smallest to the smallest distance, are obtained from "null" distributions (i.e., distributions of these quantities when a correct identification is made) generated from the data on hand. Since we are dealing with a situation in which there are sufficient data under "null" conditions (i.e., successful identification) one can obtain adequate estimates of the statistical distributions to enable reasonable assessments of the magnitudes of observed distances (or ratios) and decide whether they are small or large.

At any rate, either if an identification is suspect or if an insufficient number of comparisons have been made, the process enlarges the population of contenders by considering the speakers in additional boxes nearby. As soon as a safe identification is made, no further loops are made to add more contenders. After all the speakers have been exhausted, if the identification in terms of the closest speaker is still suspect, then the process terminates by identifying the speaker as the closest one, despite the weakness of the evidence. For the illustrative example in Fig. 7, this method led to a safe and correct identification.

Figure 8 shows a simple flow-chart of the steps involved in the above process for identifying an unknown by a preliminary limiting of the number of contenders. On the left, in Fig. 8, are shown the steps in the initial processing of the reference utterances leading to (*i*) a determination of the CRIMCOORDS, (*ii*) a representation of the speaker centroids in CRIMCOORDS space, and (*iii*) a specification of the boxes or cells in the space of the first few (e.g., two) CRIMCOORDS. On the right, in Fig. 8, is shown the identification process for an unknown utterance. From the representation of the unknown in CRIMCOORDS space, one finds which box the unknown falls into and retains for comparison all speakers whose centroids fall in a cer-

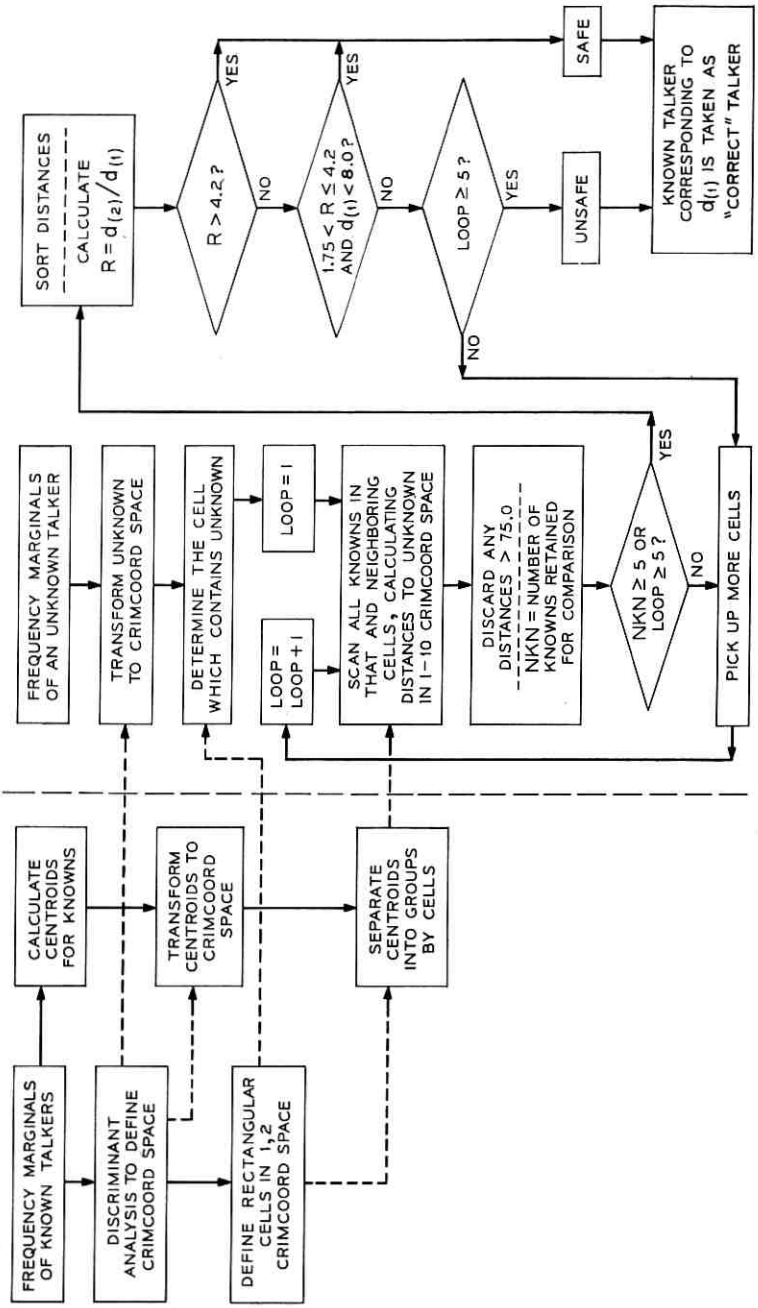

Fig. 8—Flowchart for strategic identification.

tain number of nearby boxes, while discarding all speakers who are farther away than a cut-off distance. If an adequate number of speakers have been retained for comparing the unknown against, then one computes the distance of the unknown from each of the retained speakers in an enlarged (5- to 10-dimensional) CRIMCOORDS space. If the ratio of the second smallest to the smallest is large enough (> 4.2), then the identification of the unknown with the closest speaker is assumed to be safe. Also, if this ratio is moderately large ($\leqq 4.2$ but > 1.75) and the smallest distance is small enough (< 8.0), the identification is deemed safe. If not, it is deemed suspect and more speakers in additional boxes are included for comparison with the unknown. Furthermore, if the number of speakers compared with an unknown is not large enough, then also one adds more speakers by considering additional adjacent boxes.

An efficient set of computer programs implementing this process is in use (cf. K. W. Wachter[14]). The programs provide for flexible specification of many of the parameters involved (e.g., number and size of the boxes, cut-off values for comparing the smallest distance or the ratio of the second smallest to the smallest, etc.).

Using a single word for identifying talkers in the second set of data, the above strategy yielded 81 percent correct identifications, i.e., for 81 percent of the unknowns the first most likely match was correct. In fact, if one counted the percent of times that the correct speaker was either the closest or second closest then one obtains 90 percent. The comparable percentages to these figures of 81 percent and 90 percent are 84 percent and 93 percent when one performs an exhaustive check of the unknown against every speaker. The computational cost for the exhaustive comparisons in this example involving 172 talkers, is about 70 to 90 percent more than that involved in the strategy based on preliminary limitation of the number of contenders for an unknown. The difference in computational cost will, of course, vary as one changes the number and size of the boxes chosen and the other specifications involved in the method. Also, with much larger populations of speakers, the cost differential between the two approaches would be expected to increase substantially. In the present example, the computer cost per identification is approximately 1.4 cents for the scheme which initially limits the number of contenders for an unknown.

The percentages of correct identification appear to be improvable by utilizing the identification information in additional words. Thus, instead of using the single word, *one*, when one combines the information from the separate identification results for the two words, *one* and *two*,

the percent correct identification moves up to 94 percent from the earlier stated 81 percent. Hence, the preferable direction for large populations appears to be to stay with the type of strategy described here but to combine information from more than one word.

Not all methods for combining the information from two or more words will be equally successful; however, a scheme has been developed which appears to be promising and, in fact, led to the improvement from 81 percent to 94 percent in percent correct identifications. Figure 9 shows a flowchart of the procedure. If the identification on the basis of the first word is deemed safe, then no use is made of the second word. If, on the other hand, the identification using the first word is suspect, then one looks at the identification results for the second word. If the same speaker is the closest one to the unknown utterances in both words, then this is taken as a safe indication that he is in fact

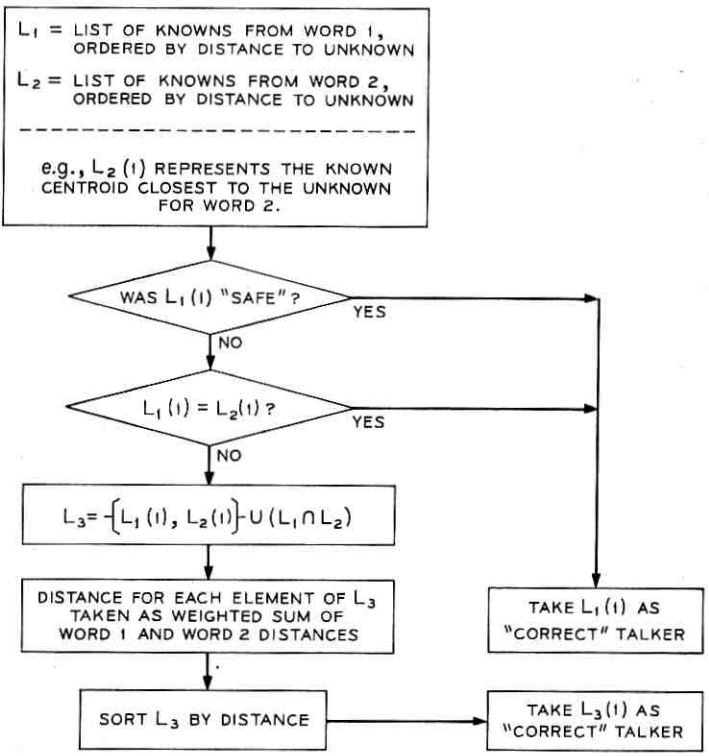

Fig. 9—Combination of word 1 and word 2 information into a single identification.

the speaker despite the weakness of the evidence for this in considering the first word by itself. If two different speakers turn out to be closest for the two words, then one considers these two speakers along with all speakers who appear concurrently on the lists of a certain number (e.g., 10) of closest speakers for both the words. For each of these speakers, one can compute a new squared distance by calculating a weighted sum of the squared distances of the speaker centroid from the unknown as obtained in the separate analyses of the two words. The weights for combining the squared distances could reflect the discrimination abilities of the two words. (Note: Implicit to this scheme is an assumption that the first word is more useful for discriminating talkers than the second.) The new squared distances may then be sorted and the identification would be made as the closest speaker in terms of this pooled measure of distance.

VI. DISCUSSION

The emphasis in the present report has been on the statistical facets of talker identification rather than on the acoustic significance of the results. The gratifying identification successes have been achieved, in fact, with relatively unsophisticated representations of the data (viz., energy-(time)-frequency analyses of whole words). We have already mentioned that interpretation of CRIMCOORDS beyond the first is elusive. At this juncture, we approach the relation between identification techniques and acoustic factors from the other end, asking what speech production theory and related experimental results have to say about augmenting or modifying our representations for future work.

In the course of replicating our second body of data, we encountered two factors which will be dealt with systematically in forthcoming studies. The first of these is inter-session variation within talkers. W. A. Hargreaves and J. A. Starkweather[8] as well as J. E. Luck[2] have reported that this effect is so strong as to render identification or verification significantly poorer when reference and test recordings are made at widely separated times. We are now collecting new recordings from talkers who return at scheduled times on different days, having found evidence of a sessions effect for those few talkers who returned to our unattended booth voluntarily. The other factor was "circuit variability." The collection of data from the unattended booth involved a second set of 172 speakers in addition to the set of 172 used in the earlier discussion in this paper. The samples from the two sets of speakers were, however, processed separately at two different times,

and the two sets of data could not be combined because of unrecoverable variations in the "circuit" (the process involved in going from the physical utterance to its digital representation, especially the behavior of the analog filter bank). Our approach to this problem is two-pronged: (*i*) We are using elaborate control and calibration procedures in making the new recordings, and obtaining our spectral energy representations directly from Fast Fourier Transforms performed on a digital computer. (*ii*) We shall deliberately vary the circuit (by making some telephone recordings simultaneously with the high-quality recordings and by passing them through switched connections) to learn how to make identification robust in the face of circuit variations.

Another major concern is with the use of information from different words and the number of replications required from each speaker for constituting the reference set of utterances. Both Pruzansky[5] and J. W. Glenn and N. Kleiner[4] found improvement when they combined utterances in the simplest way, at the level of spectral analysis. It is worth noting that the work of S. K. Das and W. S. Mohn,[3] the most successful of the verification studies, used separate analyses of ten different segments (of a fluently uttered phrase), while the other two[1,2] used only one or two. In connection with the question of number of replications, no statement about the ultimate resolving power of automatic voice identification schemes can be made until the relationship between performance and number-of-samples-known-to-be-from-one-talker is better understood.

Perhaps the gravest issue is whether measures thought to have acoustic or speech-theoretic significance should supplant or supplement raw spectral energy representations of the utterances. Examples of such measures, used with success by J. J. Wolf,[7] are glottal fundamental frequency, nasal resonance frequency, vowel formant frequencies, and voice-onset time in voiced stop-consonants. The basic argument for this approach is that a talker's uniqueness lies perhaps in the shape of his vocal apparatus, and we should use measures sensitive to that shape. Glenn and Kleiner,[4] taking an extreme position, maintain that nasal sounds are ideal because the apparatus is stationary during the time the oral passage is occluded and radiation is chiefly from the nose. Das and Mohn[3] worked with features chosen to be relevant to their acoustic segmentation, but no report on the relative merits of their many (405 in all) features is available.

One might well have reservations about using features which are significant in speech synthesis to perform talker recognition, because what is signal in the former problem may be noise in the latter. How-

ever, it is worth noting that some recent analysis-synthesis schemes for speech transmission (e.g., R. W. Schafer and L. R. Rabiner[15]) are reported to be capable of producing speech that sounds strikingly like the original, though based on only a few parameters per time sample. Although such resynthesized speech may not be capable of reflecting subtle variations of the shapes of intra-cranial cavities, it typically quite accurately reflects two important characteristics of the individual: his average "pitch" (glottal fundamental frequency) and the temporal pattern of changing glottal and formant frequencies.

"Pitch" is clearly a vital talker cue. The present work evolved a CRIMCOORD devoted to this characteristic even though our input data did not include an explicit measure of it. Wolf[7] found pitch to be the most important of his features, and B. S. Atal[16] based an entire small-population recognition scheme on it. We are investigating economical means of including such a measure in our future work.

As for the temporal aspect of utterances, it should be recalled that certain representations of time information did augment frequency information to advantage in the analysis of our first set of data. In fact, Gnanadesikan and Wilk[17] found that transforming the energies logarithmically (the common "decibel" transformation) improved the "additivity" of the frequency and time effects. Finally, it is worth learning how to use both time and "pitch" information for one very important reason: neither is unduly affected by common variations among speech transmission circuits, whereas the raw spectrum is very vulnerable.

The search for efficient representations of the speech signal is now at a choice-point. In one direction lies the extraction of features based on speech production theory, with its current high cost but the promise of robustness in the face of circuit variation and perhaps other sources of interference. In the other direction is the development of procedures for correcting obtained spectra to compensate for distortions due to the circuit, with a non-negligible cost and unknown ultimate technical feasibility. In the last analysis, technical and economic considerations will determine which of these types of representation will play the major role in practical talker identification techniques.

REFERENCES

1. Li, K. P., Dammann, J. E., and Chapman, W. D., "Experimental Studies in Speaker Verification, Using an Adaptive System," J. Acoust. Soc. Amer., *40*, No. 5 (November 1966), pp. 966–978.
2. Luck, J. E., "Automatic Speaker Verification Using Cepstral Measurements," J. Acoust. Soc. Amer., *46*, No. 4 (October 1969), pp. 1026–1032.

3. Das, S. K., and Mohn, W. S., "Pattern Recognition in Speaker Verification," AFIPS Conf. Proc., Fall Joint Computer Conference, *35* (1969), pp. 721–732.
4. Glenn, J. W., and Kleiner, N., "Speaker Identification Based on Nasal Phonation," J. Acoust. Soc. Amer., *43*, No. 2 (February 1968), pp. 368–372.
5. Pruzansky, S., "Pattern-Matching Procedure for Automatic Talker Recognition," J. Acoust. Soc. Amer., *35*, No. 3 (March 1963), pp. 354–358.
6. Pruzansky, S., and Mathews, M. V., "Talker-Recognition Procedure Based on Analysis of Variance," J. Acoust. Soc. Amer., *36*, No. 11 (November 1964), pp. 2041–2047.
7. Wolf, J. J., "Simulation of the Measurement Phase of an Automatic Speaker Recognition System," J. Acoust. Soc. Amer., *47*, No. 1 (January 1970), p. 83 (A).
8. Hargreaves, W. A., and Starkweather, J. A., "Recognition of Speaker Identity," Lang. & Speech, *6*, No. 2 (April–June 1963), pp. 63–67.
9. Smith, J. E. K., "Decision-Theoretic Speaker Recognizer," J. Acoust. Soc. Amer., *34*, No. 12 (December 1962), p. 1988 (A).
10. Ramishvili, G. S., "Automatic Voice Recognition," Engineering Cybernetics, (September–October 1966), pp. 84–90.
11. Gnanadesikan, R., and Wilk, M. B., "Data Analytic Methods in Multivariate Statistical Analysis," *Multivariate Analysis II*, (Editor, P. R. Krishnaiah), New York: Academic Press, pp. 593–638. (especially Section 4.)
12. Becker, M. H., Gnanadesikan, R., Mathews, M. V., Pinkham, R. S., Pruzansky, S., and Wilk, M. B., "Comparisons of Some Statistical Distance Measures for Talker Identification," Unpublished memo. [See also abstract in J. Acoust. Soc. Amer., *36*, No. 10 (October 1964), p. 1988.]
13. Gnanadesikan, R., and Lee, E. T., "Graphical Techniques for Internal Comparisons Amongst Equal Degree of Freedom Groupings in Multiresponse Experiments," Biometrika, *57*, No. 2 (August 1970), pp. 229–237.
14. Wachter, K. W., "Talker Recognition on Large Populations," Talk presented at the 78th Acoustical Soc. meetings in San Diego, November 1969. [See also abstract in J. Acoust. Soc. Amer., *47*, No. 1 (January 1970), p. 66.]
15. Schafer, R. W., and Rabiner, L. R., "System for Automatic Formant Analysis of Voiced Speech," J. Acoust. Soc. Amer., *47*, No. 2 (February 1970), pp. 634–648.
16. Atal, B. S., "Automatic Speaker Recognition Based on Pitch Contours," Polytechnic Institute of Brooklyn Doctoral Dissertation, June 1968.
17. Gnanadesikan, R., and Wilk, M. B., "Statistical Techniques for Effective Condensation of Talker Identification Data," Talk given at the European Regional Meetings of the Inst. of Math. Statist., September 1966. [See also abstract in Ann. Math. Stat., *37*, No. 5 (October 1966), p. 1415.]

THE BELL SYSTEM TECHNICAL JOURNAL
Vol. 50, No. 4, April, 1971
Printed in U.S.A.

Estimated Outage in Long-Haul Radio Relay Systems with Protection Switching

By W. Y.-S. CHEN

(Manuscript received November 24, 1970)

A general outage formula relating a number of important system outage factors has been derived for long-haul radio relay systems utilizing in-band or crossband automatic channel switching. This formula is used to estimate the outage of TD and TH systems with various switching strategies.

The results indicate that the crossband 2 × 18 protection-to-working channel switching system appears to be a very attractive arrangement from the standpoints of good system reliability and efficient use of the radio frequency spectrum.

I. INTRODUCTION

In order to achieve the high reliability demanded for long-haul TD and TH microwave radio relay systems, frequency diversity by automatic channel switching is used as an effective means to protect services against outages due to propagation, equipment failure, and maintenance activity. In this arrangement, each radio relay route is divided into a number of switching sections. One or two of the total number of radio channels in a given band are designated as protection channels. The automatic protection switching system uses protection channels to replace failed or otherwise unavailable regular channels by operating either IF or baseband switches at the transmitting and receiving ends of the switching section.

The first protection switching system developed for use with the long-haul TD-2 system (TDAS) is capable of protecting up to five regular working channels with one protection channel (1 × 5 switching).[1] It was first placed in service in 1953, and it accounts for about 45 percent of the long-haul radio switching systems now in the field. Another frequency diversity switching system was developed for application to the 6-GHz TH-1 system which was overbuilt on TD-2

routes or used on new routes. It was initially installed in 1960 and forms about 10 percent of the switches now existing in the field. This switching system uses two protection channels to protect up to six regular channels (2 × 6 switching).[2] About 1960, the TD-2 radio route capacity was expanded to a total of 12 channels through the use of channels placed interstitially between the original six assignments, and a second one-for-five switching system was initially required to provide protection for these interstitial channels. A much more reliable overall protection switching arrangement could be realized by combining the regular and the interstitial channels into a two protection and ten regular working channel system (2 × 10 switching), and accordingly, the 100A protection switching system was developed.[3] The 100A system was originally designed to operate with both the existing TD-2 system and the new solid-state TD-3 system. Subsequently, it was modified to provide 2 × 6 protection for the TH-3 system. Since 1964, the 100A system has become the primary heavy-route protection facility for the microwave network in this country.

Each switching installation is now operated exclusively either in the 4-GHz band (the TD systems) or in the 6-GHz band (the TH systems), and for reasons of reliability, with the exception of TDAS, two protection channels in each band usually are specified. Thus, a total of four channels out of 20 on a fully loaded route are reserved for system protection use. In order to utilize the frequency spectrum efficiently, the number of protection channels should be kept to a minimum consistent with the system requirements on reliability. The large-scale use of solid-state devices in TD-3 and TH-3 and higher fade margins achieved in these systems should result in less system outage* with present switching arrangements. This leads to reduced demand for protection channels and the observation that a reduction in the number of protection channels might be made possible by combining 4 and 6 GHz in one crossband switching operation because the fading correlation is relatively small between 4- and 6-GHz channels.

In this paper, outage is estimated for systems using various in-band and crossband diversity switching arrangements. A general expression for the system outage of a working channel is first derived considering the number of channels, fading, equipment failure, maintenance,

* In this paper, "outage" refers to the case in which the number of channels simultaneously unavailable because of fading, equipment failure, maintenance, or any other cause exceeds the number of protection channels. It therefore implies an interruption of service to one or more of the working loads.

and other outage factors. The derived formula is then applied to various TD and TH systems to estimate the reliability* to be achieved by automatic channel switching. Recommendations of switching strategies are made, based on comparison of reliabilities and utilization of the radio frequency spectrum.

II. OUTAGE FACTORS

2.1 *Selective Fading*

The most serious source of outage encountered in current 4- and 6-GHz microwave radio systems is considered to be selective fading caused by the multipath transmission of microwave signals. The mechanism and effects of multipath transmission have been discussed quite thoroughly in numerous articles published in the past two decades.[4–6] Selective fading is characterized by deep excursions of the received microwave signal level below its free space value. The time scale varies from a few seconds for large excursions (average duration of 40-dB fades) to a few hundred seconds for small excursions (average duration of 10-dB fades). The distribution of fading variation with time depends upon variable or temporary conditions in the transmission path in a complex manner. Enough data now exists to support an empirical formula relating the most important parameters.[4] Consideration of all pertinent and available selective fading data in general indicates that the fading distribution for a single hop is characterized by a fixed slope of 10 dB of fade per decade of probability for fade depth greater than 20 dB, i.e., the slope but not necessarily the amplitude of the Rayleigh distribution. Since this type of fading is frequency selective, the use of either frequency or space diversity would be effective in reducing its effect on outage.

2.2 *Flat Fading*

In addition to selective fading, there are occasional long periods of depressed signal in a microwave path caused by "earth bulge" or obstructive fading. This type of fading is rare and occurs only under substandard atmospheric conditions. In areas of high moisture content, stable calm air conditions at night and during the hours of early morning and ground fog are usually conducive to fading of this type. Widely separated frequencies and vertically spaced antennas are

* The term "reliability" is being used in the general sense and the more appropriate terminology might be "availability."

affected alike with regard to the average signal level (Ref. 6, page 72). Therefore, protection against flat fading can be accomplished only by providing adequate vertical path clearance and restricting the length of radio paths.

2.3 *Equipment Failure and Maintenance*

Unlike selective fading, the outages due to equipment failure and maintenance are of relatively long duration. Most microwave radio stations are unmanned, and therefore, the down time of a channel due to an equipment failure is longer than the average repair time actually used. Routine maintenance also increases the hazard of outages because the number of protection channels available in a system is reduced when routine maintenance is being done on any of the channels. It has been recognized that the equipment failures and maintenance can control the system outages in a long-haul system having only one protection channel.[7-9] In the past, inband frequency diversity with two protection channels has been used effectively for both fading and equipment protection. New solid-state systems are expected to be more reliable than vacuum tube systems. Thus, lower equipment outage rates would be expected from the newer TD-3 and TH-3 systems.

2.4 *FM Terminal Failure and Others*

Solid-state 3A FM terminal equipment together with solid-state 3A wire line entrance link equipment and the 200A protection switching system (a 1 × 12 baseband to IF system) have been introduced for maintenance and baseband circuit protection. Therefore, it is expected that the level of system outage resulting from terminal failures will be small.* Other system outage factors are power failure, human error, and switch failures.† These outages can be made small in a long-haul system.

III. ANALYSIS AND COMPUTATIONAL TECHNIQUES

Here we develop a method for the calculation of 4000-mile two-way annual outage resulting from the joint effects of selective fading, equipment failure, and maintenance for a radio system with auto-

* Reliability analysis of the FM terminals using a 200A switch indicates that the average outage from FM terminals in a 4000-mile system is less than 0.001%.[7]

† The effect of using protection channels for restoration and occasional TV service on system outage is a separate area of interest. No attempt has been made to study this effect in detail in this paper.

matic channel switching. It is noted that, without protection switching systems, the outage from the aforementioned factors in a 4000-mile route would be several hundred (about 800 in the 2 × 10 TD-2 system) times the total outage of the system with protection switching. Thus, these three factors are among the most important in the consideration of system reliability.

3.1 *Assumptions*

The basis of any estimation of the reliability of a system is a mathematical model of that system. Assumptions are made as to the behavior of this model which we expect will give the model the attributes of the working system. The following assumptions were made in the study of radio system reliability:

3.1.1 *Fading and Fading Frequency Correlation*

Fading rates are based on the MIDAS 1966 West Unity data.[4] These data, shown for a 68-day summer period (July 22 to September 28, 1966) are given in Fig. 1. The average fading rate shown in the figure represents the percent probability of the signal being faded to a certain depth (or greater) relative to free space for the total time of 68 days. Fading versus frequency correlation is based on an empirical formula developed by W. T. Barnett.[4]

3.1.2 *Fading Activity*

Fading is assumed to occur only during a six-hour period per day. This is a reasonable assumption over the fade depth of 35-40 dB and is supported by the Bryan-Wauseon data.[10] Figure 2 shows the ratio of fading rates during the midnight to 6 A.M. period of measurement divided by that observed during the 8 P.M. to midnight period. Fading activity was negligible during the remaining times.

3.1.3 *Fading Simultaneity*

Outage resulting from simultaneous fading activity in different hops in the same switching section is calculated on a daily basis. Daily fading rate assumed as a variable is given in Fig. 3.[9]

3.1.4 *Fading Hops*

Fading is assumed to occur in only one-half of the hops.

3.1.5 *Annual Fading Distribution*

Heavy fading is assumed to occur for two months, medium fading

(rates reduced by 1/2) for two months, and negligible fading is assumed for the remaining eight months of the year.

3.1.6 *Switching System Operation*

To simplify the computation, the switching system is assumed to have no hysteresis, that is, no width or threshold in the "channel good" versus "channel bad" decision maker (Initiator) and no differentiation between regular and protection channels with regard to the switch point. It is also assumed that the switch point (fade depth at which a protection switch is requested) is equal to the fade margin.

3.1.7 *Joint Fading and Maintenance*

Fading activity and maintenance activity are assumed to be mutually exclusive as a result of maintenance rules.

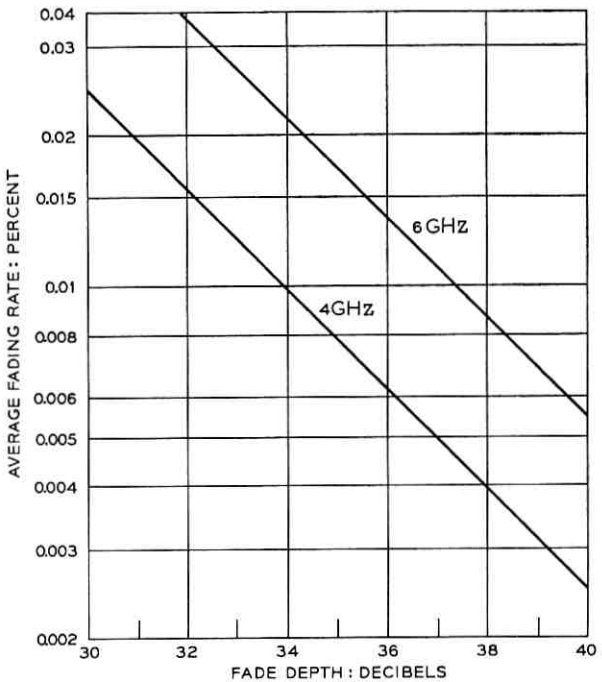

Fig. 1—Average fading rate of a 4- or 6-GHz channel based on the MIDAS West Unity data (July 22 through September 28, 1966).

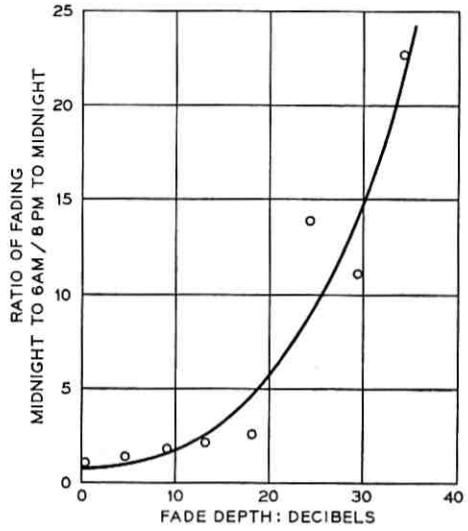

Fig. 2—Ratio of fading rates based on the Bryan-Wauseon data.

3.1.8 *Maintenance*

The maintenance rate for solid-state equipment is assumed to be the same as for TD-2, i.e., 4-1/2 hours per year per T/R bay (1-1/2 hours per T/R bay at four-month intervals). Maintenance is assumed to be concentrated during a six-hour period per day.

3.1.9 *Equipment Failure*

The failure rate for the solid-state repeater is assumed to be 0.014 failure per T/R bay per month. This represents about 3 to 1 improvement over present vacuum tube TD-2 equipment failure rates. The failure rate of TD-2 is estimated at one per T/R bay every two years, and the average time to repair an equipment failure is assumed to be 2-1/4 hours.* This corresponds to a fractional outage rate per vacuum tube T/R bay of 0.013 percent. The solid-state rate is taken to be 0.0043 percent.

3.1.10 *Two Constraints on Maintenance Operation*

(*i*) Maintenance is not to be undertaken on one channel while any other channel in the same switching section has an equipment failure.

* This is the average time required to restore a channel under equipment failure.

(*ii*) In the event of an equipment failure on any other channel while maintenance is in progress, the channel under maintenance will be restored to service within a short specified interval (say, 10 minutes).

3.1.11 *Distribution of Switching Section Lengths*

The switching section length distribution is assumed as indicated by Fig. 4. This distribution is based on the results of a 1962 TD-2 survey with the exception that 50 percent of the one-hop switching sections were deleted to compensate for the number of one-hop message sidelegs not found in a main route. The results of a 1967 TD-2 survey (with 50 percent of the one-hop sections deleted) substantially agree with the assumed distribution.

3.1.12 *Repeater Spacing*

The average repeater spacing is assumed to be 27 miles. This is based on TD-2 route data as of 6-30-65 indicating an average hop length of 26.65 miles.

3.2 *The Weighted Average Outage*

Consider a multichannel radio relay switching section having n channels of which $(m - 1)$ are protection channels. At least m simul-

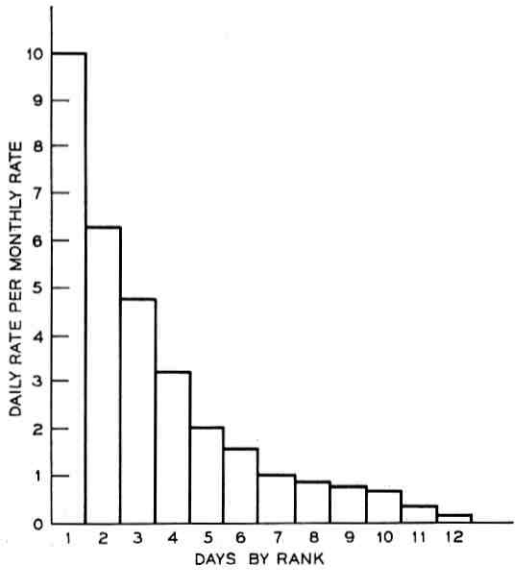

Fig. 3—Daily fading rate based on the Bryan-Wauseon data.

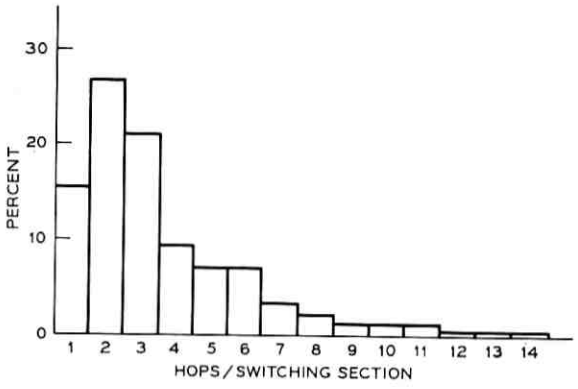

Fig. 4—Normalized distribution of switching section lengths based on the results of 1962 and 1967 TD-2 surveys with the exception that 50 percent of the one-hop sections are deleted.

taneous failures or interruptions are required before there is an actual outage or a loss of service. Those outages corresponding to more than m simultaneous channel failures should be weighted in the system outage computations since, for example, the event of two working channels failed and unprotected simultaneously is obviously twice as serious as the event of one working channel failed and unprotected at a time in a given system. Thus, we may define the weighted average outage of a working channel as follows:

ϕ_{av} = the weighted average outage of a working channel,

$$= \frac{\left[\begin{array}{c}\text{the expected number of working channels failed} \\ \text{and not protected at a time}\end{array}\right]}{[\text{the total number of working channels}]}$$

Expressed in probability notation, we have

$$\phi_{av} = \frac{1}{n - m + 1} \sum_{j=0}^{n-m} (j + 1) \Pr (\text{exactly } (m + j)) \qquad (1)$$

where Pr (exactly $(m + j)$) is the probability of exactly $(m + j)$ channels being failed simultaneously in a given system.

3.3 *Derivation of the Weighted Average Outage From a Switching Section*

Let us now compute the weighted average outage from a switching section based on equation (1). Referring to Fig. 5, the switching sec-

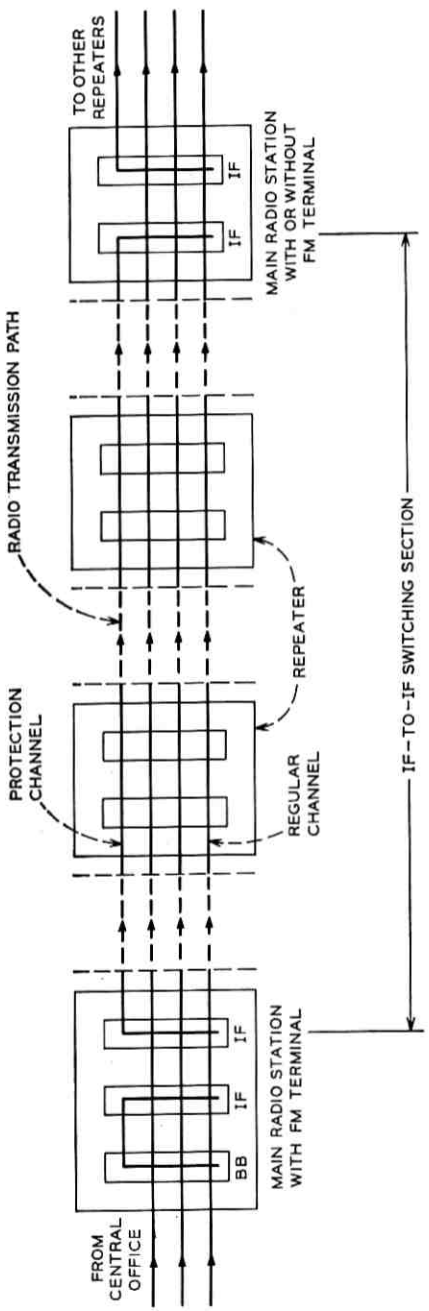

Fig. 5—Geometry of a TD or TH IF-to-IF switching system.

tion on a TD or TH route forms a link of a chain. Each switching section is completely self-contained and has no switching connection with adjacent sections. A switching section protects both directions of transmission simultaneously and independently. Thus, it is necessary only to compute one-way outage and double the result. In order to apply to MIDAS data and the empirical formulas in equation (1), it is required that we express the weighted average outage ϕ_{av} in terms of the purely simultaneous unavailability of $(m + j)$ channels, i.e., to eliminate explicit inclusion in the probability statement of channels which are not suffering a failure. It can be shown that a different representation for ϕ_{av} is

$$\phi_{av} = \frac{1}{n - m + 1}\left[\sum_{j=0}^{n-m} (-1)^j C_{m-2}^{m+j-2} \sum_{(m+j)_s} \Pr\left((m + j)_s\right)\right] \tag{2}$$

where C_{m-2}^{m+j-2} is the number of ways we may choose $(m - 2)$ out of $(m + j - 2)$ objects without regard to order and $(m + j)_s$ is a particular set of $(m + j)$ channels suffering simultaneous failures. The notation $\sum_{(m+j)_s} \Pr\left((m + j)_s\right)$ means that the outage of all possible $(m + j)$ simultaneous channel failures are to be summed (there will be C_{m+j}^{n} of them). Equation (2) is a very general expression in which no restriction on channel independence has been made. Observe that equation (2) is an alternating series which converges if all channels are independent and if the failure rate of each individual channel is low. The series converges very slowly if the channel failures are highly correlated as the MIDAS data has shown. Thus, we will consider all the terms in the series related to fading for system outage computations.

The unavailability of a single channel per hop is given by

$$P_s = P_f + P_e + P_m \tag{3}$$

where

P_f = unavailability due to multipath fading,
P_e = unavailability due to equipment failure, and
P_m = unavailability due to maintenance.

The unavailability of a single channel in a switching section is then modified as follows:

$$P_{ss} = rP_f + hP_e + hP_m, \qquad 0 \leqq r \leqq h, \tag{4}$$

where h is the number of hops in the switching section, and r is the number of hops in the switching section which are liable to experience heavy fading.

In order to apply equation (2) for the computation of outage from a switching section, we first assume that the channels fail independently of each other, i.e., that the failure of an arbitrary set of channels does not change the availability of the other channels, the correlation among channels due to fading will be considered later in our mathematical development. When all channels are independent, we obtain from equation (2)

$$\phi_{av} = \frac{1}{n-m+1}\left[\sum_{j=0}^{n-m}(-1)^j C_{m-2}^{m+j-2} C_{m+j}^{n} P_{ss}^{m+j}\right] \tag{5}$$

where P_{ss} is the unavailability of a channel in a switching section given by equation (4).
Let

$$\begin{aligned} P &= C_{m+j}^{n} P_{ss}^{m+j}, \\ &= C_{m+j}^{n}(rP_f + hP_e + hP_m)^{m+j}. \end{aligned} \tag{6}$$

By grouping the first and third terms in the parentheses of equation (6) and applying the binomial expansion, one gets

$$\begin{aligned} P &= C_{m+j}^{n} \sum_{k=0}^{m+j} C_k^{m+j}(rP_f + hP_m)^{m+j-k}(hP_e)^k, \\ &= \sum_{k=0}^{m+j} C_k^{n-(m+j-k)} C_{m+j-k}^{n}(rP_f + hP_m)^{m+j-k}(hP_e)^k. \end{aligned} \tag{7}$$

Further expand the common factor $(rP_f + hP_m)^{m+j-k}$ in equation (7) as follows:

$$\begin{aligned} &(rP_f + hP_m)^{m+j-k} \\ &\quad = \sum_{s=0}^{m+j-k} C_s^{m+j-k}(rP_f)^{m+j-k-s}(hP_m)^s, \qquad m+j-k \neq 0 \\ &\quad = 1, \qquad m+j-k = 0. \end{aligned} \tag{8}$$

Those cross terms in equation (8) which have factors $P^{m+j-k-s}P_m^s$ for $m+j-k-s \geqq 1$ and $s \geqq 1$ will be ignored because daytime maintenance routines have been put into effect in practice, and therefore, selective fading and maintenance are not considered to occur simultaneously. Thus, equation (8) is simply reduced to

$$\begin{aligned} (rP_f + hP_m)^{m+j-k} &= (rP_f)^{m+j-k} + (hP_m)^{m+j-k}, \qquad m+j-k \neq 0, \\ &= 1, \qquad m+j-k = 0. \end{aligned} \tag{9}$$

Substitution of equation (9) in equation (7) yields

$$P = \left\{C^n_{m+j} + \sum_{k=0}^{m+j-1} C^{n-(m+j-k)}_k C^n_{m+j-k}[(rP_f)^{m+j-k} + (hP_m)^{m+j-k}]\right\} \cdot (hP_e)^k. \tag{10}$$

From equations (5), (6) and (10), we obtain

$$\phi_{av} = \frac{1}{n - m + 1} \left\{\sum_{j=0}^{n-m} (-1)^j C^{m+j-2}_{m-2} \cdot \left\{C^n_{m+j} + \sum_{k=0}^{m+j-1} C^{n-(m+j-k)}_k C^n_{m+j-k}[(rP_f)^{m+j-k} + (hP_m)^{m+j-k}]\right\} \cdot (hP_e)^k\right\}. \tag{11}$$

Observe that all those terms in equation (11) having factor P_m^{m+j-k} with $m + j - k \geqq 2$ vanish because maintenance is a controlled activity, and the rules of operation prohibit simultaneous maintenance of two or more channels in the same direction in a switching section (i.e., maintenance is assumed to be done on one channel at a time). It follows, therefore, from equation (11) that

$$\begin{aligned}\phi_{av} = {} & \frac{1}{n - m + 1} \\ & \cdot \left\{\sum_{j=0}^{n-m} \left[(-1)^j C^{m+j-2}_{m-2} \cdot \sum_{k=0}^{m+j-1} C^{n-(m+j-k)}_k C^n_{m+j-k} (rP_f)^{m+j-k} (hP_e)^k\right]\right. \\ & + \sum_{j=0}^{n-m} (-1)^j C^{m+j-2}_{m-2} C^{n-1}_{m+j-1} C^n_1 (hP_m)(hP_e)^{m+j-1} \\ & \left. + \sum_{j=0}^{n-m} (-1)^j C^{m+j-2}_{m-2} C^n_{m+j} (hP_e)^{m+j}\right\}. \end{aligned} \tag{12}$$

It may be verified that the last two series on the right hand side of equation (12) converge rapidly when the factors P_m and P_e are small and independent. Thus far, we have considered only events of outage arising from independent channels in a given system. Let us now impose multipath fading. This will modify term by term the first series on the right hand side of equation (12). We see that a common factor in the series is

$$C^n_{m+j-k}(rP_f)^{m+j-k}$$

which denotes the probability of $(m + j - k)$ uncorrelated channels fading simultaneously. Actually, simultaneous fading can occur in two

ways; either all the fading may occur in one hop and be highly correlated, or it may occur in different hops in the section with less correlation. Since there are r fading hops, all fades in the same hop can occur r ways, and fades in t different hops can occur C_t^r ways (without regard to order). The probability P_{ff} of simultaneous fading of $(m + j - k)$ correlated channels becomes

$$P_{ff} = \sum_{t=0}^{r} [C_t^r \sum_{(m+j-k)_s} P_t((m + j - k)_s)] \tag{13}$$

where $\sum_{(m+j-k)_s} P_t((m + j - k)_s)$ is the unavailability of all possible $(m + j - k)$ simultaneous failures in t different hops of a switching section. For example, if three channels fade simultaneously in two hops, i.e., $m + j - k = 3$ and $t = 2$, then we have

$$\sum_{(m+j-k)_s} P_t((m + j - k)_s) = \sum_{3} P_2(3), \tag{14}$$

where $P_2(3)$ is the unavailability of three arbitrary channels in the set of n which fade simultaneously in two different hops. Therefore, if all channels are correlated due to fading, we may write equation (12) as

$$\begin{aligned}\phi_{av} = \frac{1}{n - m + 1} \Bigg\{ & \sum_{j=0}^{n-m} \sum_{k=0}^{m+j-1} \sum_{t=0}^{r} (-1)^j D_{m-2}^{m+j-2} C_k^{n-(m+j-k)} C_t^r \\ & \cdot [\sum_{(m+j-k)_s} P_t((m + j - k)_s)](hP_e)^k \\ & + \sum_{j=0}^{n-m} (-1)^j C_{n-2}^{m+j-2} C_{m+j-1}^{n-1} n(hP_m)(hP_e)^{m+j-1} \\ & + \sum_{j=0}^{n-m} (-1)^j C_{m-2}^{m+j-2} C_{m+j}^{n} (hP_e)^{m+j} \Bigg\}. \end{aligned} \tag{15}$$

Since the fading is assumed to occur only during a six-hour period and since we want an average outage, the terms in the first series of equation (15) having the factor

$$\sum_{(m+j-k)_s} P_t((m + j - k)_s)$$

should be multiplied by a time weighting factor τ^{t-1} where τ in this case is 4, and fading in different hops should involve a factor α_t to account for the peakedness of daily fading among t fading hops.* Let us designate the first series in equation (15) by S_1. Then the complete expression for S_1 becomes

* The expression of α_t in terms of t is given in Appendix B.

$$S_1 = \frac{1}{n-m+1}\left\{\sum_{j=0}^{n-m}\sum_{k=0}^{m+j-1}\sum_{t=0}^{r}(-1)^j C_{m-2}^{m+j-2} C_k^{n-(m+j-k)} C_t^r \tau^{t-1} \cdot \alpha_t [\sum_{(m+j-k)_s} P_t((m+j-k)_s)](hP_e)^k\right\}. \quad (16)$$

The formula can be modified for reduced fading rates in other months by expressing the fading rate as $b_i P_f / B_i$ where $b_i < 1$, $B_i \geqq 1$ to account for fading in other months. In nonfading months, $b_i = 2/3$, $B_i = \infty$; in medium fading months, $b_i = 1/6$, $B_i = 2$; and in heavy fading months, $b_i = 1/6$, $B_i = 1$. The joint equipment failure and maintenance outage term in equation (12) should also be modified, based on maintenance constraints. Let

$$P(m, e) = P_m P_e^{m+j-1} \quad (17)$$

Reference to Appendix A will show that this expression may be modified as follows:

$$P(m, e) = P_m P_{EQ}^{m+j-1} \quad (18)$$

where

P_{EQ} = the equivalent equipment failure probability;

$$= \frac{\tau_r}{\tau_e} P_e ;$$

τ_e = assumed duration of one equipment failure; and

τ_r = time required to restore a channel under maintenance to service in the event of an equipment failure on any other channel.

Summarizing then, the weighted average outage of a working channel, as defined in equation (1), in a switching section one may be expressed as:

$$\phi_{av} = \frac{1}{n-m+1}\left\{\sum_{i=1}^{l}\sum_{j=0}^{n-m}\sum_{k=0}^{m+j-1}\sum_{t=0}^{r}(-1)^j C_{m-2}^{m+j-2} C_k^{n-(m+j-k)} C_t^r \tau^{t-1}\alpha_t \cdot \frac{b_i}{B_i^t}[\sum_{(m+j-k)_s} P_t((m+j-k)_s)](hP_e)^k + \sum_{j=0}^{n-m}(-1)^j C_{m-2}^{m+j-2} C_{m+j-1}^{n-1} n h^{m+j} P_m P_{EQ}^{m+j-1} + \sum_{j=0}^{n-m}(-1)^j C_{m-2}^{m+j-2} C_{m+j}^{n}(hP_e)^{m+j}\right\} \quad (19)$$

where

n = total cross-sectional number of channels in the system;
$m - 1$ = number of protection channels;
h = number of hops in the switching section;
r = number of fading hops in the switching section;
τ = hourly variation parameter;
α_t = daily variation parameter;
b_i, B_i = monthly variation parameters; and
l = upper limit for the index of monthly variation parameters.

3.4 *Empirical Formulas for the Correlated Fading Channels in the Same Hop* ($t = 1$)

An empirical formula derived by W. T. Barnett[11] can be used to evaluate the simultaneous fading of an arbitrary set of $(m + j - k)$ channels at 4 and 6 GHz:

$$P_1((m + j - k)_s) = \frac{2^{(2l/m+j-k)}L^4}{\frac{4}{m + j - k}\sum_{ij}\Delta_{ij}} \tag{20}$$

where

$m + j - k$ = total number of channels in set;
l = number of 6-GHz channels in set; and
$\sum_{ij}\Delta_{ij}$ = sum of fractional frequency difference between all possible pairs in the set (there are C_2^{m+j-k} of them).

The value of (Δ_{ij}) can be calculated when the pair is from the same common carrier band. For the crossband case when one channel is from the 6-GHz band, a value of 0.05 has been used.[12]

3.5 *Annual Outage From a 4000-mile Two-Way Circuit*

Results given in this work are based on annual outage* for a 4000-mile two-way system. In order to evaluate the equations derived so far, it is necessary to assume values for h, the number of hops in a switching section. In actual computation, the distribution of hop length and switching section in a 4000-mile route are used. The computation procedure involves computing switching section performance for various combinations of h and r, multiplying the (h, r) reliability estimate by the appropriate weighting factor determined from the data, summing the results and extrapolating the answer to give an estimate of 4000-mile two-way performance.

* Including outage due to flat fading.

IV. RELIABILITY OBJECTIVES

The usual measure of reliability is outage, i.e., the total time that the circuit does not deliver the signal information within the limits of acceptable performance. This is generally considered to be at a noise level of 55 dBrnc0 or worse, or no service. The outage that can be tolerated is generally based on the worst fading month. However, there is an approximate relation between the outages in the worst month and yearly outage, so the radio relay system requirement is specified on a yearly basis. The present reliability objective for a long-haul microwave system (4000 miles two-way) is that outage time of a channel should not exceed 0.02 percent or 1-3/4 hours per year. This objective has historically been allocated among contributory causes as follows:

(*i*) Outage due to flat fading	$\leqq 0.01\%$
(*ii*) Outage due to selective fading equipment failure and maintenance	$\leqq 0.008\%$
(*iii*) Outage due to FM terminal failure and others	$\leqq 0.002\%$
(*iv*) Total	$\leqq 0.02\%$

V. RESULTS

The general expression developed in Section III was used to compute the outages for various TD and TH systems. Figure 6* shows the TD-2 1 × 5 switching performance at 4 GHz for the six original channels 1, 2, 3, 4, 5, 6 or the six interstitial channels 7, 8, 9, 10, 11, 12. A value of 0.013 percent is assumed for the unavailability due to equipment failure (see Section 3.1.9). It is seen that, for these systems, the 0.02 percent outage objective cannot be met even with very high fade margin because of the high equipment failure rate for vacuum tube systems. The effect of equipment failure can be seen by comparing the bottom two curves in the figure. As a measure of the sensitivity of these results to changes in equipment failure rate, the outage was recomputed after doubling and then after redoubling the equipment failure rate. For high fade margins, the equipment failure rate controls the system outage.

* In this figure, the annual average outage in percent is expressed in terms of fade margin which is a fixed number for a given system design. For example, the fade margin of a given system may be 35 dB. The reason for assuming the fade margin to be a variable is to show the controlling factors and how they change with different switching strategies.

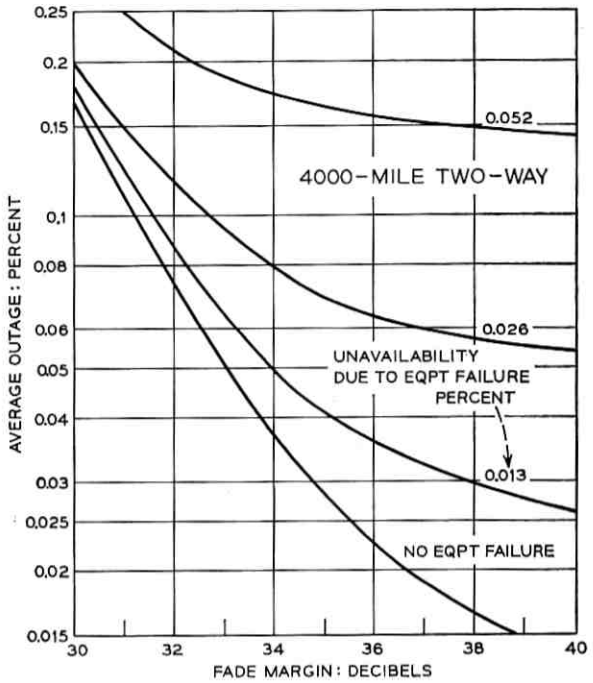

Fig. 6—Expected average outage of a vacuum tube 4-GHz system with 1 × 5 switching.

In Fig. 7, 1 × 5 switching is contrasted with 2 × 10 switching. It is noted that a reduction in the outage floor is obtained by virtue of the second protection channel. In contrast to the 1 × 5 system, the outage from a 2 × 10 system is a strong function of fade margin, and equipment failure no longer controls the system outage. The 1 × 11 curve illustrates the result of full time use of one protection channel of a 2 × 10 system; the "1 × 11 no maintenance" condition is obtained during part time use of one of the two protection channels in a 2 × 10 system when maintenance is deferred as for example when restoration is in progress. It is seen that the objective can be met at fade margin of 35.9 dB.

Figure 8 shows a set of comparable curves for 6-GHz systems.* The 2 × 6 system meets the reliability objective at 39.6-dB fade margin. Since the outage from selective fading at 6 GHz is higher than at 4

* In Fig. 8, the value of 0.0043 percent is the unavailability per T/R bay per channel due to solid state equipment failure as indicated in Section 3.1.9.

GHz, the outage is a strong function of fading margin for both the 2 × 6 and 1 × 7 arrangements.

Figure 9 shows the limits for a vacuum tube system operating in crossband diversity up to 2 × 18 capacity and, of course, 2 × 12, 2 × 14, etc., would fall between these curves.

The curves in Fig. 10 show the insensitivity of a 2 × 18 system to reasonable equipment failure rates. Again, an unavailability of 0.013 percent is assumed for vacuum tube equipment failures. Note the effect of doubling this rate once, twice, three times. The conclusion to be made is that 2 × 18 reliability is relatively insensitive to the equipment failure rate.

The effect of using one protection channel for other service, full or part time, in a 2 × 18 system is indicated in Fig. 11.

The outage from a 3 × 17 system was also computed as shown in Fig. 12 in contrast with the 2 × 10 and 2 × 18 systems. The improvement using three protection channels is not large because, in this sys-

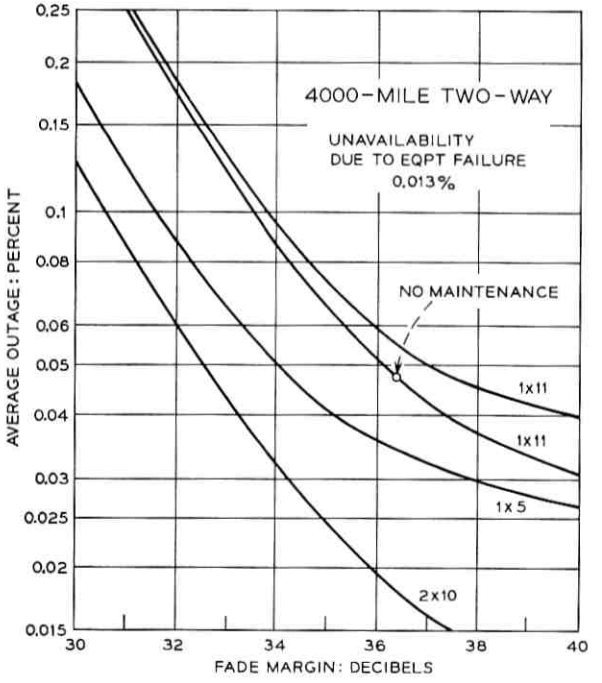

Fig. 7—Expected average outage of a vacuum tube 4-GHz system with various switching strategies.

tem, outage is controlled by the fading, and it is indicated from the MIDAS data that fading is a highly correlated phenomenon.

VI. OUTAGE FROM A SYSTEM IN THE ABSENCE OF SELECTIVE FADING

A question arises as to whether, by use of space diversity,[12] one protection channel might be enough to achieve the operational objectives in a long-haul system. To answer this question, we compute the outage by suppressing the selective fading terms in the total system outage expression, i.e., assume that there is no selective fading on the propagation paths. Table I shows the results of this computation. Note that the circled items exceed the basic 0.02 percent objective. All the circled items correspond to vacuum tube systems having only one protection channel. We may thus say that one protection channel is not enough for vacuum tube equipment protection in a long-haul system.

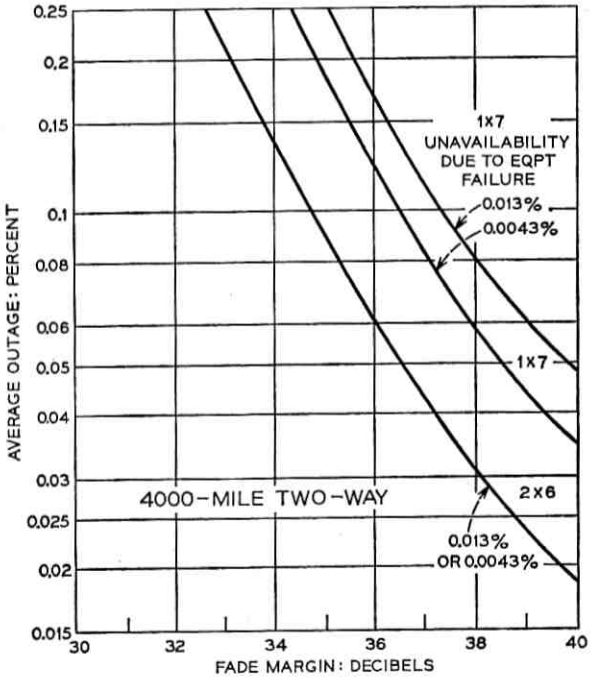

Fig. 8—Expected average outage of a vacuum tube or solid-state 6-GHz system with 2×6 and 1×7 switching.

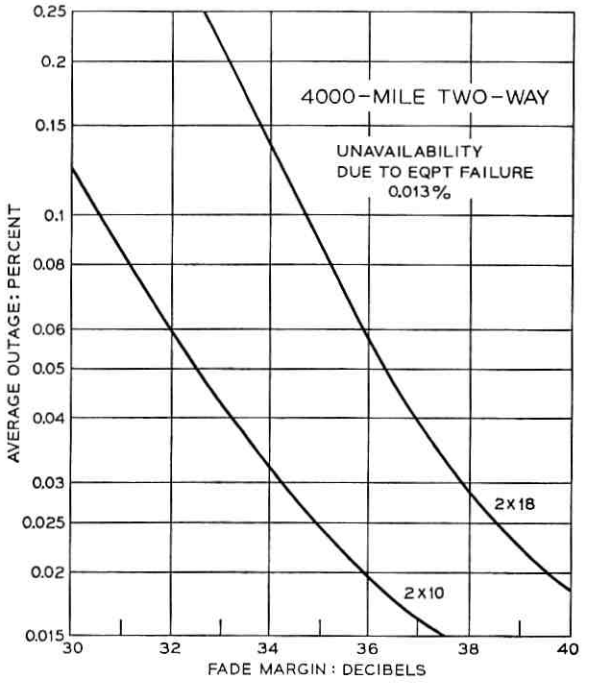

Fig. 9—Expected average outage of a 4- and 6-GHz crossband 2 × 18 system versus the 2 × 10 system.

VII. CONCLUSIONS AND RECOMMENDATIONS

The reliability of long-haul radio relay systems utilizing automatic channel switching is estimated under a few realistic assumptions. The results are illustrated in figures for various arrangements for comparison. The conclusions and recommendations drawn from these reliability curves are as follows:

(*i*) System outage is a strong function of fade margin when the fade margin is low (~ 30 dB) for all cases.

(*ii*) In systems having one protection channel, the variation of outage is strongly influenced by the equipment failure rate. With two protection channels, the outage rate is not very sensitive to equipment failure.

(*iii*) A reduction of the total number of protection channels can be achieved by crossband operation without seriously affecting the system reliability.

(*iv*) For vacuum tube systems, one protection channel does not offer adequate reliability and should not be used for long-haul applications.

(*v*) Two protection channels are sufficient to protect up to at least 18 crossband working channels (vacuum tube or solid state) assuming a fade margin of 40 dB. Multipath fading will be the primary outage variable beyond the 0.012 percent flat fading and terminal allowances.

VIII. ACKNOWLEDGMENT

The author would like to thank Messrs. H. D. Griffiths, F. H. Lanigan, and R. O. Davidson for helpful discussions on the switching systems, U. A. Matson for discussions on FM terminal equipment and switching, Mrs. B. A. Fink and Mrs. J. M. Littlefield for computer programming, and Messrs. A. C. Longton and R. P. Slade for suggestions and guidance during the course of this work.

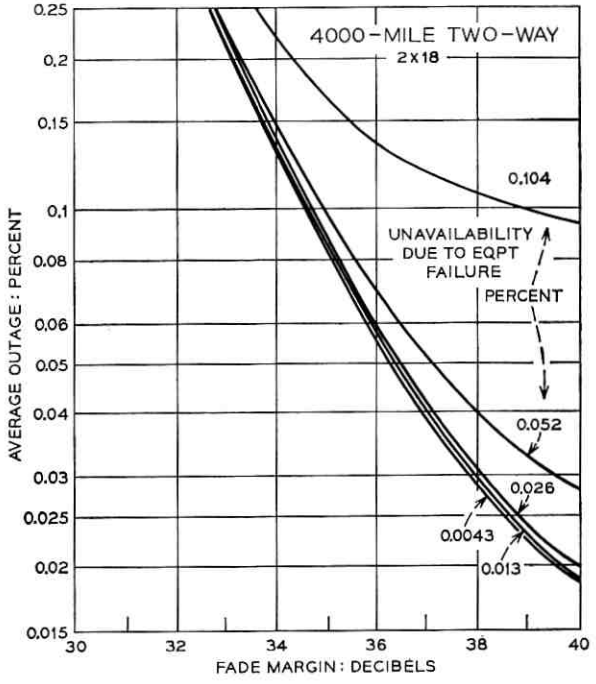

Fig. 10—Sensitivity of a 2 × 18 system to equipment failures.

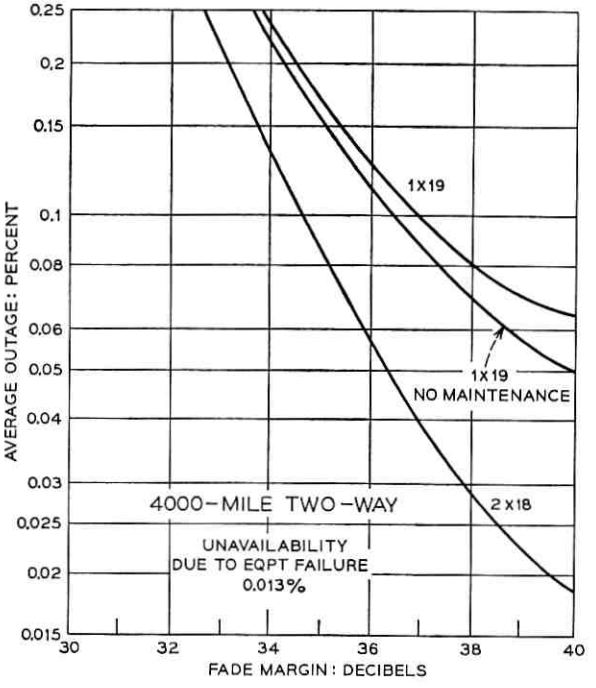

Fig. 11—Expected average outage of crossband 1 × 19 and 2 × 18 vacuum tube systems.

APPENDIX A

Outage Due to Equipment Failure and Maintenance with Constraints

This appendix develops a method to compute the outage in a multichannel radio system due to the joint effects of equipment failures and maintenance when two maintenance constraints are applied.

A.1 *Outage Due to Joint Equipment Failure and Maintenance Without Constraints*

Let us consider the simultaneous unavailability of $(l + 1)$ radio channels in which l channels experience equipment failure and one channel is being maintained. Over an interval of time τ, the per-bay unavailabilities due to equipment failure and maintenance are given by

$$P_e = \frac{\rho_e \tau_e}{\tau} \tag{21}$$

$$P_m = \frac{\rho_m \tau_m}{\tau} \tag{22}$$

where

τ_e = duration of one equipment failure;
τ_m = duration of one maintenance routine on a radio bay;
ρ_e = equipment failure rate over the interval τ; and
ρ_m = maintenance rate over the interval τ.

When P_e and P_m are independent, the outage rate due to equipment failure and maintenance without constraints is given by

$$P(m, e) = P_m P_e^l = \frac{\rho_m \rho_e^l}{\tau^{l+1}} \tau_m \tau_e^l \,. \tag{23}$$

A.2 *Evaluation of Outages with Constraints*

Let us consider first the case of one protection channel ($l = 1$). When $l = 1$, equation (23) becomes

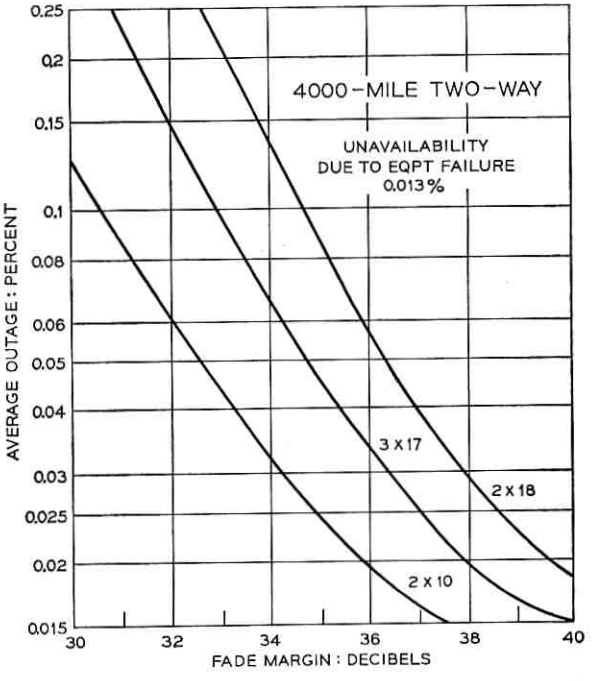

Fig. 12—Expected average outage of a 3 × 17 crossband system versus the 2 × 10 and 2 × 18 systems.

TABLE I—4000-MILE TWO-WAY OUTAGE DUE TO FLAT FADING, EQUIPMENT FAILURE, MAINTENANCE, AND FM TERMINALS, NO SELECTIVE FADING INCLUDED

Switching System	Band	Outage in Percent		
		$P_e = 0.0043\%$ (Solid State)	$P_e = 0.013\%$ (Vacuum Tube)	$P_e = 0.026\%$ (Vacuum Tube)
1 × 5	4	0.0143	0.0241	0.0515
2 × 10	4	0.0120	0.0121	0.0124
1 × 11	4	0.0166	0.0362	0.0910
2 × 6	6	0.0120	0.0120	0.0122
1 × 7	6	0.0151	0.0281	0.0647
2 × 18	4 + 6	0.0120	0.0122	0.0132
1 × 19	4 + 6	0.0197	0.0523	0.1440

$$P(m, e) = \frac{\rho_m \rho_e}{\tau^2} \tau_m \tau_e \ . \tag{24}$$

Let S be the starting time of an equipment failure with respect to the starting time of maintenance. It can be shown that equation (24) can be expressed in a different form:

$$P(m, e) = \frac{\rho_m \rho_e}{\tau^2} \int_{-\infty}^{\infty} F(S)\, dS \tag{25}$$

where $F(S)$ is the outage distribution shown in Fig. 13a. From equation (25), we see that $P(m,e)$ is proportional to the area under the curve $F(S)$.

Now impose the first constraint: scheduled maintenance will not be started during an equipment failure on another channel. This constraint implies that an outage will result only for equipment failure starting after maintenance is started, i.e., $S \geqq 0$. The outage distributions with the first constraint are reduced to those shown in Fig. 13b. The outage $P(m, e)$ can thus be obtained by integrating over the appropriate regions. The results are given in column 4 of Table II. It is seen that, with the first constraint, the expression of outage is multiplied by a factor which is less than 1.

In addition to the first constraint, apply the second constraint: if there is an equipment failure during maintenance, the channel under maintenance is to be restored to service in a period of time τ_r where $\tau_r < \tau_m , \tau_e$. This constraint implies that rapid restoration of the maintained channel limits the outage interval to τ_r or less. The outage dis-

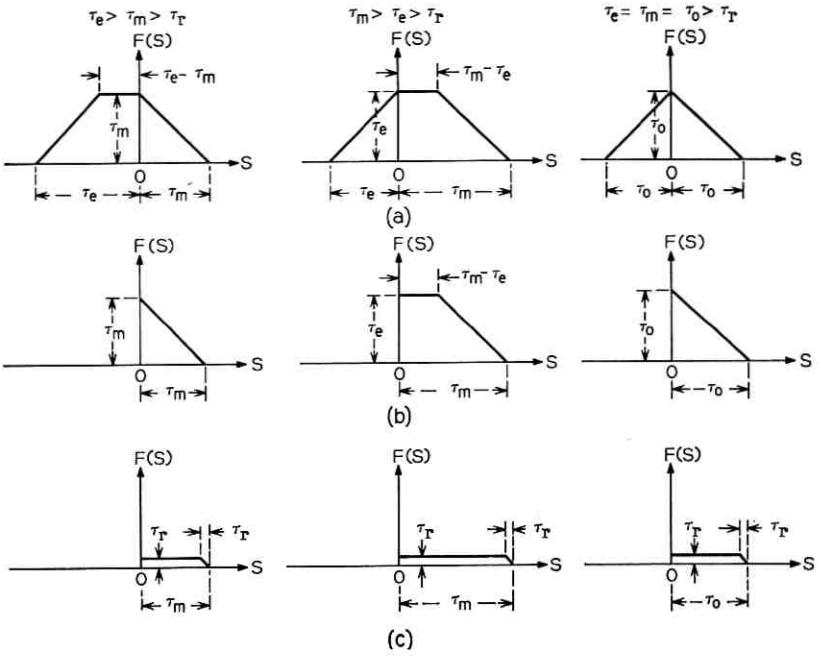

Fig. 13—Outage distributions of one variable. (a) Without maintenance constraints. (b) With the first constraint. (c) With both the first and second constraints.

tributions $F(S)$ when both constraints are applied are shown in Fig. 13c. The solutions are listed in column 5 of Table II. It is noted that the solution with both constraints is in the same form for all cases, although this is not true for the solutions obtained with the first constraint alone. Therefore, it is concluded that the first and second constraints are interrelated. The effect of the first constraint on outage is partially wiped out when the second constraint is imposed. When $\tau_r \ll \tau_m$ which is the usual case, the solutions in column 5 of Table II can be approximated by those corresponding ones in the last column of the same table. These approximations indicate that the effect of the constraints is equivalent to limiting each equipment outage to τ_r minutes.

The one-dimensional model can be extended to a two-dimensional one for the case of two protection channels ($l = 2$). The outage rate due to maintenance and double equipment failure will be of the form $P_m P_e^2$. Let S_1 and S_2 denote the starting time of equipment failures #1 and #2, respectively, with respect to the starting time of maintenance; the

TABLE II—SOLUTIONS OF OUTAGES WITH CONSTRAINTS

Number of Protection Channels	Relative Lengths of Intervals	Outage Due to Equipment Failure and Maintenance			
		No Constraints	First Constraint	First and Second Constraints	
		Exact	Exact	Exact	Approx.
1	$\tau_m < \tau_e$	$P_m P_e$	$\frac{1}{2}\frac{\tau_m}{\tau_e} P_m P_e$	$\left(1 - \frac{\tau_r}{2\tau_m}\right) P_m P_{EQ}$	$P_m P_{EQ}$
	$\tau_m = \tau_e$	$P_m P_e$	$\frac{1}{2} P_m P_e$	$\left(1 - \frac{\tau_r}{2\tau_m}\right) P_m P_{EQ}$	$P_m P_{EQ}$
	$\tau_m > \tau_e$	$P_m P_e$	$\left(1 - \frac{1}{2}\frac{\tau_e}{\tau_m}\right) P_m P_e$	$\left(1 - \frac{\tau_r}{2\tau_m}\right) P_m P_{EQ}$	$P_m P_{EQ}$
2	$\tau_m < \tau_e$	$P_m P_e^2$	$\frac{1}{3}\left(\frac{\tau_m}{\tau_e}\right)^2 P_m P_e^2$	$\left(1 - \frac{2}{3}\frac{\tau_r}{\tau_m}\right) P_m P_{EQ}^2$	$P_m P_{EQ}^2$
	$\tau_m = \tau_e$	$P_m P_e^2$	$\frac{1}{3} P_m P_e^2$	$\left(1 - \frac{2}{3}\frac{\tau_r}{\tau_m}\right) P_m P_{EQ}^2$	$P_m P_{EQ}^2$
	$\tau_m > \tau_e$	$P_m P_e^2$	$\left(1 - \frac{2}{3}\left(\frac{\tau_e}{\tau_m}\right)^2\right) P_m P_e^2$	$\left(1 - \frac{2}{3}\frac{\tau_r}{\tau_m}\right) P_m P_{EQ}^2$	$P_m P_{EQ}^2$

outage is then a function of S_1 and S_2 . Assume that the durations of the two equipment failures are equal. The outage distribution for various situations is shown pictorially in Fig. 14. The outage rate for maintenance and double equipment failure can be derived by using the following integral which is an extension of Equation (25).

$$P(m, e) = \frac{\rho_m \rho_e^2}{\tau^3} \int_{-\infty}^{\infty} \int_{-\infty}^{\infty} F(S_1 , S_2)\, dS_1\, dS_2 \tag{26}$$

where $F(S_1 , S_2)$ is the outage distribution of two variables given in Fig. 14. Observe that $P(m , e)$ is proportional to the volume under the surface $F(S_1 , S_2)$. The effect of the first and second constraints on $F(S_1 , S_2)$ is also shown in Fig. 14. The solutions for various cases are presented in the lower half of Table II.

It is seen that, when $\tau_r < \tau_m , \tau_c$, an approximate solution for $P(m, e)$ with both maintenance constraints for arbitrary l can be expressed by

$$P(m, e) = P_m P_{EQ}^l \tag{27}$$

where

$$P_{EQ} = \frac{\tau_r}{\tau_e} P_e . \tag{28}$$

Equations (27) and (28) indicate that the effect of the two constraints is once again equivalent to limiting the durations of equipment failures to a short period equal to τ_r . The equivalent equipment unavailability is then equal to $(\tau_r/\tau)\rho_e$ which is equivalent to equation (28). Comparing with the outage given by equation (23), we see that the outage with constraints can be treated by replacing P_e by P_{EQ} in the expression without constraints.

APPENDIX B

Derivation of the Daily Variation Parameter, α_t

The purpose of this appendix is to explain the use of the parameter α_t in the outage expressions for fading in different hops.[10]

Consider t channel failures due to fading which occur simultaneously in t different hops of a switching section. Assuming independence of fading among hops, the probability of t simultaneous failures is P_f^t , where P_f is the probability of a fade on a single channel and fades in different hops on different channels are assumed here to have the same probability, since P_f is normally given in terms of a monthly average. If data on which the P_f is based is examined in greater detail, it will be

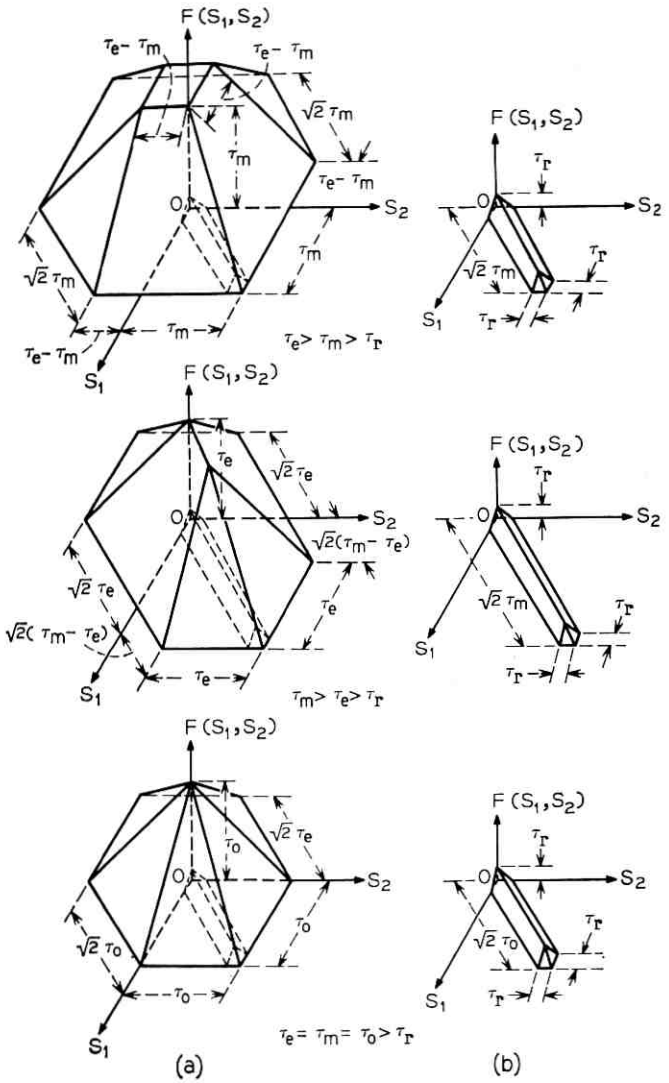

Fig. 14—Outage distributions of two variables. (a) Without constraints. (b) With constraints.

noticed that this fading is not equally distributed among the days of the month. Some days have considerably more fading than others. If P_{fi} represents fading on the ith day, then P_f may be expressed as

$$P_f = \frac{1}{T} \sum_{i=1}^{T} P_{fi} . \tag{29}$$

The joint fading on the ith day is

$$P_{fi}^t, \tag{30}$$

and the average daily fading rate for the period would then be

$$\frac{1}{T} \sum_{i=1}^{T} P_{fi}^t . \tag{31}$$

Each day's fading can be related to the monthly fading rate by the expression

$$P_{fi} = \overline{\alpha_i} P_f \tag{32}$$

so that equation (31) could be written as

$$\frac{1}{T} \sum_{i=1}^{T} (\overline{\alpha_i} P_f)^t . \tag{33}$$

Since P_f is independent of i, the actual joint fading (33) becomes

$$\left(\frac{1}{T} \sum_{i=1}^{T} \overline{\alpha_i}^t\right) P_f^t = \alpha_t P_f^t \tag{34}$$

where

$$\alpha_t = \frac{1}{T} \sum_{i=1}^{T} \overline{\alpha_i}^t . \tag{35}$$

Thus, in computing simultaneous fading activity on t channels in t different hops where fading probabilities are given in terms of monthly averages, a factor α_t should be included to account for the daily fading variation. The model for daily fading used in this paper is given in Fig. 3. Based on this model, we have

$$\alpha_2 \cong 6$$

and

$$\alpha_3 \cong 46.$$

REFERENCES

1. Welber, I., Evans, H. W., and Pullis, G. A., "Protection of Service in the TD-2 Radio Relay System by Automatic Channel Switching," B.S.T.J., *34*, No. 3 (May 1955), pp. 473–510.
2. Giger, A. J., and Low, F. K., "The Automatic Protection Switching System of TH Radio," B.S.T.J., *40*, No. 6 (November 1961), pp. 1665–1715.
3. Griffiths, H. D., and Nedelka, J., "100A Protection Switching System," B.S.T.J., *44*, No. 10 (December 1965), pp. 2295–2336.
4. Barnett, W. T., "Microwave Line-of-Sight Propagation with or without Frequency Diversity," B.S.T.J., *49*, No. 8 (October 1970), pp. 1827–1871.
5. Crawford, A. B., and Jakes, W. C., Jr., "Selective Fading of Microwaves," B.S.T.J., *31*, No. 1 (January 1952), pp. 68–87.
6. Kaylor, R. L., "A Statistical Study of Selective Fading of Super-High Frequency Radio Signals," B.S.T.J., *31*, No. 5 (September 1953), pp. 1187–1202.
7. Chen, W. Y. S., unpublished work.
8. Prielipp, R. C., unpublished work.
9. Williams, A. D., unpublished work.
10. Curtis, H. E., unpublished work.
11. Barnett, W. T., unpublished work.
12. Vigants, A., "Space-Diversity Performance as a Function of Antenna Separation," IEEE Trans. Com. Tech., *COM-16*, No. 6 (December 1968), pp. 831–836.

THE BELL SYSTEM TECHNICAL JOURNAL
Vol. 50, No. 4, April, 1971
Printed in U.S.A.

Some Extensions of the Innovations Theorem*

By THOMAS KAILATH†

(Manuscript received December 4, 1970)

Consider an observed process that is the sum of a Wiener noise *process and the integral of a not necessarily gaussian* signal *process. The innovations process is defined as the difference between the observed process and the integral of the causal minimum-mean-square-error estimate of the signal process. Then if the integral of the expected value of the absolute magnitude of the signal process is finite, we show that the innovations process is also a Wiener process. The present conditions are a substantial weakening of those previously used in which the integral of the signal variance had to be finite. The new result is obtained by using some recent results in martingale theory. These results also enable us to obtain similar results when the Wiener process is replaced by a square-integrable martingale.*

I. INTRODUCTION AND DISCUSSION OF RESULTS

We shall be concerned with stochastic processes of the form

$$dy = z\,dt + dw, \quad \text{i.e.,} \quad y(t) = \int_0^t z(s)\,ds + w(t), \qquad 0 \leqq t \leqq T \tag{1}$$

where $w(\cdot)$ is a Wiener process with

$$E[w(t)] = 0, \quad E[w(t)w(s)] = \min\,(t, s) \tag{2}‡$$

and $z(\cdot)$ is a not necessarily gaussian process such that, for every $0 \leqq s < t \leqq T$

$$w(t) - w(s) \perp\!\!\!\perp \mathfrak{F}_s = \sigma\{y(\tau),\ 0 \leqq \tau \leqq s\} \tag{3}$$

* This work was supported by the Applied Mathematics Division of the Air Force Office of Scientific Research under contract AF 44-620-69-C-0101 and in part by Bell Telephone Laboratories (Summer 1969) and a Guggenheim Fellowship.

† Stanford University, Stanford, California 94305.

‡ Later we shall replace $w(\cdot)$ by a square-integrable martingale (cf., Theorem 3).

where $\sigma\{\cdot\}$ denotes the smallest sigma-field generated by $\{\cdot\}$ and, following K. Itô, the symbol $\perp\!\!\!\perp$ will be used to denote statistical independence. In our earlier work,[1] we also assumed that

$$E\int_0^T |z(t)|^2\,dt < \infty. \tag{4}$$

This assumption not only enabled us to define the conditional expectation,

$$E[z(t) \mid \mathfrak{F}_t] = \hat{z}(t), \quad \text{say} \tag{5}$$

but also to conclude that $|\hat{z}(\cdot)|$ and $|\hat{z}(\cdot)|^2$ (as well as $|z(\cdot)|$ and $|z(\cdot)|^2$) have finite integrals a.s. Then in Appendix I of Ref. 1 and independently in Refs. 2 through 4, the following result was proved:

Theorem 1: *Under the assumptions* (1) *through* (4), *the 'innovations' process* $\{\nu(t), \mathfrak{F}_t\}$ *where*

$$\nu(t) = y(t) - \int_0^t \hat{z}(s)\,ds, \qquad 0 \leqq t \leqq T \tag{6}$$

is a Wiener process, relative to the sigma-fields $\mathfrak{F}_t$ *generated by* $y(\cdot)$. *Moreover,* $\nu(\cdot)$ *has the same statistics as the original Wiener process* $w(\cdot)$.

The reasons for the name "innovations" and some applications of the concept are discussed in Refs. 1 through 5, and the references therein, so that we shall not pursue them here. Our interest will be in relaxing the conditions under which the theorem is true. In particular we shall show that the condition (4) can be replaced by the weaker condition

$$E\int_0^T |z(t)|\,dt < \infty. \tag{7}$$

This is a substantial relaxation of (4), since now we can even consider cases in which $z(\cdot)$ need not have finite variance and need not be square-integrable in t a.s., (examples of this type are easy to find for gaussian $z(\cdot)$, cf., Ref. 6).

Nevertheless, even this weakening is not the best possible. Such a claim seems surprising, since to begin with, the standard definitions (see e.g., J. L. Doob[7]) of conditional expectation require that

$$E|z(t)| < \infty.$$

In our problem, however, L. Shepp has pointed out by example that even this condition on $z(\cdot)$ is not always necessary.[8] In Shepp's example,

$$z(t) = \eta, \quad \text{a Cauchy distributed random variable, independent of } w(\cdot).$$

Then it is easy to verify that $z(\cdot)$ as defined below by equation (8) can be used to define the innovations process $\nu(\cdot)$, even though $E \mid z(t) \mid$ does not exist. Nevertheless, Bayes' theorem shows that

$$\hat{z}(t) = \frac{\int_0^t \eta \exp\left[\eta w(t) - \frac{\eta^2 t}{2}\right] p(\eta)\, d\eta}{\int_0^t \exp\left[\eta w(t) - \frac{\eta^2 t}{2}\right] p(\eta)\, d\eta}. \tag{8}$$

It is true that there is a generalized definition of conditional expectation (see, e.g., p. 342 of Ref. 9) that can be used when $E \mid z \mid$ does not exist, but the exact sense in which equation (8) fits this generalized definition and the more general problem of trying to define $\hat{z}(\cdot)$ under just the assumptions (1) through (3) requires further investigation. So much for the assumption (4). To see that equation (3) is also not always necessary, we can let $z(t) = w(T)$, $0 \leqq t \leqq T$. By using the results of Ref. 6, it can be shown that even in this case we can define a variable $\hat{z}(\cdot)$ such that the process $\nu(\cdot)$ of equation (6) is still a Wiener process. Having discussed such examples however, let us quote precisely the results that we can prove. The first is:

Theorem 2: *Under the assumptions* (1)-(3) *and* (7), *the innovations process* $\{\nu(t), \mathfrak{F}_t\}$ *defined by equation* (6), *is a Wiener process with the same statistics as* $w(\cdot)$.

Besides extending the range of applicability of the innovations process, Theorem 2 is of interest, at least to us, because of the relatively new techniques used to prove it. Thus Theorem 1 was proved in Ref. 1 by using a martingale theorem of Lévy and Doob (cf., p. 384 of Ref. 7) to the effect that a continuous-path, finite-variance martingale with conditional variance equal to t must be a Wiener process. The assumption (4) that was made in Theorem 1 enabled us, with some computation,[1] to establish the finite-variance and conditional variance properties. In Theorem 2, the process $z(\cdot)$ may itself have infinite variance and we cannot easily apply the theorem of Lévy and Dobb. Fortunately, however, some recent developments in martingale theory, due to H. Kunita and S. Watanabe[10] and to P. Meyer,[11,12] have provided a generalized form of the Lévy-Doob theorem that we can use to prove Theorem 2, and in fact with less computation than was needed in Ref. 1 for Theorem 1. Moreover, the results in Refs. 10 through 12 have suggested our second result, which in fact includes the first one.

Theorem 3: Let $dx = z\,dt + dM$, *where*

$$E\int_0^T |z(t)|\,dt < \infty,\ M(t) - M(s) \perp\!\!\!\perp \mathfrak{F}_s \tag{9}$$

and $M(\cdot)$ *is a square-integrable martingale. Then* $\{\mu(t,\omega), \mathfrak{F}_t, P\}$, *where*

$$\mu(t) = x(t) - \int_0^t \hat{z}(s)\,ds, \qquad \hat{z}(t) = E[z(t) \mid \mathfrak{F}_t],$$

is a locally square-integrable martingale with quadratic variation the same as that of M.

P. Frost has obtained the result of Theorem 3 under the stronger hypotheses that $E|z(\cdot)|^2$ is integrable and $M(\cdot)$ is continuous.[13]

A special form of Theorem 3 was obtained earlier[5] by use of a result of Doob (See p. 449 of Ref. 7) that a continuous square-integrable martingale $\{M(t), \mathfrak{B}_t\}$ satisfying

$$E\{[M(t) - M(s)]^2 \mid \mathfrak{B}_s\} = E\left\{\int_0^t |G(\tau,\omega)|^2\,d\tau \mid \mathfrak{B}_s\right\}$$

can be written as a stochastic integral with respect to a Wiener process. In other words, this leads us to extend equation (1) by allowing a stochastic coefficient for dw; we may note that Kunita and Watanabe have shown that a (locally) square-integrable martingale of a Wiener process can also be written as a stochastic integral.

Finally we may remark that the proof of Theorem 3 also yields the following.

Corollary 4: Theorem 3 remains valid if hypothesis (7) *is replaced by*

$$\hat{z}(\cdot) \text{ exists and } \int_0^T \hat{z}(t)\,dt < \infty \text{ a.s.} \tag{10}$$

Note that condition (7) guarantees (10), not just for conditional expectations with respect to the sigma-fields $\{\mathfrak{F}_t\}$ generated by $dx = z\,dt + dw$, but with respect to any family of sigma-fields $\{A_t\}$; clearly the condition (7) is too strong and does not, as we also noted earlier, exploit the special nature of our problem. We have as yet found no condition on $z(\cdot)$ simpler than (7) that will imply (10). It seems that what will be needed is a condition on $x(\cdot)$ rather than on $z(\cdot)$ and $M(\cdot)$ separately. In fact, we may observe that in all our examples [in the lines below (7)], the process $x(\cdot)$ is absolutely continuous with respect to a Wiener process; however, we have not yet worked out all the implications of absolute continuity.

II. PROOFS OF THE THEOREMS

We shall begin with some definitions; general references for the following material are the paper of Kunita and Watanabe,[10] and the book[11] and lecture notes[12] of Meyer.

All our random variables will be defined on a probability space $(\Omega, \mathcal{B}, P)$. We shall also assume that we have an increasing and right-continuous family, $\mathcal{B}_t$, $0 \leqq t \leqq T$, of subsigma-fields of $\mathcal{B}$, each $\mathcal{B}_t$ containing all the null sets; we shall write $\mathcal{B}_T = \mathcal{B}$.

A process $\{M(t, \omega)\}$ will be called an *L_2-martingale* or a *square-integrable martingale* if $M(\cdot)$ has a.s. right-continuous sample paths* and if

$$EM^2(t, \omega) < \infty \quad \text{and} \quad E[M(t, \omega) \mid \mathcal{B}_s] = M(s, \omega) \quad \text{a.s.}$$

Every L_2-martingale $\{M(t, \omega)\}$ has associated with it an increasing function, called its *quadratic variation* $[M(t), M(t)]$, that can be calculated as (cf., p. 92 of Ref. 12)

$$[M(t), M(t)] = \lim_{\max |t_{i+1} - t_i| \to 0} \sum_{0}^{n-1} [M(t_{i+1}) - M(t_i)]^2 \qquad (11)^\dagger$$

where $(t_0, t_1, \cdots, t_n)$ is any partition of $(0, t)$ and the convergence of the sum is in L^1, i.e., in the norm $||A||^2 = E|A|$. When $M(\cdot)$ has continuous sample-paths, the quadratic variation is often written $\langle M, M \rangle$, and can be identified as the unique increasing process such that process $M^2(t) - \langle M(t), M(t) \rangle$ is a martingale.

A positive random variable $\tau(\omega)$ is called a *stopping time* if for every $t > 0$, the event $\{\tau(\omega) \leqq t\}$ belongs to $\mathcal{B}_t$, i.e., it depends only upon the history up to t.

A example of a stopping time is the first time $\langle M(t) \rangle$ exceeds a given level. An important property of a stopping time is that if $M(t)$ is a martingale process, then the "stopped" process $M(t \wedge \tau)$ is also a martingale.‡

A process $M(t, \omega)$, $0 \leqq t \leqq T$, is said to be a (continuous) local L_2-martingale, or a locally square-integrable martingale, if there exists a sequence of stopping times $\tau_1 \leqq \tau_2 \leqq \cdots$, increasing to T such that the stopped processes are all (continuous) L_2-martingales. The unique

---

* Meyer (p. 45 of Ref. 11) has shown that if $E[M(t, \omega)]$ is right-continuous (and if, as assumed above, $\{\mathcal{B}_t\}$ is right-continuous) then there always exists a right-continuous modification of $M(\cdot)$. If the paths of $M(\cdot)$ are a.s. continuous, we shall call the martingale continuous.

† This notation is a shorthand (cf. Meyer[12]) for the usual procedure involving a sequence of partitions.

‡ We use the notation $a \wedge b = \min(a, b)$.

(continuous) increasing function $\lim_{n\to\infty} [M(t\Lambda\tau_n)]$ will be called the function associated with the local L_2-martingale M, or often, the quadratic variation of M.

2.1 *Example*

The Itô integral

$$I(t) = \int_0^t f(s, \omega)\, dw\,(s, \omega) \tag{12a}$$

can be defined as a continuous function of t, $0 \leqq t \leqq T$, for every $f(\cdot\ ,\ \cdot)$ such that $f(\cdot\ ,\ \cdot)$ is independent of future increments of $w(\cdot\ ,\ \cdot)$ and

$$\int_0^T f^2(s, \omega)\, ds < \infty \quad \text{a.s.} \tag{12b}$$

If *in addition* $f(\cdot)$ obeys

$$E\left[\int_0^T |\, f(s, \omega)\,|^2\, ds\right] < \infty \tag{13}$$

then the Itô integral $I(t)$ is an L_2-martingale and its quadratic variation is

$$[I(t), I(t)] = \langle I(t), I(t)\rangle = \int_0^t f^2(s, \omega)\, ds.$$

By defining

$$\tau_n = \begin{cases} \min\left\{t: \int_0^t f^2(s, \omega)\, ds \geqq n\right\}, \\ T, \text{ if } \{\cdot\} \text{ is empty,} \end{cases}$$

we see that the Itô integral under equation (12) is always a continuous local L_2-martingale, with quadratic variation

$$[M(t), M(t)] = \lim_{n\to\infty} \int_0^{t\Lambda\tau_n} f^2(s, \omega)\, ds = \int_0^t f^2(s, \omega)\, ds.$$

2.2 *Proof of Theorem 3*

We note first that, with $\tilde{z}(t) = z(t) - \hat{z}(t)$,

$$\mu(t) = y(t) - \int_0^t \hat{z}(s)\, ds = \int_0^t \tilde{z}(s)\, ds + M(t)$$

is a martingale relative to the fields $\{\mathfrak{F}_t\}$ because for $\tau < t$,

$$E[\nu(t) \mid \mathfrak{F}_\tau] = \nu(\tau) + E\left[\int_0^t [\bar{z}(s)\, ds + dM(s)] \mid \mathfrak{F}_\tau\right],$$

$$= \nu(\tau) + \int_\tau^t E[\bar{z}(s) \mid \mathfrak{F}_s \mid \mathfrak{F}_\tau]\, ds + E[M(t) - M(\tau) \mid \mathfrak{F}_\tau],$$

$$= \nu(\tau) + \int 0\, ds + 0 = \nu(\tau). \tag{14}$$

The interchange of $E[\cdot]$ and the integral is justified by Fubini's theorem and the assumption (7).

Now define a sequence of $\mathfrak{F}_t$-measurable stopping times by

$$T_n = \{\inf t : t \geqq 0,\ \mu(t) \geqq n\} \Lambda T. \tag{15}$$

Since $\mu(t) < \infty$ a.s., the $\{T_n\}$ increase to T. Also it is clear that, for each n, $\mu(t \Lambda T_n)$ is a square-integrable martingale. Therefore, $\mu(\cdot)$ is a locally square-integrable martingale. To find its quadratic variation, we first show that

$$[\mu(t \Lambda T_n),\ \mu(t \Lambda T_n)] = [M(t \Lambda T_n),\ M(t \Lambda T_n)]. \tag{16}$$

To obtain equation (16), we use the definition (12), the fact that $[\cdot, \cdot]$ is zero for a continuous process of bounded variation, and the inequality

$$\sum_i [\mu(t_{i+1}) - \mu(t_i)]^2 \leq \sum \left[\int_{t_i}^{t_{i+1}} z(s)\right]^2 + \sum [M(t_{i+1}) - M(t_i)]^2.$$

Finally by letting n tend to infinity, we see that

$$[\mu(t),\ \mu(t)] = [M(t),\ M(t)],\quad 0 \leqq t \leqq T.$$

This completes the proof of Theorem 3.

2.3 *Proof of Theorem 2*

When $M(t)$ is a Wiener process, its quadratic variation is t. To obtain Theorem 2 from Theorem 3, we now use a theorem of Lévy and Doob (See p. 384 of Ref. 7), as extended by Kunita and Watanabe (See p. 217 of Ref. 10), that a continuous locally square-integrable martingale with quadratic variation t must be a Wiener process.

It is interesting to point out that the Kunita-Watanabe proof of the extended result is also considerably simpler than the original proof because the new proof utilizes the powerful new tools of the stochastic integral for L_2-martingales and the Itô differential rule for such processes.

2.4 *Proof of Corollary 4*

We note that hypothesis (10) suffices to ensure that $\mu(\cdot)$ is a.s. finite, so that the $\{T_n\}$ of equation (15) are well defined and tend to T, and also to ensure that $\mu(t \wedge T_n)$ is a square-integrable martingale. These are the essential ingredients of the proof of Theorem 3.

The present wider conditions under which we have been able to establish the innovations result will, of course, extend the range of problems in which the innovations can be used. In particular, we have applied Theorem 2 to show[14] that a general likelihood-ratio formula, derived in Ref. 5, for processes obeying equations (1) through (4) remains valid if equation (4) is replaced by the weaker conditions that $\int z^2(t)\, dt < \infty$ a.s. and $\int E \mid z(t) \mid dt < \infty$.

REFERENCES

1. Kailath, T., "A General Likelihood-Ratio Formula for Random Signals in Gaussian Noise," *IEEE Trans. on Infm. Theory, IT-15*, No. 3, (May 1969), pp. 350–361.
2. Frost, P. A., "Estimation in Continuous-Time Nonlinear Systems," Ph.D. Dissertation, Dept. of Electrical Engineering, Stanford University, Stanford, Calif., June 1968.
3. Shiryaev, A. N., "Stochastic Equations of Nonlinear Filtration for Purely Discontinuous Markov Processes," *Prob. Pered. Informatsii, 2*, (1966), pp. 3–22.
4. Kallianpur, G., personal communication, August 1969.
5. Kailath, T., "A Further Note on a General Likelihood-Ratio Formula," *IEEE Trans. on Infm. Theory, IT-16*, No. 4, (July 1970), pp. 393–396.
6. Kailath, T., "Likelihood Ratios for Gaussian Processes," *IEEE Trans. on Infm. Theory, IT-16*, No. 3, (May 1970), pp. 276–288.
7. Doob, J. L., *Stochastic Processes*, New York: J. Wiley & Sons, Inc., 1953.
8. Shepp, L., personal communication.
9. Loève, M., *Probability Theory*, New Jersey: Van Nostrand Book Co., Third Edition, 1963.
10. Kunita, H. and S. Watanabe, "On Square Integrable Martingales," *Nagoya Math. J., 30*, August 1967, pp. 209–245.
11. Meyer, P., *Probability and Potentials*, Waltham, Mass.: Blaisdell Book Co., 1966.
12. Meyer, P., *Intégrales Stochastiques*, I–IV, Lecture Notes in Mathematics *39*, Springer, Berlin, 1967, pp. 72–162.
13. Frost, P. A., "The Innovations Process and Its Application to Non-Linear Estimation and Detection of Signals in Additive White Noise," *Proc. UMR-Mervin J. Kelly Communications Conference*, Rolla, Missouri, October 1970, pp. 7-3-1 to 7-3-6.
14. Kailath, T., "The Structure of Radon-Nikodym Derivatives with Respect to Wiener and Related Measures," *Annals Math. Stat.*, to appear, 1971.

Contributors to This Issue

PHILIP BALABAN, Dipl. Ing., 1949, Technical University, Munich; Ph.D., 1966, Polytechnic Institute of Brooklyn; Scientific Dept., Israel Ministry of Defense, 1950–1956; Contraves AG, Zurich, 1956–1958; Computer Systems Inc., 1958–1963; Bell Telephone Laboratories, 1967—. Mr. Balaban has been engaged in research and development in the areas of analog and digital computers, circuit design, and system theory. His current work involves the application of computer aids to the design of transmission systems. Mr. Balaban has recently returned from a leave of absence to the Israel Institute of Technology. Member, IEEE, Sigma Xi.

MATTHEW D. BALKOVIC, B.S.E.E., 1960, Carnegie Mellon University; M.E.E., 1962, New York University; Bell Telephone Laboratories, 1960—. Mr. Balkovic has worked on the systems engineering aspects of analog and digital data transmission over voicebandwidth telephone channels. He is presently Supervisor of a group conducting studies on data transmission performance. Member, IEEE, Eta Kappa Nu, Tau Beta Pi, Phi Kappa Phi.

PETER D. BRICKER, B.A., 1950, Bucknell University; M.A., 1952, and Ph.D., 1954, The Johns Hopkins University; Bell Telephone Laboratories, 1955—. Mr. Bricker has been concerned with human performance, perception, and judgment, particularly with regard to speech communication behavior. He is currently studying listener perception of potential electronic calling signals. Member, Acoustical Society of America, American Psychological Association, Phi Beta Kappa.

E. M. BUTLER, B.E.E., 1964, and M.S., 1965, Cornell University; Ph.D., 1969, University of California, Berkeley; Bell Telephone Laboratories, 1969—. Mr. Butler is currently working on techniques for computer-aided analysis and design. Member, IEEE, Eta Kappa Nu.

IVAN A. CERMAK, B. Eng., 1963, M. Eng., 1967, and Ph.D., 1969, McGill University, Montreal, Canada; Bell Telephone Laboratories,

1969—. Since joining Bell Laboratories, Mr. Cermak has been concerned with computer-aided circuit design. He supervises a group responsible for nonlinear analysis and the operation of the Holmdel Transmission Systems Development Division computing facility. Member, IEEE.

WESLEY YUNG-SEN CHEN, B.S.E.E., 1960, National Taiwan University; M.S.E.E., 1963, and Ph.D., 1967, University of Washington; Bell Telephone Laboratories, 1967—. Mr. Chen is a member of the Digital Radio and Microwave Facilities Department and has worked on problems related to radio relay systems. Member, Sigma Xi.

J. CHERNAK, B.E.E., 1960, Polytechnic Institute of Brooklyn; M.E.E., 1961, New York University; Bell Telephone Laboratories, 1960—. Mr. Chernak has been concerned with computer-aided design techniques and their applications. As Director of the Transmission Technology Laboratory, he is involved in computer-aided analysis and the design of transmission components and networks. Member, IEEE, Eta Kappa Nu, Tau Beta Pi.

TA-SHING CHU, B.S., 1955, National Taiwan University; M.S., 1957, and Ph.D., 1960, Ohio State University; Bell Telephone Laboratories, 1963—. Mr. Chu has been concerned with problems involving electromagnetic wave propagation and microwave antennas. Member, IEEE, Commission 2 of URSI, Sigma Xi, Pi Mu Epsilon.

GOBIND T. DARYANANI, B.S.E.E., 1963, Calcutta University; M.S., 1965, Virginia Polytechnic Institute; Ph.D., 1968, Michigan State University; Bell Telephone Laboratories, 1969—. Mr. Daryanani has been working on the analysis and synthesis of active filters. Member, IEEE, Eta Kappa Nu, Phi Kappa Phi.

ALTON C. DICKIESON studied electrical engineering at Brooklyn Polytechnic Institute and joined the Western Electric Company Engineering Department in 1923. At Bell Laboratories, Mr. Dickieson's responsibilities included long-distance communications systems; military telephone, sonar, and torpedo guidance systems during World War II; and transmission and radio systems engineering. In 1951 he became Director of Transmission Systems Development and subsequently directed the planning for the communication and detection

systems used in the first Distant Early Warning stations. He became Executive Director of the Transmission Division in 1961, in which position he had general responsibility for the TELSTAR® communications satellite experiment. Mr. Dickieson was appointed Vice President of Transmission Development in 1966. He retired from Bell Laboratories on September 1, 1970. Naval Ordnance Development Award, 1945; Gen. H. H. Arnold Trophy of the Air Force Association (with Dr. J. R. Pierce), 1962; Gen. H. S. Vandenberg Award of the Arnold Air Society (with Dr. J. R. Pierce), 1963; National Academy of Engineering, 1970; Fellow, IEEE.

FRANCIS P. DUFFY, B.A., 1965, King's College; M.S., 1968, Stevens Institute of Technology; Bell Telephone Laboratories, 1965—. Mr. Duffy has been involved in conducting transmission performance surveys of the toll telephone network. His activities have centered on computer applications and data analysis.

HOWARD C. FLEMING, B.S.E.E., 1932, and M.S., 1936, New York University; Bell Telephone Laboratories, 1937—. After four years in the Education and Training Center, Mr. Fleming was assigned to development of Bell System and military carrier telephone communication systems. This period was interrupted by work on submarine detection systems during World War II. The development assignment was followed by military communication systems engineering, and more recently, Bell System data communications planning. At present, he supervises a group conducting data systems studies, chiefly concerned with accuracy of data transmission. Senior Member, IEEE; Member, Iota Alpha, Tau Beta Pi.

RAMANATHAN GNANADESIKAN, B.Sc. (Hons), 1952, and M.A., 1953, University of Madras (India); Ph.D., 1957, University of North Carolina; Bell Telephone Laboratories, 1959—. Mr. Gnanadesikan has worked on developing new statistical methods for use in data analysis and on a variety of applications of statistics including the problem of talker identification, the selection of semiconductor devices for submarine cable repeaters, and the empirical grouping of corporations based on their economic characteristics. He is Head of the Statistics and Data Analysis Research Department. Fellow, American Association for the Advancement of Science, American Statistical Association, Institute of Mathematical Statistics, and Royal Statistical Society;

Member, Biometric Society, International Association for Statistics in Physical Sciences, Mathematical Association of America.

DAVID J. GOODMAN, B.E.E., 1960, Rensselaer Polytechnic Institute; M.E.E., 1962, New York University; Ph.D., 1967, University of London; Bell Telephone Laboratories, 1960–62, 1967—. A member of the Systems Theory Research Department, Mr. Goodman has studied principles of digital signal processing including analog-to-digital conversion and the statistical approach to digital filter design. Member, IEEE, Eta Kappa Nu, Tau Beta Pi.

GERALD D. HAYNIE, B.S.E.E., 1956, Virginia Polytechnic Institute; M.E.E., 1961, New York University; Bell Telephone Laboratories, 1956—. Mr. Haynie has been engaged in the development of precision measuring systems used in transmission systems development. Recent emphasis of this work has been in computer-operated systems. He is Head of the Measuring Systems Design Department. Member, IEEE, Eta Kappa Nu, Tau Beta Pi.

ROBERT M. HUTCHINSON, JR., B.S.E.E., 1966, Pennsylvania State University; M.S.E., 1967, University of Pennsylvania; Bell Telephone Laboratories, 1966—. Mr. Hutchinson has worked on the measurement and characterization of low-speed data transmission performance. Member, IEEE, Tau Beta Pi.

THOMAS KAILATH, B.S. (Telecommunications Engineering), 1956, University of Poona, Poona, India; M.S., 1959, and D.Sc., 1961, Massachusetts Institute of Technology; L.D. College of Engineering (Ahmedabad, India), 1956–57; Jet Propulsion Laboratories, Pasadena, California, 1961–62; Professor of Electrical Engineering, Stanford University, 1963—. Mr. Kailath, employed by Bell Laboratories during the summer of 1969, was a Guggenheim Fellow and Visiting Professor at the Indian Institute of Science, Bangalore, India, for the academic year 1969–70. His research interests are in statistical data processing in communications and control. Member, Institute of Mathematical Statistics, SIAM, Sigma Xi. Fellow, IEEE.

BARRY J. KARAFIN, B.S.E.E., 1961, University of Pennsylvania; M.E.E., 1963, New York University; Bell Telephone Laboratories,

1961—. Mr. Karafin has been engaged in the areas of digital communication systems, computer language and compiler design, and numerical analysis. He currently heads a department concerned with the application of computers to circuit and system design.

MRS. DOROTHY B. KIRBY, B.A., Mathematics, 1952, University of Vermont; M.S., 1961, New York University; Bell Telephone Laboratories, 1952—. Mrs. Kirby has been concerned with the use of digital computers as a tool in the design and analysis of electrical circuits and communication systems. She has developed programs used for studying equalization of a high-speed digital transmission system repeatered link and for producing statistics on radio signal fading. Most recently, she has worked on the analysis of nonlinear circuits.

HARRY W. KLANCER, B.E.E., 1966, University of Detroit; M.S.E.E., 1967, University of Michigan; Bell Telephone Laboratories, 1966—. Mr. Klancer has worked on problems relating to wideband and voiceband data transmission. He has recently been involved in the evaluation of the switched network for voiceband data transmission. Member, Tau Beta Pi, Eta Kappa Nu.

STEPHEN W. KLARE, B.S., 1968, and M.S., 1969, George Washington University; Bell Telephone Laboratories, 1969—. Mr. Klare has worked in data transmission systems engineering. He is presently involved in the evaluation of the performance of the switched network for voiceband data transmission. Member, IEEE, Sigma Tau.

JOHN LOGAN, B.Sc. (1st Hons. Electrical Engineering), 1961, and B.Sc. (1st Hons. Mechanical Engineering), 1962, Glasgow University, Scotland; Ph.D. (Electronics), 1966, University of Cambridge, England; Bell Telephone Laboratories, 1966—. Mr. Logan developed techniques for simulation of circuits for both analog and digital transmission systems. In 1968 he was appointed Supervisor of a group responsible for characterization and analysis support of transmission systems and modeling and measurements of semiconductor devices. He currently heads the computer aided analysis and characterization department in the Transmission Technology Laboratory at Merrimack Valley.

MAX V. MATHEWS, B.S., 1950, California Institute of Technology; M.S., 1952, and Sc.D., 1954, Massachusetts Institute of Technology; Bell Telephone Laboratories, 1955—. Mr. Mathews has worked on various facets of acoustics research including speech analysis, as it pertains both to automatic speech recognition machines and to low channel capacity speech transmission, and computer music. He is currently the Director of the Behavioral and Statistical Research Center. Member, IEEE, Acoustical Society of America, Sigma Xi.

WILLIAM G. MCGRUTHER, B.S.E.E., 1965, Syracuse University; M.S., 1967, Johns Hopkins University; Bell Telephone Laboratories, 1965—. Mr. McGruther has worked in data transmission systems engineering. He is currently studying data system performance. Member, Tau Beta Pi, Eta Kappa Nu, Pi Mu Epsilon.

RONALD G. OLSEN, B.S.E.E., 1967, and M.S.E.E., 1968, Massachusetts Institute of Technology; Bell Telephone Laboratories, 1967—. Mr. Olsen has been engaged in the development of computer programs and techniques for the simulation and analysis of communications circuits and systems. He is a member of the Computer-Aided Analysis Department at Holmdel. Member, IEEE, Tau Beta Pi, Eta Kappa Nu, Sigma Xi.

LAWRENCE A. O'NEILL, B.S.E.E., 1956, University of Maryland; M.E.E., 1959, Catholic University of America; Ph.D., 1966, The Johns Hopkins University; Department of Defense, 1956–1967; Bell Telephone Laboratories, 1967—. Mr. O'Neill has been involved in the application of both digital and hybrid computers to digital transmission system development. He has worked on design, optimization, tolerance analysis, and the development of the computer-controlled manufacturing tests. Currently he supervises a group engaged in the computer simulation of transmission systems. Member, IEEE, Tau Beta Pi, Eta Kappa Nu, Sigma Xi, Phi Kappa Phi.

MISS SANDRA PRUZANSKY, A.B., 1959, Indiana University; M.S., 1960, University of Wisconsin; Bell Telephone Laboratories, 1960—. Miss Pruzansky has been engaged in research on human auditory perception and speech communication. She is currently concerned with the use of

computers in the study of speech perception. Member, Acoustical Society of America, American Speech and Hearing Association.

CHARLES L. SEMMELMAN, B.E.E. and B.Sc., Phys., 1939, Ohio State University; Bell Telephone Laboratories, 1940–1942 and 1946—; Signal Corps Engineering Laboratories, 1942–1946. Mr. Semmelman has been engaged in the design of filters and equalizers. He supervises a group preparing computer programs for the analysis, synthesis, and optimization of transmission networks and systems. Associate, Sigma Xi; Member, Tau Beta Pi, Eta Kappa Nu, Pi Mu Epsilon, Sigma Pi Sigma.

MRS. DOROTHEA B. SNYDER, A.B., Mathematics, 1952, Bucknell University; Bell Telephone Laboratories, 1952—. Mrs. Snyder has been concerned with the development of various programming aids for the design of transmission circuits and systems.

T. W. THATCHER, JR., B.S.E.E., 1942, Iowa State University; Bell Telephone Laboratories, 1942—. Mr. Thatcher initially was concerned with engineering, test, and installation of terminals of a military speech privacy system. For most of his career, he has been responsible for objectives, field trials, application engineering information, and improvements to the N and P families of short-haul toll and subscriber carrier systems. Currently, he is responsible for telephone network surveys as supervisor of the Measurements and Reports Group of the Transmission Performance Department. Member, IEEE.

PAUL A. TUKEY, B.A., 1967, Princeton University; Bell Telephone Laboratories, 1969—. Mr. Tukey has worked on the development of statistical techniques for automatic speaker recognition, on statistical applications of computer graphics, and on the analysis of data from the Holmdel rainfall experiment. Member, American Statistical Association, Phi Beta Kappa.

KENNETH W. WACHTER, B.A., 1968, Harvard University; Bell Telephone Laboratories, Summer 1967, 1968–1970. Mr. Wachter is currently working towards a Ph.D. in statistics at Cambridge University. While at Bell Laboratories, he worked on the theoretical problem of determining the statistical configuration of Wishart eigenvalues besides contributing to the work on talker identification.

EDWARD D. WALSH, B.S.E.E., 1965, Gannon College; M.Eng., 1966, and Ph.D., 1968, Rensselaer Polytechnic Institute; Bell Telephone Laboratories, 1968—. Mr. Walsh engaged initially in the frequency domain characterization of high-frequency active and passive devices. Later he worked on the extraction, from measured data, of large signal transistor model parameters. He is presently working on computer-aided analysis programs for large networks. Member, IEEE, Sigma Xi.

JACK L. WARNER, B.S., 1962, and M.S., 1966, Virginia Polytechnic Institute; Bell Telephone Laboratories, 1965—. Mr. Warner has worked on computer applications of statistical methods for use in data analysis, and on the development of software for data processing and data retrieval. Member, Pi Mu Epsilon.

S. YANG, B.S.E.E., 1961, Seoul National University, Korea; Electronics Officer in the Korean Navy, 1961–1964; Radio Instructor for the International Development Corporation, Seoul, 1965–1967; M.S.E.E., 1969, Virginia Polytechnic Institute; currently working toward a Ph.D. in electrical engineering at Polytechnic Institute of Brooklyn; Bell Telephone Laboratories, 1968—. Mr. Yang's work to date has included exploratory studies in the area of computer-aided network adjustment, design for computer-aided measurement, and data processing programs. Currently, he is engaged in the design of computer control, graphics, and software for a computer-operated transmission measurement system. Member IEEE, Phi Kappa Phi.